Coordination of Generator Protection and Control in the Over and Under Excited Regions

A Thesis Submitted

to the College of Graduate Studies and Research

in

Partial Fulfillment of the Requirements

for the Doctor of Philosophy Degree

in the Department of Electrical and Computer Engineering
University of Saskatchewan

by

Eli Pajuelo

Saskatoon, Saskatchewan, Canada

Permission to Use

In presenting this thesis in partial fulfillment of the requirements for a Postgraduate degree from the University of Saskatchewan, it is agreed that the Libraries of this University may make it freely available for inspection. Permission for copying of this thesis in any manner, in whole or in part, for scholarly purposes may be granted by the professors who supervised this thesis work or, in their absence, by the Head of the Department of Electrical and Computer Engineering or the Dean of the College of Graduate Studies and Research at the University of Saskatchewan. Any copying, publication, or use of this thesis, or parts thereof, for financial gain without the written permission of the author is strictly prohibited. Proper recognition shall be given to the author and to the University of Saskatchewan in any scholarly use which may be made of any material in this thesis.

Request for permission to copy or to make any other use of material in this thesis in whole or in part should be addressed to:

Head of the Department of Electrical and Computer Engineering
57 Campus Drive
University of Saskatchewan
Saskatoon, Saskatchewan, Canada
S7N 5A9

Abstract

This thesis deals with the coordination of protection and control functions associated with the synchronous generators. The excitation control functions are a key component in maintaining the stability of machines and the network. The overall objective of coordination is simple; to allow excitation control functions, the automatic recovery from excursions beyond normal limits, and only take protective action as a last resort. This thesis focuses on four areas of generator control and protection : a) Loss of excitation protection, b) Dynamic underexcitation coordination, c) Dynamic Overexcitation coordination, and d) a generic protective relay development platform for hardware and software development.

Loss of excitation (LOE) is a condition in the underexcited region that presents a risk of severe damage to a generator. The state of the art in the detection of a loss of excitation condition is based on the principle that, for a zero Thevenin voltage, the generator becomes a reactance as seen from the power system. The difficulty in detecting a loss of excitation is that several other disturbances may temporarily present a similar behavior, for instance a fault followed by a power swing. In this part of the work, a new algorithm for the detection of a loss of excitation condition is proposed by using the Support Vector Machine (SVM) classification method and a careful design of the necessary feature vectors. The proposed method is robust to changes in conditions including initial load, fault types, line impedance, as well as generator parameter inaccuracies.

Coordination in the underexcited region presents difficulties due to the commonly used static characteristics instead of dynamic simulation. The underexcited limit presents an overload characteristic that is not normally known or used. Once the limit is exceeded, the limiting control action is a control loop that presents a dynamic behavior not typically represented in studies in the current industry practice. It is also important to properly model and include dynamic performance of protection functions. An important consideration not

typically taken into account is the actual stability limit, which depends on the characteristics and the mode of excitation control used. This thesis includes all the above considerations necessary to achieve the required coordination using the more accurate dynamic simulations. Specific scenarios that present risk to the machine or the system are included to assess the coordination achieved. A real generator from the Alberta power system is used as a case study to demonstrate the proposed coordination methodology.

Coordination in the overexcited region again presents practical difficulties due to static characteristics instead of dynamic simulation of conditions that exercise the overexcitation limits. The problems observed relate to coordination methodology and modeling methods for both protection and control limits. Once the limit boundary characteristic is exceeded, the limiting action is a control loop that presents dynamic behavior that needs to be represented. Similar considerations need to be made with the protection function protecting against rotor overload. Current modeling methods mostly use low bandwidth simulations, i.e., transient stability studies. A modeling methodology as well as specific model improvements to the IEEE ST1A excitation control model are proposed to achieve the required coordination. The ST1A type is one model that can represent a wide variety of system models from different manufacturers. The proposed modeling methodology applies to high bandwidth simulations such as electromagnetic simulations. Specific important scenarios, such as severe temporary reactive overload or severe power swing conditions, where the protection and control are required to coordinate but that present risk to the machine or the system are proposed as part of the coordination considerations.

The detection of LOE conditions by the proposed SVM method and by traditional methods was implemented in hardware by using a digital signal processor (DSP) platform and tested using real time power system simulations. A new platform for real time protective relay development was designed and used for the purpose of implementation. In the proposed platform, a processor independent code is used so that development can be performed using native host computer development tools. By using the proposed platform-independent code, off line testing can be performed either interactively or in batch mode for evaluating multiple cases.

Acknowledgments

I would like to express my gratitude and appreciation to Dr. R. Gokaraju for his guidance, support and patience throughout the extended time to complete this work. His advice and assistance with respect to the preparation of this thesis are thankfully acknowledged.

I also would like to express my sincere thanks to Prof. M.S. Sachdev for providing funding from his NSERC grant for my PhD studies.

I would like to thank Don Robinson and Hiten Patel from Saskpower for the invaluable field experience with synchronous generator testing, as well as Roger Berube and Les Hajagos from Kestrel Power for the thorough technical material produced as a result of those tests.

Also, I would like to thank the IEEE Excitation Systems and Control Subcommittee and to Jose Taborda in particular for his interesting discussions and encouragement as well as the IEEE Power System Relaying Committee for their important work and useful discussions and material produced that made a significant impact on my knowledge to complete this thesis.

I am grateful to professors and student colleagues in the Department of Electrical and Computer Engineering, too many to name them all here, that have contributed with useful discussions, encouragement, and friendship during my longer than usual time to complete my PhD program.

Financial support provided by the Natural Sciences and Engineering Research Council (NSERC) of Canada and the University of Saskatchewan is thankfully acknowledged.

The author would also like to thank his beloved wife Erlinda Huamani, for her patience and unconditional support during all of this work. Also, the author would like to thank his parents Fortunato and Ricardina for their continued moral support and encouragement.

Dedicated to my

beloved wife Maribel

and children Diego, Mara, and Andres

Table of Contents

List of Tables

List of Figures

List of Symbols and Abbreviations

A/D	Analog to Digital
AESO	Alberta Electric System Operator
ANN	Artificial Neural Networks
ATP	Alternative Transient Program
AVR	Automatic Voltage Regulator
COMTRADE	Common Format for Transient Data Exchange
CPU	Central Processing Unit
CT	Current Transformer
DFT	Discrete Fourier Transform
DSP	Digital Signal Processor
DYSL	Dynamic Stability Limit
ECS	Excitation Control System
EDMA	Enhanced Direct Memory Access
EMTP	Electro Magnetic Transients Program
ESCSC	Excitation Systems and Control Subcommittee
FCL	Field Curent Limiting
FCR	Field Current Regulator
FFT	Fast Fourier Transform

FIR	Finite Impulse Response
GCC	Generator Capability Curve
GPP	General Purpose Processor
GTAO	RTDS analog output card
IEC	International Electrotechnical Commission
IIR	Infinite Impulse Response
IRAM	Internal RAM
LED	Light Emitting Diode
LFC	Load Frequency Control
LOE	Loss of Excitation
NERC	North American Eletric Reliability Corporation
OEL	Over Excitation Limiter
PC	Personal Computer
PSS	Power System Stabilizer
PSS/E	Power System Simulator from PTI
PT	Potential Transformer
PTI	Power Technologies Inc.
RAM	Random Access Memory
ROM	Read Only Memory
RTDS	Real Time Digital Simulator
SDK	Software Development Kit

SDRAM	Synchronous Dynamic RAM
SSSL	Steady State Stability Limit
SVM	Support Vector Machine
TACS	Control System Modeling Tools in ATP
TNA	Transient Network Analyzer
UEL	Under Excitation Limiter

List of Publications

My Ph.D. has produced the following publications to date:

List of Journal Papers:

[J1] E. Pajuelo, R. Gokaraju, and M. S. Sachdev, "Identification of generator loss of excitation from power swing conditions using a fast pattern classification method", *IET Generation, Transmission and Distribution*, Vol. 7, Issue 1, pp. 24-36, 2013.

[J2] E. Pajuelo, and R. Gokaraju, "Generator Coordination Methodology in the Underexcited Region", *IEEE Transactions on Power Delivery*, Submitted on January 2015.

List of Conference Papers:

[C1] E. Pajuelo, R. Gokaraju, and M. S. Sachdev, "Coordination of overexcitation limiter, field overcurrent protection and generator control", Panel session paper invited by the IEEE Excitation Controls Subcommittee, July 25-29, 2010, Paper No. 2010GM1560, Panel Paper, Presented at the IEEE PES General Meeting in Minneapolis, MN.

List of Poster Presentations:

[PO1] E. Pajuelo, R. Gokaraju, and M. S. Sachdev, "Loss of Excitation Protection for Generators Using a Support Vector Machine Technique", July 26-29, 2009, Poster presented at the IEEE PES General Meeting in Calgary, AB.

[PO2] E. Pajuelo, R. Gokaraju, and M. S. Sachdev, "Coordination of underexcitation limiter, loss of excitation protection and generator control", July 25-28, 2011, Poster presented at the IEEE PES General Meeting in Detroit, MI.

List of Patents

My Ph.D. has produced the following patents to date:

[PA1] E. Pajuelo and R. Gokaraju, "Identification of generator loss of excitation from power swing conditions using a fast pattern classification method", This work has been filed with the Patent Cooperation Treaty Patent Application No. PCT/CA2014/050067 for METHODS AND APPARATUS FOR DETECTION OF GENERATOR FAULTS on February 3, 2014.

Chapter 1

Introduction

1.1 Background

For a normal power system operation, a balance is required between the power produced and the power consumed. Voltage and frequency at all buses must remain within certain tolerances, and every operating state of the system should be stable even during the worst possible contingencies. Such requirements are achieved with the help of protection and control systems.

1.1.1 Power Systems Protection

Protection systems are responsible for detecting and removing fault conditions in the power system. Protection systems do not detect a fault before it happens, nor do they prevent it from happening. The prevention of faults is achieved by proper design of the power system components. The role of protection systems is to reduce the consequences (such as damage to power equipment) of a fault by quickly isolating the faulted equipment.

The most common type of fault is the short circuit. The consequences of a short circuit depend on where it happens in a power system. In an overhead transmission line, for instance, the insulating air recovers quickly after de-energizing the fault arc. In a generator or transformer, however, the insulating material becomes permanently damaged by a short circuit. The isolation of a fault typically requires two components: a) a protective relay and b) a circuit breaker. The protective relay uses voltage and current measurements to identify the presence of a fault in the protected area. The circuit breaker performs the

electrical isolation following the decision from the relay. One special case is the fuse, in which detection and isolation are incorporated in a single device; fuses needs to be replaced after each protective operation. The protective function concept is illustrated in Fig. 1.1 .

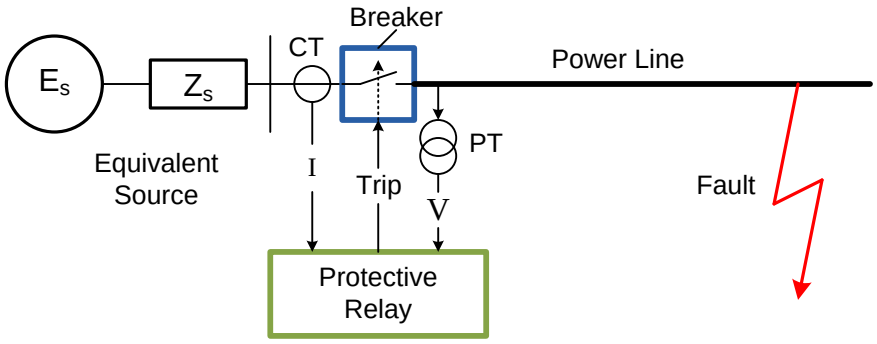

Figure 1.1: Basic protective function concept

Other types of faults are not short circuits. These type of faults are abnormal conditions that may be allowed temporarily as long as they return back to normal within a given period of time. An example of such faults is when certain variables move above or below normal levels by a relatively small percentage, with the most typical being a) over/under frequency, b) over/under voltage, and c) active/reactive over/under power. Compared to short circuit faults in which a decision should be made quickly once the condition is detected, these abnormal conditions require the protection to be coordinated with any control action responsible to return the condition to normal.

The power system is susceptible to not only faults but also to many other normal disturbances, such as line switching, sudden load changes, and turbine input changes, to name a few. Therefore, there is a risk of incorrect operation of the protection system. To achieve correct operation, the protection system must meet certain requirements: a) selectivity, b) sensitivity, c) speed, and d) reliability. Selectivity helps to identify faults inside the protected area from other disturbances. Sensitivity is a measure of how small a fault can be detected. Speed is important to reduce the impact of the fault on the power system. Reliability is obtained by a compromise between dependability and security.

1.1.2 Numerical Relays

At present, protection functions are implemented with technologies based on microprocessor architectures. The basic components of a numerical relay are: a) current and voltage inputs, b) contact inputs, c) fault detection element(s), d) contact outputs, and e) a target or alarm display. The current and voltage inputs perform instantaneous measurement of these signals, converting them to numbers, i.e. the current and voltage samples. The contact inputs monitor the status of variables that have two states, such as breaker position, i.e., open or closed. The fault detection element consists of two main elements: a phasor estimator and a protection function. The phasor estimator converts the voltage and current measurements to phasor form. The protection function identifies using these phasors whether or not a fault exists in the protected area. The contact outputs transmit the protective decision to the circuit breakers. The target or alarm visually indicates the last protective operation performed.

Additional functions are included in numerical relays thanks to advanced capabilities of the microprocessor architectures, such as a) recording, b) communications, and c) self-test. Information recorded includes: a) events with time stamp, b) oscillography waveforms and digital flags, and c) fault reports. Communication capabilities help during maintenance and also allow integration with the supervisory control and data acquisition system. Self-test, also known as autodiagnostic, helps in improving the reliability by continuously monitoring the status of different components inside a numerical relay so that internal failure is detected before the equipment is required to operate.

1.1.3 Power Systems Controls

Power systems controls are categorized into three major areas: a) system, b) transmission, and c) generation. System control includes the load frequency control (LFC) , which is responsible for restoring the frequency to normal by increasing or decreasing the overall generation. It also includes economic allocation, which decides how much each generator should produce to keep the overall cost at a minimum. Transmission control includes reactive power

(var) control to maintain voltage levels within the tolerances, and others. Generation control includes active power and output voltage controls. One of the main subjects of this research work is generation control, and therefore a more detailed description is given in Chapter 2.

1.2 Motivation for the Proposed Research

1.2.1 Problems Associated with Coordination of Generator Protection with Control

The basic coordination concept between generator protection and control is simple and can be summarized as follows: a) an abnormal condition happens, b) control action should be allowed to return the generator to normal, and c) only if control action fails should the protection trip and take action to protect the generator. This concept is illustrated in Fig. 1.2. However, this simple concept is not necessarily easy to implement in practice.

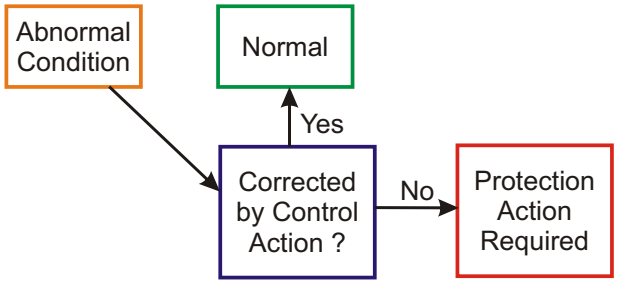

Figure 1.2: Basic concept of coordination between generator protection and control

Disturbance events have occurred in recent years in which generator protection tripped units that still had available capability to support the system [2–8]. For instance, a large disturbance happened on the North America Western System Coordinating Council (WSCC) area on July 2, 1996 in which around 12 GWs of load was lost [2, 9]. In this event, several generating units tripped due to field excitation overcurrent protection, and at least one due to suspected loss of excitation condition. Another major disturbance happened on the North Eastern part of the North American System on August 14, 2003, in which a record 53 GWs of generating units tripped, with many of these trips happening due to field excitation

overcurrent, loss of excitation, and abnormal frequency, among other protection functions [3,10]. One important issue identified in these disturbances is the lack of proper coordination between protection and control functions that monitor similar operating quantities of a generator.

The coordination of generator protection and control in the over and under excited regions should provide the maximum available reactive capability in these regions [11, 12] and therefore it presents a number of challenges. One challenge is due to the method commonly used to define the generator protection settings, which is based on static characteristics representing generator capability, control limits, or protective relay characteristics. In general, these characteristics vary in time and are dependent on several variables, such as terminal voltage, disturbance severity and duration time, and dynamics of the particular generating unit, as well as the plane on which they are plotted (complex power plane or impedance plane). An example of the dynamic behavior for the overexcitation limit (OEL) is shown in Fig. 1.3. In Fig. 1.3, the OEL dynamic limit depends of the maximum allowable time, T_{MAX}, for a given level of field current I_{FD}.

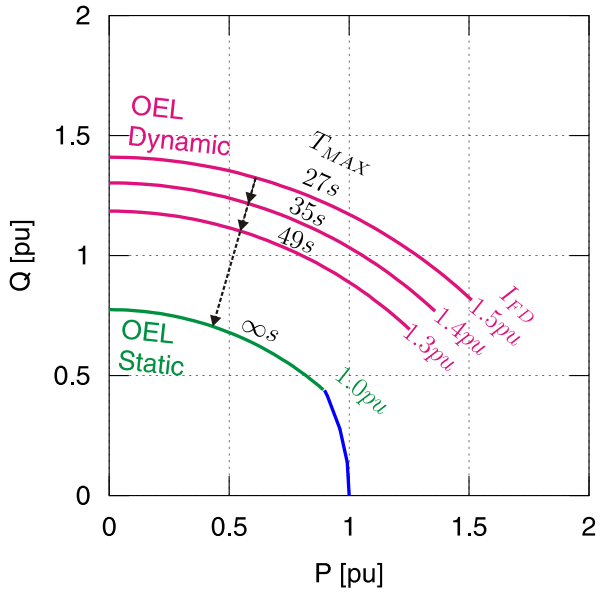

Figure 1.3: Basic concept of static versus dynamic characteristic for the OEL limit

Static modeling concepts were developed at a time when computer technology was very

limited. Thus, the use of static characteristics is, in fact, an attempt to simplify the coordination process by assuming large conservative safety margins between these characteristics as well as large and safe operating time delays. The dynamic behavior of the generators is not taken into account.

Another challenge is with regard to modeling the functions that need to be coordinated, i.e., the protection and control functions of interest. Examples of these functions are the loss of excitation protection function and the underexcitation limiter control function. The dynamic response of these functions needs to be properly represented placing special consideration to their performance when the machine moves temporarily beyond the normal operating limits. Considerable modeling effort is required to incorporate these functions into the dynamic power systems network database and simulation tools. Practical considerations for generator and excitation design to meet regulations also play an important role [13].

In addition to the accuracy in modeling the generator, as well as its control and protection, the conditions that are more important to verify the coordination need to be identified and considered. With the models obtained, several different scenarios can be verified that in many cases are not physically possible without risk to damage the machine.

1.2.2 Literature Review

A working group report from IEEE PSRC published in 2004 [6] provides a review of past performance of generator protection functions during wide area disturbances and highlights recommendations to improve the performance by reducing the possibility of maloperations. This report describes, among several events, the major disturbance on 1996 in the WSCC network area above indicated. In the 1996 WSCC disturbance, the report indicates that several generation units tripped out of service due to miscoordination between excitation control and protection functions [6]. The other major disturbance in North America on August 2003 previously indicated, could not be considered in the IEEE PSRC 2004 report because this report was submitted prior to this event. In the event of 2003 there were many generator taken out of service by protective operations, with many of them suspected of being

unnecessary trips due to miscoordination between generator protection and control [10].

To address the issues just described, the IEEE PSRC produced another report published in 2007 [14] with recommendations to adjust the generator protection functions in order to better coordinate with generator control functions. This IEEE PSRC report basically summarizes and provides guidelines for the coordination between protection and control, but only using static characteristics without the use of dynamic modeling and simulation. These recommendations for static coordination were included in the IEEE C37.102-2006 standard, with examples in the appendix of that document. More recently, the North American Electric Reliability Corporation (NERC) produced a technical report [10] with updated guidelines based on the prior IEEE PSRC 2007 report. One important addition in this report from NERC is the suggestion to use dynamic simulation to improve coordination between generator control and protection.

In this thesis, a more extensive literature review that is more specific to the different subjects presented is provided in later chapters in order to improve clarity and avoid the reader to jump back and forth between this brief literature review and the corresponding chapters.

The synchronous machine and its modeling for dynamic simulations is one of the key components of this thesis and is described in the next section.

1.3 Synchronous Machine and Modeling

1.3.1 Park's Equations

One of the most widely used mathematical representations of the synchronous machine is provided by Park's equations [15], which are based on a transformation between stator phase quantities to a stationary frame with respect to the rotor. This transformation is called the dq0 transformation and is given by (1.1):

$$\begin{bmatrix} y_d \\ y_q \\ y_0 \end{bmatrix} = [\mathbf{S}] \begin{bmatrix} y_a \\ y_b \\ y_c \end{bmatrix} \tag{1.1}$$

where:

y : instantaneous current i or voltage v

$\mathbf{S}$: transformation matrix

a, b, c : phase designation

The transformation matrix $\mathbf{S}$ is given by (1.2):

$$[\mathbf{S}] = \frac{2}{3} \begin{bmatrix} \cos(\theta) & \cos(\theta - 120^\circ) & \cos(\theta + 120^\circ) \\ \sin(\theta) & \sin(\theta - 120^\circ) & \sin(\theta + 120^\circ) \\ \frac{1}{2} & \frac{1}{2} & \frac{1}{2} \end{bmatrix} \tag{1.2}$$

where:

θ : rotor angle of d axis with respect to stator phase a

An overview of the synchronous generator showing the equivalent circuits as well as the dq0 rotating frame concept used to develop Park's equations is shown in Fig. 1.4.

In Fig: 1.4

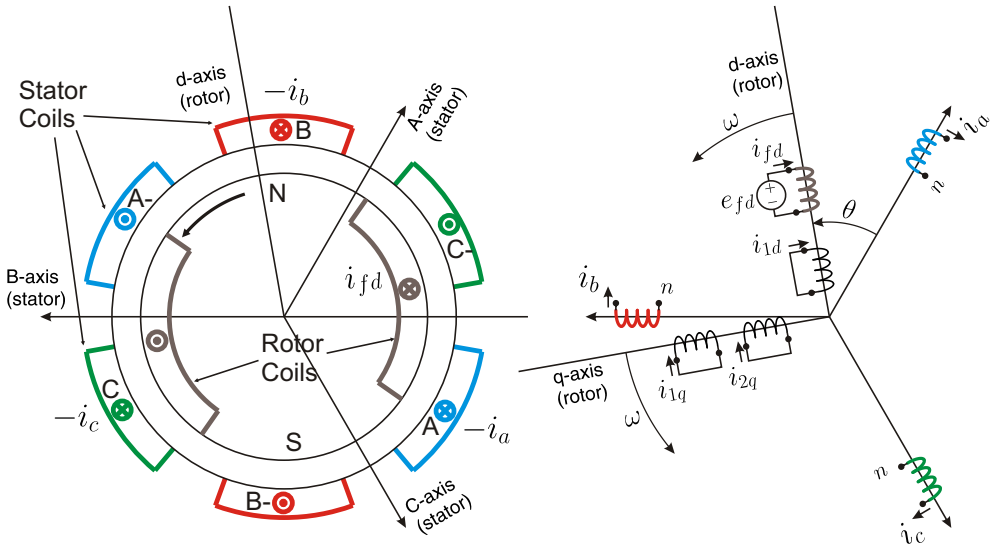

Figure 1.4: Synchronous machine overview and equivalent circuits for Park's modeling

fd : rotor field winding

$1d, 1q$: damper winding representation

$2q$: deep eddy current in rotor representation

θ : rotor angle respect to stator

ω : rotor speed

Based on Fig. 1.4, Park's equations define the relationship between currents, voltages, flux linkages as given by (1.3) and (1.4):

$$\begin{bmatrix} \Psi_d \\ \Psi_q \\ \Psi_0 \\ \Psi_{fd} \\ \Psi_{1q} \\ \Psi_{1d} \\ \Psi_{2q} \end{bmatrix} = \begin{bmatrix} -L_d & 0 & 0 & L_{ad} & 0 & L_{ad} & 0 \\ 0 & -L_q & 0 & 0 & L_{aq} & 0 & L_{aq} \\ 0 & 0 & -L_0 & 0 & 0 & 0 & 0 \\ -L_{ad} & 0 & 0 & L_{ffd} & 0 & L_{f1d} & 0 \\ 0 & -L_{aq} & 0 & 0 & L_{11q} & 0 & L_{aq} \\ -L_{ad} & 0 & 0 & L_{f1d} & 0 & L_{11d} & 0 \\ 0 & -L_{aq} & 0 & 0 & L_{aq} & 0 & L_{22q} \end{bmatrix} \begin{bmatrix} i_d \\ i_q \\ i_0 \\ i_{fd} \\ i_{1q} \\ i_{1d} \\ i_{2q} \end{bmatrix} \tag{1.3}$$

where:

Ψ : flux linkage

$L_{ffd}, L_{11q}, L_{11d}, L_{22q}$: self inductances of rotor windings

L_d, L_q, L_0 : stator equivalent self inductances in dq0 coordinates

L_{ad}, L_{aq} : mutual inductances between stator and rotor windings

L_{f1d} : mutual inductance in d axis between fd and 1d windings

$$\begin{bmatrix} e_d \\ e_q \\ e_0 \\ e_{fd} \\ 0 \\ 0 \\ 0 \end{bmatrix} = \begin{bmatrix} -R_a & 0 & 0 & 0 & 0 & 0 & 0 \\ 0 & -R_a & 0 & 0 & 0 & 0 & 0 \\ 0 & 0 & -R_a - 3R_n & 0 & 0 & 0 & 0 \\ 0 & 0 & 0 & R_{fd} & 0 & 0 & 0 \\ 0 & 0 & 0 & 0 & R_{1q} & 0 & 0 \\ 0 & 0 & 0 & 0 & 0 & R_{1d} & 0 \\ 0 & 0 & 0 & 0 & 0 & 0 & R_{2q} \end{bmatrix} \begin{bmatrix} i_d \\ i_q \\ i_0 \\ i_{fd} \\ i_{1q} \\ i_{1d} \\ i_{2q} \end{bmatrix} + \frac{1}{\omega_{base}} p \begin{bmatrix} \Psi_d \\ \Psi_q \\ \Psi_0 \\ \Psi_{fd} \\ \Psi_{1q} \\ \Psi_{1d} \\ \Psi_{2q} \end{bmatrix} + \frac{\omega}{\omega_{base}} \begin{bmatrix} \Psi_q \\ -\Psi_d \\ 0 \\ 0 \\ 0 \\ 0 \\ 0 \end{bmatrix} \tag{1.4}$$

where:

$$R_a : \text{stator winding resistance}$$

$$R_n : \text{stator neutral resistance}$$

$$R_{fd}, R_{1q}, R_{1d}, R_{2q} : \text{rotor windings resistance}$$

$$p : \frac{d}{dt} \text{ derivative of time operator}$$

$$\omega_{base} : \text{nominal speed of rotor}$$

One difficulty in the implementation of models based on Park's equations (1.3) (1.4) is the estimation of the inductance matrix, which is not typically available. Several methods have been proposed to measure and validate parameters for generator modeling [16–22]. The parameters of a synchronous generator typically available and used by the industry are listed in Table 1.1 [23–27]. The conversion between the parameters in Table 1.1 and those used in (1.3) and (1.4) is performed by numerical methods [28].

Table 1.1: Typical Synchronous Machine Parameters Available

Description	Parameter
Synchronous Inductance	L_d
	L_q
Transient Inductance	L'_d
	L'_q
Subtransient Inductance	L''_d
	L''_q
Transient OC Time Constant	T'_{d0}
	T'_{q0}
Subtransient OC Time Constant	T''_{d0}
	T''_{q0}
Stator Leakage Inductance	L_l
Stator Resistance	R_a

Canay's Reactance: One difficulty with Table 1.1 is that the equivalence from these parameters to those of (1.3) and (1.4) is not unique. This was pointed out by Canay [29–33] and the major difficulty caused by the above mentioned approach is the error introduced in the calculation of rotor field currents during transient conditions. Canay proposed the use of at least one additional characteristic reactance X_C.

Despite acknowledgement that Canay's reactance is very important, it has not been widely used due to difficulties associated with its measurement. Current regulations from the North American Electric Reliability Corporation (NERC) require the verification and modeling of generators [34] but do not specifically require the measurement of this characteristic reactance X_C.

Most electromagnetic transient simulation programs in current use provide the option to

consider this characteristic reactance, X_C, if its value is known. However, current practice with transient stability simulation programs does not consider X_C as its value is not typically measured or available. A method to measure or estimate the X_C has been proposed by Canay [33].

In Chapter 3 of this thesis, one of the issues dealt with is control and limiting of the field current, for which the Canay's reactance becomes very important. An example of field current calculated for a transient condition by electromagnetic simulation is shown in Fig. 1.5. In this example, the difference between assuming that the Canay's reactance is equal to the leakage reactance ($X_C = X_L$) and obtaining the X_C reactance from the manufacturer can be observed. The problem is aggravated in transient stability simulation because the generator modeling typically used does not represent the high frequency oscillations observed in Fig. 1.5.

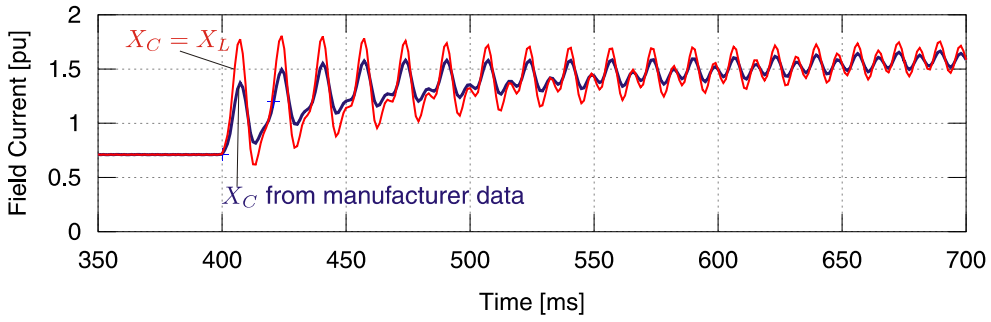

Figure 1.5: Comparison of field current calculated with known and unknown characteristic reactance X_C

1.3.2 Mechanical Equations

The mathematical representation of a synchronous machine used in most studies follows the physical representation of a single rotating mass [35], as given by (1.5):

$$T_m - T_e - \frac{D}{\omega_s}\frac{d\delta}{dt} = \frac{2H}{\omega_s}\frac{d^2\delta}{dt} \tag{1.5}$$

where:

T_m : mechanical torque

T_e : electrical torque

D : damping coefficient

H : inertia constant of the machine

w_s : synchronous speed

δ : rotor angle

The electrical torque T_e in (1.5) is based on Park's equations (1.3) and (1.4), as given by (1.6):

$$T_e = \Psi_d i_q - \Psi_q i_d \tag{1.6}$$

1.4 Simulations

1.4.1 Transient Stability

Transient stability studies deal with the ability of rotating machines, typically synchronous generators, to maintain synchronism with the power system during severe disturbance events [35]. The length of the study period is usually the time required to observe a full swing at the oscillation frequency of interest, on the order of 2 seconds to 10 seconds, or enough to observe if the machine angle stabilizes or loses synchronism with the rest of the system. The disturbance events typically considered are short circuit faults for: a) different fault types, b) different fault durations, c) different fault locations, d) protective relay operation for these faults, and e) possible reclose after a fault trip. An example of the machine angle response for the most severe limit condition for stability of this machine is shown in Fig. 1.6.

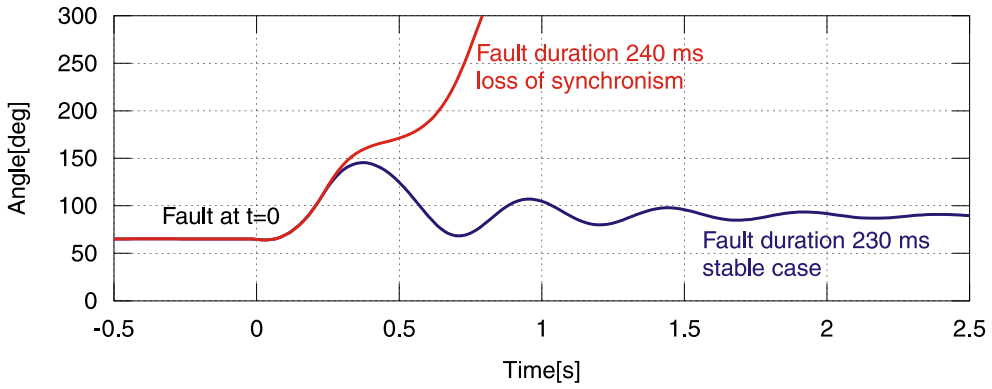

Figure 1.6: Comparison of machine angle responses for a stable and an unstable case

The mathematical representation for transient stability studies does not require the instantaneous time domain voltage and current signal sinusoidal waveforms to be obtained, but instead uses phasor representations of them, i.e., magnitude and angle. The sampling period, or integration time step, for this type of simulation is not very high, on the order of 2 ms to 5 ms. Thus, mathematical modeling of the components simulated needs to consider the corresponding bandwidth for the integration time step used, on the order of 200 Hz to 500 Hz (for the 5 ms to 2 ms integration time step). This type of simulation is considered low bandwidth, as compared to the electromagnetic transient simulations described next.

1.4.2 Electromagnetic Transient Simulations

This type of simulation is capable of solving a network and producing a time domain response with a very high bandwidth, i.e., typically on the order of 10 kHz or more. With careful modeling, an electromagnetic transient simulation is capable of reproducing the actual voltage and current waveforms in the time domain that would be observed from a real power system disturbance. An example of the voltage and current signals calculated for a fault between phases A and B to ground is shown in Figs. 1.7 and 1.8.

Typically, electromagnetic simulations have been used for: a) switching transient studies, b) lightning overvoltage studies, and c) power electronics studies. Compared with a transient stability study, an electromagnetic transient study requires significantly more effort in

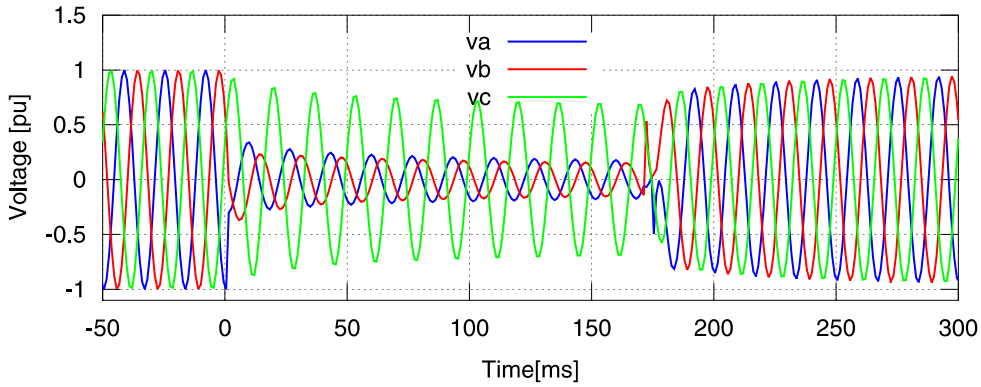

Figure 1.7: Voltages in time domain for ABG fault calculated by electromagnetic transient simulations

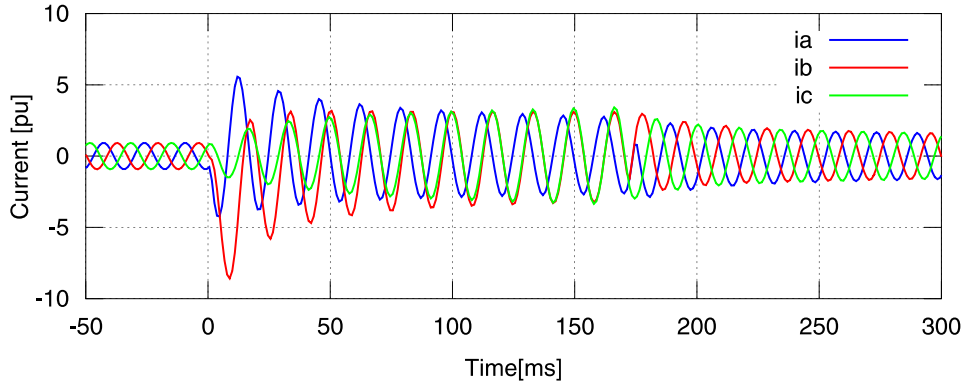

Figure 1.8: Currents in time domain for ABG fault calculated by electromagnetic transient simulations

modeling and computing resources for the same size of system.

Initially, this type of simulation was performed using model power systems based on physical components, sometimes called transient network analyzer (TNA) systems. Later on, offline computing methods were implemented based on the work of Dommel [36]. The offline simulation results can be played back to test protection systems [37]. Nowadays, real time implementations of electromagnetic simulations on special hardware platforms [38] [39] are being used.

1.4.3 Hardware-in-the-Loop Simulation

This type of simulation is useful when testing a hardware implementation of a function being considered, such as a protection or control function. This concept is illustrated in Fig. 1.9. During a hardware-in-the-loop simulation, the practicality of a proposed algorithm is evaluated and tested. Real time electromagnetic simulations are needed for two reasons: a) to produce the voltage and current signals to be measured by the hardware prototype, and b) to make the simulated power system take the actions indicated by the control signals fed back from the hardware prototype.

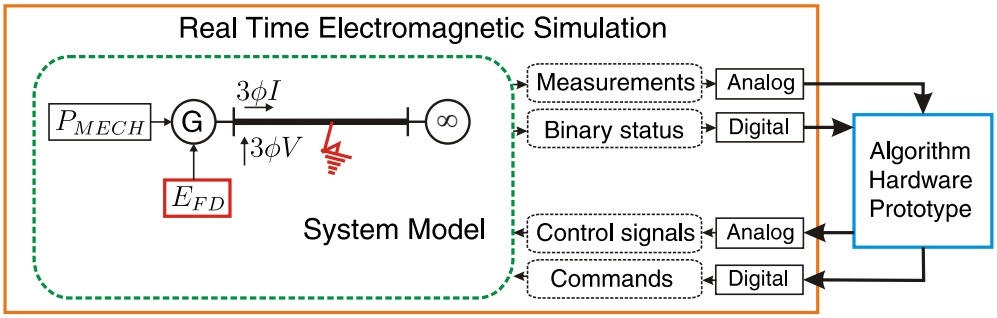

Figure 1.9: Hardware in the loop concept

1.5 Simulation Tools Used

1.5.1 Power System Simulator (PSS/E)

The PSS/E is a software program developed by PTI (now Siemens PTI) that allows several type of studies, with power flow, voltage stability, transient stability, and short circuit among the most important [40]. Several utility networks and/or areas of the North American power system network are already modeled using this simulation tool.

1.5.2 Alternative Transients Program (ATP)

The ATP is a software program originally developed by Bonneville Power Administration, under the name of EMTP (Electro-Magnetic Transients Program) [41].

1.5.3 Real Time Digital Simulator (RTDS)

The RTDS [38] is a software and hardware platform that implements the electromagnetic simulation of power systems in real time, with the capability to produce analog or digital outputs as well as receive analog or digital inputs as feedback into the model. The RTDS hardware is capable of solving the complete network being simulated in a time period shorter than the integration step used by the electromagnetic simulation. In Fig. 1.9, the RTDS corresponds to the Real Time Electromagnetic Simulation block.

1.6 Thesis Objective

Proper coordination between generator protection and control functions have become very important in recent times due to various operational and regulatory factors. One operational need is to use the full capability of the generator during stressed system conditions. Deregulation has resulted in slowing down the development of additional generation despite the load growing steadily. The separation of generation and transmission companies has also resulted in problems performing such studies due to disintegration of special studies groups involving the various companies.

There are other factors outside deregulation. One problem is due to the use of traditional methods for protection and control studies. In many cases, the protection department uses analysis tools and static characteristics that are mostly suitable for short circuit studies. However, the control department may mostly use time domain step response methods, root locus, and frequency response methods to study and define the expected performance of control functions. As a result, disturbance events have occurred in recent years in which

generator protection tripped units, i.e., took them out of service, that still had available capacity to support the system. This is, in part, due to a lack of studies that consider the dynamic behavior of protection and control functions to achieve proper coordination.

One aspect of the coordination considered in this thesis is modeling of the excitation control loop while considering the dynamic limiter performance and interaction during severe disturbances. In particular, the overexcitation limiter control function has not been widely used in transient stability studies, and several operations report occasions when the field overcurrent protection has taken a generator out of service due to extended field forcing conditions [10]. Therefore, one of the objectives of this thesis is to improve the modeling of the overexcitation limiter (OEL) function for dynamic coordination studies of generator protection and control. In this part of the work, two improvements are proposed: a) custom modeling of an OEL considering the overall dynamic performance during a disturbance, and b) modeling that can be applied to electromagnetic simulations instead of just transient stability simulations.

Another problem studied in this thesis is the loss of excitation protection function that has been associated with several false trips of generators not necessarily at a loss of excitation condition, resulting in extension of the disturbance to a larger portion of the network [10]. So, another objective of this thesis is improvement of the loss of excitation protection function. A method to detect the loss of excitation condition is proposed, based on a modern yet simple and practical pattern classification tool using a Support Vector Machine (SVM) . This method correctly identified a loss of excitation condition from all other disturbances, such as faults, power swings, switching, and automatic control action, among others. It is important to point out here that the classical methods used by the industry, such as mho impedance zones, are also pattern classification methods. These traditional methods have been developed based on studies of trajectories using simulations to define characteristics and regions in the impedance plane that allow the identification of loss of excitation from other conditions. Therefore, in the proposed method, the key component is not necessarily the use of the SVM method alone, but the definition of distinctive features that allow improved identification of a loss of excitation from any other condition.

Another problem studied in this thesis is generator protection and control coordination in the underexcited region. The protection and control aspects that are investigated include: a) underexcited thermal capability, b) underexcited stability limit, c) reliability of the excitation control scheme, d) underexcitation limiter modeling, e) loss of excitation protection modeling, f) extreme loading conditions, and g) critical faults and contingencies. To address all of these considerations, a methodology is proposed to achieve coordination with traditional protection functions. This methodology is based on the use of dynamic simulation and is verified in a practical scenario from a real system. For comparison, the new SVM method for detection of LOE conditions is also verified on the same system.

The final objective is practical implementation. The proposed SVM method for LOE detection is tested and verified using a hardware-in-the-loop simulation study and compared with offline simulation results published in the literature. The implementation of a protective relaying algorithm prototype for hardware-in-the-loop testing is a task that requires knowledge in several areas, with signal processing, real time embedded architectures, protection algorithm modeling, and electromagnetic simulations among the most important. One of the main difficulties in developing and debugging protective relay algorithms such as the proposed SVM LOE method with real signals is that the power system cannot just be paused at a desired time instant to analyze the performance of a given algorithm. Another difficulty in protective relay development is that these are typically embedded architectures with processor specific development tools that make use of hardware or software emulators; this makes the development process cumbersome and relatively inefficient. The last contribution from this thesis is addressing these considerations while keeping in mind a general and flexible design that could be used to develop not only the proposed method but also any other protection function or algorithm.

Thus, a consolidated protective relaying development platform is proposed to enable the development of any protection function to be considered.

1.7 Thesis Outline

This thesis consists of seven chapters. An outline is provided for each of the chapters below.

In Chapter 1, a brief introduction is provided for power systems protection and controls followed by an introduction to problems related to coordination of generator protection and control. Also in this chapter, synchronous machine modeling and the necessity of doing dynamic simulations are introduced. The chapter concludes with the thesis objective, how some of the problems identified are addressed, and a thesis outline.

In Chapter 2, an extended introduction to overall generator protection is provided. A similar discussion about overall generator excitation controls, including the limiters and their importance, is also presented. Finally, the problem and current state of the art in coordination for generator protection and control, the concept of static and dynamic coordination, as well as basic considerations for coordination in the overexcited, underexcited, and loss of synchronism conditions are given.

In Chapter 3, the overexcited capability of synchronous generators, the steady state, and transient overload limits are described. The basic interaction between different modes of control in the overexcited region and the basic coordination requirement with the corresponding field overcurrent protection are discussed. The model proposed to complement existing standard excitation control models from IEEE is described in detail. This model is used to study some severe reactive overload conditions only possible or practical through simulation and in which coordination is expected to successfully support the system.

In Chapter 4, a new method is proposed to detect a loss of excitation condition using the Support Vector Machine method. The chapter starts with an introduction to the loss of excitation condition, risk for the machine, as well as typical detection methods. The concept of pattern recognition is introduced, including the concepts of feature vector, training, mapping functions, and, in particular, the Support Vector Machine classification method. The new loss of excitation detection method is developed, in particular the selection of features based

on careful study of the trajectories in the power plane and the impedance plane. Another key component of the new method is the required training to cover a wide range of generator operating conditions. Finally, test results and a sensitivity study provide validation with respect to the stability of the proposed method.

In Chapter 5, a methodology for coordination in the underexcited region of synchronous generators is proposed, followed by an example coordination for a real power generator connected to an Alberta power system network. The chapter starts with a discussion about limitations of existing coordination methods and the different limits to be considered (e.g., thermal and stability limits). Modeling of limiter controls not typically present in current existing network databases is described. The considerations for static and dynamic coordination are also described, and these are tested in different scenarios for which the protection and control functions need to be coordinated. Finally, the performance of the proposed SVM method for detection of LOE conditions is studied for these same scenarios to assess the coordination achieved.

In Chapter 6, a new protective relaying development platform is described along with implementation of the proposed SVM method for LOE detection in the proposed platform for hardware-in-the-loop testing. The considerations used in the design of this relay development platform are described in detail, with hardware and software architectures, the platform independent design, the use of IEEE COMTRADE standard for signal recording, and electromagnetic offline and real time simulations for validation and debugging among the most important. The implementation of the proposed SVM method for LOE detection is described and the experimental test results are compared with previous work performed within the electromagnetic simulation tool.

Finally, Chapter 7 provides a summary, contributions, conclusions of this thesis, and future work.

Chapter 2

Generator Protection and Control

2.1 Generator Protection

An overview of synchronous generator protection is shown in Fig. 2.1. In Fig. 2.1, it is observed that a protective decision may result in one or all of the following: a) tripping of the main breaker, b) tripping of the field breaker, and c) shutdown of the generator prime mover. The protective relay operation as well as the required speed of operation depends on the type of fault or abnormal condition [42]: a) short circuit fault, b) prime mover abnormal condition, c) excitation system fault, d) stability condition, e) system backup fault, or others.

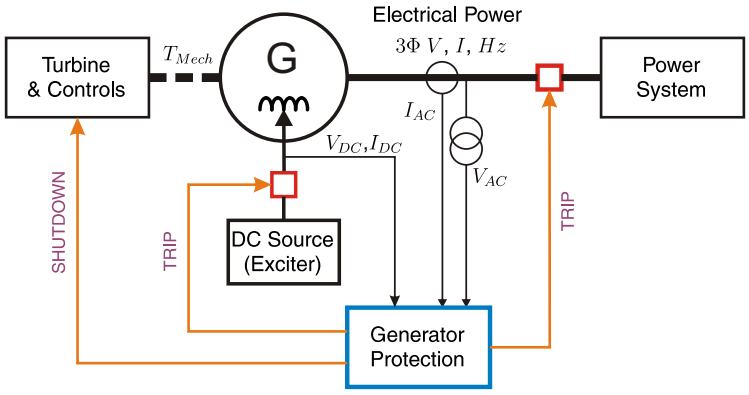

Figure 2.1: An overview of synchronous generator protection

In this section, only the most important generator protection functions are discussed. From the point of view of coordination with excitation control, not all protection functions need to be considered; this will be pointed out in each subsection.

2.1.1 Short Circuit Protection

The relaying function applicable depends on the type of short circuit as well as the location of the fault. Short circuit protection can be classified into three categories: stator ground, field ground, and current differential. Short circuit protection does not require any different modeling consideration to coordinate with excitation control, as these faults must be cleared as soon as they are detected to prevent further risk or damage to the machine.

2.1.1.1 Stator Ground

The protection philosophy applied for detection of ground faults depends on the type of grounding that the generator is using. There are three basic methods of grounding synchronous generators: low impedance grounding, high impedance grounding, and hybrid grounding [43].

The low impedance grounding approach typically limits the fault current for a ground fault in the range between approximately 200 A primary up to 150% of the rated generator current. The protection function typically used to detect ground faults is ground current differential function 87N, which compares zero sequence currents from the neutral and from the residual current obtained at generator terminals. The 87N concept for detection of stator ground faults is illustrated in Fig. 2.2.

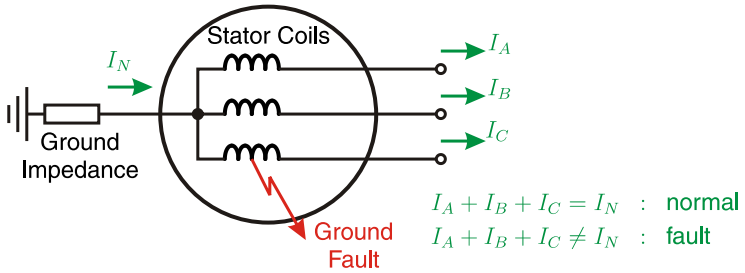

Figure 2.2: Ground fault detection for low impedance grounding by 87N

The high impedance grounding approach typically limits the fault current for a ground fault on the order of 3 to 25 A primary. In this case, the detection of ground faults is largely

based on two principles: neutral overvoltage at fundamental frequency, and third harmonic at neutral or from calculated residual obtained at generator terminals. The neutral overvoltage function 59N measures the fundamental frequency voltage drop at the grounding resistance and detects faults from the generator terminal down to about 5% from the neutral of the generator. The neutral overvoltage principle is illustrated in Fig. 2.3. The most typical third harmonic approach is the neutral undervoltage function 27TH, which is based on the continuous presence of third harmonic voltage at the neutral during normal conditions. In cases where the generator design does not produce enough third harmonic to apply the 27TH function, subharmonic voltage injection is more suitable to ensure protection.

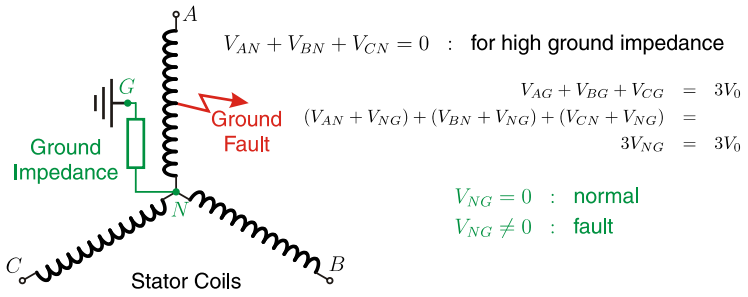

Figure 2.3: Ground fault detection for high impedance grounding by 59N

The hybrid grounding approach combines both types of grounding, i.e. the low and high impedance, keeping the low impedance for normal operation and only switching to high impedance during tripping in order to limit damage to the generator.

2.1.1.2 Field Ground

The rotor field circuit of synchronous generators is typically a DC ungrounded circuit, and thus a single ground fault is unlikely to cause any significant damage. A second fault to ground closes the circuit and may cause damage depending on how many turns are shorted [43]. One effect of this type of fault is field unbalance and thus vibration, which may be severe and cause mechanical damage. Another effect of this double fault is thermal damage by the fault current flowing through the iron laminations.

The rotor ground fault protection function 64F is mostly based on detection of the DC

voltage shift of the overall field and excitation circuit caused by the ground fault. However, there is a fault location in the rotor that presents zero voltage difference with ground, making it difficult to detect by typical 64F protection function. To detect this and all other rotor faults, detection methods that use voltage injection are more effective.

2.1.1.3 Current Differential

The current differential detection method is based on the Kirchoff law, which states that the sum of all currents entering a node must be zero. Current differential protection function 87G primarily detects faults involving more than one phase with or without ground as well as some severe ground fault conditions [43]. The concept of current differential protection function 87G is illustrated in Fig. 2.4.

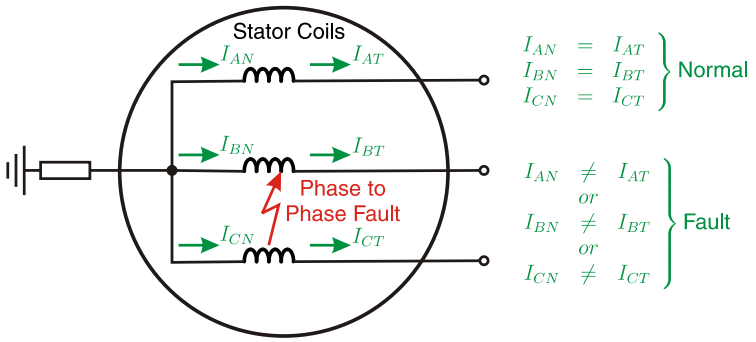

Figure 2.4: Fault detection principle by phase differential 87G

The main issue with the application of the current differential protection principle is the error in the current measurement by the current transformers. Two kind of errors need to be considered: a) saturation of the current transformer core and b) external stray flux entering the current transformer core. Saturation of the current transformer core is directly related to the area calculated by the integral of the current over time during a given disturbance. Thus, a large balanced current on the order of 20 times the rated value would typically cause saturation, but a relatively low current on the order of 3 times the rated value with a slowly decaying superimposed DC component would also cause the same amount of saturation. The stray flux caused by external magnetic fields, such as the proximity of another phase

carrying large currents, may also produce enough noise current to cause maloperation of the current differential function.

There are three basic types of current differential methods in use: a) percent differential, b) high impedance, and c) self balancing. The percent differential method assumes that the measurement error is a percentage of the through current. This method uses a small percentage level when currents are low and there is no risk of saturation, but uses a large percentage level when currents and the risk of saturation are high. The high impedance method uses a physical connection between current transformers to a common point where a high impedance is connected. In this method, an internal fault is detected by the overvoltage caused in the high impedance element. In the self balancing method, the physical currents are magnetically subtracted by encircling both conductors, i.e., the input and the output, by the current transformer core.

The current differential methods just described are unable to detect faults between turns, i.e., interturn, in the same phase. Several other options exist to detect interturn faults, such as splitting a phase into several paths or comparing the voltage induced in each phase. The split phase detection method compares the currents on each path, assuming that they are identical. The voltage comparison calculates the zero sequence from the sum of the voltage induced in each phase of the generator, which should result in a zero sum in normal operation.

2.1.2 Prime Mover

The protection functions in this category do not need special considerations to coordinate with excitation control. However, correct modeling of the excitation control as well as the prime mover control is required when defining settings for these protection functions to simulate the conditions described next.

2.1.2.1 Reverse Power

The reverse power protection function 32 is responsible for detecting the loss of prime mover and consequent damage to it [43]. The sensitivity and speed requirements for this protection function depend on the type of prime mover being considered.

The reverse power protection function needs to consider specific application requirements, such as: a) intentional motoring during starting of a generator, b) synchronous condenser applications, c) pumping stations, d) temporary motoring during sequential tripping.

2.1.2.2 Frequency

The abnormal frequency protection function 81 detects over and/or under frequency conditions. The allowable operating region and duration are different for the generator and the prime mover, and also different for different types of prime movers [43].

The operating region for a generator is specified for newer generators by IEC standard 60034:2007 in a frequency vs. voltage plane, between +/- 2% of nominal frequency and between +/- 5% of nominal voltage [44]. This frequency vs. voltage characteristic is illustrated in Fig. 2.5.

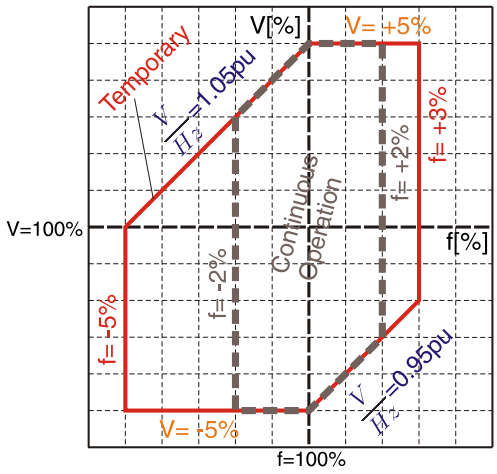

Figure 2.5: Voltage-frequency generator capability according to IEC600034 standard.

The operating region for the prime mover is typically more restrictive for thermal units,

such as steam turbine units, combustion turbine generating units, and combined cycle units. These types of turbines present an operating region in the frequency vs. time plane that is specific and provided by the manufacturer. Overfrequency protection is not commonly applied because generator controls are relied upon to bring the machine back to normal speeds. However, the underfrequency protection function is typically applied, and this needs to coordinate with the generator operating frequency-time region as well as the underfrequency load shedding schemes used [45, 46].

In the case of hydro prime movers, frequency deviations are much wider and overspeeds of up to 150% of nominal are possible due to physical limits on the governor control action. Thus, overfrequency protection is mostly applied in the case of hydro prime movers as a backup to overspeed limiting control action. Underfrequency protection is not applied to this type of prime movers.

2.1.3 Excitation

The protection functions in this category need to be carefully considered with respect to coordination with excitation control, as will be indicated for each individual function.

2.1.3.1 Loss of Excitation (LOE)

An example of synchronous generator response to a loss of excitation condition followed by a loss of synchronism is illustrated in Fig. 2.6. This is 104.4 MVA, 13.8 kV, 3600 rpm synchronous generator, whose parameters are provided later in Section 4.5. The severity of a loss of excitation condition is dependent on several factors: a) initial loading, b) type of machine rotor, c) size of the generator, d) strength of the system network, and e) fault cause, among others [12]. Higher loading conditions are more severe as they may cause a rapid loss of synchronism with large currents and pulsating torques in the shaft of the machine. In Fig. 2.6, the loss of synchronism occurs just after 3 seconds, producing pulsating power of more than 1.0 *pu* in amplitude, producing induced currents and current inversion in the rotor.

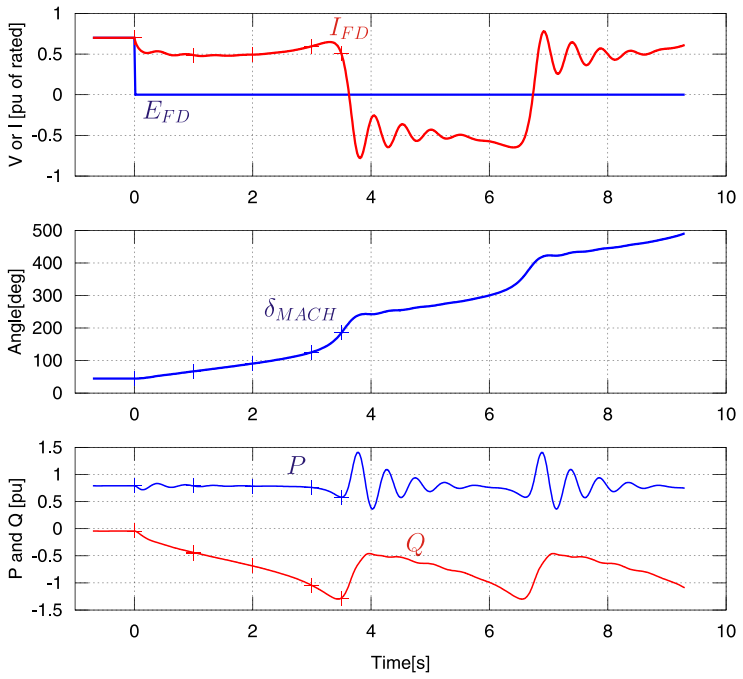

Figure 2.6: Loss of excitation condition response: field voltage E_{FD} and current I_{FD}, machine angle δ_{MACH}, active power P, and reactive power Q

Machines with round rotors present a thermal limit in the underexcited region that encroaches and restricts the capability of the machine to absorb reactive power. On the other hand, machines with salient pole rotors present a thermal limit that is typically far from the generator capability and does not necessarily restrict it, being capable of maintaining synchronism during loss of excitation conditions with relatively light loading [47, 48]. Larger machines subjected to a loss of excitation condition present a risk to the system because they become a large reactive power load and cause a voltage collapse with a risk of voltage instability in the same vicinity within the network [49]. The risk of voltage stability is less in strong systems as the voltage may not drop significantly. The loss of excitation condition does not pose the same risk if this condition is caused by an incorrect trip of the field breaker compared to a case where the fault is caused by an arc flashover in the field circuit [50–54].

The subject of loss of excitation is one of the main topics of this research work and is discussed in more depth in Chapters 4 and 5.

2.1.3.2 Overexcitation

The term "overexcitation" has been used by the protective relaying industry to refer to the condition where the magnetic flux exceeds normal operating levels [43, 55]. It should not be confused with the same "overexcitation" term used by the excitation control industry, which refers to a condition where the amount of DC voltage applied to the rotor field exceeds normal operating levels.

The detection of overexcitation from the protective relaying point of view is based on the measurement of the voltage to frequency ratio, V/Hz. The limit imposed by V/Hz is a thermal limit and should consider both the generator capability as well as the associated step up transformer capability, which are specific and provided by the manufacturers of the equipment [56]. The V/Hz protection should be coordinated with the V/Hz limiting control action so that the generator is not tripped unnecessarily. The V/Hz characteristics and a typical coordination example are shown in Fig. 2.7. In Fig. 2.7, the limiter control characteristic is reached first, then the monitor characteristic is performed by the redundant backup control in case the main control fails, and last is the protection that trips the machine from the system [57].

The V/Hz method of detection can be analyzed from two angles: constant frequency and variable frequency. The constant frequency scenario is observed during normal operation and, in this case, the V/Hz essentially becomes a maximum voltage limit for the generator. The variable frequency scenario is observed both during start-up and in case of overspeed. Low frequencies are experienced during start-up, which must be accompanied by proportionally low excitation voltages. In overspeed conditions, the V/Hz ratio may not present a risk of overflux in the machine, but a dangerous overvoltage may be produced.

The overexcitation condition as seen from the excitation control point of view is described in the following section as rotor overload.

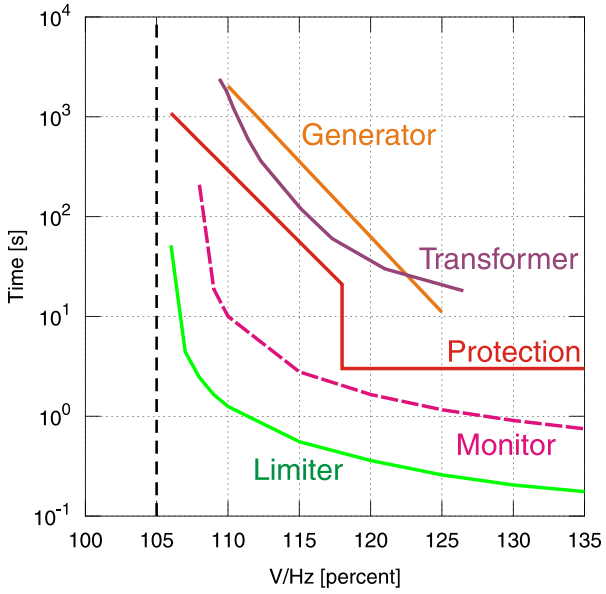

Figure 2.7: V/Hz characteristics coordinated: limiter and monitor control, protection, generator and transformer capability limits

2.1.3.3 Rotor Overload

The field overcurrent protection, i.e., rotor overload, is based on DC current measurement of the rotor field current [43]. The rotor winding is capable of a temporary overload according to IEEE standard C50.13 [58], which is sometimes necessary to provide reactive power support to the system network during voltage collapse conditions. An example of a voltage collapse condition where a generator is providing additional reactive power to the system is shown in Fig. 2.8. This result is based on a 360 MVA, 13.8 kV synchronous generator and its parameters are provided later in Section 3.5.1. The field overcurrent protection needs to be coordinated with overexcitation limiter control action to allow the use of the overload capability without exceeding the thermal capability of the machine.

The subject of field overcurrent protection and overexcitation limiter control is one of the main subjects of research in this thesis and is discussed in more depth in Chapter 3.

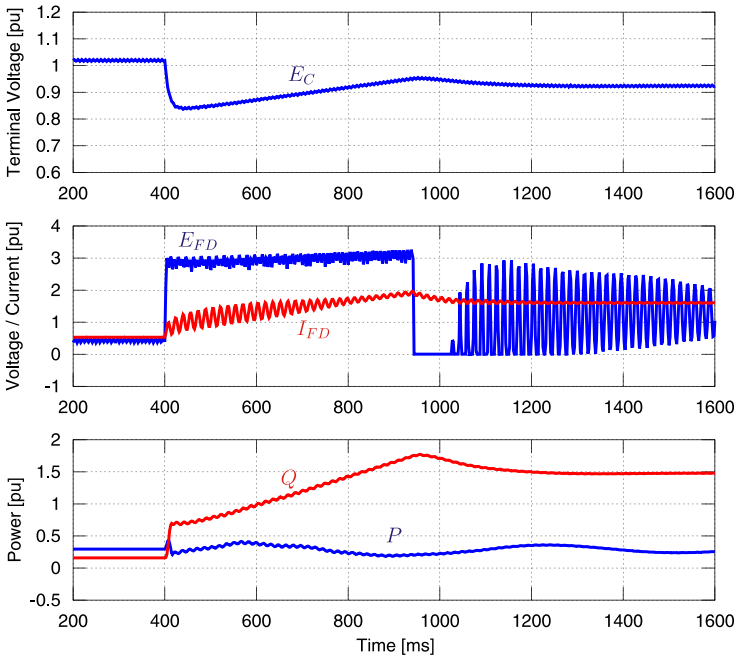

Figure 2.8: Network voltage collapse condition: terminal voltage E_C, field voltage E_{FD} and current I_{FD}, active power P and reactive power Q

2.1.4 Stability

From the point of view of coordination, the main issue involved with loss of synchronism protection is correct modeling of the machine and the network system to make sure the protection is effective for all scenarios.

2.1.4.1 Loss of Synchronism

A synchronous generator keeps itself synchronized with the power system network with a synchronizing torque, i.e., a torque in the direction that brings the machine back into synchronism. When a fault happens in the system close to a synchronous generator, an accelerating torque is produced due to a temporary imbalance between mechanical power and electrical power. The accelerating torque is in the direction opposing the synchronizing torque. Depending on the location and the severity and the duration of the fault, the synchronous generator may lose synchronism with the system. The most typical method

used for detecting a loss of synchronism is based on estimation of the angle between the internal machine equivalent source and the system network. These methods are commonly represented in the complex impedance plane and require parameters such as generator and system impedances, critical clearing angle, and speed of the fastest unstable swing. The impedance parameters are typically available, but obtaining the last two parameters is not as straightforward and requires a dynamic simulation of the generator connected to the actual system [59, 60].

The synchronous generator may also lose synchronism for reasons other than a fault in the system. For example, loss of synchronism can happen following a severe loss of excitation condition. In this case, the loss of excitation protection is expected to trip the machine before the loss of synchronism happens.

2.1.5 System Backup

From the point of view of coordination, backup functions need to be studied using dynamic performance studies, i.e., simulations taking into account the machine dynamics, excitation control, and the network system. Another important issue to consider in system protection is the impact of external faults or switching operations on generator shaft torsional fatigue [61, 62].

2.1.5.1 Distance/Overcurrent

The system backup protection trips the generator from the system when all protection and breakers downstream of the fault point fail to clear a fault [43]. Depending on the type of protection functions being used downstream from the generator, two types of protection principles are used: overcurrent and distance.

The use of overcurrent protection presents difficulty due to the synchronous machine behaviour with two basic effects to consider: time dependent source impedance and internal voltage levels [63–66]. The apparent impedance of a synchronous machine continuously varies

in time during a fault condition between the subtransient X''_d, transient X'_d, and synchronous X_d reactance values, such that $X''_d < X'_d < X_d$. The internal voltage, i.e., excitation voltage level, is directly associated with both the active and reactive power operating point of the machine. For a fixed active power, a large internal voltage corresponds to reactive power being supplied to the system; a lower value of internal voltage corresponds to reactive power being absorbed. If the reactive power is considered fixed, a maximum value of internal voltage corresponds to a larger active power supplied to the system. With all of these considerations, the minimum current supplied to a fault must be used in setting the overcurrent pickup level of the protection. The overcurrent pickup level just described is below the rated current of the generator and, for this reason, some form of voltage restraint or supervision is used in these types of protection. An example of a balanced fault condition in the line connecting the generator with the power system is shown in Fig. 2.9, i.e., keeping the exciter and prime mover levels constant. This result is based on a 360 MVA, 13.8 kV synchronous generator and its parameters are provided later in Section 3.5.1. In Fig. 2.9, the fault current level below the normal rated generator levels presents difficulty for typical overcurrent protection based on current alone. Therefore, the terminal voltage level information is needed to confirm that a fault is present.

The use of distance protection overcomes the difficulties just described for overcurrent protection. Two zones of distance protection are suggested: one short and relatively fast zone to protect the step up transformer, and a second larger and slower zone to protect the remote bus associated with the longest line from the generating substation. The backup coverage provided needs to be balanced with restrictions including the maximum emergency load and the generator capability curve. More recently, stability studies have been proposed to define the limits of backup protection to be provided [10].

Backup protection for ground faults is typically provided in the high voltage side of the step up transformer by using neutral time overcurrent protection. The coordination of this protection is not as difficult as the previously described phase overcurrent protection because ground currents are only present when there are faults.

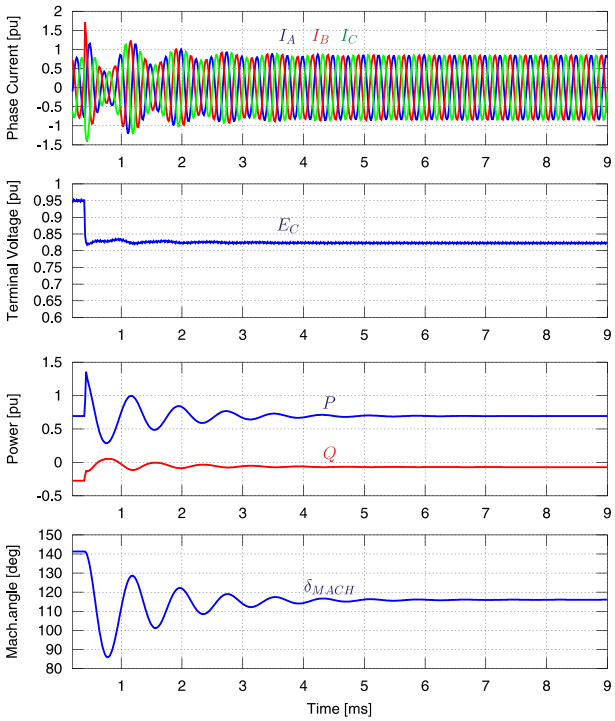

Figure 2.9: Response to a three phase fault in the system: instantaneous fault currents I_A, I_B, I_C, terminal voltage E_C, active power P and reactive power Q, and machine angle δ_{MACH}

2.1.6 Other Schemes

The protection functions in this category do not need special consideration for coordination with the excitation control functions.

2.1.6.1 Current Unbalance

The presence of a current unbalance condition produces negative sequence currents, which results in a magnetic field component rotating in the opposite direction as the rotor and with synchronous speed relative to the stator. This negative sequence magnetic field component rotates at two times the synchronous speed relative to the rotor and induces stray currents that produce overheat and may cause damage. The thermal limit of the rotor in terms of negative sequence is defined by IEEE standard C50.12 [67] for salient pole machines

and by IEEE standard C50.13 [58] for round rotor machines. This thermal limit is given by a temporary overload current vs. time characteristic as well as a continuous unbalance level allowed for a given type and size of machine. The negative sequence overcurrent protection for a generator is very important because of its sensitivity and the fact that no other downstream protection provides the required coverage. The continuous capability for phase current unbalance of synchronous generator ranges between 5 and 10%, depending on the presence of damper windings, the type of cooling, and the size and type of the machine as indicated in IEEE standards C50.12 and C50.13.

2.1.6.2 Accidental Energization

In the case of an accidental energization, a synchronous generator behaves like an induction motor; this is a very dangerous condition for the machine. This induction motor behavior produces localized heating in the rotor due to large induced currents in paths not designed to carry them, damaging or even destroying the generator in a relatively short time. An accidental energization is typically produced in two scenarios: a generator breaker or switch is accidentally closed with generator offline, or breaker flashover occurs just prior to synchronizing or just after removing the machine from the system. One difficulty in detecting an accidental energization is the fact that this protection needs to be active when the machine is offline, while all other protection functions are typically active with the machine online. The most common method for detecting an accidental energization condition is by using an overcurrent detection supervised by undervoltage.

2.2 Generator Excitation Controls and Modeling

2.2.1 Excitation Types

2.2.1.1 DC, AC, and Static

Excitation control systems are classified into three categories according to IEEE standard 421.5 [68]: DC types, AC types, and static. The difference between these categories is based on the source of electric power supplying the main generator field winding.

The DC type of excitation control system takes power from a DC commutated generator, i.e., the exciter, and the IEEE standard considers up to four different variations, designated DC1A, DC2A, DC3A, and DC4B. These variations cover differences in the type of control scheme used to drive the field of the exciter DC generator, including non-continuously acting, continuously acting, and retrofit of older units with new controls.

The AC type of excitation control system takes power from an AC rotating generator, i.e., the exciter, and uses a rectifier to obtain DC power for field winding. The IEEE standard considers eight different variations, designated AC1A, AC2A, AC3A, AC4A, AC5A, AC6A, AC7B, and AC8B. These variations cover numerous differences, with the most noticeable being the type of control, the type of rectifier used, the source of power for the control, and special compensation to achieve high initial response.

The static type of excitation control system does not make use of a rotating generator to obtain the DC supply for field winding. The IEEE standard considers seven different variations, designated ST1A, ST2A, ST3A, ST4B, ST5B, ST6B, and ST7B. These variations also cover numerous differences, with the most significant being the type of control, type of supply for the rectifier, use of additional internal loops like a field voltage control loop, and location of the input of auxiliary signals.

The IEEE 421.5 standard is focused on modeling for low bandwidth simulations. However, some commercial electromagnetic simulation tools provide high bandwidth version of these models. The details of the high bandwidth modeling are dependent on the implemen-

tation [69]. Additional models not described in the IEEE 421.5 standard are available in the literature from most manufacturers [70, 71], including in some cases details of the hardware implementation [72–74].

2.2.1.2 IEEE ST1A Model

The IEEE ST1A model is recommended in IEEE 421.5 standard to represent excitation systems with a solid state controlled rectifier, as shown in Fig.2.10. The voltage supply to this rectifier typically comes from a step down transformer located at the terminals of the generator.

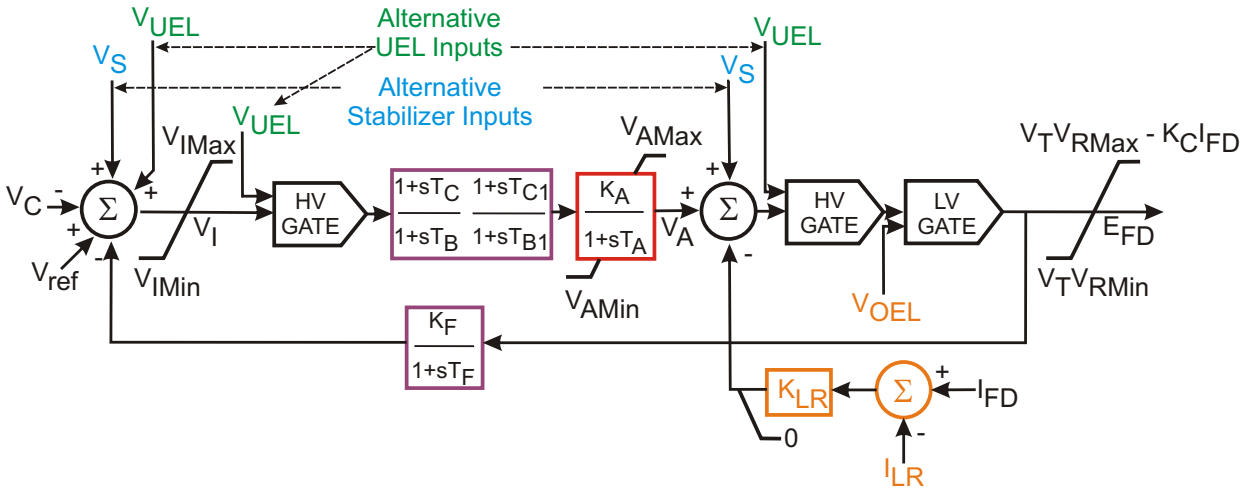

Figure 2.10: IEEE ST1A exciter model - potential source controlled rectifier exciter

In Fig.2.10:

V_{ref} is the reference or desired terminal voltage

V_C is the terminal voltage measured

E_{FD} is the excitation voltage output

I_{FD} is the field current measured

K_A, T_A represent the main exciter control loop

T_C, T_{C1}, T_B, T_{B1} represent the lead lag compensating control loop

K_F, T_F represent the stabilizing feedback control option

V_S represents auxiliary signals, e.g., power system stabilizer (PSS)

V_{UEL} is the underexcitation limiter signal

V_{OEL} is the external overexcitation limiter (OEL) signal

K_{LR}, I_{LR} represent an OEL limiter included on ST1A

$V_{IMax}, V_{Imin}, V_{AMax}, V_{AMin}$ represent internal limits of the control signals

V_T, V_{RMax}, V_{RMin} represent floor and ceiling levels dictated by the potential source

K_C represents the rectifier regulation

2.2.2 Automatic Voltage Regulator

The main function of excitation system is to maintain a constant voltage level, i.e., automatic voltage regulation or AVR control. In most cases, the controlled variable is generator terminal voltage but in other cases can be the voltage level at a different bus. An example of AVR control action to a system voltage change of about 5% is shown in Fig. 2.11. This result is based on a 360 MVA, 13.8 kV synchronous generator and its parameters are provided later in Section 3.5.1.

AVR control action helps improve the transient stability of the machine, i.e., stability during large disturbances, by increasing synchronizing torque. At the same time that transient stability is improved by AVR control, small signal stability is reduced by a reduction in the damping torque for machine oscillations.

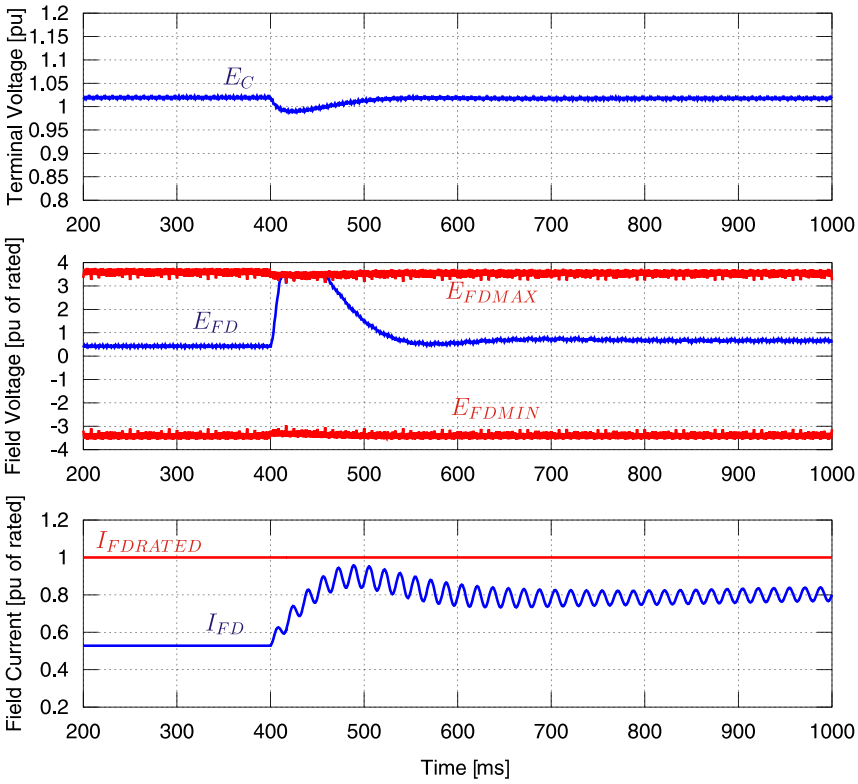

Figure 2.11: AVR control action to a system voltage change of about 5%: terminal voltage, field voltage, and field current

Synchronizing and Damping Torque: The concept of synchronizing and damping torques can be better understood by considering the linearized version of the equation of motion for a synchronous machine [35, 75] as given by (2.1):

$$\frac{2H}{\omega_s}\frac{d^2(\Delta\delta)}{dt^2} + \frac{D}{\omega_s}\frac{d(\Delta\delta)}{dt} + K_1\Delta\delta = 0 \tag{2.1}$$

where:

$\Delta\delta$: rotor angle deviation

H: inertia constant of the rotor

D: damping coefficient

w_s: synchronous frequency

K_1: synchronizing coefficient

In (2.1) the first term represents the torque component due to machine acceleration. The second term corresponds to damping, and is a value proportional to speed change in the direction necessary to bring the machine back to the initial speed. The third term is the synchronizing torque, and is a value proportional to the angle change in the direction necessary to bring the machine back to synchronism.

The AVR performance for large and small signals can be characterized by a set of parameters defined in IEEE 421.2 standard [76, 77].

2.2.3 Power System Stabilizer

The role of power system stabilizer (PSS) controls is to overcome the reduction in small signal stability caused by AVR control. An example of PSS control action to power oscillations caused by a fault in the system is shown in Fig. 2.12. This result is based on a 360 MVA, 13.8 kV synchronous generator and its parameters are provided later in Section 3.5.1. In this figure, the field voltage E_{FD} shows additional oscillation after the fault is cleared; this is caused by the PSS action and results in faster decay of the active power P oscillations.

PSS control action improves the small signal stability by increasing the damping torque for machine oscillations. Referring to (2.1) and calculating the integral over time of the first term, i.e., machine acceleration torque, results in a value proportional to speed change. This method, i.e., taking the integral of the machine acceleration, is one of the most common

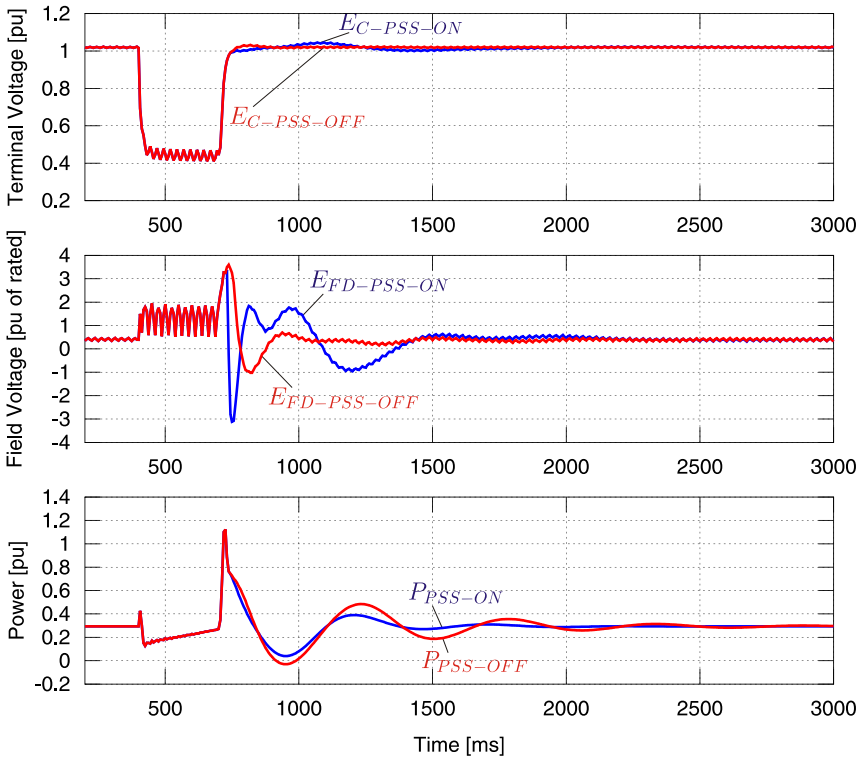

Figure 2.12: PSS control action to a power system fault: terminal voltage E_C, field voltage E_{FD}, and active power P

ways to obtain a damping signal for PSS control action. IEEE 421.5 standard [68] defines four types of PSS control, designated PSS1A, PSS2B, PSS3B, and PSS4B. The variations cover numerous differences, with the most noticeable being the number of input signals, type of input signals, and target bandwidth (s) [78, 79].

2.2.4 Limiters

While AVR and PSS control action are always present, limiter control action is activated only when the corresponding limit is exceeded and until the operating point is brought back to normal. In Fig. 2.13, a typical generator capability curve (GCC) is shown, indicating the limits that need to be monitored [80–84]. Three types of limiters are described here– underexcitation (UEL) , overexcitation (OEL), and V/Hz– although other types are also used in actual practice [85–87].

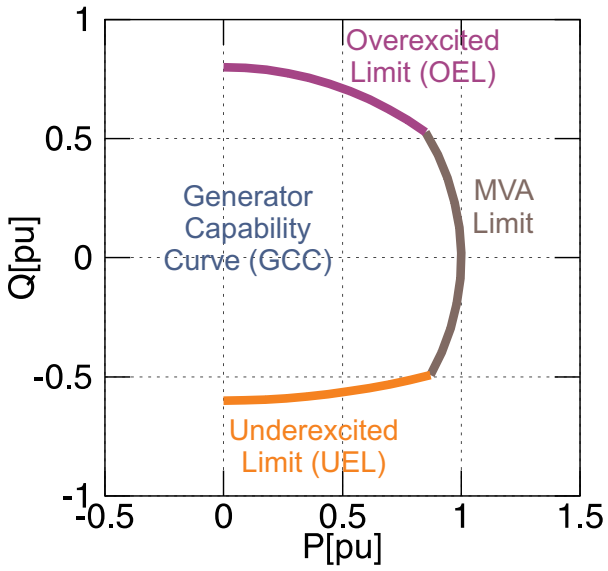

Figure 2.13: Generator capability curve and limits

2.2.4.1 Underexcitation Limiter

The underexcitation limiter (UEL) continuously monitors the lower part of the GCC curve. This limit is associated with stator end core heating, stability limits, and loss of excitation protection. The stator core ends are subject to leakage flux perpendicular to their laminations during underexcited conditions, which produces heating due to eddy currents and imposes a thermal limit in the underexcited region. Stability is maintained by the action of synchronizing torques, which are typically in the direction to bring the generator back into synchronism as long as the machine is operating within the stability limits. Beyond the stability limits, the synchronizing torque becomes zero and changes sign, causing the machine to lose synchronism.

An example of underexcited conditions and the UEL limiting control action is shown in Fig. 2.14. This result is based on a 360 MVA, 13.8 kV synchronous generator and its parameters are provided later in Section 3.5.1. Once the operating point of the machine exceeds the UEL limit, a control loop action is activated based on the reactive power difference to the limit and aimed at increasing the excitation and bringing the machine back inside the GCC. In Fig. 2.14, the UEL signal is produced based on the difference between

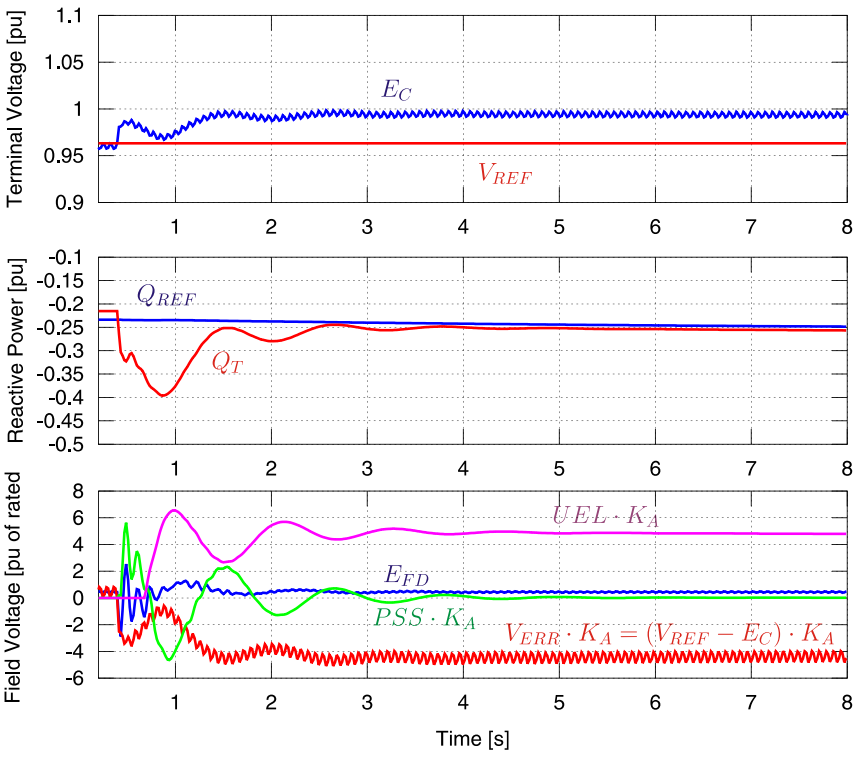

Figure 2.14: Underexcited condition and limiter control action: terminal voltage E_C and reference V_{REF}, reactive power Q_T and reference Q_{REF}, and signal components of the exciter voltage E_{FD}

the reactive power Q and the reference level Q_{REF}. This figure also shows that, for this example, the field voltage E_{FD} is a result of the sum of three components: the voltage error signal $V_{ERR} = V_{REF} - E_C$, the UEL signal, and the PSS signal. It should be noted that the reference level Q_{REF} is not constant, but depends on terminal voltage and active power levels.

IEEE 421.5 standard [68, 88] defines two types of UEL control, designated UEL1 and UEL2. The variations cover differences in the shape of characteristic, voltage dependence, and the type of control. This subject is discussed in more detail in Chapters 4 and 5 of this thesis.

2.2.4.2 Overexcitation Limiter

The overexcitation limiter (OEL) continuously monitors the upper part of the GCC curve. This limit is associated with the thermal limit of the rotor winding current carrying capability. The rotor thermal limit is capable of temporary overload and is used to provide reactive support to the system in case of voltage collapse conditions [89, 90]. An example of a voltage collapse condition is shown in Fig. 2.15. This result is based on a 360 MVA, 13.8 kV synchronous generator and its parameters are provided later in Section 3.5.1. Once the operating point of the machine exceeds the limit characteristic, a control loop action is activated based on the difference between the current and the limit level and aimed at reducing the excitation and bringing the machine inside the GCC. In Fig. 2.15, the AVR control action on the field voltage E_{FD} is followed by the limiting control action OEL to keep the field current I_{FD} at about 160%, i.e., the temporary overload level.

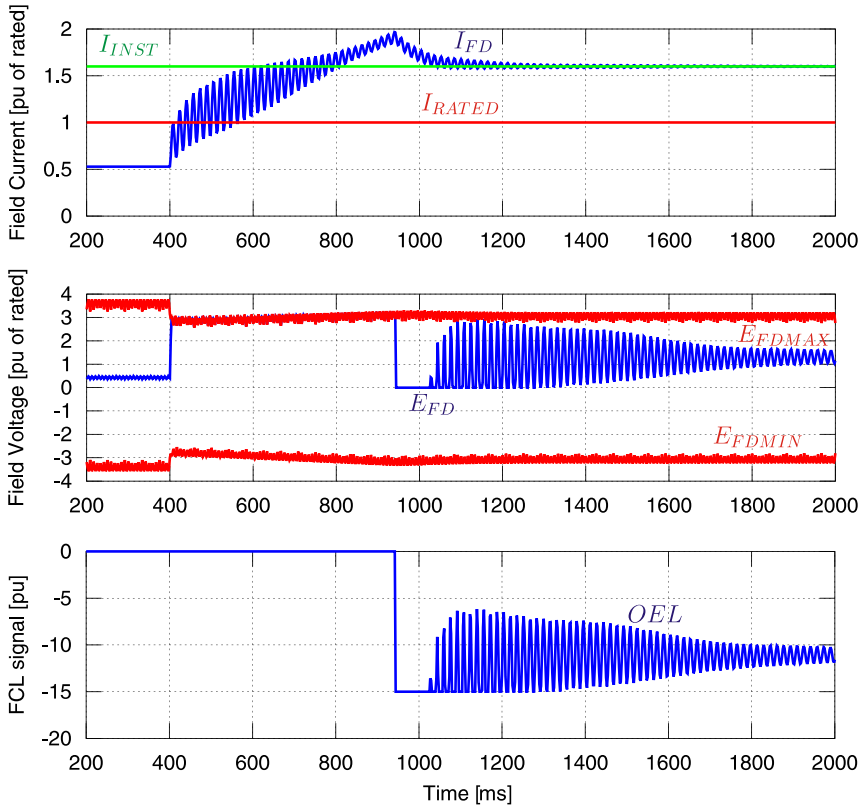

Figure 2.15: OEL control action: field current I_{FD} and limit levels I_{INST} and I_{RATED}, field voltage E_{FD}, dynamic limits E_{FDMAX} and E_{FDMIN}, and OEL signal

A model was proposed by an IEEE Task Force on Excitation Limiters in 1995 [91], but is not yet included in the corresponding IEEE standard. This subject is discussed in more detail in Chapter 3 of this thesis.

2.2.4.3 Volts/Hz Limiter

The overflux limiter continuously monitors the ratio of voltage to frequency, i.e., V/Hz. A high V/Hz ratio indicates an overflux condition, which may cause overheating and pose a risk of damage to the generator. Once the operating point of the machine exceeds the V/Hz ratio defined by the limiter, a control loop action is activated based on the difference between the V/Hz measured and the setpoint and aimed at reducing the excitation and keeping the V/Hz ratio within safe levels. A model was proposed by an IEEE Task Force on Excitation Limiters in 1995 [91], but has not yet been included in the corresponding IEEE standard [56, 92, 93].

2.2.5 Review of Current Industry Practices on Limiters

The use of underexcitation limiters for synchronous generators dates back to the use of AVR control itself [94, 95]. In general, overexcitation, underexcitation, overflux, and other types of limiters have been widely used in actual synchronous generator applications.

The mathematical representation of limiters is not common practice, even at the present time. Current regulations proposed by the North American Electric Reliability Corporation (NERC) require verification and modeling for dynamic simulation of the generator [96–101] , exciter [92, 102–104], voltage regulator [105], impedance compensation, and power system stabilizer [34]. These regulations do not explicitly require the verification and modeling of limiters.

Dynamic simulation tools provide some support for the modeling of limiters. One of these tools is PSS/E [106] from Siemens PTI, which provides several underexcitation limiter model blocks as recommended by IEEE 421.5 standard. This tool provides simplified overexcitation

limiter model blocks only, and largely relies on user-defined modeling for more complete OEL models. Another tool is TSAT [107] from Powertech, which only allows modeling of UEL and OEL as defined by the user.

The network database for system studies used by utilities does not necessarily include limiter models. One example is the AESO base case [108], which essentially includes all of the dynamic information required by NERC but not the dynamic limiter models.

2.3 Coordination of Generator Protection and Control

2.3.1 NERC and IEEE Recommendations

The coordination of generator protection and control is important and needs to be considered to ensure safe operation of the generator and to maximize use of the generator capability. Working Group J-5 of the Rotating Machinery Subcommittee of the IEEE Power System Relaying Committee proposed a set of recommendations for achieving coordination between generator protection and control [14]. These recommendations were proposed from the point of view of the protective relaying industry and suggest simplified rules that are generally applicable without the need to perform dynamic simulations [109]. The NERC System Protection and Control Subcommittee also proposed a set of recommendations for achieving coordination between generator protection and control [10]. The NERC recommendations improve upon the IEEE recommendations by suggesting the use of dynamic simulation for verification of the coordination [110–112].

2.3.2 Static and Dynamic Coordination

Static coordination is based on the comparison of characteristics in the complex impedance plane or in the complex power (PQ) plane. Several curves are calculated and plotted in these planes, among the most important of which are: a) GCC curves, b) limiters such as OEL and UEL, c) protection functions such as distance (function 21), loss of excitation (LOE or function 40), and out of step (function 78), and d) other limits such as the

stability limit. These curves are plotted assuming extreme conditions so that the margins obtained are safe and conservative. An example of the characteristic curves used for static coordination in the underexcited region is shown in Fig. 2.16. One important observation in Fig. 2.16, is that the mapping between planes depends on the voltage level used; for instance, the LOE characteristic is constant in the impedance (Z) plane but its location varies in the power plane (PQ) as a function of the present voltage level.

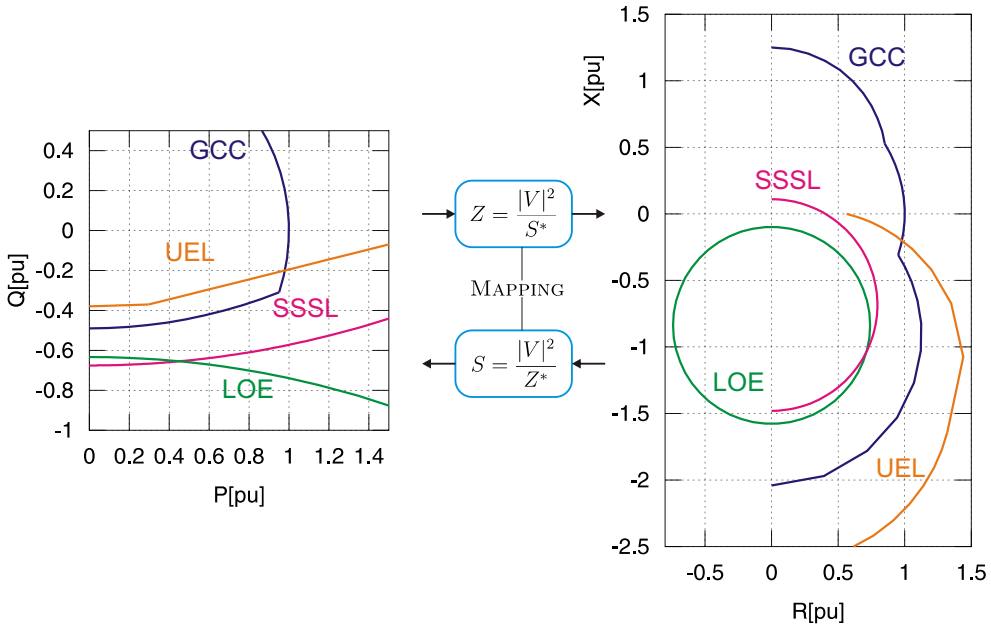

Figure 2.16: Characteristics used for static coordination in the underexcited region

The dynamic coordination also makes use of these characteristics but in their natural plane of origin; for instance, a loss of excitation protection is plotted in the impedance plane where it is usually defined rather than mapping it into a PQ plane. In dynamic coordination, the overall system is modeled with particular attention paid to synchronous generator dynamics, as described in Section 1.3, and excitation control including dynamic limiters, as described in Section 2.2. The contingency cases are selected considering the most credible severe conditions that bring the operating point beyond normal limits and into the protection zones where there is increased risk of maloperation or miscoordination. The resulting trajectories are studied in the protection function characteristic plot to verify correct or incorrect operation [113, 114].

2.3.3 Overexcited Region

2.3.3.1 Rotor Overload

The field overcurrent protection uses an inverse time characteristic that is typically based on the short time rotor overload capability, but considering a safe margin in the current vs. time plane. The rotor thermal limit is not constant in the power plane and depends on variables such as the terminal voltage and field current as shown in Fig. 2.17. This result is based on a 360 MVA, 13.8 kV synchronous generator and its parameters are provided later in Section 3.5.1.

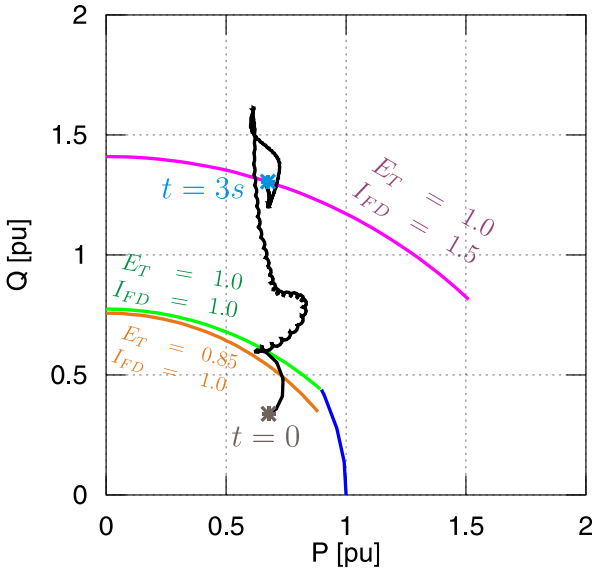

Figure 2.17: Dynamic behavior of the OEL characteristic in the PQ plane

2.3.3.2 OEL

The overexcitation limiter presents a dynamic behavior in the current vs. time plane during a reactive overload condition. The OEL does not initially apply any control action, allowing free AVR control, i.e., the field forcing period. In Fig. 2.15, the field forcing period is from $400ms$ up to $940ms$. Once the specified field forcing expires, the OEL applies instantaneous limiting control if the field current exceeds a predefined threshold, i.e., the

instantaneous limiting period. In Fig. 2.15, the instantaneous limiting period starts at $940ms$. The OEL also uses an inverse time characteristic that is faster than the protection characteristic but by a safe coordination margin. When this inverse time characteristic is reached, the OEL applies inverse time limiting control action as the machine cannot provide any more reactive support to the system beyond the nominal [115].

2.3.3.3 System Backup

The considerations for coordination depend on the type of backup provided, i.e., overcurrent or distance. For overcurrent protection, voltage control or voltage restraint is typically used and careful review of considerations should be made, with the most important being the most severe voltage collapse, a full load current larger than the steady state fault current, the time margin, and the stator thermal capability. For overcurrent with voltage control or voltage restraint, dynamic simulation should make the coordination effort easier if the dynamic behavior of the protective function is also modeled.

The distance function is typically split into two zones: one zone to protect the step up transformer and a second zone to provide backup to the longest line. Protection of the step up transformer does not present serious difficulties unless there is a very short line immediately connected to the generating station. The second zone needs to carefully consider several aspects: a) the longest line leaving the generating station, b) the maximum emergency load at the rated power factor, c) the maximum reactive overload, and d) the stator thermal capability.

An example of a system with the corresponding impedance plane considering static coordination of the distance function is shown in Fig. 2.18. In this figure, the zone 2 distance element provides backup for substation SUB1 only; this element should not operate for the maximum reactive overloads Z_{PQ1} and Z_{PQ2} defined by NERC and should not operate for the maximum overload $ZL_{150\%}$ up to $ZL_{200\%}$. However, the separation between the generator capability curve GCC and the distance element Z_2 region allows a different shape of the distance element providing coverage for additional substations, assuming that the maximum

reactive overloading conditions are not realistic for a given system.

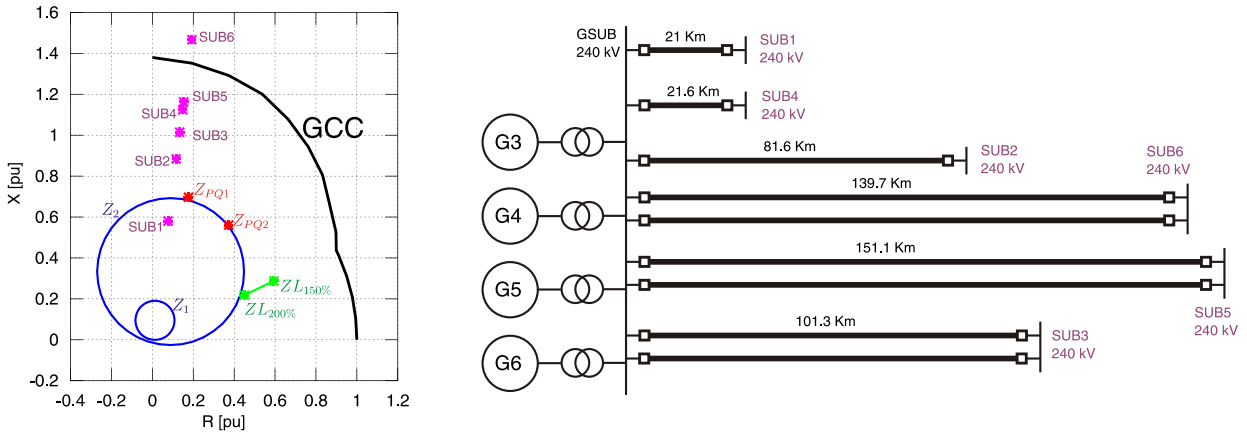

Figure 2.18: System backup coordination: impedance plane and example system

The recommendations by NERC on this subject anticipate a severe restriction in backup coverage will result and suggest the use of dynamic simulation studies as an additional option.

2.3.3.4 Reactive Overload

Coordination in the overexcited region needs to consider cases that exercise the reactive capability of the generator. To achieve this, NERC proposed the use of a voltage collapse down to 85% with reactive overload conditions between 150 and 175%. In Fig. 2.18, these reactive overload points are shown as Z_{PQ1} and Z_{PQ2}. However, a more reasonable approach is to review the network neighboring the generator for possible contingencies to produce a maximum voltage collapse condition that is recoverable.

2.3.4 Underexcited Region

2.3.4.1 Loss of Excitation (LOE)

Loss of excitation (LOE) protection is studied in the complex power or impedance plane, initially considering a safe margin using the static coordination method. However, static coordination is not capable of providing complete security against external disturbances as

the duration of these disturbances can only be measured from a dynamic simulation or from a real system disturbance [50, 116–119] .

2.3.4.2 UEL

An initial coordination is achieved by reviewing the margin between the UEL characteristic, GCC, LOE, and stability limit. However, it is very important when modeling the corresponding underexcitation limiter (UEL) to test and make corrections in the coordination between the LOE and UEL dynamic response.

An example of an underexcited condition with the corresponding UEL limiting control action is shown in Fig. 2.19. This result is based on a 360 MVA, 13.8 kV synchronous generator and its parameters are provided later in Section 3.5.1. In Fig. 2.19, the static coordination in the PQ plane seems to provide a safe margin between the GCC curve and the LOE protection. Also in this figure, the response of two sets of UEL control, each with different gain in the limiting control loop, show that a delay needs to be used in the LOE protection and this delay is highly dependent on the dynamics of the given machine, controls, and system network.

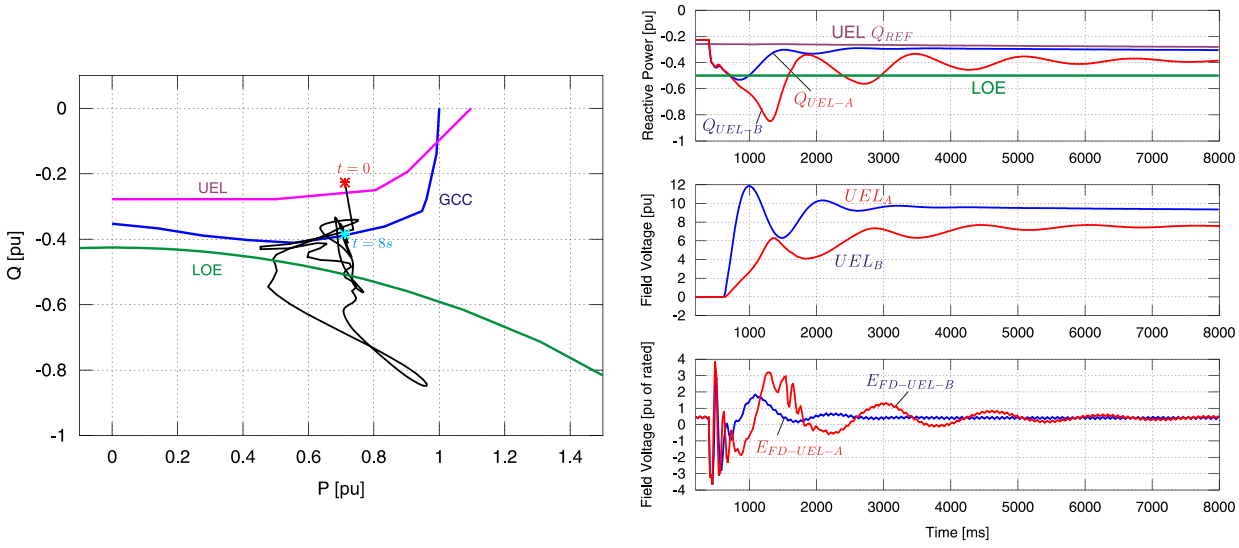

Figure 2.19: Underexcited condition response: UEL control action impact on LOE protection

2.3.4.3 Stability

The stability limit needs to be considered based on the specific generator control philosophy, with AVR type, PSS usage, and redundancy of controls being the most important. In some cases, the steady state stability limit with manual control would be applicable; in most cases, however, the stability limit would not restrict the generator capability due to the use of redundant AVR and PSS controls. The dependence of the steady state stability limit with the AVR control action is illustrated in Fig. 2.20.

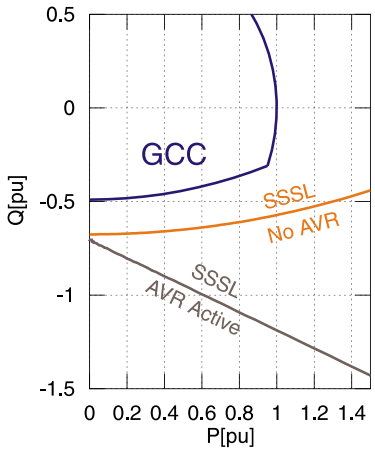

Figure 2.20: Steady state stability limit and AVR action

2.3.5 Interaction of Generator Protection with Loss of Synchronism Conditions

The loss of synchronism condition is dangerous for a generator and, if possible, needs to be detected at the first unstable swing. However, detection at the first swing requires careful study of the dynamic performance of the generator for different loading scenarios.

In general, it is not desirable for other functions, such as distance or loss of excitation, to trip during a loss of synchronism condition as there is no control over the angle between the machine and the power system. The tripping of the generator during a loss of synchronism needs to consider the breaker capability, as the breaker may be subjected to twice the rated voltage in cases when the angle between the generator and power system is most open. An

example of the risk for the LOE protection to operate during a loss of synchronism condition is shown in Fig. 2.21. Another example of the risk of distance protection operating during a loss of synchronism condition is shown in Fig. 2.22. The synchronous generator in these two examples is a 360 MVA, 13.8 kV and its parameters are provided later in Section 3.5.1.

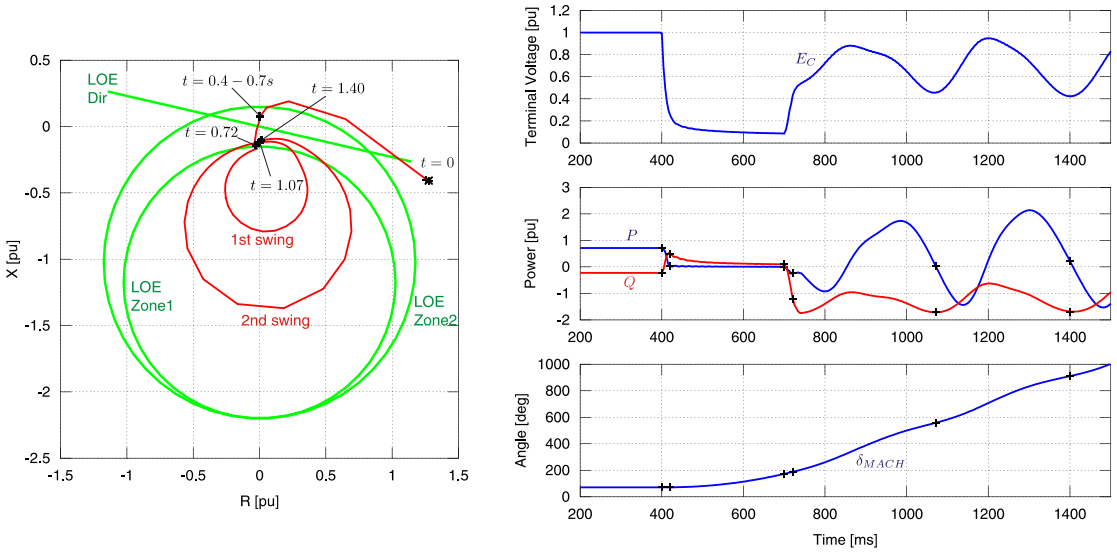

Figure 2.21: Loss of synchronism condition and LOE protection

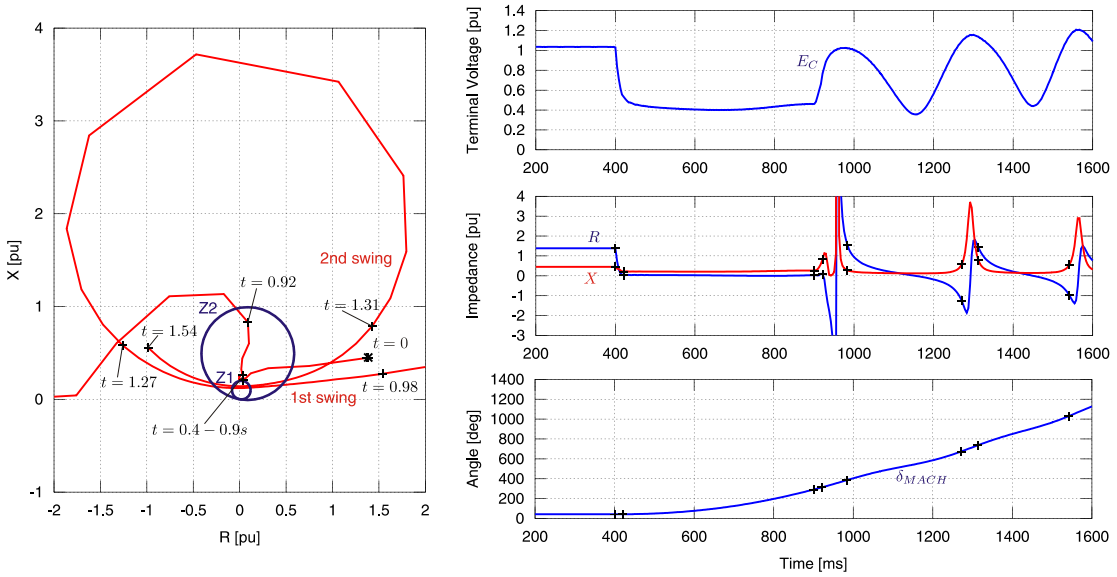

Figure 2.22: Loss of synchronism condition and distance protection

2.4 Summary

In this chapter, some of the most important generator protection functions were described in detail. The protection functions that need to be considered for coordination with excitation control are excitation protection, stability protection, and system backup protection. Other protection functions do not need special consideration to coordinate with excitation control, as their operation is needed regardless of the control action. The important generator excitation control functions were also described in detail. The main control actions commonly used in power system studies are the automatic voltage regulator (AVR) and power system stabilizer (PSS). However, for proper coordination between generator protection and excitation control, the limiter control actions need to be correctly represented. Current industry practices do not use accurate modeling of the limiters– underexcitation limiters (UEL), overexcitation limiters (OEL), and overflux limiters (V/Hz)–in power system studies. Coordination between generator protection and excitation control was discussed and a brief explanation of the current recommendations by NERC and IEEE was given. Static versus dynamic coordination were described. Coordination in the overexcited region requires that two issues be addressed: coordination with the system backup protection functions and coordination for temporary rotor overload conditions. Coordination in the underexcited region requires that several factors be considered–loss of excitation (LOE) protection, underexcitation limiter (UEL), and stability limit–all of which need to be correctly modeled and studied. Coordination with loss of sychronism protection is also important because the protection functions being considered up to this point are affected by this machine condition.

In the next chapter, coordination between OEL, AVR, and field overcurrent protection is discussed in detail. Modeling methods valid for high bandwidth simulations, i.e., on the order of 1 kHz or more, are presented and the coordination performance is demonstrated by dynamic simulations.

Chapter 3

Proposed OEL Modeling for IEEE ST1A Exciter

3.1 Importance of OEL

The operating requirements of power systems networks have become more demanding in recent times. One of these requirements is to maximize the availability and use of the reactive generating capability [12]. This reactive capability directly impacts the voltage stability of the system [14, 91]. For a synchronous generator, the reactive capability is given by the rotor field winding thermal limit [58]. Making full use of this capability helps to retain the voltage stability of the system during stressed conditions, but without damaging the generator [89, 120].

Two main functions are responsible for the maximum reactive capability of a synchronous generator: the excitation control system (ECS) and the field overcurrent protection. The excitation control system, in particular the automatic voltage regulator (AVR) and the overexcitation limiter (OEL), are responsible for keeping the machine within limits [91, 121–123]. The field overcurrent protection is responsible for taking the machine out of service in case control actions fail to keep operation within overexcitation limits [12, 124]. Coordination between excitation control and protection is critical [14]. Coordination studies are, in most cases, based on generator and excitation control parameters and characteristics. Practical tests to verify the coordination present risk for the machine and the power system [121, 123, 125, 126].

In this section, coordination between the OEL limiter, AVR, and field overcurrent protec-

tion is discussed in detail. Coordination performance is verified for severe conditions where coordination is required. Performance is verified by simulation, and therefore modeling accuracy is very important. Modeling methods suitable for electromagnetic (high bandwidth) simulations are presented. It should be noted that typical simulation studies are based on low bandwidth methods, and several models for such studies are available in the literature. The main reference for modeling details of AVR, PSS, and UEL controls is IEEE 421.5 standard and references therein [68, 127]. Additional models for OEL, underexcitation (UEL), volts per hertz (V/Hz), and overvoltage limiters have been described to complement those provided in the IEEE standard [91, 121, 122, 128–130].

The subject of this section should not be confused with the volts per hertz limiter, which is sometimes called overexcitation protection in the protective relaying literature.

3.2 Overexcitation Capability

The overexcitation limit is important because it defines the amount of reactive power available if needed by the power systems. This reactive power is needed to maintain the voltage levels in the power system and prevent voltage collapse. It is in this way that the reactive support from the generator improves the voltage stability of the system. Two types of limits can be identified: steady state and dynamic.

3.2.1 Steady State Overexcitation Limit

The steady state overexcitation limit defines the maximum reactive power that can be supplied continuously. This maximum is not a fixed value, but is actually a characteristic curve in the PQ plane.

The overall Generator Capability Curve (GCC) indicates the operating limits of a synchronous generator and is shown in Fig. 3.1. In this figure, the overexcitation limit is the upper portion of the GCC curve. This limit is defined by the rated current capability of the rotor field winding and, in many cases, also by the generator step up transformer ratio [131].

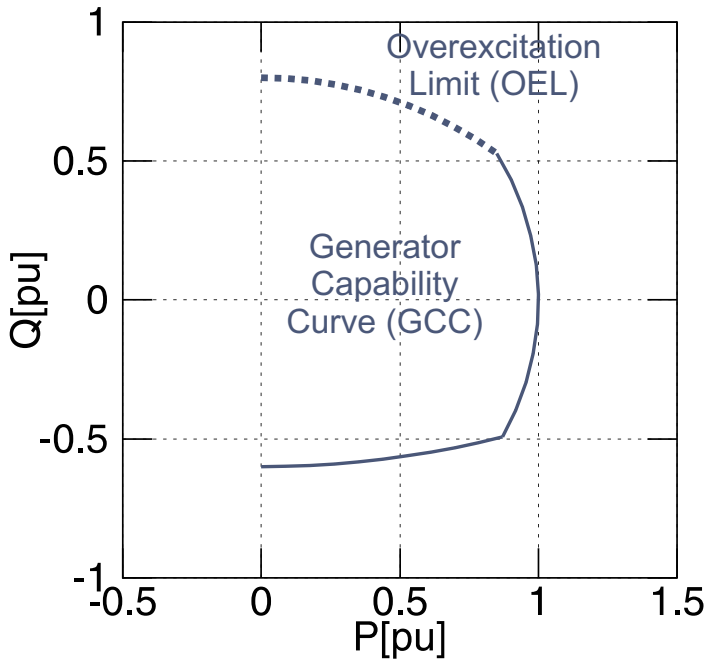

Figure 3.1: Generator capability curve

3.2.2 Dynamic Overexcitation Limit

The dynamic limit defines the additional reactive power that the generator can supply during disturbance events. This limit is dynamic because the maximum rotor current is a function of time.

This dynamic limit is given by the rotor winding short-time thermal capability, which is described by a characteristic in the current-time plane. IEEE C50.13 standard [58] defines the rotor winding short-time thermal requirements as a curve with the following equation 3.1.

$$I_{FD} = 100 \cdot \sqrt{\frac{33.75}{t} + 1} \tag{3.1}$$

where I_{FD} is rotor field current as percent of rated and t is the time in seconds.

In this equation, the IEEE C50.13 standard provides four points as a reference, as given in Table 3.1.

Table 3.1: Rotor winding short-time thermal capability

Time(seconds)	10	30	60	120
Rotor current(percent)	209	146	125	113

The resulting curve is shown in Fig. 3.2:

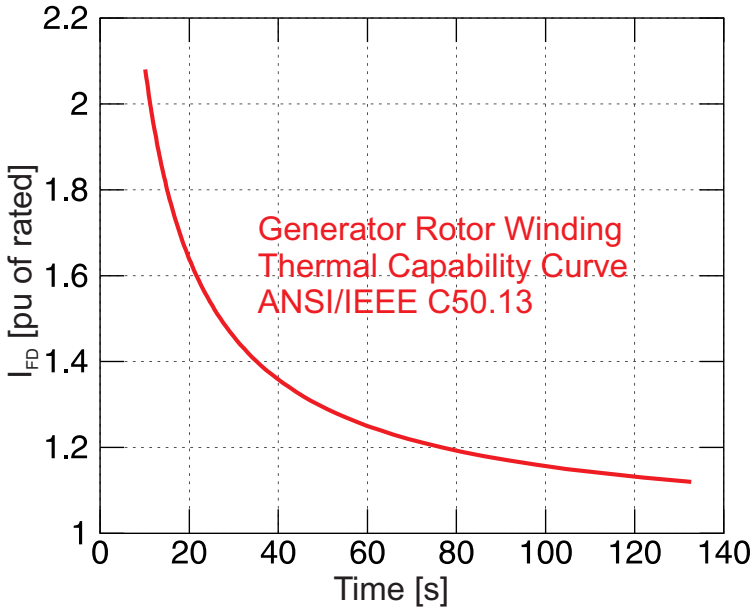

Figure 3.2: Rotor winding short-time thermal requirements in IEEE C50.13

3.2.3 Disturbance Events that Exercise Overexcitation Limits

Power system disturbances that cause voltage collapse will result in an excitation voltage increase due to AVR control action. If this increase is above the maximum reactive capability of the machine, then the OEL limiter will be activated. One important condition to consider is a fault in the power system network close to the generator. The field current may increase significantly during the fault and also during a power swing that may follow the fault being cleared.

Another condition, which could be more severe, is an overload with voltage reduction. Consider an overload condition that demands reactive generation close to the machine limit.

In this scenario, if some other vital supply of reactive power in the network is lost, then the voltage will collapse if the generator is unable to resupply the lost reactive power. One example of reactive power loss could be loss of excitation (LOE) in an adjacent generator in the same power plant.

3.3 Interaction between Excitation Control, Limiter, and Protection

3.3.1 Basic Interaction

An overview of the main components involved in the overexcited region is given in Fig. 3.3.

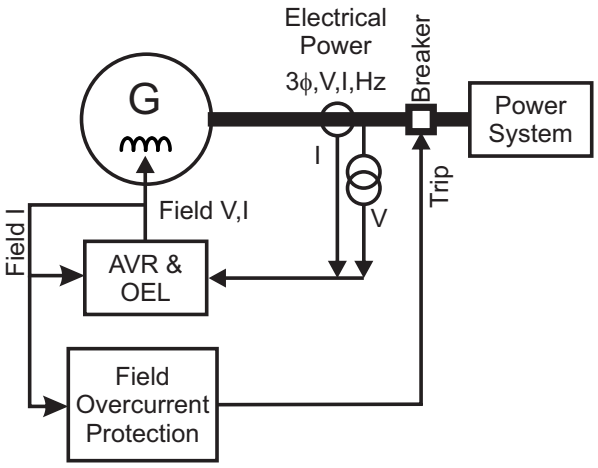

Figure 3.3: Overview of AVR, OEL, and field overcurrent protection functions

3.3.1.1 Normal Control

The main control action when the machine is operating within limits is terminal voltage control, i.e., AVR control action. The AVR keeps the terminal voltage magnitude constant at the desired level set by the AVR input reference.

3.3.1.2 OEL Limiting Control

Overexcitation limiting (OEL) control is activated as soon as the operating point of the generator is beyond the overexcitation limit. In the PQ plane, this is represented as a point moving outside and above the upper curve of the GCC. In the current-time plane, this is represented as a current level above the rated value.

The OEL action is responsible for returning the operating point to within GCC limits. In the process, the OEL makes use of the rotor short-time overload capability as needed.

3.3.1.3 Field Overcurrent Protection

The field overcurrent protection is always monitoring the rotor current level. However, it should only take the machine out of service in case all actions to return it to within limits fail.

3.3.2 Overexcitation Disturbance Conditions

Several conditions can be identified during an overexcitation disturbance event, as shown in Fig. 3.4:

- Field Forcing
- Field Current Limiter Instantaneous
- Field Current Limiter Inverse Time
- Field Overcurrent Protection

3.3.2.1 Field Forcing Condition

This condition starts when the field rotor current exceeds the rated current level. The AVR is allowed free control action during the field forcing time interval. High values of

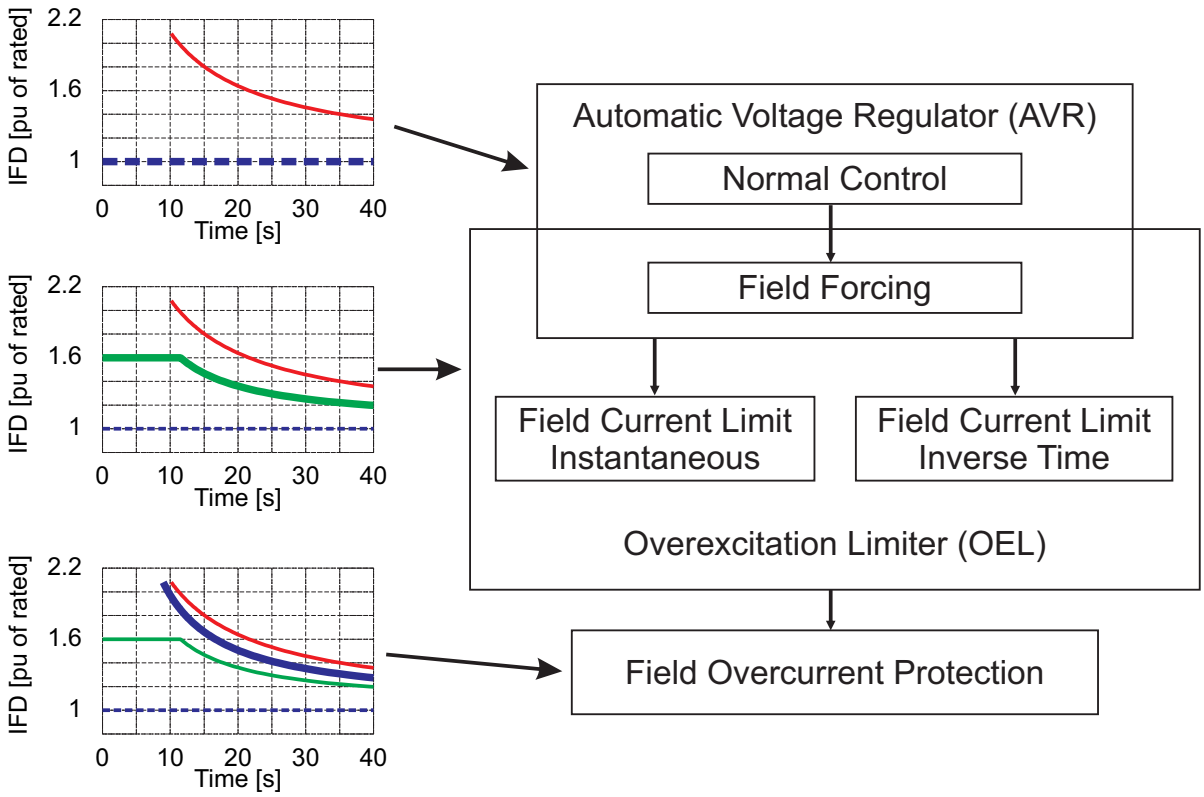

Figure 3.4: Interaction between AVR, OEL, and field overcurrent protection

excitation voltage may be applied up to the ceiling voltage level available, typically on the order of 3.50 *pu*. This ceiling voltage may be reduced during a disturbance that causes voltage collapse in the system, limiting the field forcing action. The field forcing duration is typically on the order of 100 milliseconds to 1.0 seconds. This duration is configurable in the excitation control system; however, there is no clear rule available for setting its value.

3.3.2.2 Field Current Limiting Instantaneous Condition

After the field forcing interval, the field rotor current is typically limited to a maximum value, i.e., an instantaneous limiting level. This maximum level is defined by the generator manufacturer and is typically on the order of 160% of the rated field current. During the field forcing interval, there is no limiting action if the field current is below the instantaneous limiting level; the limiting action is applied when the field current exceeds the instantaneous

limiting level. This limiting action is based on the difference between the field current and the current limit pickup level. The current limit pickup level is the reference input to the limiting control loop being used. The actual limiting control loop is proportional or proportional-integral and brings the field current to within desired levels. The current limit pickup level is a dynamic value, equal to the instantaneous limiting level during the field current limiting instantaneous interval.

3.3.2.3 Field Current Limiting Inverse Time Condition

In parallel with the instantaneous limiting interval, an inverse time current characteristic is typically used if the field current is above the rated field current level. This limiting curve in the current-time plane needs to be below the rotor winding short-time thermal capability defined by IEEE C50.13 standard by some margin. No inverse time limiting control action is taken until the operating condition reaches the inverse time limiting current characteristic. Once this curve is reached, the first action is to change the value of the current limit pickup to the rated field current. Then, the limiting control is activated using the limiting control loop to bring the field current down to the rated field current level.

3.3.2.4 Field Overcurrent Protection Trip Condition

This protection continuously monitors the field current level and will take the generator out of service when rotor thermal conditions approach the capability limit due to the risk of damaging the machine. However, the protection should also allow the limiting control to take action and provide sufficient time to return the machine to normal. Also, the protection should allow the machine to provide maximum reactive support to the system by the use of the short-term rotor overload capability. In order to achieve these objectives, coordination is performed using current-time curves. In the current-time plane, the IEEE C50.13 curve should be above all other curves. The curve immediately below should be that of the inverse time protection. Located below both curves are the OEL curves. In many cases for large machines, redundant excitation control systems (ECS) are used. When redundancy is used,

the backup ECS takes control if the main ECS fails. The field overcurrent protection needs to consider this and allow the redundancy to perform its function before deciding to take the machine out of service.

3.4 Modeling of Excitation, Control, Overexcitation Limiter, and Protection

There are two basic approaches for modeling overexcitation limiters and their interaction with excitation control systems, as specified by IEEE 421.5 standard:

- Custom modeling
- Modeling proposed by the IEEE Excitation Systems and Control Subcommittee (ESCSC) in a paper published on 1995 [91].

3.4.1 OEL and the IEEE ST1A Model

3.4.1.1 IEEE ST1A Model Characteristics

The IEEE ST1A model is recommended in IEEE 421.5 standard for representing excitation systems with a solid state controlled rectifier and is shown in Fig.3.5. The voltage supply to this rectifier typically comes from a step down transformer located at the terminals of the generator.

In Fig.3.5:

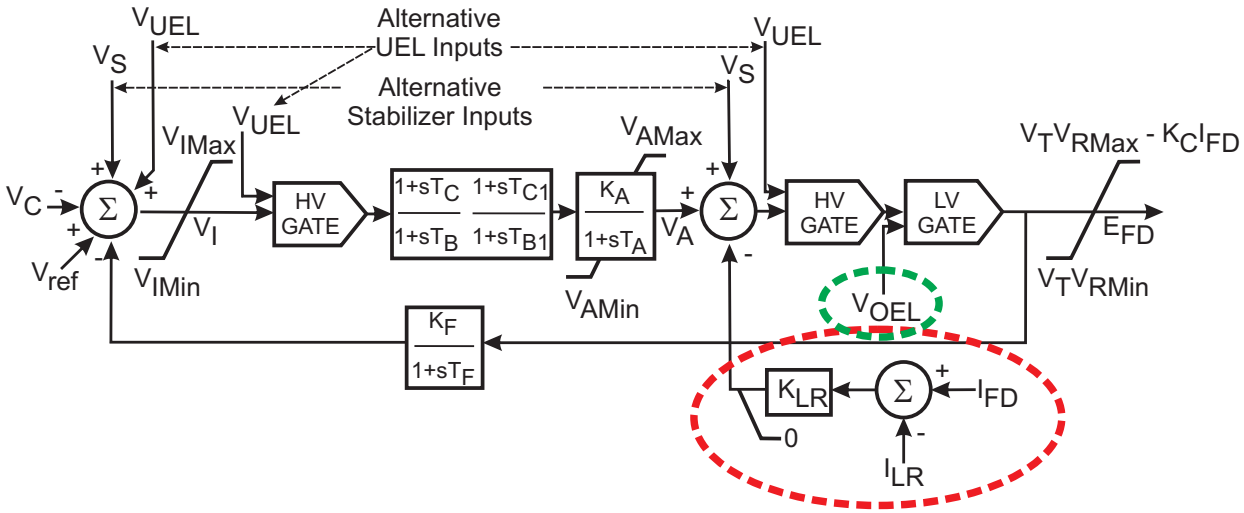

Figure 3.5: IEEE ST1A exciter model - potential source controlled rectifier exciter

V_{ref} is the reference or desired terminal voltage

V_C is the terminal voltage measured

E_{FD} is the excitation voltage output considering the rectifier effect and ceiling voltage limits

I_{FD} is the field current measured

V_S represents auxiliary signals, e.g., power system stabilizer (PSS)

V_{UEL} is the underexcitation limiter signal

V_{OEL} is the overexcitation limiter signal

K_A, T_A represent the main exciter control loop

T_C, T_{C1}, T_B, T_{B1} represent lead lag compensating control loop

K_F, T_F represent the stabilizing feedback control option

K_{LR}, I_{LR} represent an OEL limiter included in ST1A

3.4.1.2 OEL Model from IEEE 421.5 Standard

An overexcitation limiter (OEL) model is described in Section 9 of IEEE 421.5 standard, but this model cannot be interfaced with the ST1A. This OEL model is intended for long-

term dynamic studies, which require a bandwidth even lower than transient stability studies [132, 133]. This model does not represent the details on control loops required for transient stability studies. This OEL model will not be used in this work.

3.4.1.3 Interaction Between ST1A and OEL Control

The IEEE ST1A excitation system model provides two options for OEL control. One option is a summing type, which comes through the K_{LR} block in Fig.3.5. The second option is a takeover type, which comes via the input V_{OEL} to the low level LV gate in Fig.3.5.

In this proposed OEL model, the summing type is used. The advantage of the summing type is that PSS action is maintained, as opposed to the takeover type in which the V_{OEL} signal needs to include its own PSS action if needed. In the proposed OEL model, the path characterized by I_{LR}, I_{FD}, and K_{LR} is being replaced.

3.4.1.4 OEL Control Included in ST1A

The ST1A model already includes very basic OEL control of the summing type, as indicated previously. This OEL is basically an instantaneous limiting control where the maximum field current is defined by the parameter I_{LR}. Field forcing can be represented by zeroing the K_{LR} parameter for the desired field forcing duration starting from the beginning of the overexcitation disturbance.

The OEL model included in ST1A has several limitations:

- Modeling is intended for low bandwidth simulations, i.e., transient stability, but not electromagnetic types of simulations
- Field forcing time measurement is not described
- Inverse time limiting control is not described
- Dynamic behaviour of the current limit pickup is not described

- Transitions between field forcing, instantaneous, inverse time, and normal control are not clearly described

One important detail is the units used for K_{LR} and I_{LR}. In the ST1A model, these values are in per unit with base equal to the no load field current value.

3.4.2 Custom Modeling: Proposed OEL Modeling Improvements for ST1A

The model proposed in this section is based on Murdoch's work for the IEEE ST4B exciter model [121]. An overview of the model proposed is given in Fig.3.6. This model replaces the path characterized by I_{LR} and K_{LR} in Fig.3.5. In this model, the input signal is the field current measured I_{FD} and the output is the OEL limiting signal. One important improvement over Murdoch's work is that the proposed model can be used in high bandwidth studies, such as electromagnetic simulations.

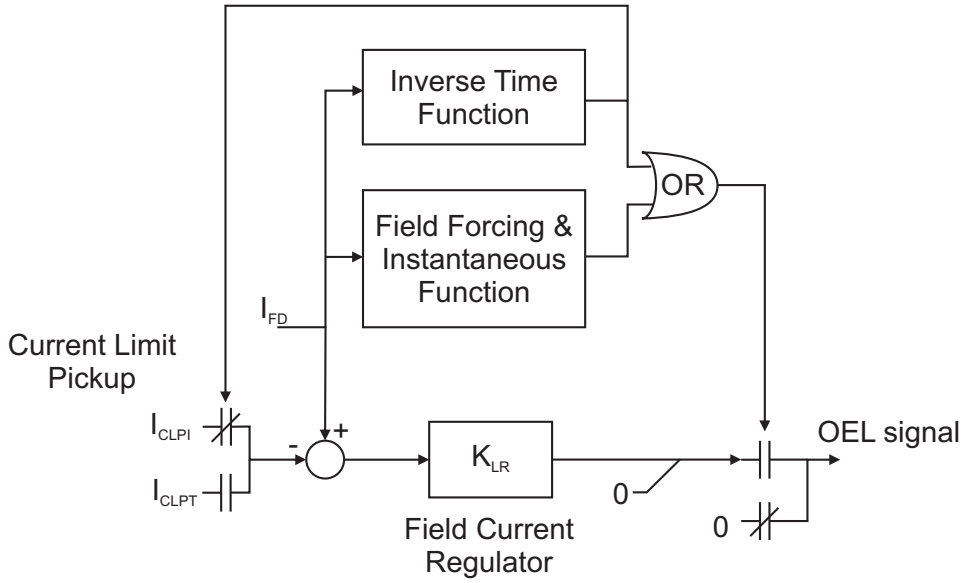

Figure 3.6: Proposed OEL model for ST1A

In the proposed OEL model, the values are in per unit with base equal to the full load rated field current value.

3.4.2.1 Field Forcing and Instantaneous Limiter

The proposed field forcing and instantaneous function is shown in Fig. 3.7.

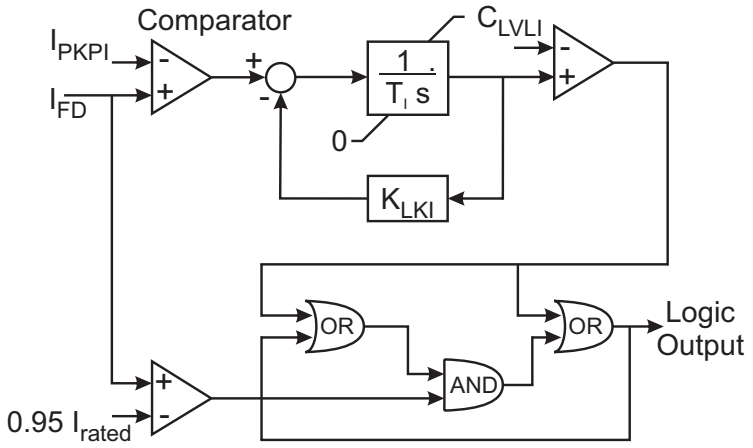

Figure 3.7: Proposed field forcing and instantaneous function block

In Fig.3.7:

I_{FD} is the field current measured in *pu* of rated

I_{PKPI} is the instantaneous pickup level, typically 1.60 *pu*

K_{LKI}, T_I are integrator loop parameters

C_{LVLI} is the integrator pickup level for the desired field forcing time

Field Forcing Mode: Initially, the field forcing and instantaneous block issues a zero logic output in Fig.3.7, causing a zero OEL signal output in Fig.3.6 by following the normally closed contact path. A logical signal level of 1.0 is achieved after the desired field forcing time.

Time Measurement: This is performed by an integrating timer that accumulates pulses coming from an input level comparator. This comparator compares the measured current

I_{FD} and the instantaneous pickup level I_{PKPI}. The integrating timer in this case is not ideal but "leaky", which means that its gain is finite ($\frac{1}{K_{LKI}}$). An output comparator is used with a preset level C_{LVLI} selected to obtain the desired field forcing duration.

A typical response in the time domain is given in Fig.3.8. This result is based on a 360 MVA, 13.8 kV synchronous generator and its parameters are provided later in Section 3.5.1. For this example, the following parameters have been selected: $T_I = 1.0$, $K_{LKI} = 0.25$, $C_{LVLI} = 0.194$, and $I_{PKPI} = 1.60$. Here, the desired field forcing time is $200ms$. The

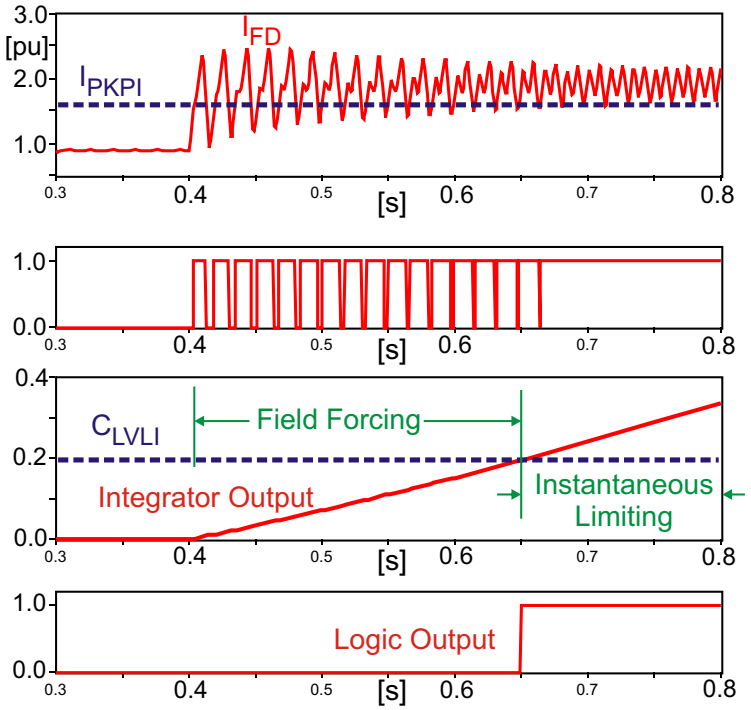

Figure 3.8: Time signals of proposed field forcing and instantaneous function

integrating timer is required in the proposed model due to the oscillating nature of the field current I_{FD} during severe disturbances. These oscillations are obtained from electromagnetic simulations but are not necessarily reproduced by the transient stability simulation methods typically used by the industry. The oscillations of field current I_{FD} may go above and below the instantaneous pickup threshold with a time period much shorter than the desired field forcing duration. A simple timer would pickup and reset many times, resulting in a significantly longer field forcing duration. However, an integrating timer adds all of the short time periods if they are close to each other and provides an effective measurement of the

field forcing duration. This level of detail is not described in IEEE 421.5 standard, but it is required in this work because electromagnetic simulations are being used.

Instantaneous Field Current Limiting Mode: As soon as the desired field forcing duration elapses, a logical output of 1.0 is issued (see Fig.3.7). This allows the output of the field current regulator limiting control loop in Fig.3.6 to become the output OEL signal by closing the normally open contact. Thus, the field current regulator limiting control action is applied at the summing point in Fig. 3.5. During the instantaneous limiting mode, the input reference to the OEL, i.e., the current limit pickup, remains at the instantaneous level I_{CLPI} to maintain the typical 160% of rated field current.

3.4.2.2 Field Current Regulator

This is the control loop responsible for producing the limiting signal applied to the main exciter loop. The controlling signal is based on the difference between the field current measured I_{FD} and the current limit pickup reference level. The control action used in the proposed OEL is proportional with a gain in K_{LR} that is dependent on the application. The output is restricted to be positive, so a zero output is produced by this limiting control loop when the field current I_{FD} is lower than the limit pickup.

3.4.2.3 Dynamic Current Limit Pickup

The behavior of the current limit pickup is dynamic and depends on whether or not the thermal operating condition has reached the inverse time limit. If the generator was operating below or at the rated field current condition prior to a disturbance, the current limit pickup is equal to the instantaneous limiting level I_{CLPI} in order to keep the field current within 160% of the rated value. If the disturbance causes the generator to reach the inverse time limiting curve, then the current limit pickup becomes the I_{CLPT} value in order to keep the field current within 100% of the rated value. The current limit pickup will remain at this level until the field current drops below 100% minus a hysteresis level of

approximately 10%. Values for 1.55 for I_{CLPI} and 0.95 for I_{CLPT} were used in the proposed OEL to achieve the desired limiting levels of 160% and 100%. The difference of 0.05 is required because the controller type proposed is proportional and of the summing type.

3.4.2.4 Inverse Time Limiter

This function starts measuring time when the field current exceeds the rated value and is shown in Fig.3.9. The time measurement is based on the difference between the field current I_{FD} and a reference level I_{PKPT} equal to the rated value plus 2%, i.e. 102%. This difference goes to a summing point and becomes the input to an integrating timer. In this way, the time integration is faster for a larger difference and slower when there is a small difference, thus generating an inverse time characteristic.

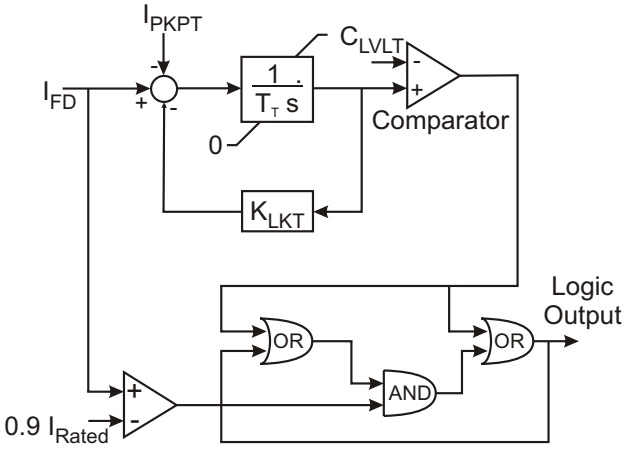

Figure 3.9: Proposed inverse time measurement function block

In Fig.3.9:

I_{FD} is the field current measured in pu of rated

I_{PKPT} is the inverse time pickup level, typically 1.02 pu

K_{LKT}, T_T are integrator loop parameters

C_{LVLT} is the integrator pickup level for the desired inverse time curve

The current time characteristic selected needs to be below the IEEE C50.13 by a safe margin, as shown in Fig. 3.10. This margin allows enough time for the field control regulator action to bring the generator back to a rated level. In Fig. 3.10, the following parameters were used: $I_{PKPT} = 102\%$, $T_T = 60.0$, $K_{LKT} = 0.255$, and $C_{LVLT} = 0.109$.

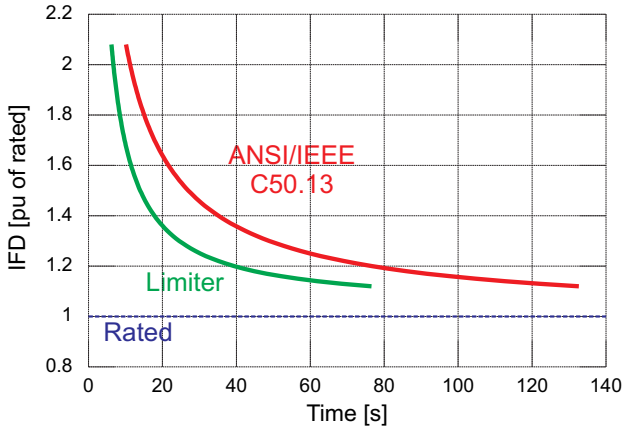

Figure 3.10: Proposed inverse time limiter current-time curve

3.4.2.5 Field Overcurrent Protection

This function block is very similar to the inverse time limiter described above. The main difference between protection and limiter characteristics is in the pickup level C_{LVLT} in Fig.3.9. The protection pickup level C_{LVLTP} should be larger than the C_{LVLT} used for limiting control. The time margin between both current-time curves considers switching to redundant ECS in case the main ECS fails. This margin should also include enough time to allow for the field current regulator (FCR) control action to bring the operating point within

normal conditions. At the same time, the curve should also be coordinated with the IEEE C50.13 standard curve. An example of this coordination is shown in Fig. 3.11.

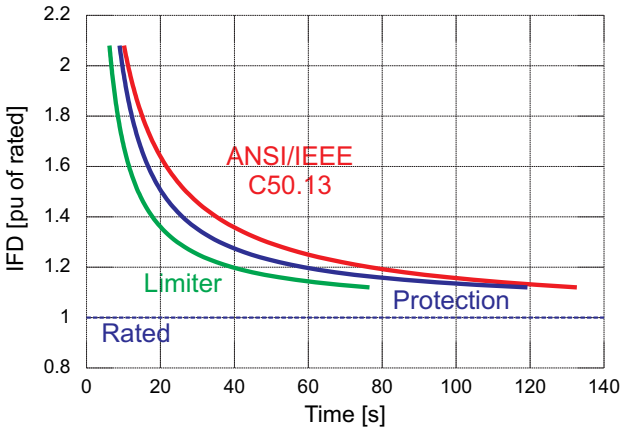

Figure 3.11: Proposed inverse time coordination between protection and control

For the simulation example shown in Fig. 3.11, the following parameter was used for the protection curve: $C_{LVLTP} = 0.156$.

3.4.3 IEEE 1995 OEL Model: Limitations and Proposed Improvements

The OEL model proposed by the IEEE was intended to be generic enough to implement any given limiter model available in the industry. This model is shown in Fig. 3.12.

In Fig.3.12:

I_{rated} is the rated field current for OEL scaling.

I_{tfpu} is the OEL timer pickup level.

I_{lim} is the OEL timed current limit.

I_{inst} is the OEL instantaneous current limit.

I_{max} is the OEL enable threshold.

T_{en} is the OEL enable time.

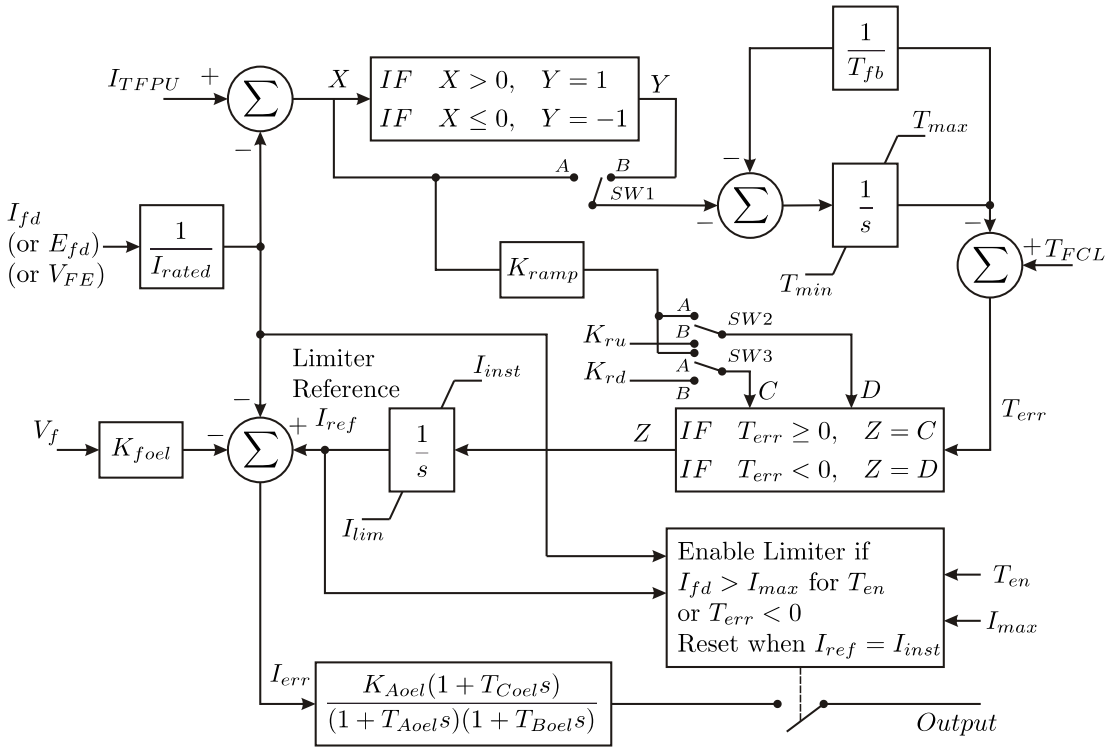

Figure 3.12: Generic OEL model proposed by the IEEE in 1995

T_{min} is the OEL timer minimum limit.

T_{max} is the OEL timer maximum limit.

T_{fcl} is the OEL timer setpoint.

T_{fb} is the OEL timing feedback time constant.

K_{rd} is the OEL fixed ramp down gain.

K_{ru} is the OEL fixed ramp up gain.

K_{ramp} is the OEL proportional ramp rate gain.

K_{aoel} is the OEL regulator gain (proportional).

K_{foel} is the OEL control system stabilizer gain.

T_{aoel} is the OEL regulator time constant.

T_{coel} is the OEL regulator time constant.

T_{boel} is the OEL regulator time constant.

3.4.3.1 Limitations of the 1995 IEEE OEL Model

The model shown in Fig. 3.12 has several limitations:

- Ramp up/down variables C and D are not restricted, i.e., $D \geq 0$ and $C \leq 0$
- Latching logic is not included, i.e., hysteresis, for a proper reset of OEL
- Only a proportional control loop is included; no integral control is available
- Time measurement for field forcing is affected by field current oscillations

These limitations were observed when trying to apply the IEEE OEL Model to reproduce the results obtained by the custom model proposed earlier. A trial and error process was followed to identify the specific limitations, making corrections until the same results were obtained with the proposed improvements described below.

3.4.3.2 Proposed Improvements to the IEEE 1995 OEL Model

To address the limitations listed above, some modifications are proposed in this thesis and are illustrated in Fig.3.13. One of the modifications is to restrict the values of ramp up/down variables C and D, so that $C \leq 0$ and $D \geq 0$. Another modification is to include a logic for latching and reset. The latching logic proposed provides flexibility by using a variable *tlck*, so that reset limits can be set independently for the instantaneous limiter with the variable *iiulk* and for the timed limiter with the variable *itulk*. One more important modification is enabling the use of proportional and/or integral control as required by a particular application. The use of integral control also requires limits be provided, as shown in Fig.3.13. The last modification proposed is to use an integrating timer similar to that described in subsection 3.4.2.1.

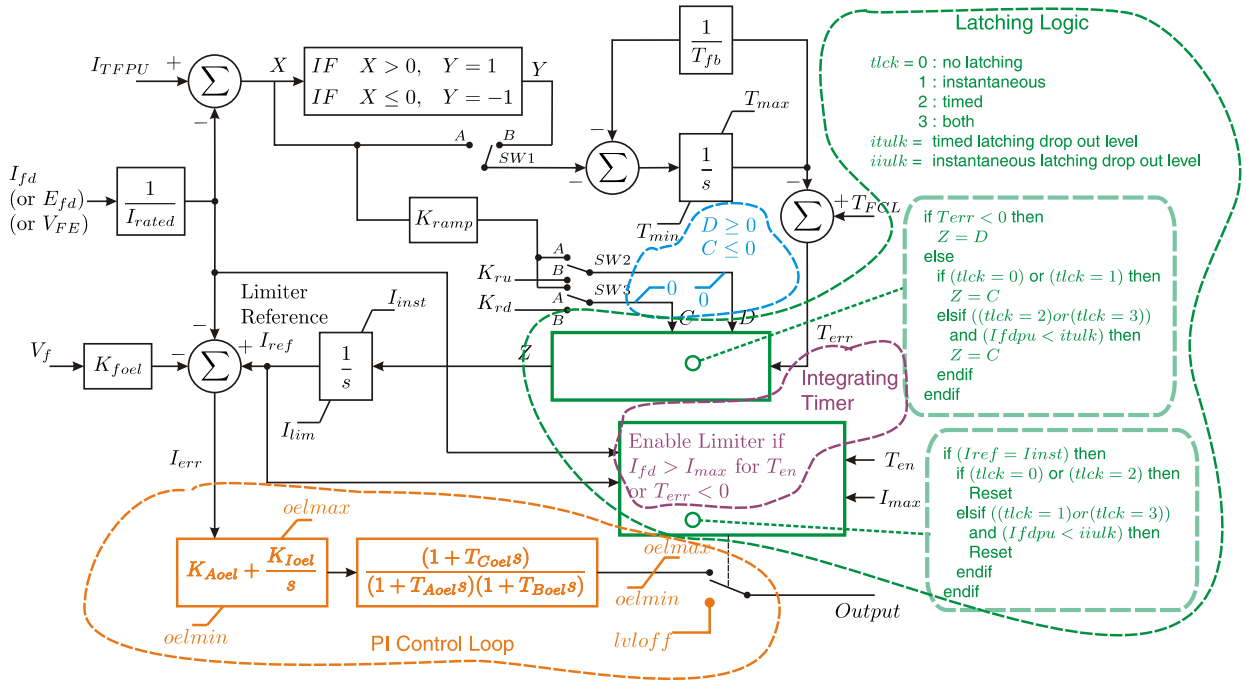

Figure 3.13: Proposed improvements to the generic OEL model proposed by the IEEE in 1995

3.5 Dynamic Coordination Tests with Proposed Custom OEL Model

In this section, the proposed OEL model is tested with an example test system for two important scenarios: close in fault and temporary overload with voltage reduction.

3.5.1 Test System

The system used to study the proposed OEL model is a 360 MVA, 18 kV round rotor generator connected to an infinite bus through a power line with 0.055 *pu* impedance. The parameters of this generator correspond to the Poplar River 2 Unit from SaskPower [134]. The generator is represented by single mass dynamics and includes governor control action. The exciter control functions represented are AVR and OEL. The simulation tool used is the ATP/EMTP software.

Table 3.2: Generator parameters

S_{base}	360	MVA	X_q	2.2	pu	X_{CAN}	0.22	pu
V_{base}	18	kV	X'_d	0.3	pu	T'_{d0}	7.1	s
H	2.89	s	X'_q	0.52	pu	T'_{q0}	1.0	s
Xn	0.001	pu	X''_d	0.26	pu	T''_{d0}	0.03	s
Rn	0.001	pu	X''_q	0.26	pu	T''_{q0}	0.06	s
X_0	0.001	pu	X_L	0.22	pu			
X_d	2.2	pu	R_a	0.0025	pu			

Table 3.3: Exciter ST1A parameters

K_A	432	pu	T_{C1}	0	s	K_C	0.172	pu
T_A	0.003	s	T_{B1}	0	s	K_F	0	pu
T_C	0	s	V_{RMAX}	10.8	pu	T_F	1.0	s
T_B	0	s	V_{RMIN}	10.0	pu			

Table 3.4: Power system stabilizer PSS2A parameters

V_{SI1}	Speed		T_3	0.04	s	N	1	
V_{SI2}	Power		T_4	0.02	s	V_{STMAX}	0.1	pu
K_{S1}	15.0	pu	T_{W1}	10.0	s	V_{STMIN}	-0.06	pu
K_{S2}	1.736	pu	T_{W2}	10.0	s	T_6	0	s
K_{S3}	1.0	pu	T_{W3}	10.0	s	T_7	10.0	s
T_1	0.05	s	T_{W4}	0	s	T_8	0.5	s
T_2	0.02	s	M	5		T_9	0.1	s

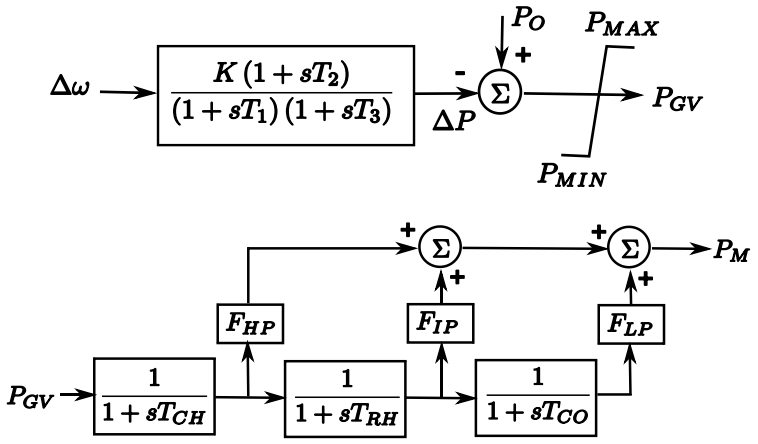

Figure 3.14: IEEE governor model

Table 3.5: Governor parameters

K	18	pu	P_{MIN}	0	pu	T_{CO}	0.28	s
T_1	0.077	s	P_{MAX}	0.95	pu	F_{HP}	0.27	pu
T_2	0	s	T_{CH}	0.025	s	F_{IP}	0.2555	pu
T_3	0.198	s	T_{RH}	7.0	s	F_{LP}	0.4745	pu

Table 3.6: Proposed OEL parameters

I_{CLPI}	1.55	pu	T_I	1.0	s	T_T	60.0	s
I_{CLPT}	0.95	pu	K_{LKI}	0.25	pu	K_{LKT}	0.255	pu
K_{LR}	224.4	pu	C_{LVLI}	0.194	pu	C_{LVLT}	0.109	pu
I_{PKPI}	1.60	pu	I_{PKPT}	1.02	pu	C_{LVLTP}	0.156	pu

3.5.2 Close In Fault Test

An overview of the system configuration and initial conditions used for the fault case test is given in Fig. 3.15. The fault applied is zero ohm BCG, i.e., phase B and C to ground. The fault is applied at time $t = 400ms$ and cleared at time $t = 700ms$.

The current measured at the generator terminal is shown in Fig. 3.16. In this figure, the

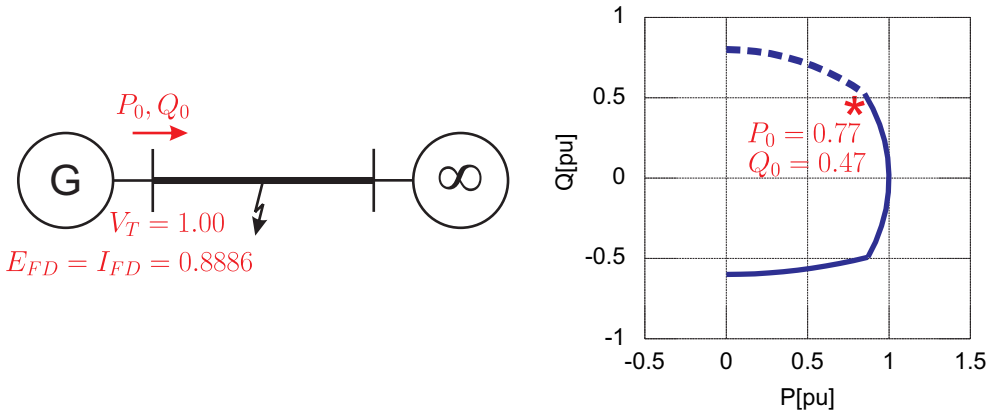

Figure 3.15: Test case of fault

generator currents reaches around 15 per unit value during the fault, then follows a stable swing after the fault is cleared.

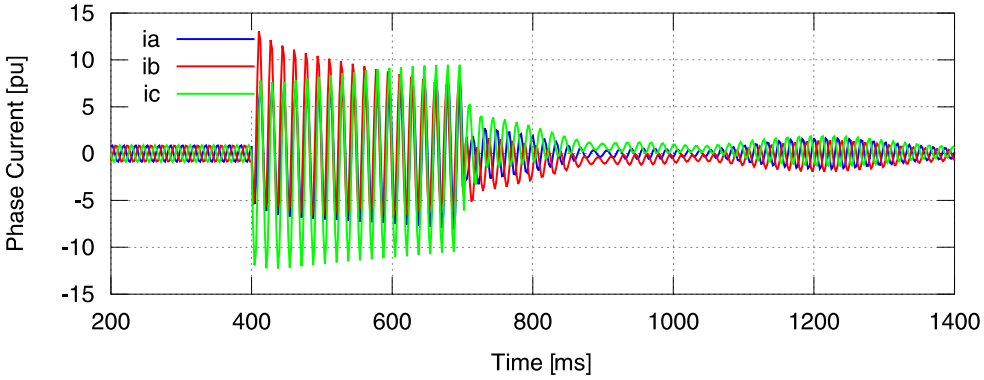

Figure 3.16: Instantaneous generator phase currents for fault case

The voltage measured at the generator terminal is shown in Figs. 3.17 and 3.18 in instantaneous and root mean square (RMS) form, respectively. The terminal voltage for phases B and C drops below 30%, corresponding to the faulted phases while the fault is present. Phase A voltage also drops to a level around 60% during the fault interval. The three phase voltages recover quickly after the fault is cleared.

The field current measured is shown in Fig. 3.19. The field current increase above the instantaneous level of 160% and oscillates as describer earlier. This current drops below the 160% level after the fault is cleared and also follows a lower frequency oscillation that corresponds to the power swing observed in the generator terminal currents.

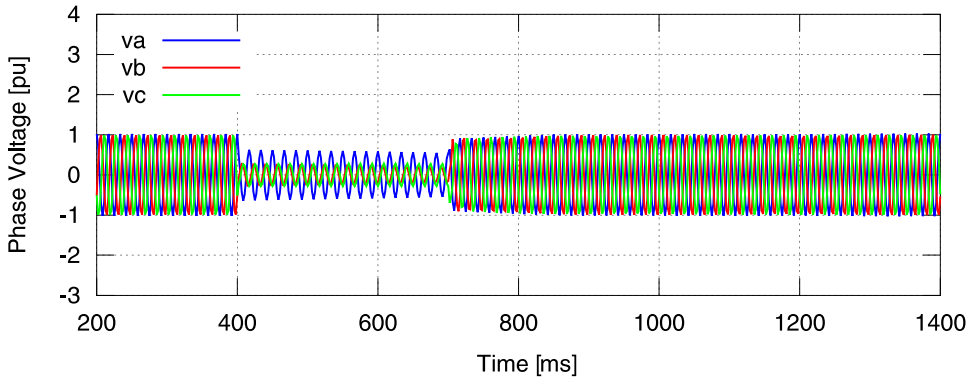

Figure 3.17: Instantaneous generator phase voltages for fault case

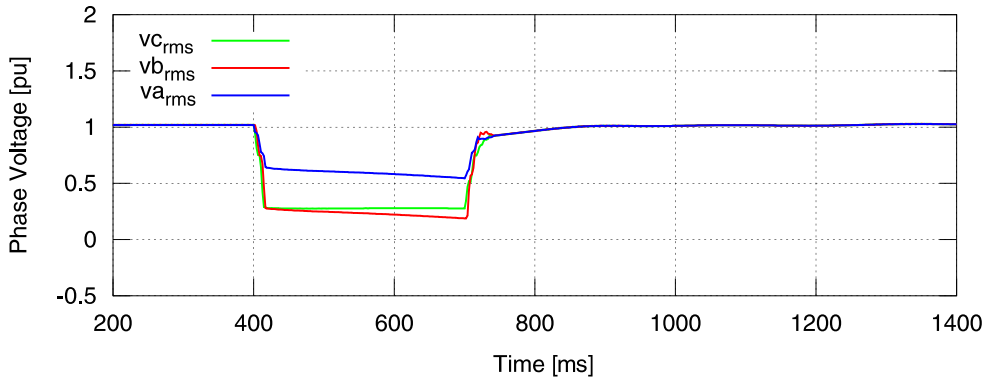

Figure 3.18: Instantaneous generator RMS phase voltages for fault case

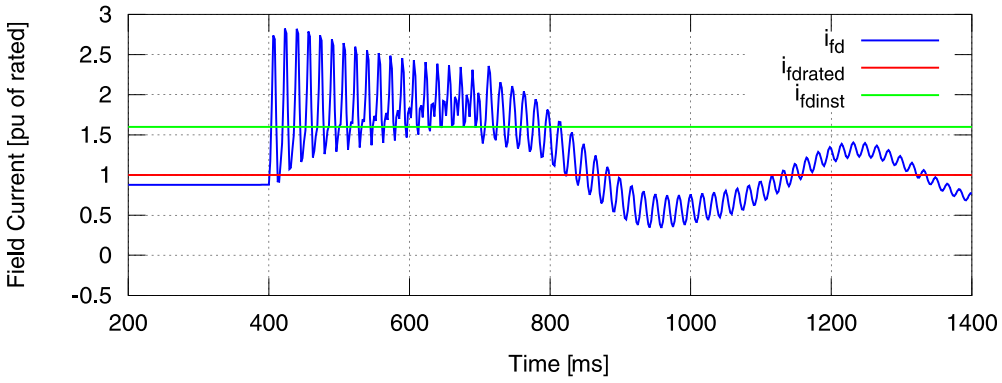

Figure 3.19: Instantaneous generator field current for fault case

The field voltage measured is shown in Fig. 3.20. This figure also shows the instantaneous excitation ceiling voltage, i.e., the maximum field voltage that can be applied at a given point in time. In Fig. 3.20, the ceiling voltage is initially around 346% of the rated value and drops to a level between 105 and 90% during the fault. The ceiling voltage is directly dependent on

the generator terminal voltage because the input to the rectifier of the exciter is taken from it. In Fig. 3.20, the field voltage applied initially tries to increase due to the AVR action, but is finally limited to the maximum allowed by the ceiling voltage. Also, this figure shows the limiting action starting at about time $t = 669ms$.

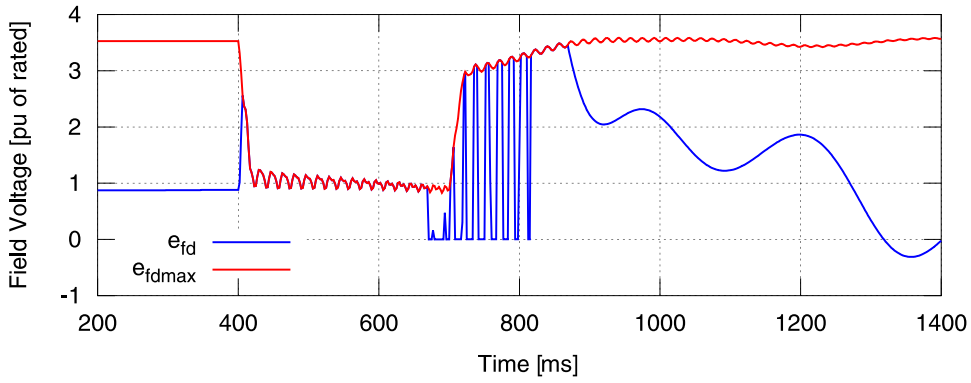

Figure 3.20: Instantaneous generator field voltage for fault case

The output of the integrator to measure field forcing time is shown in Fig. 3.21. The integrator is defined to allow $200ms$ of field forcing, but in this case the time is around $269 = (669 - 400)ms$. The larger time obtained is explained by the oscillations of the field current around the 160% level as described earlier. The integrating timer resets at time $t = 2348ms$ in this case.

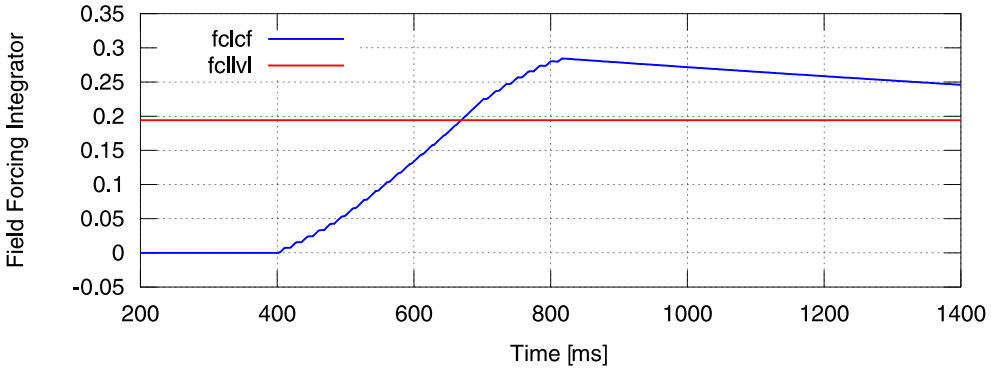

Figure 3.21: Field forcing integrator and limit for fault case

The field current limiting (FCL) signal is shown in Fig. 3.22. This signal is activated immediately after the integrating timer reaches 0.194. The FCL signal is not continuous

but pulsating because the field current oscillates around the instantaneous level of 160%. The FCL signal resets at around time t = 816 ms when the field current drops below the instantaneous level. Notice that although the FCL signal is reset, the integrating timer still allows limiting action if the field current is above the instantaneous level.

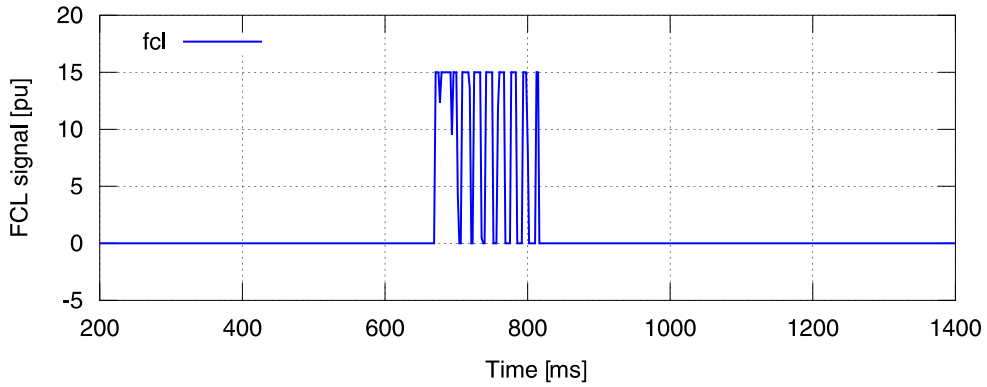

Figure 3.22: Field current limiting signal for fault case

The output of the inverse time integrator is shown in Fig. 3.23. This figure is provided as a reference because the test condition is significantly far from the thermal capability of the field rotor.

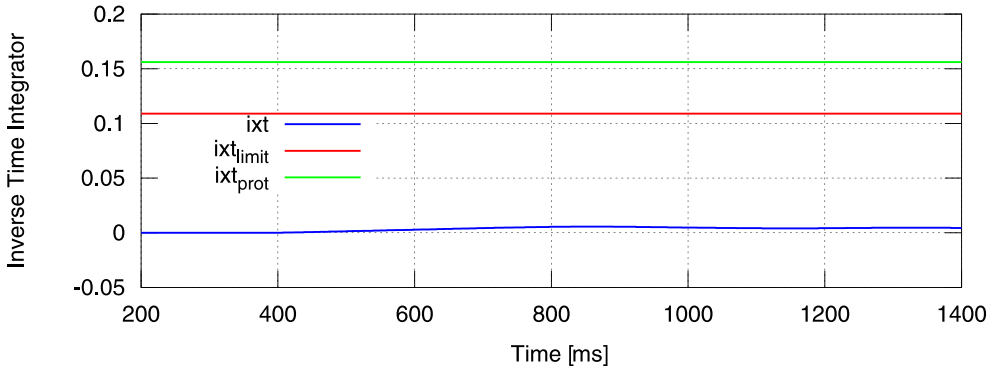

Figure 3.23: Inverse time integrator and limits for fault case

The logic flags corresponding to the inverse time and instantaneous integrators are shown in Fig. 3.24. The instantaneous flag picks up at the time $t = 669ms$; the inverse time flag does not pick up at all during the fault condition tested.

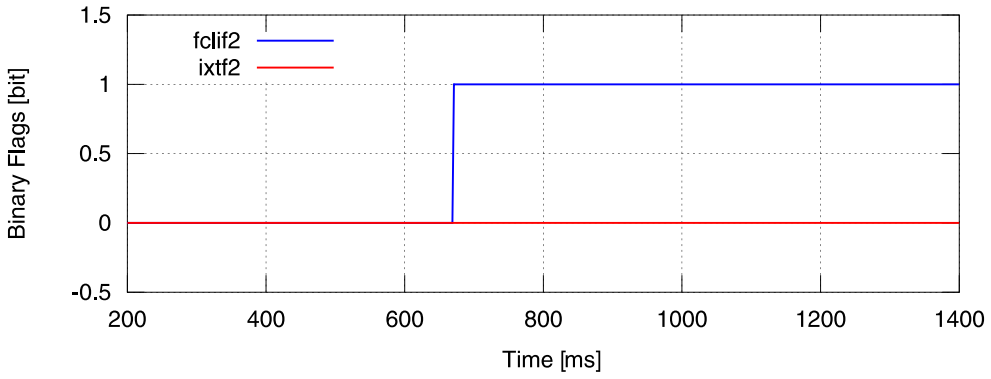

Figure 3.24: Inverse time and instantaneous OEL flags for fault case

3.5.3 Temporary Overload with Voltage Reduction Test

An overview of the system configuration and initial conditions for the overload test case is shown in Fig. 3.25. A large inductive load of 0.11 pu impedance is applied to the generator terminals at time $t = 400ms$. This inductive load is removed at time t = 25 s.

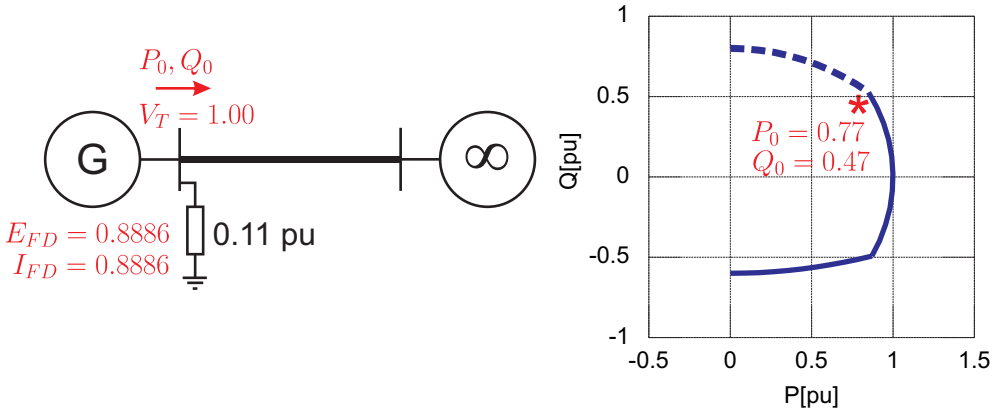

Figure 3.25: Test Case of Overload

The current measured at the generator terminal is shown in Fig. 3.26. In this figure, the generator currents reaches around 2.6 per unit value in phase B during the field forcing period, then stabilizes at about 1.9 per unit value during the instantaneous limiting period. At time $t = 12.1s$, this current begins to drop to 1.22 per unit due to the inverse time limiting action. The terminal current returns to normal after time $t = 25s$ when the overload condition is removed.

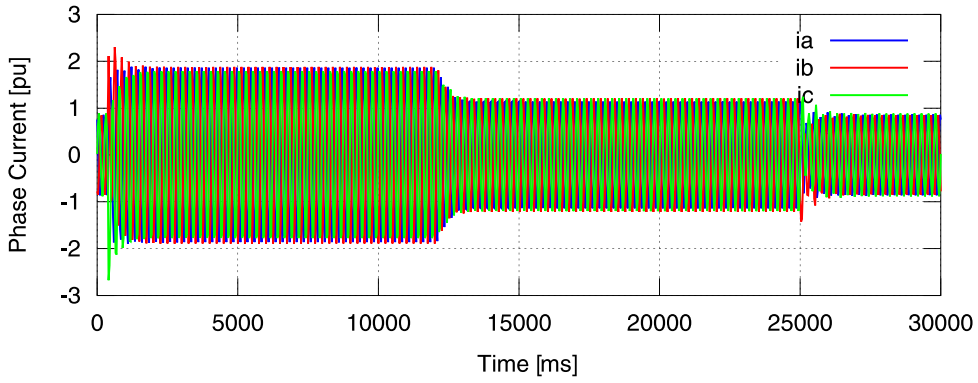

Figure 3.26: Instantaneous generator phase currents for fault case

The voltage measured at the generator terminal is shown in Figs. 3.27 and 3.28 in instantaneous and RMS form, respectively. Initially, the terminal voltage drops to about 70% for all phases. This initial voltage level is maintained during the field forcing and instantaneous limiting period. At time $t = 12.1s$, the voltage begins to drop to 66% due to the inverse time limiting action. The voltage finally recovers to the initial value when the reactive overload is removed at time $t = 25s$.

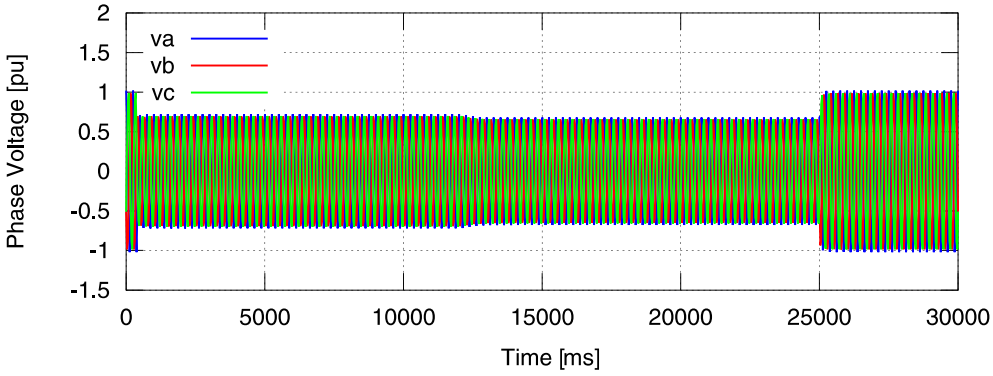

Figure 3.27: Instantaneous generator phase voltages for fault case

The field current measured is shown in Fig. 3.29. This current initially increases and oscillates around the instantaneous limit of 160% during the field forcing period and the beginning of the instantaneous limiting period. The field current stabilizes at the instantaneous limit at around time $t = 1.4s$ due to the instantaneous limiting action. At time $t = 12.1s$, the inverse time limiting action starts to reduce the field current to 100%. The change from the 160% to the 100% level is not instantaneous and takes about 700 ms. The

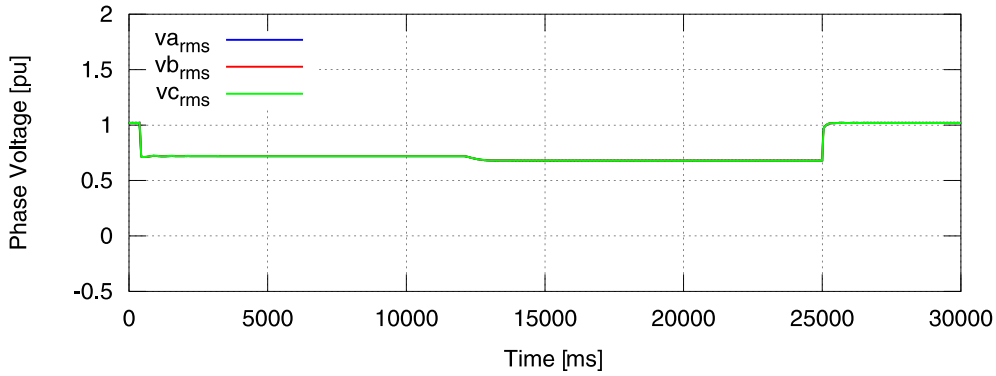

Figure 3.28: Instantaneous generator RMS phase voltages for fault case

field current remains at the 100% level until the overload is removed, then returns to the pre-disturbance level.

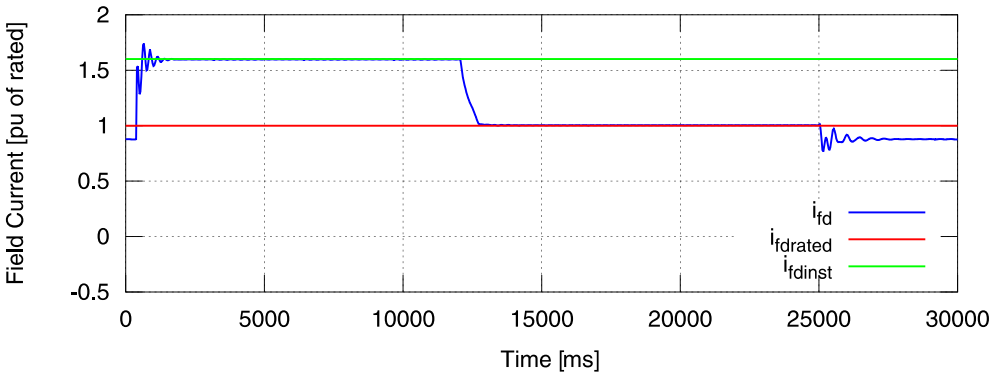

Figure 3.29: Instantaneous generator field current for fault case

The field voltage measured is shown in Fig. 3.30. This figure also shows the instantaneous excitation ceiling voltage. In Fig. 3.30, the ceiling voltage is initially around 353% of the rated value. The ceiling voltage drops to about 232% during the field forcing and instantaneous limiting period, then drops again to 228% during the inverse time limiting period, returning to normal when the overload condition is removed. The field voltage tries to increase at the start of the disturbance due to the AVR action, but is restricted by the ceiling voltage. The instantaneous limiting action starts at around time $t = 875ms$. The instantaneous limiting action is pulsating due to the fact that the field current is oscillating around the instantaneous limit of 160%. Inverse time limiting action starts at time $t = 12.1s$

by initially completely dropping the excitation voltage until time $t = 12.72s$ when the field current reaches the rated value of 100%. From this time onwards, the limiting action is maintained by keeping an excitation level lower than the one applied during the instantaneous limiting period. The field voltage returns to normal once the overload condition is removed at time $t = 25s$.

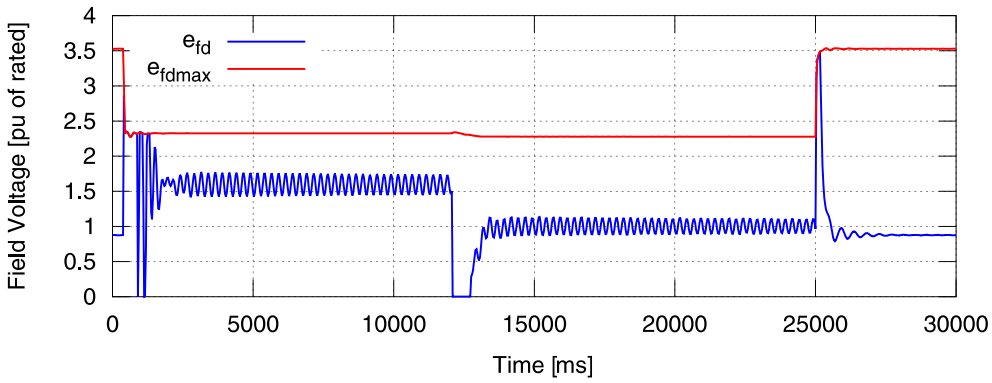

Figure 3.30: Instantaneous generator field voltage for fault case

The output of the integrator to measure field forcing time is shown in Fig. 3.31. The integrating timer picks up at time $t = 875ms$ when the integrator output reaches the 0.194 level. This implies a field forcing time of $475 = 875 - 400ms$. The integrating timer resets at time $t = 4619ms$ in this case. The instantaneous limiting action starts as soon as the integrating timer picks up and is maintained until the inverse time limiting action takes over at time $t = 12.1s$. That is, the logic implemented ensures that instantaneous limiting action remains, in spite of the integrating timer resetting at time $t = 4619ms$, as long as the field current is trying to increase beyond the instantaneous limit of 160% due to the AVR action.

The field current limiting signal is shown in Fig. 3.32. This limiting signal follows a pattern similar to the excitation voltage, showing the different periods such as field forcing, instantaneous limiting, inverse time limiting, and return to normal.

The output of the inverse time integrator is shown in Fig. 3.33. The inverse time picks up at time $t = 12.1s$ when the integrator output reaches the 0.109 limiting level. This

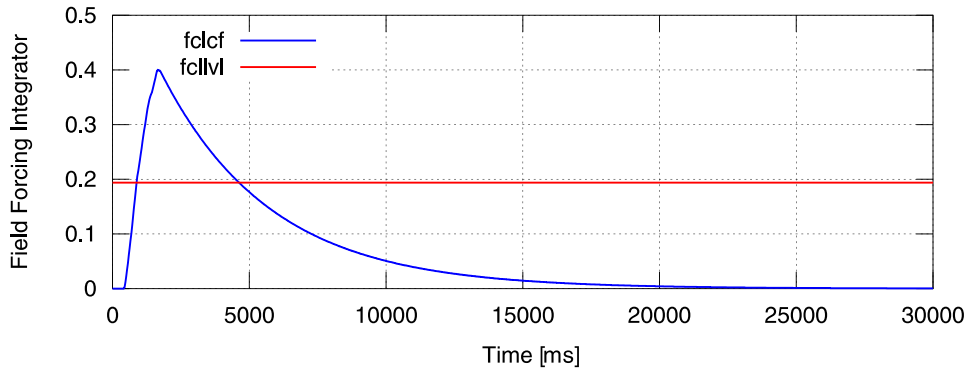

Figure 3.31: Field forcing integrator and limit for fault case

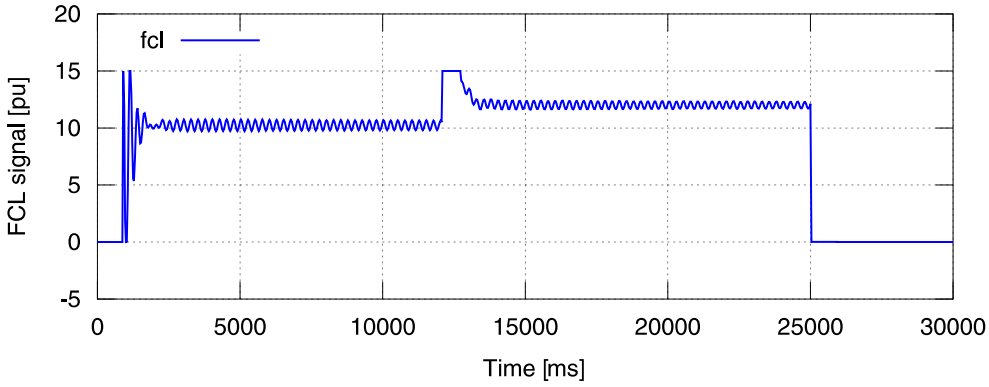

Figure 3.32: Field current limiting signal for fault case

timer slightly overshoots during the time that the inverse time limiter is driving the field current down to the rated 100% level. The margin between the protection level of 0.156 and the limiting level of 0.109 ensures that the inverse time limiter has enough time before protection would take action and trip the generator out of service. Fig. 3.33 also shows that the integrator drops very little during the inverse time limiting period, reaching 0.102 at time $t = 25s$. Once the overload is removed, the inverse time integrator drops slowly, reaching only 0.088 at time $t = 30s$. This behavior of the inverse time integrator would produce a faster pickup if a consecutive overload occurred.

The logic flags corresponding to the inverse time and instantaneous integrators are shown in Fig. 3.34. In this figure, the instantaneous limiting flag picks up at time $t = 875ms$ and the inverse time limiting flag picks up at time $t = 12.1s$. Both flags reset at time $t = 25s$ when the field current drops below 100% of the rated value.

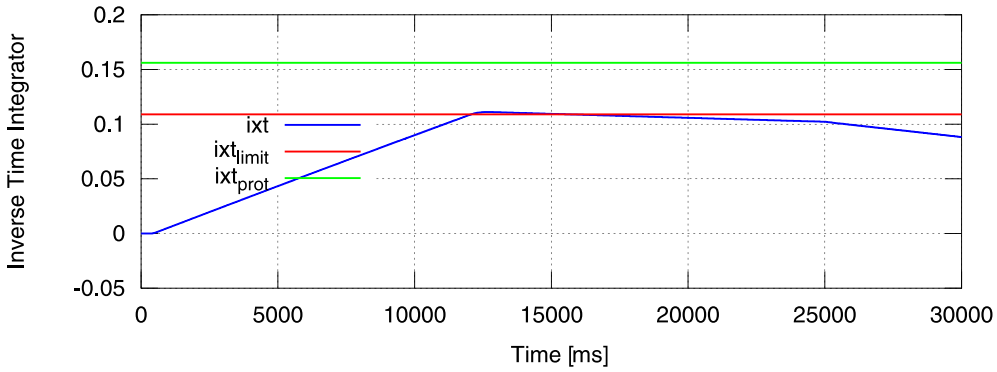

Figure 3.33: Inverse time integrator and limits for fault case

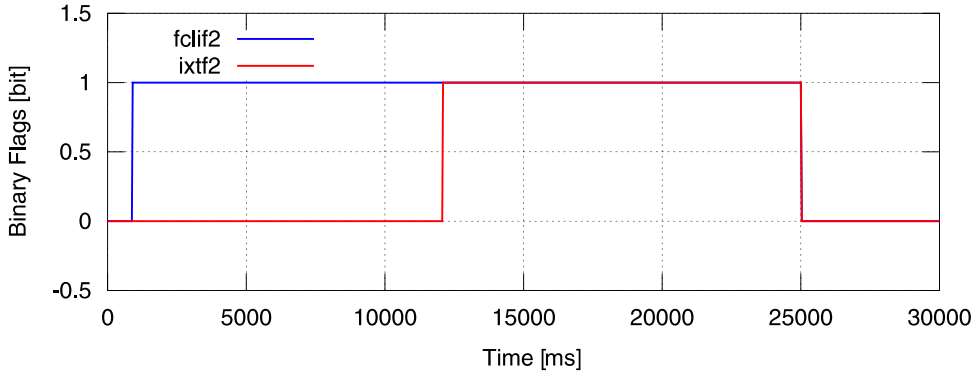

Figure 3.34: Inverse time and instantaneous OEL flags for fault case

3.6 Summary

In this section, coordination between the OEL limiter, AVR, and field overcurrent protection was discussed in some detail. Overexcitation capability and the interaction between control and protection functions associated with this capability were described. Modeling methods suitable for electromagnetic (high bandwidth) simulations using ATP/EMTP were presented. Analysis of the coordination performance was conducted for severe conditions in which coordination is required. This performance was verified by simulation, therefore modeling accuracy is very important. Current industry practices do not consider OEL models, and therefore no comparison was made with existing modeling methods.

This chapter proposes a more sophisticated OEL model that interfaces with the IEEE ST1A standard excitation model. The current ST1A model does not completely represent

the dynamics of OEL that occur in real situations. Dynamic coordination can be analyzed using this new OEL model, together with existing AVR, PSS, and protective relay models. An important contribution of the proposed model is that it can be used for electromagnetic simulations, i.e., high bandwidth simulations. Existing simplified OEL models used in the literature are intended for low bandwidth simulations only, such as transient stability or small signal stability analysis or programs. Another important contribution described in this chapter is verification of severe reactive overload scenarios that are not physically performed due to risk to the machine. These considerations become even more critical with round rotor machines.

The next chapter discusses loss of excitation protection and describes a new method for detecting loss of excitation conditions using a fast pattern classification method.

Chapter 4

Proposed Loss of Excitation Detection Algorithm

4.1 Loss of Excitation Condition

4.1.1 Risk to Machine and Power System

System impacts resulting from a loss of excitation condition depend on several factors, with the most important being the size of the generator unit, the system network, and initial operating conditions. The main effect of a loss of excitation is a reduction in the terminal voltage, which translates into a negative change in the reactive power supplied. Other reactive power sources in the surrounding area must supply the difference in reactive power to keep the system voltage at normal levels. If the machine size is relatively large, a loss of excitation event increases the risk of voltage instability in the surrounding area of the system network.

Another effect of a loss of excitation condition is a reduction in power flow due to reduced power transfer from rotor to stator. This reduction in power flow is caused by weakening of the magnetic coupling between the rotor and stator. In severe loss of excitation conditions, there is a risk of loss of synchronism of the affected machine. For a large machine, a loss of synchronism would produce severe power swing disturbances in the surrounding area of the system network and increase the risk of other machines also losing synchronism.

The impact of a loss of excitation on the affected machine is also very important. A reduction in excitation produces high stator currents and eddy currents in the end core

laminations, both of which cause overheating and increase the risk of permanent damage to the machine.

As stated earlier, a loss of excitation is followed by a loss of synchronism in severe cases, which may induce currents in the rotor due to the slip frequency, thus causing overheating. The loss of synchronism would also produce torque pulsations every time the rotor crosses the synchronously rotating stator field, increasing the risk of permanent damage to the machine shaft [135].

4.1.2 Detection Methods

The impedance measurement is one of the most widely used methods to detect loss of excitation conditions [136, 137]. This impedance is apparent, i.e., not a real impedance, but the ratio between voltage and current measured at the terminals of the generator. This detection method provides improved selectivity compared to earlier methods based on DC voltage and current [138]. The impedance is typically measured in the direction towards the power system network. The units used for this impedance are usually in per unit with generator ratings as the base.

The impedance measurement is based on voltage and current signals obtained from current and voltage transformers located at the generator terminals. From these signals, the fundamental frequency phasors are extracted using numerical techniques such as the Discrete Fourier Transform (DFT) . This impedance is analyzed considering its behavior in the impedance plane.

During a loss of excitation condition, the apparent impedance moves towards the negative imaginary axis [139], as shown in Fig. 4.1. The final impedance value towards which this impedance moves is not fixed and ranges between two values–the transient reactance X'_d, and the synchronous reactance X_d–depending on the load prior to the loss of excitation. For a higher load the final point moves closer to the transient reactance X'_d, while for a lighter load the final point moves closer to the synchronous reactance X_d. The final impedance never actually reaches the negative imaginary axis.

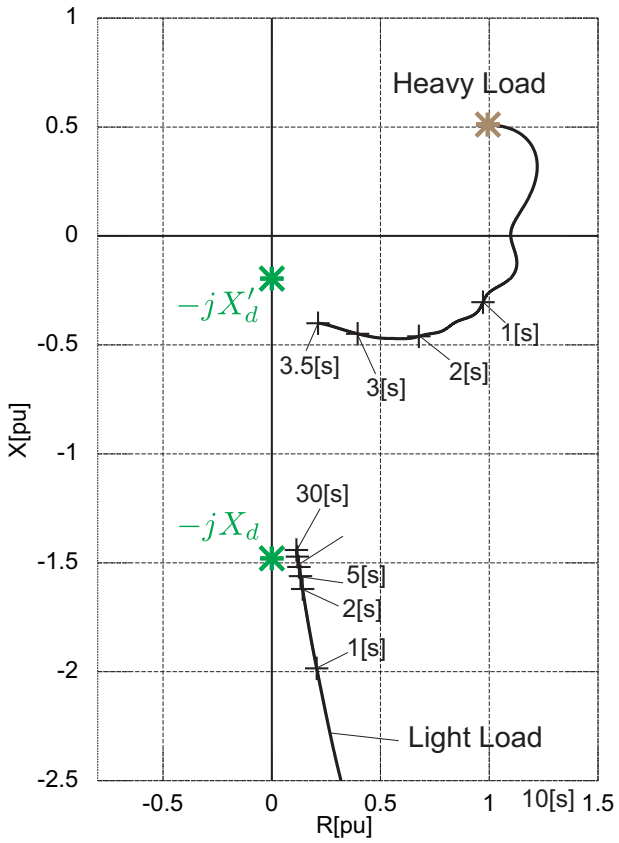

Figure 4.1: Behavior in the impedance plane for an LOE condition

One approach to detecting LOE conditions was proposed by Mason and uses a mho circle in the impedance plane. This approach is shown in Fig. 4.2. The mho circle encloses both the X_d and X'_d points in the negative imaginary axis. The Mason approach can detect an LOE condition for both a heavy or light initial load. The load condition has an impact on the detection time for an LOE condition. In the case shown in Fig. 4.2, the LOE is detected slightly after 2 s for a heavy load condition and in about 5 s for a light load condition. The mho zone maintains a safety margin with the generator capability curve (GCC), even for the lowest generator voltage condition, i.e., 95% of the rated voltage.

The actual tripping time is not the same as the detection time for security reasons that will be described in the next section. Typically, time delays between 0.5 to 2.0 s have been proposed to trip an LOE condition following the Mason approach. However, the maximum time to be applied is limited by the fact that the LOE protection function should trip

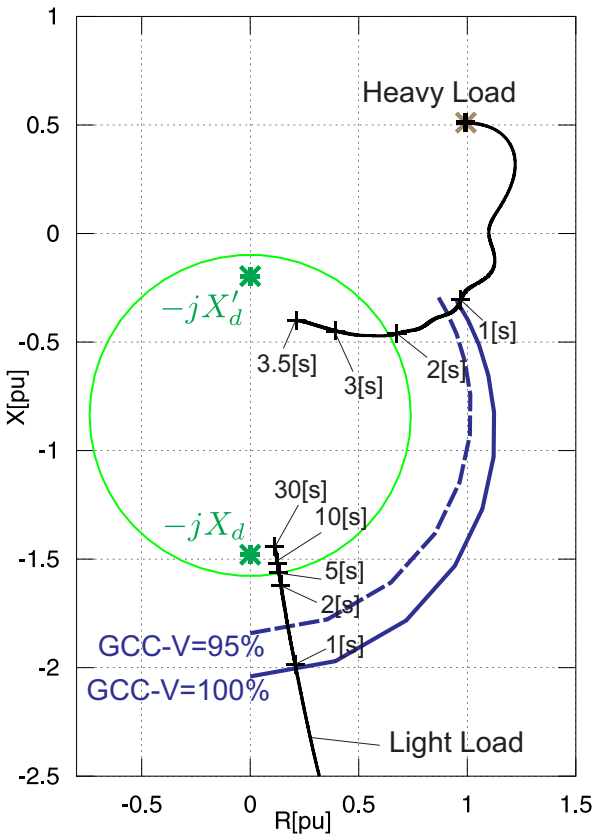

Figure 4.2: Detection of an LOE condition - Mason approach

the machine before the loss of synchronism that can occur in severe cases. In Fig. 4.2, the maximum time delay for an LOE results in about 1.5 s, measured from the time the impedance enters the mho zone at about 2.0 s to the time when loss of synchronism happens at about 3.5 s.

Another approach to detecting the LOE condition was proposed by Tremaine and Blackburn and uses a larger mho circle in the impedance plane supervised by two additional functions: directional and undervoltage. This approach is shown in Fig. 4.3. The mho circle encloses the origin in addition to the X_d and X'_d points in the negative imaginary axis. The Tremaine and Blackburn approach can detect LOE conditions for heavy and light initial loads. This approach provides a larger impedance region, and thus is more sensitive than the Mason approach. Additionally, this approach protects the machine from reaching the Steady State Stability Limit (SSSL) , while keeping some safe distance from the GCC curve

considering the lowest generating voltage condition.

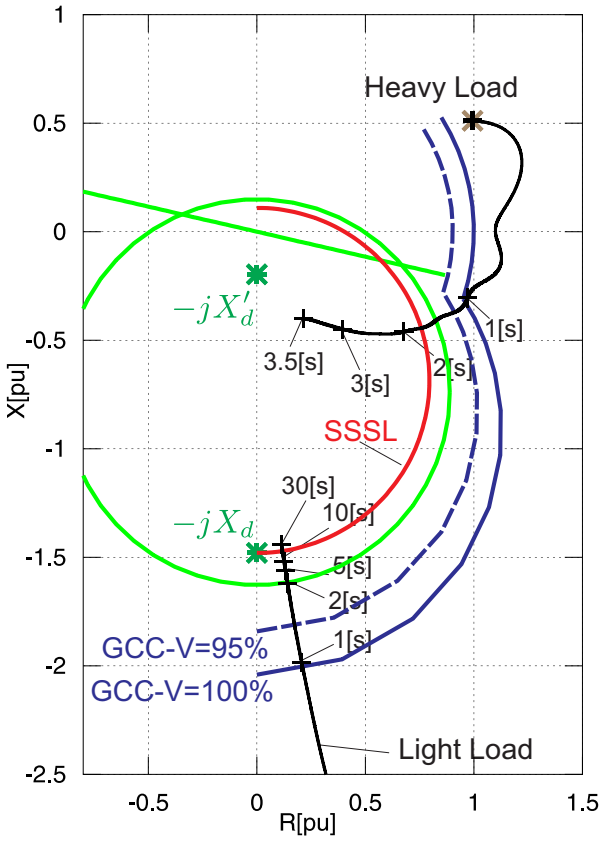

Figure 4.3: Detection of an LOE condition - Tremaine/Blackburn approach

4.1.3 Risk of Incorrect LOE Detection

The selectivity of LOE detection using mho impedance zones is not perfect, as other conditions may activate this detection function by temporarily entering the impedance region [140]. One such case is a power swing condition, which enters and leaves the LOE impedance zone for a short time compared to the time delay used in LOE identification. In this regard, the Mason approach is more secure compared to the Tremaine/Blackburn approach, due to the smaller area used in the impedance plane for LOE detection.

A power swing is typically a result of a disturbance that causes unbalance between electrical and mechanical power on a synchronous machine. Power oscillations, which may be stable or unstable, are produced. In the case of a stable power swing, the generator should

be allowed to recover; no false trips are desired as outage of the machine will impact the system causing even further oscillations. In the case of unstable power swings, a different protection function, i.e., the loss of synchronism function, is responsible for tripping the generator from the system.

The behavior of a stable power swing in the impedance plane is shown in Fig. 4.4. In this figure, the Mason approach for the detection of an LOE condition has been improved by Berdy to include an additional smaller zone that can operate faster [141]. Each zone uses an independent time delay to make the trip decision. A time delay range between 0.1 and 0.4 s has been proposed for this smaller zone trip decision. Thus, the Berdy improvement would trip the machine faster in the case of a more severe LOE condition. The larger zone in Fig. 4.4 is the original Mason approach.

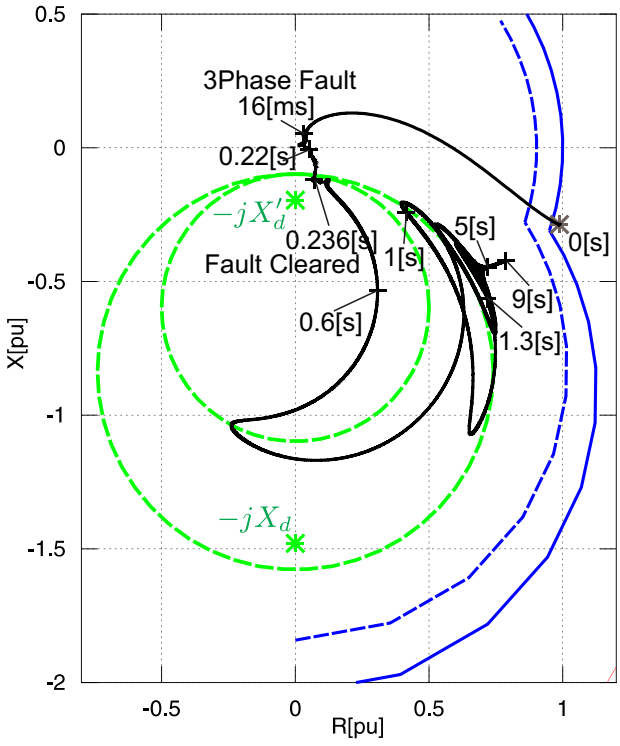

Figure 4.4: Stable power swing condition - Mason/Berdy approach

The pickup and trip times of the two LOE zones are shown in Fig. 4.5. In this example, the time delays used were 0.4 s for the smaller (LOE1) and 1.0 s for the larger (LOE2) mho zone. The large mho zone operates correctly by ignoring the power swing condition.

However, if a time delay between 0.5 and 0.6 s had been used, the large LOE zone would have maloperated by tripping the generator out of service. The small zone does maloperate when using the 0.4 s time delay, causing undesired tripping of the generator. In order to prevent the small zone from maloperating, a time delay longer than 0.6 s is required for this zone.

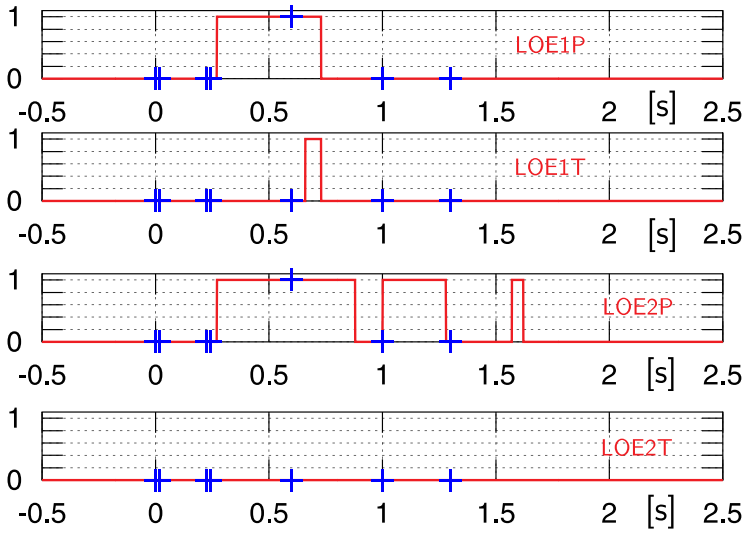

Figure 4.5: LOE zones 1 and 2 operation - Mason/Berdy approach

The discussion just presented illustrates some of the considerations required to find the correct settings for traditional LOE protection. It also highlights that the current industry practice for detection of LOE conditions must consider the dynamic performance of the generator specifically under study, but such information is not necessarily available at the present time.

4.1.4 Literature Review of Other Detection Methods

An alternative approach to combining time undervoltage in the AC and DC circuits was proposed by Lee et al. [142] for the Ontario Hydro system in 1979. Another approach that uses admittance instead of impedance is described by Herrman and Smit [143] from Siemens. Tambay and Paithankar [144] proposed the use of rate of change of the apparent reactance instead of time coordination. Furthermore, Li et al. [145] proposed the use of the δ angle

between the internal voltage and the equivalent source for identification of LOE and loss of synchronism conditions. Usta et al. [146] proposed the use of pre-calculated levels of reactive power and time delays for the detection of LOE conditions. Yaghobi et al. [147] proposed the use of a search coil to detect LOE by measuring the flux in the air gap of the machine. Shi et al. [148, 149] provide a reasonable comparison between the most common methods for detection of LOE conditions. Lee et al. [150] explain additional operational considerations that should be taken into account to reduce the risk of incorrect LOE detection. Siwang et al. [151] provide a discussion of the current IEEE recommendations with respect to setting the traditional LOE impedance zone. Morais et al. [152] evaluate an adaptive method using apparent reactance X and reactance change in time $\frac{dX}{dt}$ restricted to a square similar in size to the large negative offset Blackburn mho zone.

Application of modern digital and numerical techniques, such as adaptive filtering techniques, pattern classification techniques, artificial neural networks (ANNs), and fuzzy logic, to LOE protection has been very limited. In 1994, Sharaf and Lie [153] proposed a single-layered perceptron and a two-layer feed forward-based ANN for the identification of LOE and loss of synchronism conditions. The Sharaf and Lie classifier was based on the fast Fourier transform (FFT) of several synchronous machine variables, such as machine angle deviation, machine speed deviation, accelerating power deviation, output power, voltage, current, and apparent admittance. From the FFT result, only a few dominant components were used to assemble the input vector for the classification. This classifier produced multiple outputs: fault or normal, first swing instability or LOE, allowable clearing time (long or short), and type of LOE (short circuit or open circuit). The accuracy of this classifier ranged between 67 and 92%. In 2007, So et al. [154] proposed an algorithm to identify power swing conditions based on angular velocity and acceleration of the generator terminal voltage. In 2009, Bo et al. [155] proposed an ANN-based method for the identification of LOE conditions. In this method, the input features were the excitation voltage applied and the active power output. The accuracy of this classifier was on the order of 99%. In 2010, Morais et al. [156] proposed a method based on a fuzzy inference mechanism. In this method, the input variables are apparent impedance and generator terminal voltage. A set of rules is defined based on known

characteristic behaviours of these variables during an LOE condition. This method has a suggested accuracy of 100% in the identification of an LOE vs. power swing condition. In 2011, Bi et al. [157] proposed a method to dynamically modify the diameter of the mho LOE characteristic by using an estimate of the equivalent source impedance.

4.2 Support Vector Machine

The Support Vector Machine (SVM) is a classification method based on linear discriminant functions and has been used for pattern recognition [158]. The traditional methods for the detection of loss of excitation conditions, such as the Mason [136], Berdy [141], and Tremaine or Blackburn [137] methods that use mho impedance zones, could also be considered pattern classification methods. These traditional loss of excitation detection methods were developed based on studies of trajectories using simulation studies to define characteristics and regions in the impedance plane that allow the identification of loss of excitation from other conditions.

4.2.1 Pattern Recognition

Pattern recognition systems consist typically of several functions: sensing, segmentation and grouping, feature extraction, classification, and post-processing. Sensing is responsible for observing the objects of interest. Segmentation and grouping help to separate the objects from background information. Feature extraction obtains key information from the objects, i.e., features, to help the classification function. Classification is where the decision is made about the category of the objects. Post-processing consists of the actions performed based on the decision made by the classifier.

4.2.2 Linear Discriminant Functions

A linear discriminant function is one that uses a linear decision boundary surface, i.e., a hyperplane, that separates the two classes of data. Fig. 4.6 illustrates the classification

concept using the SVM technique.

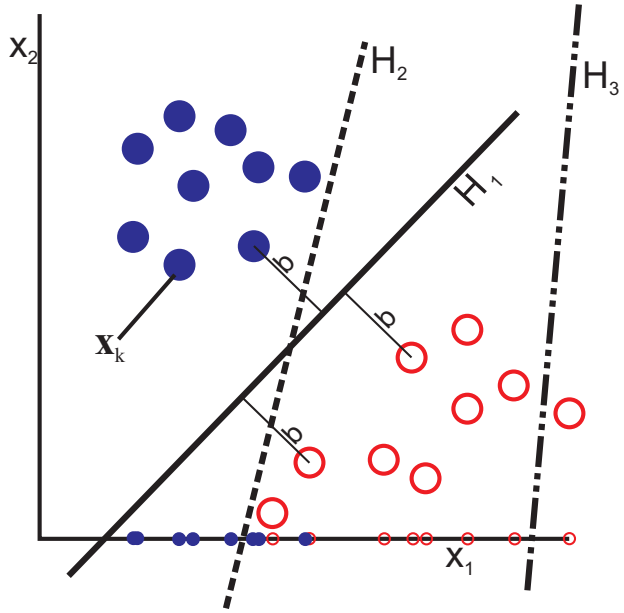

Figure 4.6: Support Vector Machine classification concept

In Fig.4.6, hyperplanes H_1 and H_2 separate the two classes of data, whereas hyperplane H_3 does not. The class of the data depends on which side of the hyperplane a given data vector $\mathbf{x}_k$ is located. A point $\mathbf{x}_p$ located in the hyperplane satisfies equation (4.1).

$$\mathbf{w}_T\mathbf{x}_p + w_0 = 0 \tag{4.1}$$

The data vector $\mathbf{x}_k$ is the pattern to be classified.

4.2.3 Feature Vector

The data vector $\mathbf{x}_k$ is also known as a feature vector because its coordinates are the values of key selected object features to help the classification process. In Fig. 4.6, the coordinates x_1 and x_2 are the values of the features used for classification. From Fig. 4.6, it can be seen that the separation between the two sets of data vectors depends on the quality of the feature chosen. In Fig. 4.6, for instance, it is not possible to obtain good classification

based on the x_1 coordinate alone; therefore, coordinate x_2 is needed. The distance from a data vector to the hyperplane is given by equation (4.2), where b is the minimum distance from any data vector to this hyperplane.

$$\left| \frac{\mathbf{w}^T}{\|\mathbf{w}\|}(\mathbf{x}_k - \mathbf{x}_p) \right| = \left| \frac{\mathbf{w}^T\mathbf{x}_k + w_0}{\|\mathbf{w}\|} \right| \geq b \tag{4.2}$$

The hyperplane parameters $\mathbf{w}$ and w_0 are defined such that the data vector $\mathbf{x}_k$ satisfies one of the two inequalities (4.3) and (4.4), depending on which side of the hyperplane it is located. The category of a particular data vector $\mathbf{x}_k$ is given by the value of z_k. The two inequalities (4.3) and (4.4) can be combined into one resulting in (4.5). Combining (4.2) and (4.5) provides the relationship (4.6) between the minimum distance b and the normal vector $\mathbf{w}$.

$$\mathbf{w}^T\mathbf{x}_k + w_0 \geq +1 \Longrightarrow z_k = +1 \tag{4.3}$$

$$\mathbf{w}^T\mathbf{x}_k + w_0 \leq -1 \Longrightarrow z_k = -1 \tag{4.4}$$

$$z_k(\mathbf{w}^T\mathbf{x}_k + w_0) \geq +1, \quad k = 1, .., n \tag{4.5}$$

$$\frac{z_k(\mathbf{w}^T\mathbf{x}_k + w_0)}{\|\mathbf{w}\|} \geq b = \frac{1}{\|\mathbf{w}\|} \tag{4.6}$$

4.2.4 Training Methods

Training of the classifier consists of finding a hyperplane that separates the two classes of data. The training is performed using vectors from both classes and whose categories are

known up front. A trained classifier produces zero classification error when the two classes of data are separable. In a separable case, there may be multiple hyperplanes that separate the two classes. The SVM method finds an optimum separating hyperplane that maximizes the distance b. In Fig.4.6, both hyperplanes H_1 and H_2 separate the two classes of data, but only H_1 maximizes the distance b and is therefore optimum. From (4.6), this is equivalent to minimizing the vector norm $\|\mathbf{w}\|$ subject to the constraints (4.5). Using the Lagrange method to minimize $\|\mathbf{w}\|$ results in (4.7). Note that the Lagrange multipliers α_k in (4.7) are restricted to values greater or equal to zero because of the constraints in (4.5). Also, note that n is the number of training vectors. From the duality principle, the problem in (4.7) becomes an optimization problem with respect to $\boldsymbol{\alpha}$ instead of with respect to $\mathbf{w}$ and w_0 as described in (4.8). Applying the two conditions to the right-hand side of (4.8) to the Lagrange function in (4.7) results in (4.9) and (4.10).

$$L(\mathbf{w}, w_0, \boldsymbol{\alpha}) = \frac{1}{2}\|\mathbf{w}\|^2 - \sum_{k=1}^{n} \alpha_k [z_k(\mathbf{w}^T \mathbf{x}_k + w_0) - 1], \qquad \alpha_k \geq 0, \forall k \tag{4.7}$$

$$\min_{\mathbf{w}, w_0, \nabla_{\boldsymbol{\alpha}} L = 0} L(\mathbf{w}, w_0, \boldsymbol{\alpha}) \longleftrightarrow \max_{\boldsymbol{\alpha}, \nabla_{\mathbf{w}} L = 0, \frac{\partial L}{\partial w_0} = 0} L(\mathbf{w}, w_0, \boldsymbol{\alpha}) \tag{4.8}$$

$$\nabla_{\mathbf{w}} L = 0 \longrightarrow \mathbf{w} = \sum_{k=1}^{n} \alpha_k z_k \mathbf{x}_k \tag{4.9}$$

$$\frac{\partial L}{\partial w_0} = 0 \longrightarrow \sum_{k=1}^{n} \alpha_k z_k = 0 \tag{4.10}$$

Substituting (4.9) and (4.10) into (4.7) gives (4.11), which is subject to the constraints given by (4.12).

$$L(\boldsymbol{\alpha}) = \sum_{k=1}^{n} \alpha_k - \frac{1}{2} \sum_{k=1}^{n} \sum_{l=1}^{n} \alpha_k \alpha_l z_k z_l \mathbf{x}_k . \mathbf{x}_l \tag{4.11}$$

$$\sum_{k=1}^{n} \alpha_k z_k = 0 \qquad \alpha_k \geq 0, \forall k \tag{4.12}$$

Solution of (4.11) and (4.12) requires solving a quadratic programming problem of the form given in (4.13)

$$L(\boldsymbol{\alpha}) = -\frac{1}{2}\boldsymbol{\alpha}^T \mathbf{H}\boldsymbol{\alpha} + \mathbf{c}^T\boldsymbol{\alpha} \tag{4.13}$$

where

$$H_{kl} = z_k z_l \mathbf{x}_k.\mathbf{x}_l \quad , \quad k, l = 1, .., n \tag{4.14}$$

$$\mathbf{c}^T = [1, 1, .., 1]_{1\times n} \tag{4.15}$$

Once $\boldsymbol{\alpha}$ is known, the values of $\mathbf{w}$ and w_0 are easily obtained using (4.9) and (4.5). The data vectors $\mathbf{x}_k$ located exactly at a distance b from the hyperplane are known as support vectors. The Lagrange multipliers α_k corresponding to the support vectors may be greater than zero whereas all other multipliers must be zero. The number of support vectors is typically much less than the total number of training vectors.

4.2.5 Mapping Functions

If the data are not separable in the original space, mapping functions such as polynomial functions, Gaussian functions, and so on are used. By doing this, the vectors can be mapped to a higher dimensional space where the two classes are linearly separable. In this newly mapped space, the hyperplane is constructed and the methods described before can be applied to find the SVM classifier. Compared to the ANN, the SVM has advantages of being

not as complex and having training needs that are not as demanding. In this work, superior classifications could be achieved with an SVM by proper selection of input features without the need for applying a more complex ANN.

4.3 Feature Selection Specific to LOE Behavior

An alternative approach to traditional time coordination is proposed in this work. It can be seen from Figs. 4.1 and 4.4 that the trajectories for an LOE condition and for a power swing condition have some noticeable differences. These differences are with respect to the path and the duration of the two types of disturbances in the complex plane plot (Figs. 4.1 and 4.4). One of the contributions of this work is the identification of such differences to find the appropriate features of each disturbance, and this is described in detail in the following section.

This work uses the SVM pattern recognition method to distinguish an LOE from a stable power swing or other conditions. With this new approach, there is no need to use additional elements, such as a second smaller zone and directional or undervoltage elements. Time coordination is also improved.

4.3.1 Selection of Level of Calculation

The features are based on measurements of the fundamental frequency voltage and current made over a given time window. The level of calculations performed to obtain the features is important to determine the quality of these features in classifying the desired conditions.

4.3.1.1 Raw Samples: V or I

The measurement of currents and voltages results in raw samples collected a rate of 15,360 Hz. Three phase voltages and three phase currents are measured to obtain six sets

of samples at each sampling time. Prior to sampling, the analog signals are filtered by a low pass anti-alias filter with a cutoff frequency of 7680 Hz. The raw samples taken directly represent a wide spectrum of frequencies. However, from prior knowledge about the LOE phenomenon, the most important behaviour to observe is that of the fundamental frequency. Thus, it was decided that the use of raw samples as direct input to the classifier would not be optimum as it would place an additional burden on the classifier with respect to performing the fundamental frequency estimation.

4.3.1.2 Phasor Calculations

The fundamental frequency phasors are calculated for each of the three current and three voltage channels. These calculations are made using Discrete Fourier Transform (DFT) with a window of 256 samples. The sampling rate of 256 samples per cycle is a typical speed for state of the art numerical relay technology. By observing the behavior of the voltage or current phasors, a general relationship to clearly distinguish an LOE condition from others was not immediately obvious. Using prior knowledge of the LOE phenomenon, a combination of voltage and current, such as impedance, was found to be a more meaningful parameter for the proposed classification method.

4.3.1.3 Positive Sequence

The initial approach in this work was to use only one phase of voltage and current, i.e., phase A. One phase is enough for detection of an LOE condition because it is typically a balanced three phase condition. However, the proposed classification method must be stable for any type of disturbance, such as power system faults that in most cases are unbalanced conditions. The positive sequence is a combination of the three phases and attenuates the effect of unbalanced conditions, such as faults; thus, it was selected as a more appropriate feature for the proposed classifier. During an LOE condition, the positive sequence values are identical to the single phase values.

4.3.1.4 Additional Filtering

The phasors are calculated every time a new sample is available, i.e., every 65.1 μs. However, the LOE detection can be performed with a lower time resolution on the order of $50ms$ because the decision needs to be made within 0.5 to 1.0 s. This is equivalent to downsampling the phasor real and imaginary component signals from 15,360 Hz to 20 Hz. Transient conditions such as transitions from prefault to fault, transitions from fault to power swing, fault conditions, and power swing conditions are relatively fast compared with the $50ms$ resolution. To avoid errors caused by transient conditions, anti-alias filtering is performed by a low pass filter with a cutoff of 10 Hz.

4.3.1.5 Impedance (Z) / Power (S)

The apparent impedance Z is calculated based on the positive sequence voltage and current phasors to observe its behaviour in the complex impedance plane. The apparent power S is also calculated using the same positive sequence voltage and current phasors to observe its behaviour in the complex power plane. The apparent impedance Z and power S are scaled to per unit using the generator ratings as base values. The impedance Z and power S are not used as direct inputs to the classifier because their values alone are insufficient to produce a good classification.

4.3.2 Time Window

Selection of the time window is important and two parameters need to be balanced: length of time and number of points. A longer time window provides more information, but a shorter time window results in a faster decision. More points mean more detail is captured, while fewer points result in fewer calculations. A time window of 1.0 s is used in the proposed classification method, i.e., a total of 20 measurements each one taken every 50 ms. It should be noted that 1.0 s is a typical time used in traditional LOE detection methods.

4.3.3 Behavior of Z or S

As discussed before, one of the key contributions of this work is finding the actual features that are useful for distinguishing a power swing from an LOE condition. This was based on observing the trajectories of the two conditions in the complex power plane and the impedance plane. The time measurements were taken with a resolution of $^1/_{4th}$ of one millisecond or better.

4.3.3.1 First Feature

This feature was obtained by looking at the trajectories in the impedance plane. In Figs. 4.1 and 4.4, the points outside the mho zone are not considered an LOE condition. Therefore one feature chosen is the distance in the impedance plane from the most recent point in the 1.0 s window to the centre of the traditional large mho zone, as described in (4.16). In (4.16), Z_{19} is the most recent impedance measurement in the 1.0 s window. However, this feature alone is not enough for a complete classification because, in cases such as that of Fig. 4.4, a power swing condition may enter the mho zone.

$$x_1 = \left| Z_{19} - \frac{(-jX_d - jX'_d)}{2} \right| \tag{4.16}$$

4.3.3.2 Second Feature

This feature and the following two features are found by looking at the behaviour of the LOE condition and the power swing condition in the power plane, as shown in Figs. 4.7 and 4.8. As a reference, the corresponding behaviour of the apparent impedance, i.e., the first feature, as well as the active and reactive power plotted as function of time are shown in Figs. 4.9 and 4.10. It is interesting to note in Figs. 4.7 and 4.9 that the active power increases during the fault condition, causing a slow down of the machine and bringing it into the motoring region temporarily as soon as the fault is cleared, which explains the negative power observed. In Figs. 4.7 and 4.8, the generator capability curve (GCC) is plotted at

rated voltage conditions. The GCC is not constant and varies with the generator terminal voltage.

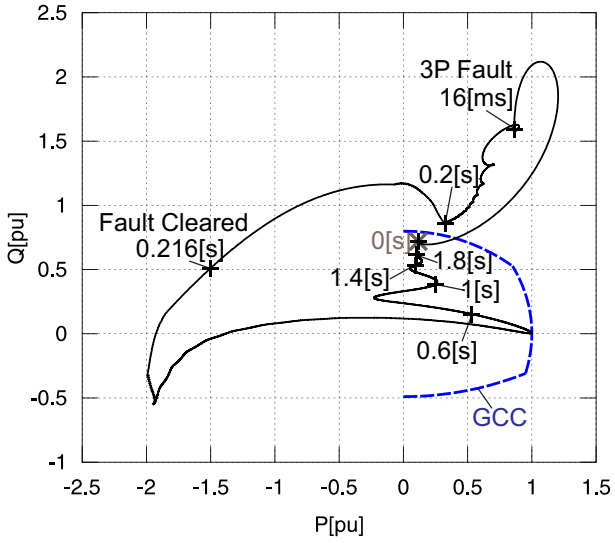

Figure 4.7: Behavior of power swing conditions in the power plane.

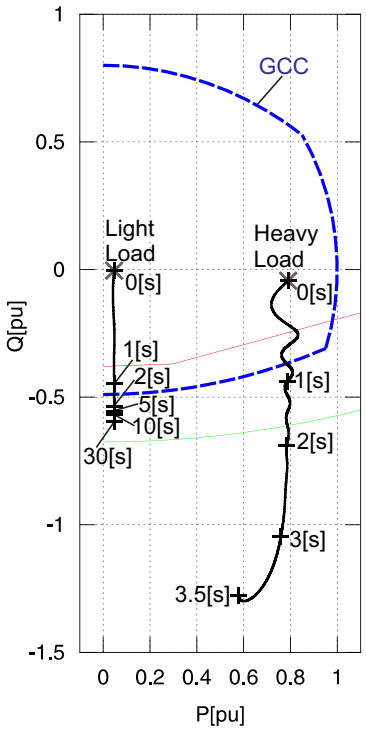

Figure 4.8: Behavior of LOE conditions in the power plane.

From Fig. 4.8, we can see that the trajectory for an LOE follows a negative imaginary

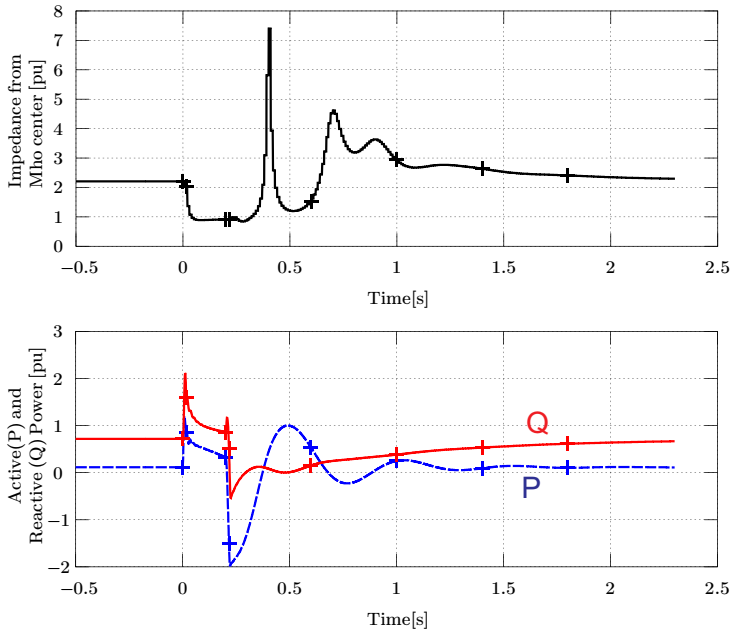

Figure 4.9: Impedance and active and reactive power for stable power swing condition.

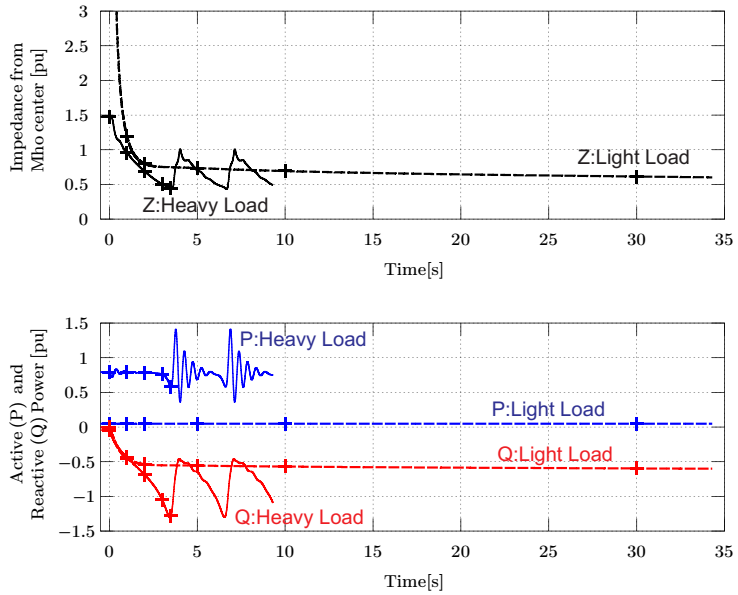

Figure 4.10: Impedance and active and reactive power for LOE conditions.

direction. However, this behaviour is only valid up to the time the machine loses synchronism at about 3.5 s, as seen in Fig. 4.10. In contrast, Fig. 4.7 shows the trajectory for a power swing follows a positive imaginary direction if the prefault condition ($t < 0s$), transition between prefault to fault condition ($t = 0.0 - 16.0ms$), fault condition ($t = 16ms - 2s$), and

the transition from fault to the power swing ($t = 0.2 - 0.216s$) are disregarded. Therefore, the next feature is chosen as the imaginary component of the total displacement in the 1 s window, as described in (4.17).

$$x_2 = \Im\{S_{19} - S_0\} \tag{4.17}$$

In (4.17), S_0 and S_{19} are the oldest and the most recent apparent power measurement points, respectively, in the 1.0 s window. It should be noted again that this feature alone is not enough to classify an LOE condition correctly because the 1.0 s window includes the transition and the fault conditions that must be isolated.

4.3.3.3 Third Feature

From Figs. 4.7 and 4.8, it can also be noted that an LOE has a more direct path, that is, closer to a straight line, compared with a power swing condition. The more direct path means that the total length travelled in the path for a given time window is closer to the length of a straight line from the start to end of that path. Therefore, the feature chosen is the ratio between these two values and is described mathematically in (4.18). The value of the ratio for a more direct path will be a number closer to 1.0.

$$x_3 = \frac{\sum_{i=1}^{19} |S_i - S_{i-1}|}{|S_{19} - S_0|} \tag{4.18}$$

The feature just described above is useful for identifying the power swing condition period (Fig. 4.7). Let us consider the time window from 0.216 to 1.216 s in Fig. 4.7. This time window includes the power swing condition. It can easily be seen that the value of x_3 will be much larger than 1.0.

It is worth mentioning that the characteristics during the transition periods from prefault to fault (0.2-0.255 s) and from fault into the power swing (0.4-0.425 s) are primarily influenced

by the response of the full cycle DFT phasor estimation method. For instance, the transition from prefault to fault is practically instantaneous in the time domain, that is, a fraction of a millisecond. During this transition, the DFT window uses samples collected from prefault and fault, therefore producing phasor values in between these two conditions.

The first three features were able to discern LOE conditions from other conditions in most cases, except during the transition periods just described. To overcome this, an additional feature was chosen and is described below.

4.3.3.4 Fourth Feature

From Figs. 4.8 and 4.10, it can be seen that the point in the path moves relatively slowly during an LOE condition before loss of synchronism occurs. That is, no large sudden changes are observed during an LOE condition. This fact is included as a feature and is chosen based on the maximum change in the path over two consecutive points during the 1.0 s window. The fourth feature is then calculated as the distance that would be travelled if that maximum change was constant over the 1.0 s as described in (4.19). A faster movement produces a larger value of this feature.

$$x_4 = (N-1)\max\left(|S_i - S_{i-1}|\right) \quad , \quad N = 20, i \in [1..(N-1)] \tag{4.19}$$

4.3.3.5 Proposed Feature Vector

Overall, the proposed feature vector has four coordinates, as shown in (4.20), and each coordinate is described mathematically by the relationships (4.16) - (4.19).

$$\mathbf{x}_k = [x_1,\ x_2,\ x_3,\ x_4] \tag{4.20}$$

The performance of the features presented for LOE in Fig. 4.8 and for stable power swing conditions in Fig. 4.7 are illustrated in Figs. 4.11 and 4.12. The first feature drops

below 1.0 *pu* during an LOE condition before a loss of synchronism occurs. However, this same feature also drops temporarily during a power swing condition. The second feature is negative during an LOE condition, although its value eventually becomes very small for a light load condition. During a power swing condition, this feature may also become temporarily negative. The third feature is a value close to 1.0 for an LOE condition. This feature is larger than 1.0 during a power swing, but this difference is not as noticeable while the fault is present ($t = 0 - 0.2s$). The fourth feature is clearly about 1.0 *pu* during the LOE condition. This same feature is larger than 10 *pu* for a stable power swing condition, which especially helps during periods of rapid change in the variables considered.

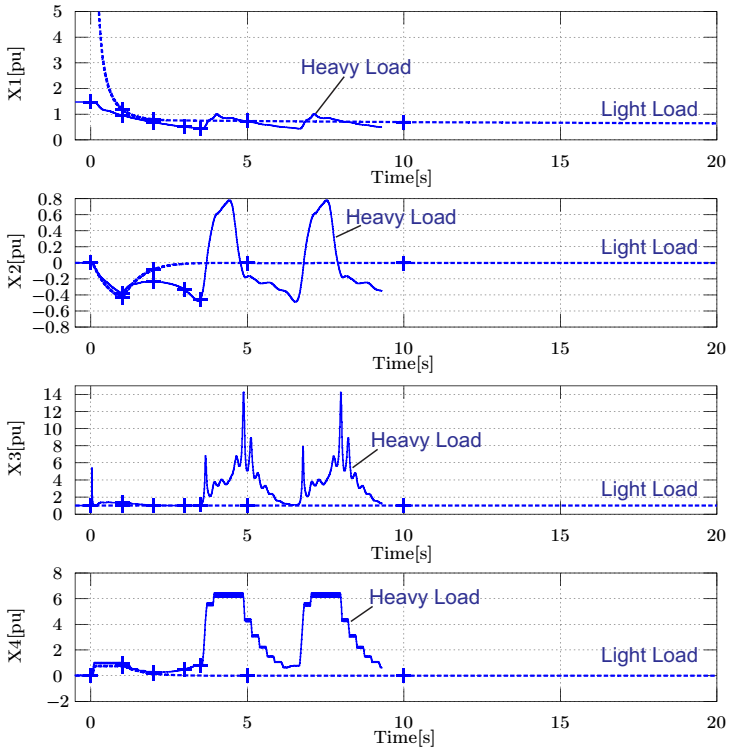

Figure 4.11: Behaviour of features for LOE conditions.

The majority of the techniques using SVMs for power systems fault analysis techniques use generic higher dimension mapping functions such as Gaussian or polynomial functions to separate the data vectors. However, the features described in this thesis using (4.20) [1] were obtained by looking at the actual characteristics and mapping the original time-domain samples instead of just using generic mapping functions. This helped in obtaining better

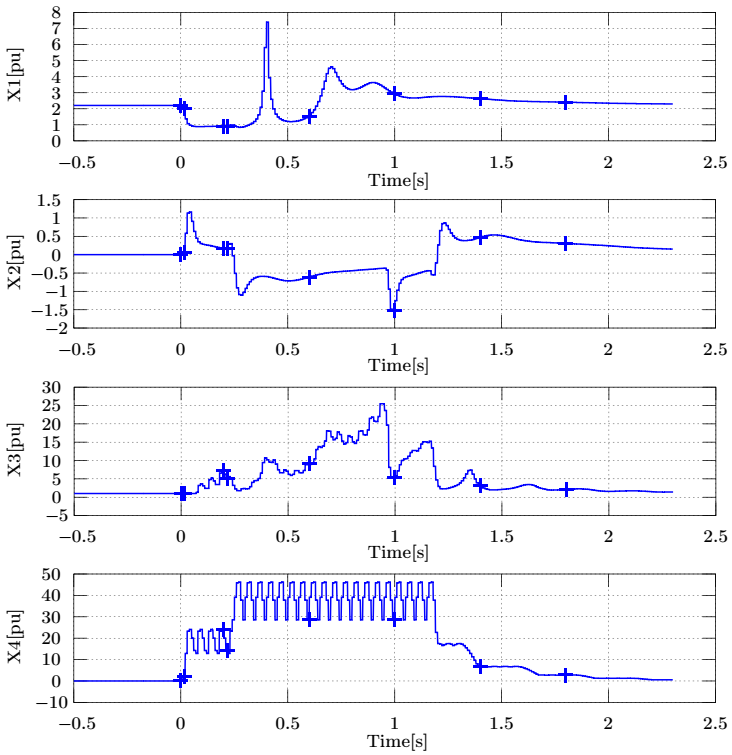

Figure 4.12: Behaviour of features for power swing conditions.

classification accuracy.

4.4 Training Considerations

The training consists of finding the hyperplane parameters $\mathbf{w}$ and w_0 of the desired classifier using the SVM method.

4.4.1 System Modeling

A generator connected to an infinite bus through a power line is used. A time-domain model of the synchronous machine using $dq0$ transformation is used to represent the generator. The mechanical behaviour is represented by a lumped mass. The prime mover and excitation controls are set in manual mode during the simulation for the following reasons. For prime mover control, the time constants are relatively large compared to the simulation

time so there is no need to include the prime mover dynamics in the simulation model. When the excitation control is in manual mode, the worst swing scenarios can be easily generated. Here, the worst swing condition means that the impedance obtained is closer to and inside the LOE impedance region during a stable power swing condition. The power line is represented by a lumped impedance. A fault resistance is connected at 50% of the line. For simplicity, a step up transformer is not included; regardless, the proposed method is expected to work with or without the presence of this power transformer.

4.4.2 Initial Conditions

To make the classifier more general, the training cases consider all limits of the GCC. A total of six cases are used, combining load and power factor variations such as high and light load and leading, lagging, and unity power factors. To achieve these initial load conditions, two parameters are varied:

- Voltage magnitude, within $+/-5\%$.
- Angle, within a 90° stability limit and the generator leading the infinite bus.

The initial loads used are illustrated in Fig. 4.13. These loads are located as close as practically possible to the specified conditions. For instance, there is no need to achieve an absolute unity power factor but to be as close as possible during training.

4.4.3 Selection of Disturbances

Stable power swing conditions are obtained by applying a three phase short circuit and removing it after a short period of time. For generating the power swing cases, the following two considerations are taken into account:

- The impedance temporarily enters the LOE mho zone during the power swing.
- The system actually recovers, that is, returns to a stable condition.

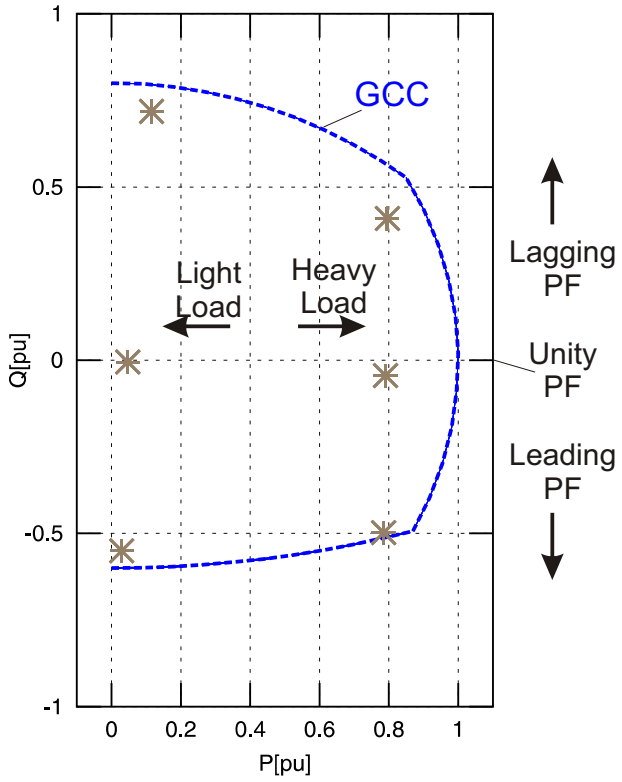

Figure 4.13: Initial loads in the PQ plane.

The LOE conditions are obtained by using the following sequence:

- Starting with an initial load, the field voltage is adjusted to produce the desired load conditions in the PQ plane.
- Zeroing the field voltage until the end of the simulation period.

4.4.4 Simulation

The alternative electromagnetic transients program (ATP/EMTP) [41] is used to obtain the time domain solution of the model described above. A solution time step of 65.1 μs, equivalent to 256 samples every power system cycle, is used. This time step allows us to properly reproduce a bandwidth of 0.00 to 7.68 kHz. Thus, most of the transients are considered. The total time duration of simulation is chosen such that both kinds of disturbances (LOE and power swing) can be clearly observed. In the case of a power swing, it

is important to verify that the generator returns to a stable condition. It should be noted that unstable power swings of any kind are not considered in this work as this condition is typically detected by other protection functions, such as out-of-step relays. It should be also noted that, during a power swing, the fundamental frequency at the generator terminal may vary significantly (+/- 1.0 Hz or more). In the case of an LOE condition, it is also important to confirm if and when a loss of synchronism follows.

4.4.5 Selection of Data Vectors

After the simulation is done, the data vectors are calculated and consolidated as described in section 4.3, using the mathematical program Octave. As described before, the impedance characteristics present a more direct path when they start approaching the mho zone and, therefore, the following three restrictions are taken into consideration for choosing the training vectors.

- During a heavy loading condition, the training vector is chosen from the instant when the most recent of the 20 points on the characteristic is just inside the mho zone (Fig. 4.2).
- For lightly loaded cases, the first 1.0 s after the beginning of an LOE disturbance is disregarded (Fig. 4.2).
- The loss of synchronism that may follow an LOE condition is not included, as discussed before.

For a stable power swing condition, all possible data vectors are used without restrictions. This means that the prefault, fault, power swing, and final load data vectors are included. The transitions between these conditions are also included. The resulting classifier is actually trained to identify a non-LOE condition instead of just a stable power swing condition.

4.4.6 SVM Solution

In this work, the numerical solution is obtained using the quadratic programming function $qp()$ from the mathematical program Octave. First, $\boldsymbol{\alpha}$ is obtained and then $\mathbf{w}$ and w_0 are obtained, as described in Section 4.2. Once $\mathbf{w}$ and w_0 are obtained, the classifier is verified using (4.3) and (4.4) for all training data vectors. A zero classification error confirms that the data are separable in the original space.

4.5 Test Results

To demonstrate improvements gained through the proposed method, a 104.4 MVA, 13.8 kV, 3600 rpm, and wye connected synchronous generator as described in Subsection 4.4.1 is studied using electromagnetic simulation. The synchronous machine parameters of this generator are given in Table 4.1 and correspond to the sample system in reference [12]. The machine used here is different from that used in Chapter 3, as this part of the thesis work was performed earlier and before a more complete generator model was available. This generator is connected to the infinite bus through a line of $0.11\angle 84.3°$ pu impedance in generator base units. A fault resistance of 0.005 pu is used, which is connected at 50% of the line.

Table 4.1: Generator parameters

S_{base}	104.4	MVA	X_q	1.42	pu	X_{CAN}	0.14	pu
V_{base}	13.8	kV	X'_d	0.193	pu	T'_{d0}	3.59	s
H	3.09	s	X'_q	0.484	pu	T'_{q0}	0.312	s
Xn	0.001	pu	$X"_d$	0.136	pu	$T"_{d0}$	0.033	s
Rn	0.001	pu	$X"_q$	0.132	pu	$T"_{q0}$	0.084	s
X_0	0.001	pu	X_L	0.14	pu			
X_d	1.48	pu	R_a	0.00144	pu			

4.5.1 Training Data and Resulting SVM Classifier

The data vectors used for training are taken from both classes of disturbances: stable power swing scenarios and LOE scenarios. To produce a stable power swing, the three phase fault is applied at $t = 0s$ and removed at 200 ms in the simulation time scale. To produce an LOE, the field voltage is reduced to zero at $t = 0s$ in the same time scale. The total length of the simulation is 35 s. The duration of power swing observed is between 2.0 and 5.0 s. The duration of the LOE depends on the loading conditions. For a high load, the LOE lasts between 2.8 and 3.7 s before a loss of synchronism occurs. For a light load, the LOE may not cause loss of synchronism within the 35.0 s simulation.

A total of 116 data vectors are used for the training. These cases are listed in Table 4.2. After the training vectors are specified, the SVM equation is solved. A total of four support vectors are obtained, with two stable power swings and two LOE. The parameters of the resulting classifier are given in (4.21) and (4.22). The classification error is then verified using the training vectors and the two classes are confirmed to be separable.

Table 4.2: Simulation runs and training data vectors

Case No.	Load/PF	Initial P+jQ, *pu*	Number of vectors	Type of case	
1	light/lagging	0.12+j0.72	8	LOE	47
2	light/unity	0.05-j0.01	10	LOE	vectors
3	light/leading	0.03-j0.55	11	LOE	
4	heavy/lagging	0.80+j0.41	6	LOE	
5	heavy/unity	0.79-j0.04	3	LOE	
6	heavy/leading	0.78-j0.50	9	LOE	
7	light/lagging	0.12+j0.72	8	PS-3P	69
8	light/unity	0.05-j0.01	8	PS-3P	vectors
9	light/leading	0.03-j0.55	10	PS-3P	
10	heavy/lagging	0.80+j0.41	12	PS-3P	
11	heavy/unity	0.79-j0.04	14	PS-3P	
12	heavy/leading	0.78-j0.50	17	PS-3P	

PS: power swing, 3P: three phase fault used.

$$\mathbf{w}^T = [17.6668238.7866.102622.7685] \tag{4.21}$$

$$w_0 = -19.730 \tag{4.22}$$

4.5.2 SVM Implementation

In this work, the method described in Section 4.3 is implemented using the foreign models compiled object in ATP. Two methods of LOE detection were implemented in this foreign models object for performance comparison: the SVM classifier and the traditional two mho zone LOE. The phasor estimation was implemented using DFT with angle normalization,

so that a steady state fundamental frequency condition produces a fixed phasor value. The three phases of current and voltage were used to obtain the positive sequence current and voltage phasor. These positive sequence phasors are used by the SVM method described. The SVM classifier is defined mathematically by (4.3) and (4.4) using the parameters (4.21) and (4.22) obtained from the SVM solution. The output of this classifier in time is used to assess the performance.

4.5.3 Test Consideration and Results

Two types of measurements were obtained: a) active and reactive power, and b) time. The active and reactive power were obtained by sensors based on fundamental frequency phasors inside the electromagnetic simulation tool. The time was obtained by inspection of the signals in time with a resolution of $^1/_{4th}$ of one millisecond or better.

4.5.3.1 New Cases Similar to the Training Cases

These cases are obtained using the same disturbances used for training. In Table 4.3, the traditional LOE detection is shown as a reference. In Table 4.4, the SVM method results are shown for comparison. These results are also illustrated in Figs. 4.14 and 4.15. The SVM pickup time is the time it takes for the proposed method to confirm an LOE condition. The SVM reset time also indicates the time when loss of synchronism occurs. In these cases, good results are more likely because of the similarity between the data vectors and the ones used for training.

Table 4.3: New cases similar to training cases - two MHO zone LOE

				Two MHO zone			
				Large MHO Time, s		Small MHO Time, s	
Case No.	Load/PF	Initial P+jQ, *pu*	Type of case	Pickup	Trip	Pickup	Trip
1	LL/lag.	0.12+j0.72	LOE	7.7222	8.7133	-	-
2	LL/unity	0.05-j0.01	LOE	4.5423	5.5335	-	-
3	LL/lead.	0.03-j0.55	LOE	0.9520	1.9432	-	-
4	HL/lag.	0.80+j0.41	LOE	2.1591	3.1502	2.7405	3.1304
5	HL/unity	0.79-j0.04	LOE	1.7824	2.7735	2.5027	2.8924
6	HL/lead.	0.78-j0.50	LOE	0.7758	1.7603	1.6612	2.0511
				Pickup	Reset	Pickup	Reset
7	LL/lag.	0.12+j0.72	PS-3P	-	-	-	-
8	LL/unity	0.05-j0.01	PS-3P	0.27090	0.31055	-	-
8(*)				0.51210	0.63103		
9	LL/lead.	0.03-j0.55	PS-3P	0.25554	2.82820	0.26433	0.77536
10	HL/lag.	0.80+j0.41	PS-3P	0.26433	0.29076	-	-
11	HL/unity	0.79-j0.04	PS-3P	0.25554	0.33483	0.25554	0.31719
12	HL/lead.	0.78-j0.50	PS-3P	0.24668	0.76651	0.24668	0.56385
12(*)				0.88108	1.16300		

LL: light load, HL: heavy load, PS: power swing, 3P: 3 phase fault used, (*) picked up twice

Table 4.4: New cases similar to training cases - SVM method

Case No.	Load/PF	Initial P+jQ, *pu*	Type of case	SVM Time, s Pickup	SVM Time, s Reset	Loss of Synch. time, s
1	LL/lag.	0.12+j0.72	LOE	0.26739	24.410	25
2	LL/unity	0.05-j0.01	LOE	0.40160	-	-
3	LL/lead.	0.03-j0.55	LOE	0.22071	-	-
4	HL/lag.	0.80+j0.41	LOE	0.21257	3.7512	3.76
5	HL/unity	0.79-j0.04	LOE	0.24161	3.6203	3.62
6	HL/lead.	0.78-j0.50	LOE	0.42070	2.8707	2.87

LL: light load, HL: heavy load, PS: power swing, 3P: 3 phase fault used

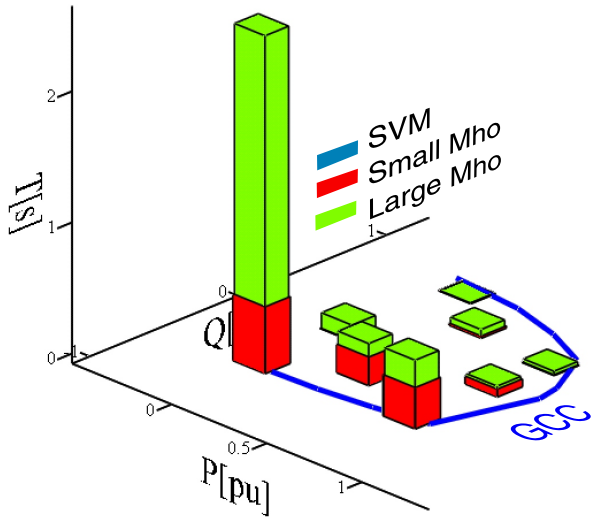

Figure 4.14: Power Swing Duration results.

4.5.3.2 Different Initial Loading

These cases are obtained by modifying the initial load conditions. Two different initial load conditions are used for the new cases. For each of these conditions, one LOE scenario

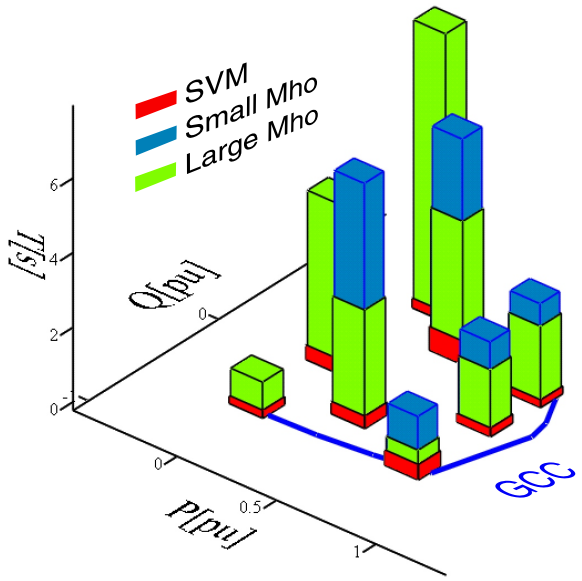

Figure 4.15: Proposed SVM Operating Pickup Times.

and one power swing scenario are generated and are listed in Tables 4.5 and 4.6. These results are also illustrated in Figs. 4.16 and 4.17.

Table 4.5: New cases with different initial loads - two MHO zone LOE

				Two MHO zone			
				Large MHO Time, s		Small MHO Time, s	
Case No.	Load/PF	Initial P+jQ, *pu*	Type of case	Pickup	Trip	Pickup	Trip
13	ML/lag.	0.37+j0.47	LOE	3.3824	4.8165	6.0143	6.4099
14	ML/lead	0.38-j0.30	LOE	3.1615	4.1462	6.5308	6.9154
				Pickup	Reset	Pickup	Reset
15	ML/lag.	0.37+j0.47	PS-3P	0.26433	0.32598	0.27311	0.29076
16	ML/lead	0.38-j0.30	PS-3P	0.24668	0.56385	0.25554	0.47577

ML: medium load, PS: power swing, 3P: 3 phase fault used

Table 4.6: New cases with different initial loads - SVM method

Case No.	Load/PF	Initial P+jQ, *pu*	Type of case	SVM Time, s Pickup	SVM Time, s Reset	Loss of Synch. time, s
13	ML/lag.	0.37+j0.47	LOE	0.6429	7.5702	7.56
14	ML/lead.	0.38-j0.30	LOE	0.3425	8.1902	8.13

ML: medium load, PS: power swing, 3P: 3 phase fault used

4.5.3.3 Different Fault Types

The power swing scenarios generated so far used three phase fault types. However, unbalanced faults occur more frequently in reality. Thus, it is important to verify the performance of the SVM approach during unbalanced fault conditions as well. Four more cases with the following fault types are used: AG, BG, ABG, and BCG. The four cases are listed in Table 4.7. To bring the impedance during a power swing closer to or inside the LOE characteristic, the worst case scenario of the six initial load conditions is used, that is, a heavy load with leading power factor (0.78 - j0.50 *pu*). The worst case scenario used in this work was described by Berdy [141] as a voltage regulator out of service, low system impedance, fault clearing time equal to critical switching time (i.e., the maximum switching time for which the machine is stable), and the machine operating at a leading power factor.

Table 4.7: New cases with different fault types - two MHO zone LOE

				Two MHO zone			
				Large MHO Time, s		Small MHO Time, s	
Case No.	Load/PF	Initial P+jQ, *pu*	Type of case	Pickup	Reset	Pickup	Reset
17	HL/lag.	0.78+j0.50	PS-AG	0.24668	0.39648	0.24668	0.31719
18	HL/lead	0.78-j0.50	PS-BG	0.2379	0.39648	0.24668	0.3084
19	HL/lag.	0.78+j0.50	PS-ABG	0.2379	0.60792	0.2379	0.36126
20	HL/lead	0.78-j0.50	PS-BCG	0.2379	0.62557	0.24668	0.37005

HL: heavy load, PS: power swing, AG/BG/ABG/BCG fault type used

4.5.3.4 Different Transmission Line

The electrical centre of the power swing moves away from the generator when the line length is increased, while the electrical centre moves closer to the generator impedance or may fall inside the generator impedance when the line length is reduced. When the electrical centre is too far from the generator impedance, then the power swing may not enter the LOE region. The length as well as the impedance of the power line that connects to the infinite bus was therefore increased from 0.11 to 0.33 *pu*. Beyond a 0.33 *pu* line length, the power swing did not enter the LOE impedance zone. Only four initial load conditions are used and combine heavy/light load and leading/lagging power factor variations. Eight more cases are considered (four power swing scenarios and four LOE scenarios), and are listed in Tables 4.8 and 4.9. The power swing is only produced using three phase faults in this part.

Table 4.8: New cases with longer line - two MHO zone LOE

				Two MHO zone			
				Large MHO Time, s		Small MHO Time, s	
Case No.	Load/PF	Initial P+jQ, *pu*	Type of case	Pickup	Trip	Pickup	Trip
21	HL/lead.	0.60-j0.28	LOE	1.6436	2.6348	2.4102	2.8066
22	HL/lag.	0.66+j0.32	LOE	2.5820	3.5731	2.9520	3.3441
23	LL/lead.	0.02-j0.29	LOE	2.6826	3.6739	-	-
24	LL/lag.	0.08+j0.31	LOE	8.9603	9.6820	-	-
				Pickup	Reset	Pickup	Reset
25	HL/lead.	0.60-j0.28	PS-3P	0.55506	0.85465	-	-
26	HL/lag.	0.66+j0.32	PS-3P	-	-	-	-
27	LL/lead.	0.02-j0.29	PS-3P	0.26433	0.68722	-	-
28	LL/lag.	0.08+j0.31	PS-3P	-	-	-	-

LL: light load, HL: heavy load, PS: power swing, 3P: 3 phase fault used

Table 4.9: New cases with longer line - SVM method

				SVM Time, s		
Case No.	Load/PF	Initial P+jQ, *pu*	Type of case	Pickup	Reset	Loss of Synch. time, s
21	HL/lead.	0.60+j0.28	LOE	0.5417	3.3355	3.34
22	HL/lag.	0.66-j0.32	LOE	0.28015	3.6062	3.62
23	LL/lead.	0.02-j0.29	LOE	0.4739	-	-
24	LL/lag.	0.08-j0.31	LOE	0.4.9332	28.186	28.0

LL: light load, HL: heavy load, PS: power swing, 3P: 3 phase fault used

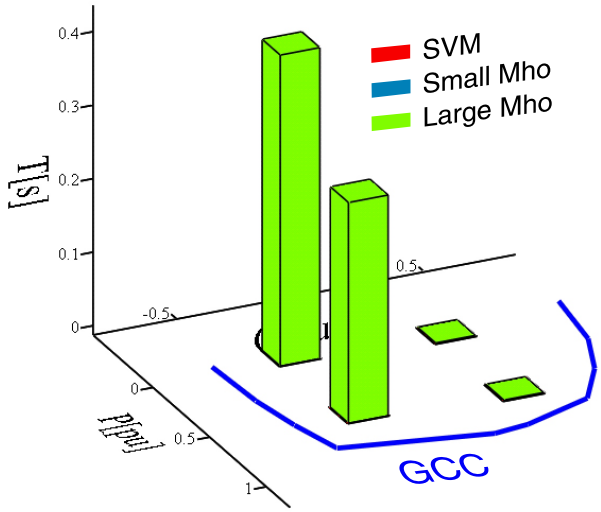

Figure 4.16: Power Swing Duration results for longer line.

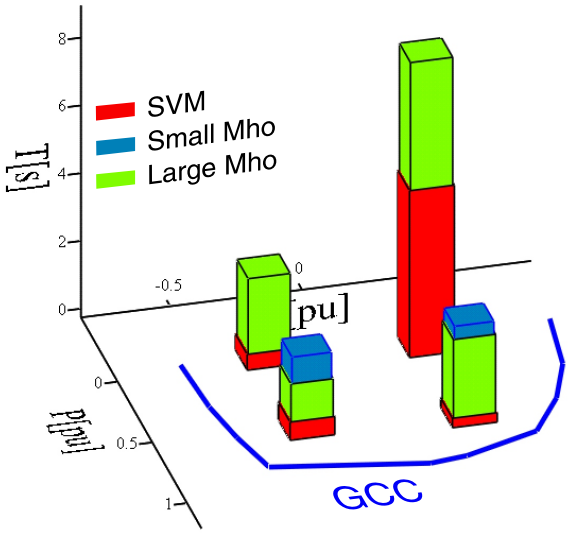

Figure 4.17: Proposed SVM Operating Pickup Times for longer line.

4.5.3.5 Sensitivity to Generator Parameters

The parameters of the generator can only be determined to a certain degree of accuracy, depending on the method used to obtain the values. Therefore, it is important to study the latency and robustness of the proposed method to small variations in the generator parameters. The cases for the most severe LOE event (case no. 6 in Tables 4.3 and 4.4)

were used to study the sensitivity of the proposed method. A variation of either +/- 5% was used, depending on which one caused the operating point to enter the LOE mho zone, i.e., increasing the risk of maloperation. The results are given in Tables 4.10 and 4.11.

Table 4.10: Sensitivity to generator parameters - two MHO zone LOE

				Two MHO zone			
				Large MHO Time, s		Small MHO Time, s	
Case No.	Parameter varied	Initial P+jQ, *pu*	Type of case	Pickup	Trip	Pickup	Trip
6	-	0.78-j0.50	LOE	0.7758	1.7603	1.6612	2.0511
	MVA+5%			0	+11 ms	+77 ms	+88 ms
	kV+5%			-33 ms	-33 ms	-198 ms	-176 ms
	X_d+5%			-22 ms	-22 ms	-77 ms	-55 ms
	X_q+5%			+11 ms	+11 ms	-11 ms	0
	X'_d+5%			0	0	-22 ms	-11 ms
	X'_q+5%			0	0	-22 ms	-11 ms
	X_d"+5%			0	0	-11 ms	0
	X_q"+5%			0	0	-11 ms	0
	T'_{do}+5%			+33 ms	+33 ms	+55 ms	+66 ms
	T'_{qo}+5%			0	0	-11 ms	+11 ms
	T_{do}"+5%			0	+11 ms	-11 ms	0
	T_{qo}"+5%			0	0	-11 ms	+11 ms
	H+5%			0	0	-11 ms	0
				Pickup	Reset	Pickup	Reset
12	-	0.78-j0.50	PS-3P	0.1913	0.6304	0.1913	0.3826
	MVA+5%			0	0	0	+28.2 ms
	kV+5%			-11 ms	+12 ms	-11 ms	+59 ms
	X_d+5%			0	+2 ms	0	+10 ms

X_q+5%	0	+1 ms	0	+19 ms
X'_d+5%	0	0	0	-2 ms
X'_q+5%	0	0	0	-22 ms
X_d"+5%	+1 ms	0	+1 ms	0
X_q"+5%	0	+2 ms	0	-1 ms
T'_{do}+5%	0	0	0	-11 ms
T'_{qo}+5%	0	+1 ms	0	-2 ms
T_{do}"+5%	0	0	0	-2 ms
T_{qo}"+5%	+1 ms	0	+1 ms	-1 ms
H+5%	0	0	0	-11 ms

LL: light load, HL: heavy load, PS: power swing, 3P: 3 phase fault used

The parameter that affected the detection of an LOE condition the most (case no. 6 in Tables 4.3 and 4.4) by the SVM method proposed was an increase in the X'_q of 5%. The impact was a delay of 33 ms in the detection as indicated in Tables 4.10 and 4.11. For the same LOE condition, the traditional two-zone mho impedance method was also affected by the parameter variation, but resulted in a faster trip time by 33 ms for an increase in the rated voltage of 5%. However, the overall decision time using the SVM method was still faster (453 ms) compared to the traditional two mho zone method (1.73 s).

Table 4.11: Sensitivity to generator parameters - SVM method

Case No.	Parameter varied	Initial P+jQ, *pu*	Type of case	SVM Time, s Pickup	SVM Time, s Reset	Loss of Synch. time, s
6	-	0.78-j0.50	LOE	0.4207	2.8707	2.87
	MVA+5%			-11 ms	+22 ms	
	kV+5%			0	-407 ms	
	X_d+5%			-11 ms	-110 ms	
	X_q+5%			+33 ms	-55 ms	
	X'_d+5%			-11 ms	-22 ms	
	X'_q+5%			-11 ms	-33 ms	
	X_d"+5%			-11 ms	-11 ms	
	X_q"+5%			-11 ms	-11 ms	
	T'_{do}+5%			-11 ms	+110 ms	
	T'_{qo}+5%			-11 ms	+11 ms	
	T_{do}"+5%			-11 ms	0	
	T_{qo}"+5%			-11 ms	+11 ms	
	H+5%			-11 ms	0	

LL: light load, HL: heavy load, PS: power swing, 3P: 3 phase fault used

On the other hand, the SVM was not affected for a power swing condition (case no. 12 of Table 4.3). The SVM classifier successfully and clearly identified all instances where the impedance entered the LOE mho zone as a non-LOE condition. However, the traditional two mho zone method was affected, because the machine was operating very close to the transient stability limit. This limit depends on two variables: the point in the PQ plane relative to the GCC curve and the fault duration. The point in the PQ plane in this case is on the limit of the GCC curve in the leading reactive region and the fault duration used for all prior cases is 200 ms. The parameters that caused the most impact on the performance of the traditional LOE detection method for this power swing condition were 5% variation

of the MVA rating, the kV rating, and the X_d synchronous reactance, which allowed the machine to lose synchronism for the fault duration of 200 ms being used. It is unlikely a machine would be operated so close to the transient stability limit, thus the fault duration time was reduced from 200 to 150 ms so there was no loss of synchronism.

4.5.4 Comparison of SVM and Traditional Methods

Based on the cases tested, the SVM method is able to identify the LOE condition before the impedance enters the mho zone. However, for increased security, a trip decision can be made when the impedance just enters the LOE mho zone. The traditional two mho zone method [141] uses time coordination, which only starts when the impedance enters either of the two mho zones; thus, it takes longer than the proposed SVM method. Take for instance case no. 4, shown in Fig. 4.2, where the impedance takes 2.16 s to reach the mho impedance zone. The proposed SVM methods detects this condition at just 213 ms. The traditional two zone LOE needs to wait 1 s after the impedance enters the zone and then only trips at 3.13 s. It should be noted that although the SVM method proposed uses a 1 s window, it can detect an LOE with less than 1 s of disturbance information. Also, it should be noted that the improvements are more significant for heavier load conditions and less significant for lighter load conditions.

4.6 Summary

A new method to distinguish LOE from power swing disturbances was presented in this chapter. This method was based on the SVM pattern recognition technique. Careful selection of identifying features was done to take full advantage of the capabilities of the SVM method. In summary, the first feature represents the distance from the most recent impedance measured to the centre of the mho zone. The second feature corresponds to the total change in reactive power within a one second window. The third feature indicates how straight the path is in the complex power plane. The fourth feature detects sudden jumps in the complex power plane within the one second window. The resulting classifier

provided accurate identification of various operating conditions of the synchronous generator. By combining this classifier with the traditional one zone mho impedance approach, the detection time for identifying LOE conditions was significantly improved compared to the traditional two mho zone method without any loss of accuracy in detecting the LOE condition.

Chapter 5

Proposed Coordination Methodology in the Underexcited Region

5.1 Limitations of Existing Coordination Methodologies

Coordination between generator protection and excitation control in the underexcited region should provide the maximum available reactive capability in this region [11]. As described before, the existing methods used by the industry are based on static characteristics, i.e., steady state characteristics, such as those shown in Figs. 5.1 and 5.2.

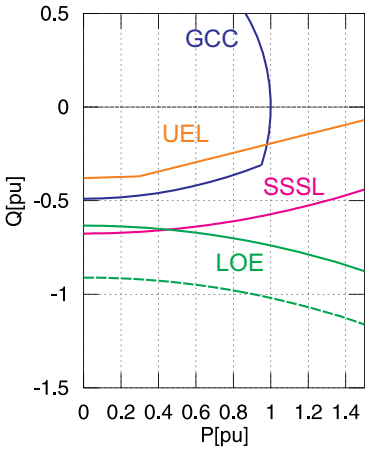

Figure 5.1: Coordination characteristics in the PQ plane

In Figs. 5.1 and 5.2, several characteristics are shown: (a) the Generator Capability Curve (GCC), (b) the Underexcitation Limiter (UEL), (c) Loss of Excitation (LOE) protection, and (d) the Steady State Stability Limit (SSSL). The static coordination verifies margins

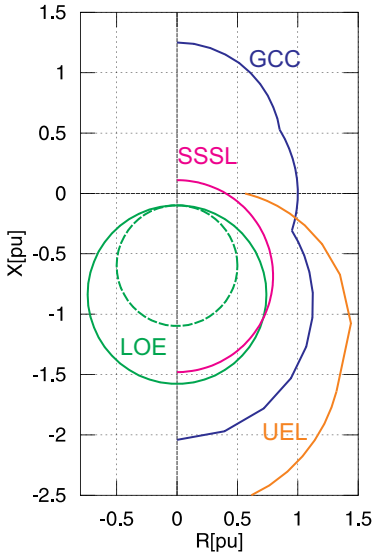

Figure 5.2: Coordination characteristics in the Z plane

between these steady state characteristics for the maximum and minimum operating voltage levels. The static coordination method has been widely applied because it does not use detailed dynamic modeling and simulation of the generator under consideration.

The limitations of the static coordination arise from the fact that dynamic simulations have not been a common practice. Some of the limitations of static coordination are as follows:

- The SSSL characteristic is generally applied although it is a severe restriction in the static coordination; the SSSL only applies when excitation control is in manual mode.
- Mapping steady state characteristics from the PQ plane to the Z plane or vice versa is only valid at the specific voltage level considered, but the coordination is typically assumed to apply to voltages outside these levels.
- The UEL limit is not a rigid limit and has a dynamic characteristic.
- LOE timings can only be truly verified by dynamic simulation plus LOE equation characteristic modeling.

5.2 Literature Review of Dynamic Coordination in the Underexcited Region

The concept of dynamic simulation to assess the correct operation of protection functions during typical disturbances has been previously proposed. Arndt [119] presents studies performed for a real generator to coordinate the LOE for power swing conditions and that represent the AVR control as well as the frequency dependence of the LOE characteristic, but does not include UEL modeling. Darron [50] examines the impact of LOE conditions on the system and the machines, considers the frequency dependence of LOE protective characteristics, and proposes load flow and transient studies, but does not mention the importance of UEL modeling. Baldwin [114] proposes improving the coordination of several functions, such as LOE and loss of synchronism among others, but does not specify the use of dynamic simulations. Pierre [117] proposes a simplified machine model to test the effectiveness of LOE protection but only for isolated systems. Choi [159] shows an example of dynamic coordination of the UEL considering stability, protection, and re-tuning of the UEL control loop, but with a simplified LOE protection characteristic. Ribeiro [160] presents dynamic modeling of the UEL and V/Hz, showing the interaction with LOE protection and the SSSL stability limit, but does not include the PSS stabilizer effect. Dias [118] studies LOE and external fault conditions by dynamic simulation, but does not represent the excitation control system in the model. Berube [161] explains the considerations for UEL tuning, the problem of stability oscillations, use of proportional integral control, and coordination with LOE protection with experimental results, but with emphasis on the control point of view. Ramos [162] describes a problem with UEL instability and coordination with the PSS on a real system with hydro units, but does not present much detail on coordination with LOE protection. Sandoval [113] describes the use of dynamic simulation for verification of LOE and loss of synchronism conditions, considering AVR/PSS but with simplified UEL modeling. Schaefer [110] discusses the coordination problem from the point of view of control, using simplified protection function representation. Mozina [112] explains the implementation of coordination between transmission protection, generator protection, and control according to NERC, but from the protective relaying industry point of view.

In this thesis, the proposed coordination approach addresses the issues discussed above and the limitations of past approaches.

5.3 Underexcited Capability

The operating limits of a synchronous generator in the underexcited region are defined by the lower part of the generator capability curve (GCC) plotted in the PQ plane, as shown in Fig. 5.1. This lower curve of the GCC is the underexcited limit and restricts the amount of reactive power that the machine can absorb from the power system. The machine approaches this limit by absorbing reactive power when trying to limit or prevent temporary overvoltage conditions. One should also consider the limitation due to the generator step up transformer ratio in the capability analysis [131, 163–165].

5.3.1 Thermal End Core Limit

The underexcited limit in the GCC curve is defined by the thermal capability of the stator core ends for this condition [166]. Underexcited conditions cause the core ends of the stator to overheat due to increased magnetic leakage flux in directions perpendicular to the stator core laminations as well as in other paths not intended to carry significant amounts of flux. This thermal limit exists in all types of synchronous machines, but become more critical in round rotor machines because it encroaches on the GCC area [167–174]. In salient pole machines, this thermal limit is far away from the GCC curve and the underexcited limit for this type of machines is the stator winding thermal limit [175,176] itself, as shown in Fig. 5.3.

5.3.2 Stability Limit

The stability limit represents a physical limit beyond which the synchronous machine cannot operate, i.e., beyond this limit the machine loses synchronism with the power system. This limit can be plotted in the PQ plane as a curve in the underexcited region. In Fig.

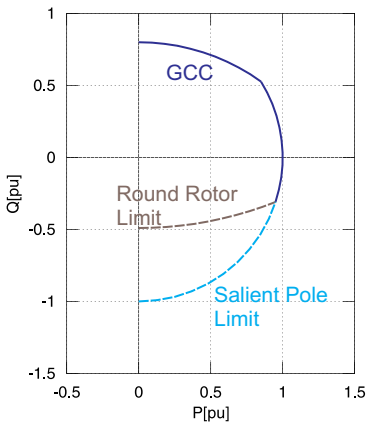

Figure 5.3: Generator capability curves for round and salient pole machines

5.1, the steady state stability limit (SSSL) is plotted. The stability is mainly a result of the effect of two types of torque: synchronizing torque and damping torque.

5.3.3 Synchronizing Torque

Synchronizing torque is proportional to a change of the machine angle $\Delta\delta$. Stability is maintained when this torque is in the direction to bring the machine back to the angle δ prior to the change. In Fig. 5.4, the mechanical power P_M is fixed and the electrical power P_E is plotted as a function of the machine angle δ with respect to the system. Considering a small increase in the machine angle $\Delta\delta$, the corresponding electrical power increase ΔP will slow down the rotor and bring the operating point back to the initial value.

The steady state stability limit (SSSL) is the operating point of the machine where the synchronizing torque becomes zero. In Fig. 5.5, the steady state stability limit is shown in the PQ plane for the excitation control cases in manual and automatic modes for comparison. In this figure, the SSSL characteristic is also shown when the difference between direct axis X_d and quadrature axis X_q reactances is neglected, which is commonly done in protective relaying applications. These characteristic curves are calculated using the method described in Appendix 7.4.

The SSSL limit is closer to the GCC curve for manual excitation control mode compared

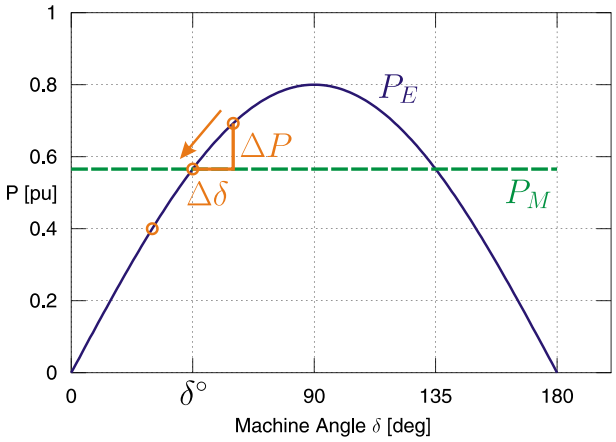

Figure 5.4: Synchronizing torque concept

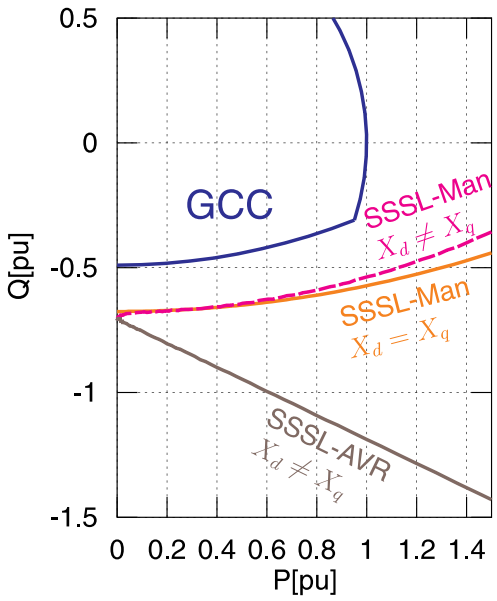

Figure 5.5: Steady state stability limit characteristics in the PQ plane

to the automatic control mode. In many cases, the SSSL limit in manual mode encroaches on the GCC curve restricting the reactive capability of the machine. For this reason, in most cases the generators are required to operate with automatic excitation control mode, i.e., with AVR active.

5.3.4 Damping Torque

The damping torque is proportional to a change of the machine speed $\Delta\omega$. Stability is maintained when this torque is in the direction to bring the machine back to the speed ω prior to the change. The dynamic stability limit (DYSL) is the operating point of the machine where the damping torque becomes zero. This limit refers to the amount of damping for oscillations between the machine and the power system. The range of frequencies typically considered for this damping is on the order of 0.1 to 4.0 Hz. In Fig. 5.6, the dynamic stability limit is shown in the PQ plane for the excitation control in manual and automatic modes [177]. These characteristic curves are calculated using the method described in Appendix 7.4.

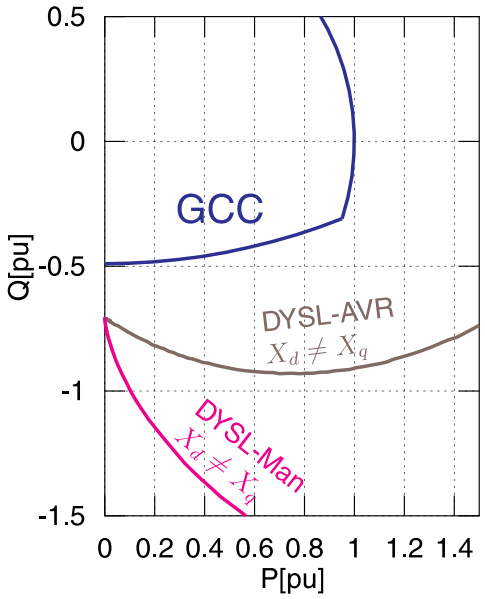

Figure 5.6: Dynamic stability limit characteristics in the PQ plane

The DYSL limit is closer to the GCC curve for automatic excitation control mode compared to the manual control mode. Thus, the AVR action has the opposite effect on the SSSL and DYSL, i.e., it improves the SSSL but makes the DYSL worse. Therefore, the DYSL becomes more important for coordination purposes.

In older machines, the gain of the AVR control is not very high and the natural damping of the machine results in a DYSL characteristic located safely away from the GCC curve.

In newer machines with fast acting static excitation units, higher gains are used and the damping is reduced to the point that the dynamic limit may, in many cases, encroach on the GCC characteristic. In these cases, an additional control action is required, known as power system stabilizing (PSS) control. The PSS control action restores the damping that was reduced by the AVR action and relocates the stability limit away from the GCC area.

5.3.5 Reliability and Stability Limit

The degree of reliability expected is associated with the importance of the generating unit being considered. Two main aspects need to be considered when studying coordination: the redundancy in the excitation control system (ECS) and the system outage used to determine the stability limit.

The excitation control system redundancy depends on the importance and size of the generating unit. Single excitation control systems are used in smaller machines. In this case, the manual control mode SSSL limit needs to be respected because failure of the ECS would cause a switch from automatic to manual mode of operation. Redundant excitation control systems are used in larger and more important machines. In most cases, these larger machines are not allowed to operate without AVR action present. The failure of one ECS would cause a switch to a secondary ECS, keeping the AVR action active. In this case, the automatic control mode DYSL is the one used as it is the characteristic closer to the GCC curve. In most cases with redundant ECS, PSS action is also present together with the AVR; thus, both stability limits, i.e., the steady state and dynamic limits, are located far from the GCC curve. In this last case, i.e., an AVR/PSS combination, the stability limits are not required to be considered for the coordination between UEL control and LOE protection.

The system outage to be considered for the calculation of the stability limit is directly related to the degree of reliability desired. A single contingency scenario may be applied to weak systems, such as outage of the largest generator connected or ECS failure without any other outage. A double contingency scenario may be applied to stronger systems, such as outage of the two largest generators connected or outage of the largest generator and ECS

failure. Obviously, the case considering double contingency provides increased reliability.

5.4 Underexcitation Limiter (UEL)

The underexcitation limiter (UEL) is responsible for monitoring and keeping the machine within the generator capability curve (GCC) limits in the underexcited region. The UEL takes action when the operating point of the machine in the PQ plane goes beyond a predefined characteristic in the negative reactive direction. When this happens, the UEL applies a control signal to the AVR loop in order to increase the excitation voltage and bring the machine back inside the GCC area [178–185].

5.4.1 UEL Characteristics

5.4.1.1 PQ plane

According to IEEE standards, there are three basic characteristic types used to define the UEL in the PQ plane: circular, single line, and multi-line. The different characteristic shapes are illustrated in Fig. 5.7. The circular shape has been used in older machines, for which coordination was focused more on the manual control mode SSSL limit. The single or multi-line types are used in more modern machines depending on the importance of the UEL limit in the particular application. The single line type is easier to define and may be used when tight margins are not required for coordination in the underexcited region. The multi-line type better approximates the shape of the GCC in the underexcited region, and helps in providing maximum capability when tight coordination margins are required.

5.4.1.2 Voltage Dependence

The dependence of the UEL characteristic on the terminal voltage is important to ensure coordination is maintained for the range of operating voltages to which the generator will be subjected. The circular type varies the UEL characteristic using the square of the terminal

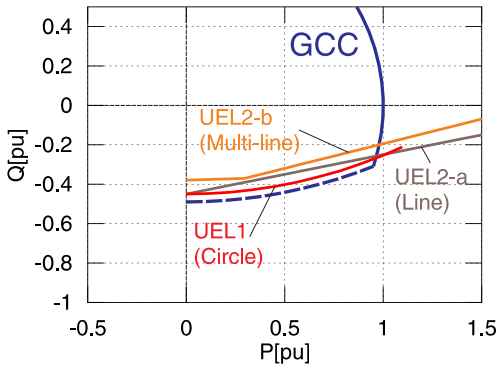

Figure 5.7: UEL characteristics in the PQ plane

voltage. This behaviour is applicable when coordination is required with the manual mode SSSL characteristic, and also to coordinate with LOE protection functions. In Fig. 5.8, the circular UEL characteristic equation is illustrated, showing the basis for the voltage dependence on the square of the terminal voltage.

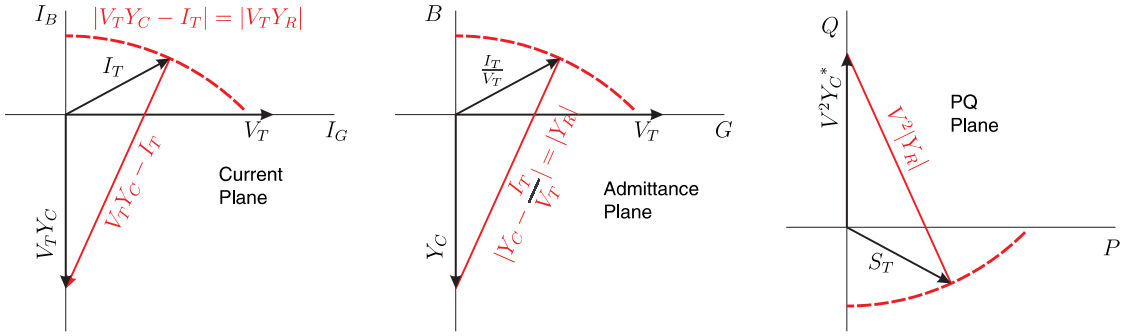

Figure 5.8: Circular UEL dependence on voltage

According to IEEE standards, the single line or multi-line characteristics are capable of providing a voltage dependence following an exponential function of the form V^k, where k is an integer value between zero and two. In this way, these relatively newer characteristics provide the traditional squared voltage dependence if coordination is required or as the application dictates.

5.4.2 Regulator Loop

The UEL control action is defined by the control loop indicated by IEEE standards [68], as shown in Fig. 5.9. In Fig. 5.9, the most important control blocks are highlighted.

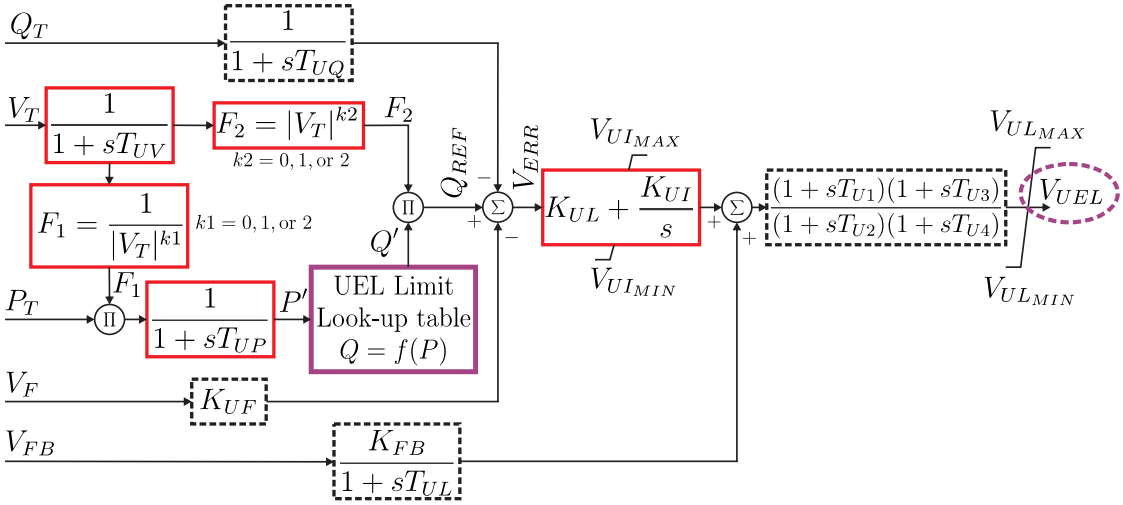

Figure 5.9: UEL control loop for single line or multi-line

The terminal voltage signal V_T and the active power signal P_T are used as reference values. From these two reference values, the current reactive power limit level Q' is obtained by using a lookup table function $Q = f(P)$. The voltage dependence is obtained using the blocks $\frac{1}{V^{k1}}$ and V^{k2}, considering that the lookup table $Q = f(P)$ is defined at a rated voltage level. The main regulating control loop is a proportional integral with parameters K_{UI} and K_{UL}. The controlled variable is the reactive power signal Q_T.

5.4.3 Summing or Takeover

The output signal V_{UEL} from the UEL control loop is applied to the main AVR control loop in order to increase the excitation to the rotor field when the operating point of the machine moves below the UEL characteristic in the PQ plane. There are two ways of applying this output signal V_{UEL} to the AVR loop: as a summing input or as a takeover input.

A summing type of UEL control action typically adds its signal to the reference voltage input signal, i.e., at the input of the AVR control loop. The summing type of control has the

advantage that other control actions being added to this summing point are still available. Of particular interest is the PSS control action, which remain active when a summing type of UEL action is applied. The UEL control action is zero in cases where the reactive power is above the UEL characteristic in the PQ plane. A disadvantage of a summing type of UEL control is that the level of this signal needs to be strong enough to overcome the main AVR control action, thus larger UEL control loop gain may be needed. At the same time, the gain of the UEL control loop needs to be carefully calculated to maintain overall stability when it is activated.

A takeover type of UEL control action typically takes over the AVR loop when the reactive power is reduced below the UEL characteristic in the PQ plane. The takeover action is performed by using an analog high level gate that compares the UEL signal with the voltage error signal typically used by the AVR loop. Here, the advantage is that the UEL action does not need to overcome the main AVR action because these two signals are not being added. A disadvantage is that any control action prior to the takeover point in the main AVR control loop is basically removed by the UEL takeover. In many cases, the PSS action is before the AVR control, in particular at the summing point at the beginning of the AVR loop. In this case, a takeover type of UEL control action is not the best option. In newer designs of AVR control, the PSS action is applied further down the loop, after the takeover points, and a takeover type of UEL can be applied. A takeover type of UEL control action needs to keep a negative offset in case the reactive power is above the UEL characteristic in the PQ plane. If a zero level were used for a takeover UEL, the limiting action would come into effect when trying to reduce the excitation within the normal operating area of the GCC curve.

5.5 Loss of Excitation (LOE) Protection

Traditional LOE detection methods were described in Subsection 4.1.2. A proposed method for LOE detection based on the Support Vector Machine (SVM) was described in Section 4.3.

5.6 Coordination Considerations

This part of the work is performed taking as a case study one of the largest generators from the Alberta system [108]. The Alberta network database is available in PSS/E (Power System Simulator from Siemens PTI) format [40]. In this network database, all generators are represented in enough detail to perform different types of studies, such as transient stability studies, load flow studies, and short circuit studies, among others. The generator used for this study is one thermal unit of 483 MVA capacity (Sundance Plant located close to City of Edmonton). The network area of study is illustrated in Fig. 5.10.

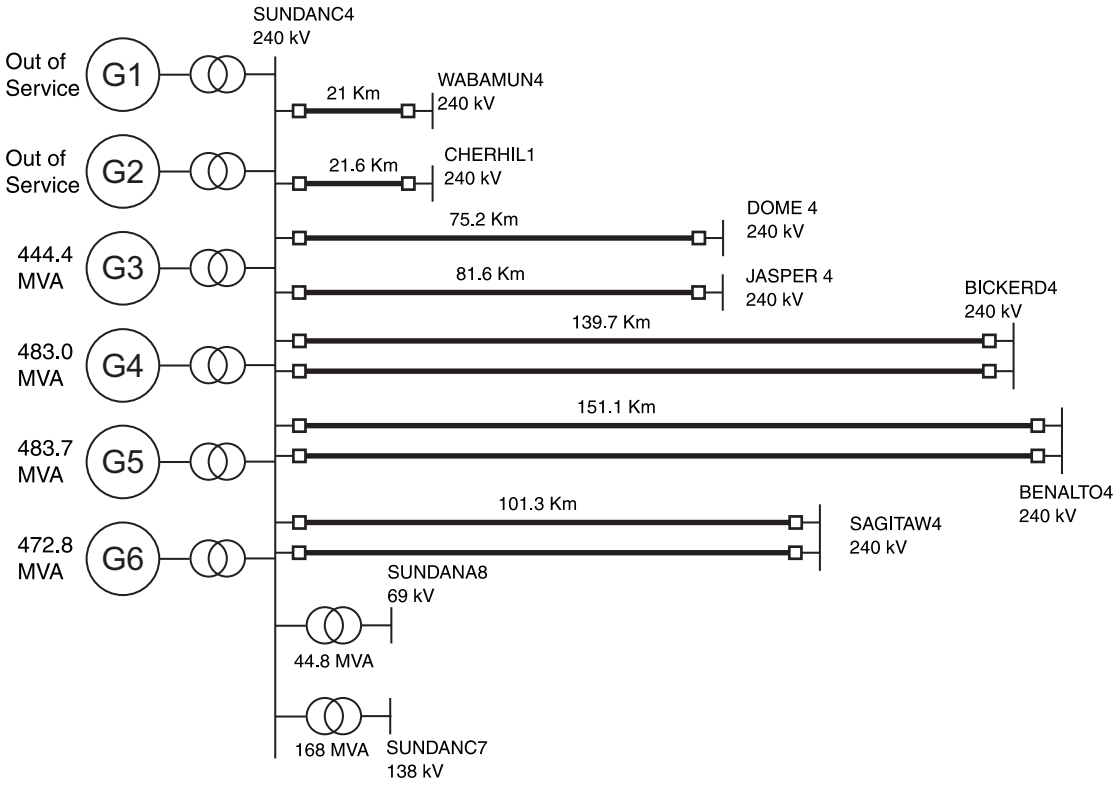

Figure 5.10: Overview of Sundance generator plant and surrounding network

5.6.1 Excitation Control Modeling

The excitation control for this generator unit is already modeled in the PSS/E AESO (Alberta Electric System Operator) base case. This excitation unit has been modeled using

the PSS/E standard model type EXST1 [106]. The EXST1 is a slightly modified version of the type ST1 model proposed by an IEEE Excitation working group in 1981 [186], and is shown in Fig. 5.11.

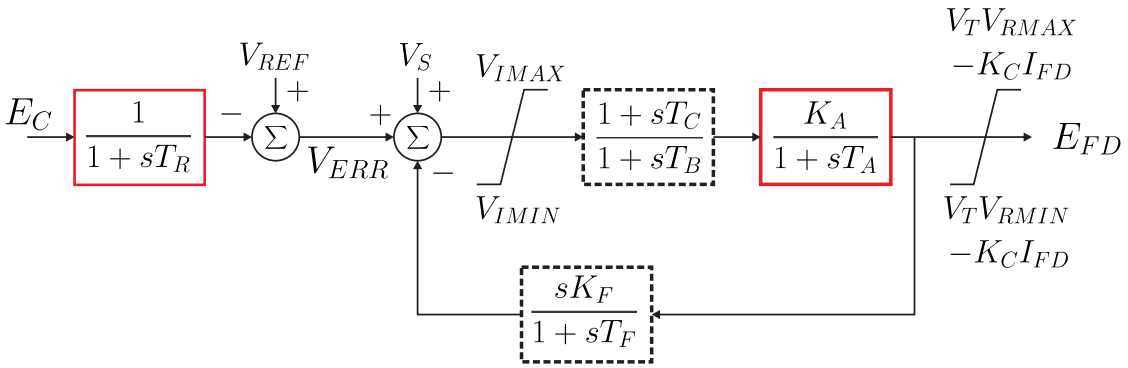

Figure 5.11: EXST1 model; PSS/E implementation of 1981 IEEE ST1 model.

In Fig. 5.11:

V_{ref} is the reference or desired terminal voltage

E_C is the terminal voltage measured

T_R is the voltage measurement delay time constant

E_{FD} is the excitation voltage output considering rectifier effect and ceiling voltage limits

I_{FD} is the field current measured

V_S represents auxiliary signals, e.g., power system stabilizer (PSS)

K_A, T_A represent the main exciter control loop

T_C, T_{C1}, T_B, T_{B1} represent the lead lag compensating control loop

K_F, T_F represent the stabilizing feedback control option

The ST1(or EXST1) model does not have a provision for including the UEL required to properly represent dynamics in the underexcited region. In fact, UEL dynamics are not represented for any generator in the AESO system.

The type of exciter being used in the machine under study is better represented by

the IEEE ST5B model. The ST5B model is recommended in IEEE 421.5 standard for the Unitrol ABB type of exciter control systems, and is shown in Fig. 5.12 [68]. This model allows proper representation of the takeover type of UEL being used in this system. One characteristic of the ST5B model is that it considers different transient gains depending on which control action is currently active, be it an Automatic Voltage Regulator (AVR), UEL, or Overexcitation Limiter (OEL). Another characteristic is that PSS action always remains active because this input is after the takeover inputs used by UEL or OEL control actions.

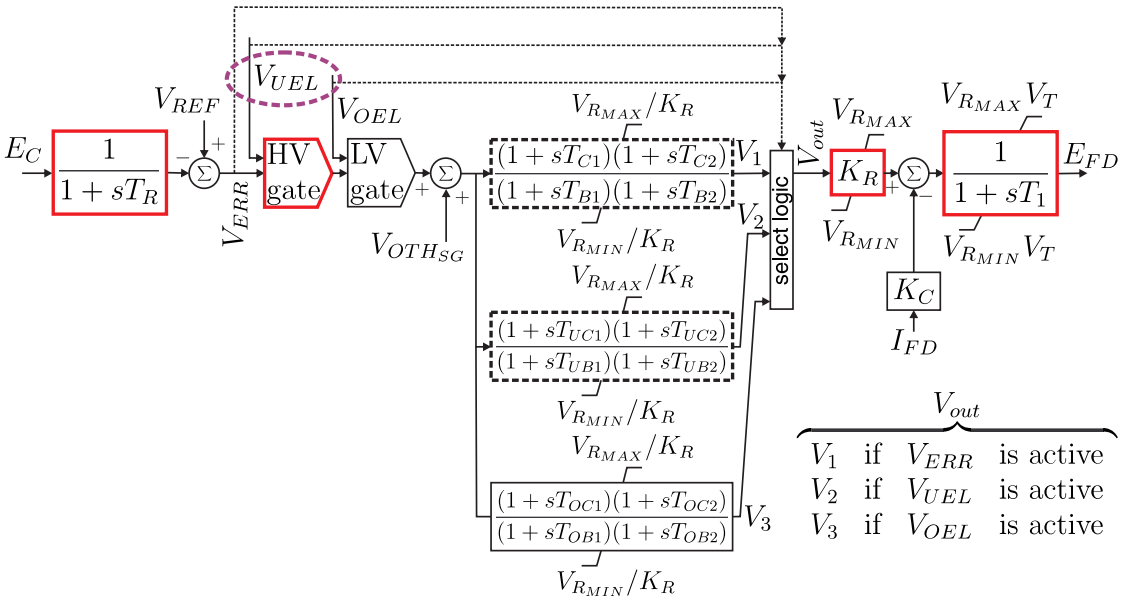

Figure 5.12: ST5B model; PSS/E implementation of IEEE ST5B model.

In Fig. 5.12:

V_{ref} is the reference or desired terminal voltage

E_C is the terminal voltage measured

T_R is the voltage measurement delay time constant

E_{FD} is the excitation voltage output considering rectifier effect and ceiling voltage limits

I_{FD} is the field current measured

K_C represents the equivalent internal resistance of rectifier

$V_{OTH_{SG}}$ represents the auxiliary signals, e.g., power system stabilizer (PSS)

K_R, T_1 represent the main exciter control loop

$T_{C1}, T_{C2}, T_{B1}, T_{B2}$ represent lead lag compensation for AVR control loop

V_{UEL} is the input signal from UEL control action

V_{OEL} is the input signal from OEL control action

$T_{UC1}, T_{UC2}, T_{UB1}, T_{UB2}$ represent lead lag compensation for the UEL control loop

$T_{OC1}, T_{OC2}, T_{OB1}, T_{OB2}$ represent lead lag compensation for the OEL control loop

The parameters of the existing ST1 model are converted to the newer ST5B model, maintaining a similar response for operation of the machine within the GCC area. The equivalence is not very complicated if we assume the same transient gains for all of the different loops, as shown in Table 5.1.

Table 5.1: Conversion of parameters between ST1 and ST5B

ST5B Parameter(s)	ST1 Parameter	Value
$T_{R_{ST5B}}$	$T_{R_{ST1}}$	0.200 s
$T_{C1_{ST5B}}, T_{UC1_{ST5B}}, T_{OC1_{ST5B}}$	$T_{C_{ST1}}$	0.568 s
$T_{B1_{ST5B}}, T_{UB1_{ST5B}}, T_{OB1_{ST5B}}$	$T_{B_{ST1}}$	5.680 s
$T_{C2_{ST5B}}, T_{UC2_{ST5B}}, T_{OC2_{ST5B}}$		0.100 s
$T_{B2_{ST5B}}, T_{UB2_{ST5B}}, T_{OB2_{ST5B}}$		0.100 s
$K_{R_{ST5B}}$	$K_{A_{ST1}}$	700 pu
$T_{1_{ST5B}}$	$T_{A_{ST1}}$	0.003 s
$K_{C_{ST5B}}$	$K_{C_{ST1}}$	0.09 pu
$V_{R_{MAX_{ST5B}}}$	$V_{R_{MAX_{ST1}}}$	9.2 pu
$V_{R_{MIN_{ST5B}}}$	$V_{R_{MIN_{ST1}}}$	-8.1 pu

For validation of the modeling, a comparison of the existing EXST1A response with the newer ST5B response for a change in $\Delta Vref$ of +5% is shown in Fig. 5.13 [187, 188].

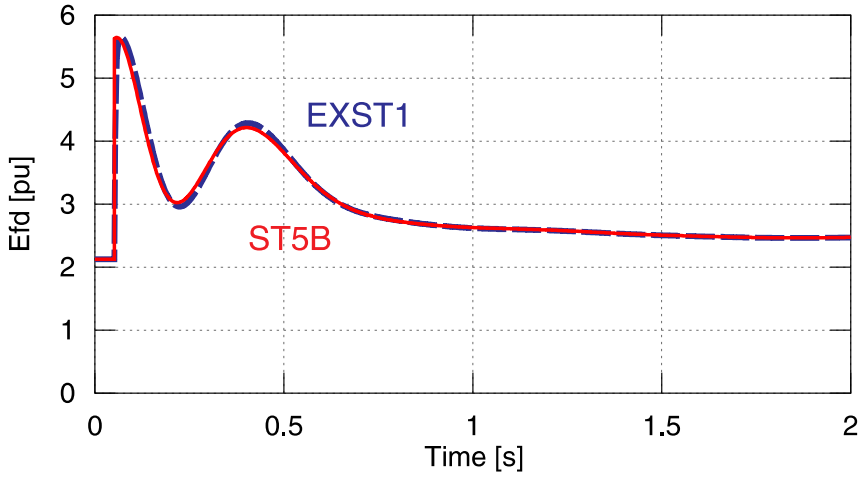

Figure 5.13: Comparison of EXST1 and ST5B responses for a $\Delta Vref = 5\%$

5.6.2 Underexcitation Limiter Modeling

The AESO network database does not include modeling of the UEL control action for any of the machines in the Alberta network. However, it is important for the dynamic coordination proposed to know the dynamic behavior of the UEL and thus a model is described here based on typical assumptions. The underexcitation limiter is modeled using the IEEE UEL2 standard model, which is shown in Fig. 5.9. Some of the parameters used for this modeling are typical (and recommended in IEEE 421.5 standard) and indicated in Table 5.2.

Table 5.2: UEL2 typical parameters

Parameter(s)	Value
T_{UV}, T_{UP}	5.0 s
T_{UQ}	0.0 s
$k1, k2$	2.0 pu
K_{UI}	0.5 pu
K_{UL}	0.8 pu
$V_{UI_{MAX}}, V_{UL_{MAX}}$	0.25 pu
K_{UF}, K_{FB}, T_{UL}	0.0
$T_{U1}, T_{U2}, T_{U3}, T_{U4}$	0.0

The remaining parameters need to be considered more carefully to match the specific GCC of the generator. The UEL limiter characteristic in the PQ plane is typically defined to maintain a margin of about 0.1 pu from the lower curve of the GCC for the particular machine. The UEL characteristic for this case is illustrated in Fig. 5.14, and the corresponding PQ parameters are given in Table 5.3.

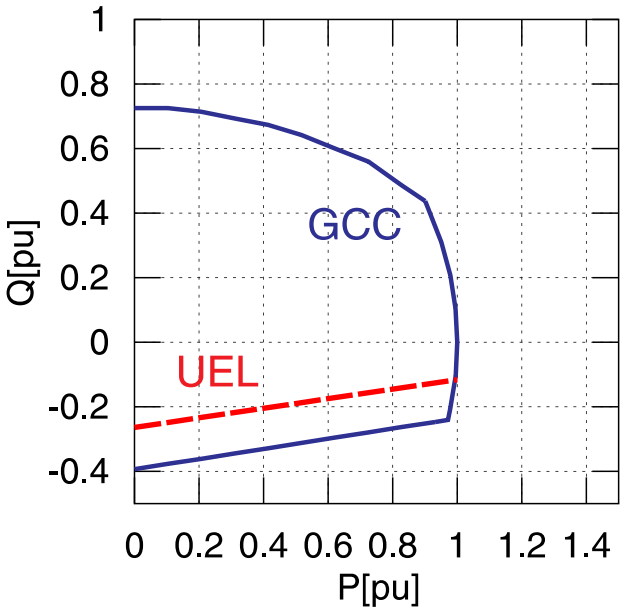

Figure 5.14: UEL characteristic in the PQ plane to coordinate with the GCC

Table 5.3: UEL2 PQ points

Parameter(s)	Value
$P_0 + jQ_0$	0.0 - j0.2635
$P_1 + jQ_1$	1.0 - j0.1158

The minimum values for parameters $V_{UI_{MIN}}$ and $V_{UL_{MIN}}$ must be different from the default zeroes as suggested by IEEE 421.5 standard, because this is a takeover type of UEL. The values selected for these two parameters are given in Table 5.4.

Table 5.4: UEL2 minimum levels

Parameter(s)	Value
$V_{UI_{MIN}}$	-0.1
$V_{UL_{MIN}}$	-0.1

Validation of the UEL model is performed by considering the response to a disturbance

such as a step change in the $Vref$ input of the AVR that causes the PQ point to move beyond the UEL characteristic. This response needs to be compared with actual tests in the machine for the same conditions. The simulation results for this test are shown in Figs. 5.15 and 5.16.

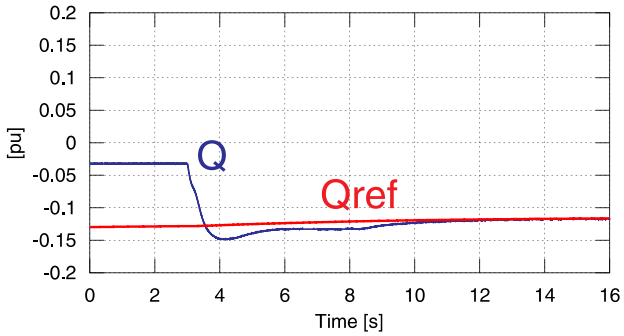

Figure 5.15: Reactive power Q and UEL limiter reference Qref response to a negative step change in Vref of 2.5%

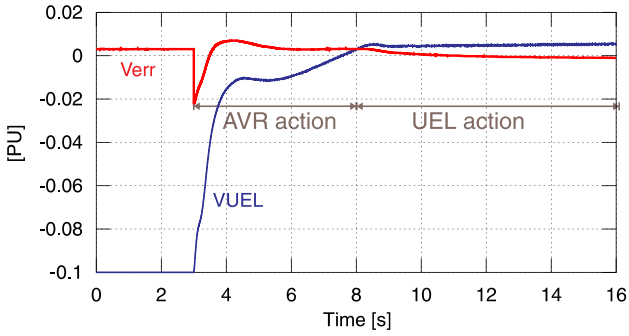

Figure 5.16: Voltage error Verr and UEL signal VUEL response to a negative step change in Vref of 2.5%

The trajectory in the PQ plane is shown in Fig. 5.17. This test is important to verify the performance of the UEL, and in particular to verify the stability of the overall control loop. Fig. 5.15 clearly shows that the reactive power Q converges to the new level without any oscillations.

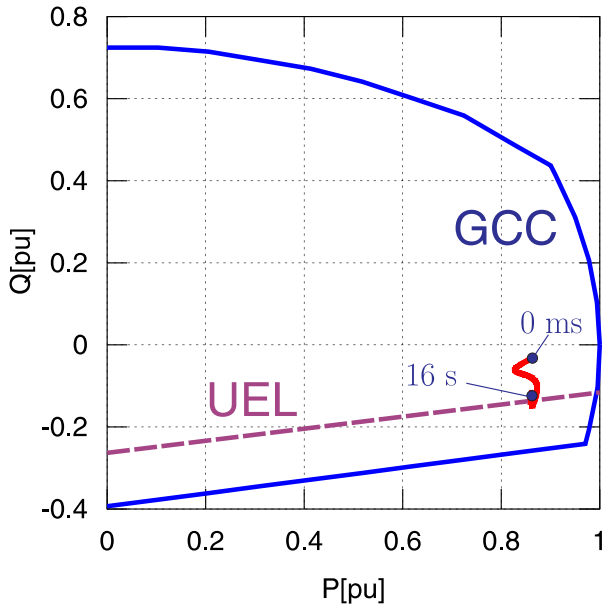

Figure 5.17: Trajectory in the PQ plane for a negative step change in Vref of 2.5%

5.6.3 Static Coordination

Static coordination is achieved based on the margin between several characteristics in the PQ plane or impedance plane, i.e., between the LOE, GCC, UEL, and stability limit if applicable [10]. Coordination between the UEL and the GCC limit due to end core heating was already achieved in Subsection 5.6.2, where a margin of 0.1 *pu* was used.

The steady state stability limits for this case are calculated as a reference to illustrate the improvement in the SSSL by the AVR control action. The SSSL for manual and automatic control is shown in Fig. 5.18. In this case, the SSSL under manual control is close to the GCC and may restrict the characteristic for different voltage conditions following the square of the terminal voltage dependence of this limit. This generator makes use of the redundant excitation control system, which maintains the AVR control action in all conditions. Under AVR control, the SSSL is far from the GCC curve and does not need to be considered in the coordination.

The dynamic stability limits are also calculated as a reference to illustrate the effect of the AVR action on this characteristic. The DYSL for manual and AVR control without PSS

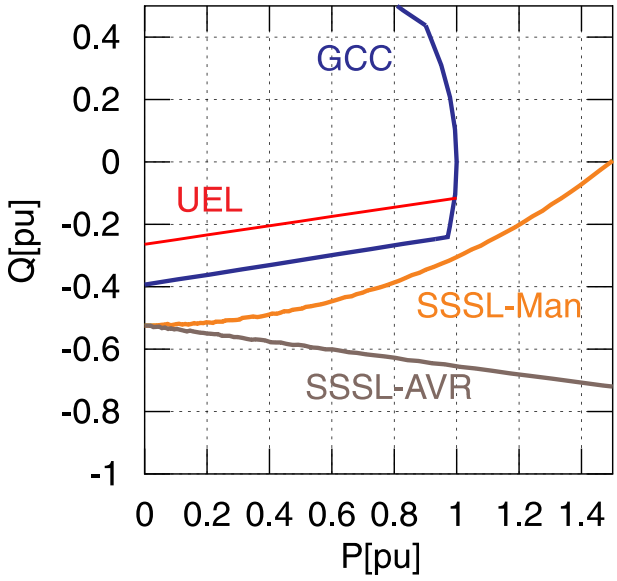

Figure 5.18: Steady state stability limit improvement due to AVR action

is shown in Fig. 5.19.

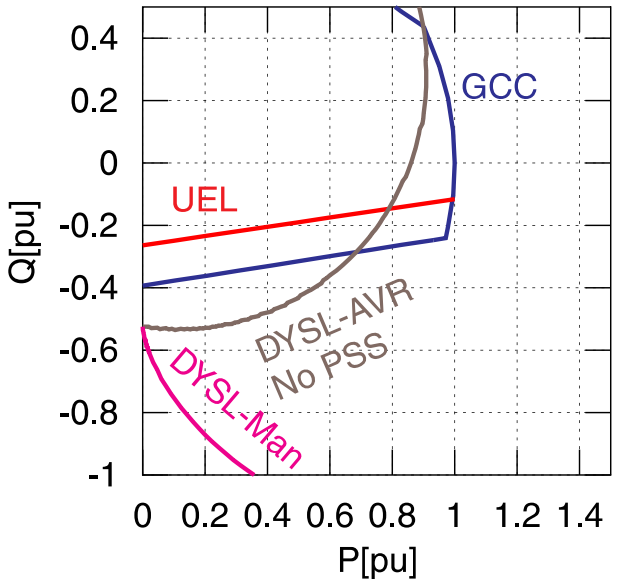

Figure 5.19: Dynamic stability limit change due to AVR action

In this case, the DYSL is the most restrictive of all stability limit characteristics observed when no PSS action is present. This generator needs not only redundant AVR action but also continuous redundant PSS action to maintain stability, especially for higher load conditions. In the AESO network database, it was observed that this generator makes use of PSS control,

and thus the dynamic limit is moved away from the GCC area. The stability limit is therefore not considered for the coordination.

The coordination only needs to consider the GCC and LOE characteristics. The resulting curves showing the coordination in the impedance plane are given in Fig. 5.20. The normal operating point will be located to the left of the GCC and UEL in the impedance plane. The coordination margin between the GCC and LOE is smaller with the larger Blackburn mho zone and directional. The coordination margin between the GCC and the larger Berdy/Mason mho zone approach is reasonable.

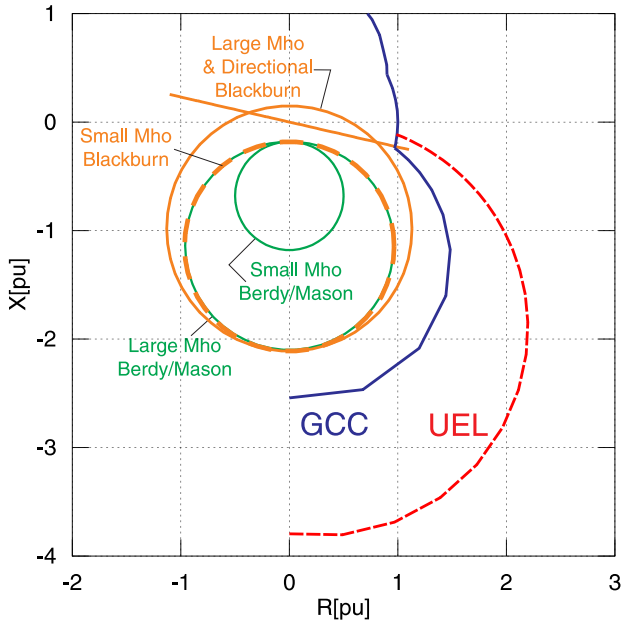

Figure 5.20: Static coordination between LOE, GCC and UEL

5.6.4 Dynamic Coordination

Three different conditions are proposed to verify that coordination is adequate: a) severe stable power swing, b) temporary system overvoltage, and c) unstable power swing. The LOE protection should not maloperate for any of these conditions.

5.6.4.1 Severe Stable Power Swing

The coordination was verified for the most severe power swing condition. The AVR control action helps to prevent the operating point from entering the LOE zones for an extended period of time. The trajectory in the impedance plane for this condition is shown in Fig. 5.21. The power swing trajectory enters the LOE zone in the case of the large Blackburn mho zone, but not the Berdy mho zone. However, the impedance stays inside for only $30ms$, i.e., from 100 to $130ms$, which is not enough to cause a trip. Larger mho zones equate to a larger risk of maloperation, i.e., the larger Blackburn zone has more risk associated with it.

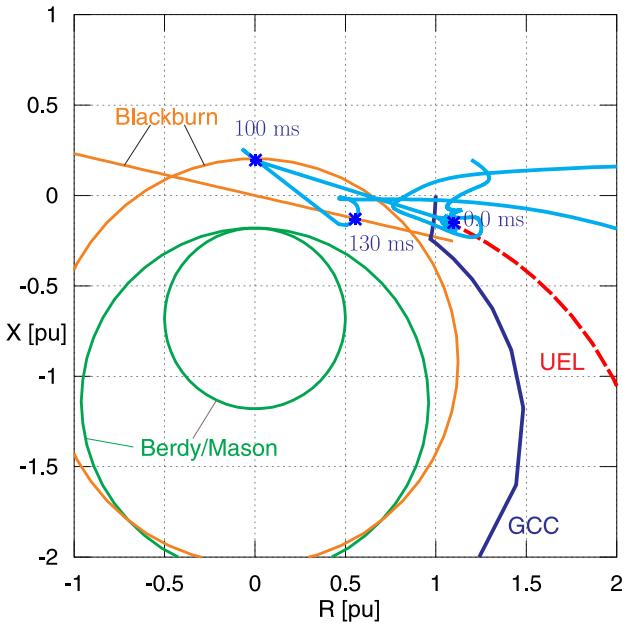

Figure 5.21: Dynamic coordination for severe stable power swing

5.6.4.2 Temporary System Overvoltage

The coordination was verified for a temporary system overvoltage condition. A system overvoltage condition causes the AVR to automatically reduce the excitation. The movement of the reactive power Q in the PQ plane activates the UEL action. The trajectory in the PQ plane for this condition is shown in Fig. 5.22.

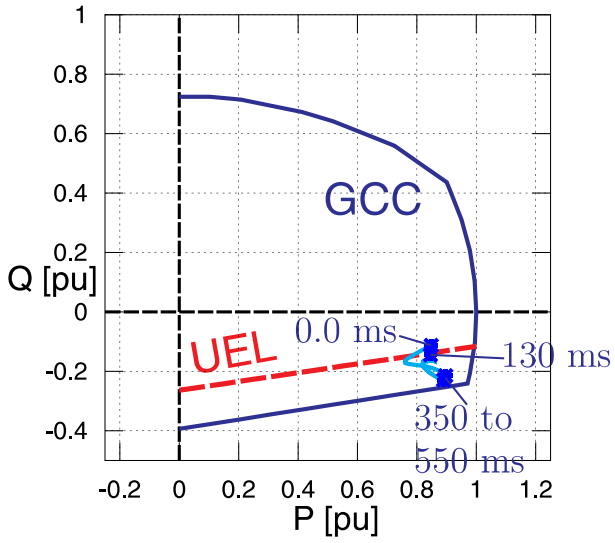

Figure 5.22: Dynamic coordination for temporary system overvoltage in the PQ plane

The trajectory in the impedance plane for this condition is shown in Fig. 5.23. In this case, the power swing trajectory stays at the edge of the LOE zone for the large Blackburn mho zone for about 200 ms, i.e., from 350 to 550 ms. There is increased risk of maloperation based on the Blackburn mho zone. The Berdy/Mason approach does not present a risk of maloperation up to this point.

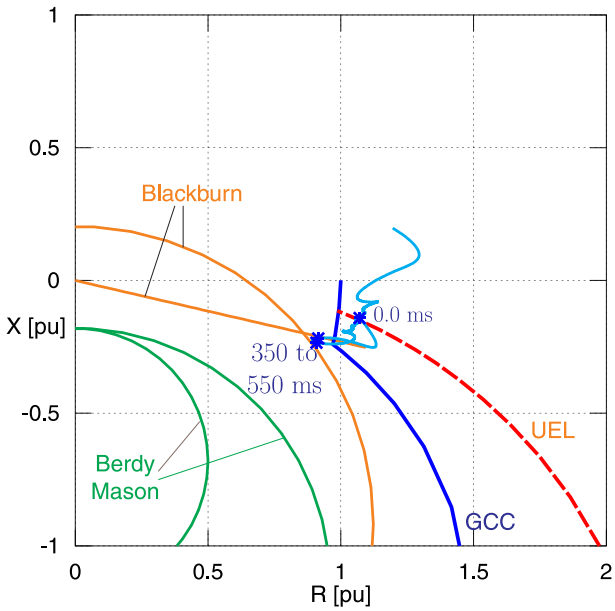

Figure 5.23: Dynamic coordination for temporary system overvoltage

The operating point goes below the UEL characteristic, activating the limiting action. Considering the PQ plane, the operating point does not leave the GCC characteristic. In the impedance plane, however, the impedance touches the large Berdy mho zone. The explanation for this apparent inconsistency is due to the fact that the voltage drops significantly during this disturbance, causing the impedance magnitude to drop and reach the mho zone.

5.6.4.3 Unstable Power Swing

The coordination was also verified for unstable power swing conditions. Unstable power swings are typically produced when a fault is cleared by delayed protections, i.e., when instantaneous protections failed. The generator loses synchronism and the first swing should be detected by the loss of synchronism protection function (function 78). The trajectory in the impedance plane for this condition is shown in Fig. 5.24. In this figure, the trajectory enters the large Berdy mho zone for a 40 ms period, i.e., from 780 to 820 ms, during the second unstable swing. Again, the larger Berdy mho zone is associated with a risk of maloperation in case the loss of synchronism should fail to remove the machine from service at the first swing.

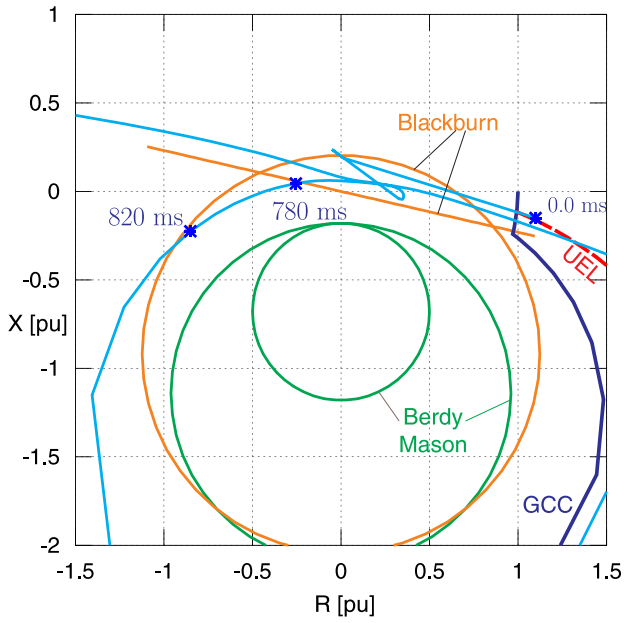

Figure 5.24: Dynamic coordination for unstable power swing

5.6.5 Dynamic Coordination with Proposed SVM Method

The SVM method for LOE detection proposed in Chapter 4 was originally trained for fixed excitation, i.e., manual voltage regulators [1]. This method was tested for several conditions, excluding system overvoltage conditions and the corresponding actions from AVR and UEL controls. Thus, this section describes the results of the SVM method trained for this case system and the coordination achieved. This case is shown in Fig. 5.25.

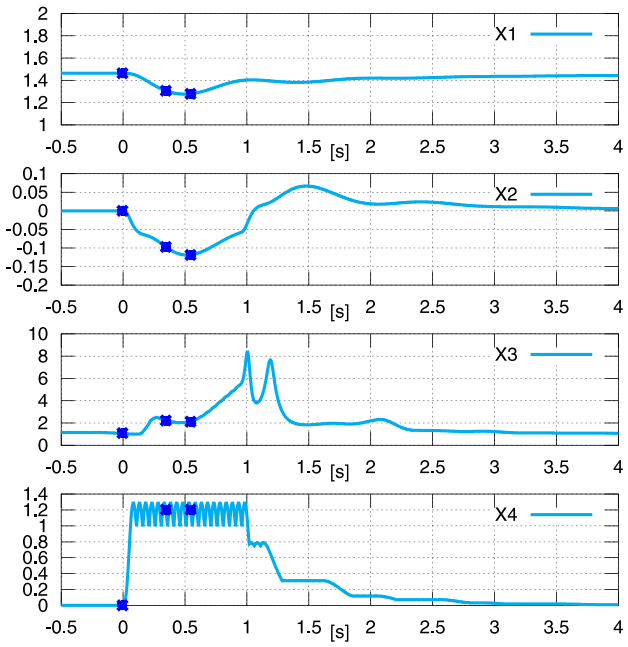

Figure 5.25: Dynamic coordination with proposed SVM LOE detection method for temporary system overvoltage

In Fig. 5.25, consider the time interval from 350 to 550 ms. The first feature $X1$ is reduced as the impedance temporarily approaches the mho centre. The second feature $X2$ is reduced as well, as the reactive power Q goes temporarily below the UEL limit. The third feature $X3$ increases as the disturbance is not a true LOE condition, and the path in the PQ plane is not straight. The fourth feature $X4$ also increases as there are rapid changes within a 1.0 s window. Correct operation of the SVM classifier, i.e., no trip for non LOE conditions, was observed in all cases tested.

5.7 Summary

In this section, the coordination between loss of excitation protection, generator capability limits, stability limits, and underexcitation control was discussed in detail. The limitations of current practice, which makes use of static characteristics for coordination, were highlighted. A case study was used to review static coordination using a real generator from the Alberta network. The proposed considerations for improved dynamic coordination were presented with results of test scenarios that verify the coordination achieved. Finally, the SVM method for LOE detection from Chapter 4 was trained and tested for this realistic case study, with successful verification of the results.

Coordination in the underexcited region basically involves the UEL control and LOE protection functions, and becomes very important in systems that may use this region of the GCC area. Systems in which voltage levels are relatively higher will be more susceptible to dropping into the negative reactive region because they absorb reactive power from the system in order to maintain voltage at acceptable levels. The underexcited region is especially critical because it is relatively closer to the stability limits of the generator, thus the actual stability limit needs to be considered based on the specific excitation control scheme being used, i.e., AVR/PSS availability and redundancy.

In the next chapter, a hardware and software implementation for the SVM method for the detection of LOE conditions is presented. The hardware and software platform design is open and generic to enable the implementation of any other protective relaying algorithm.

Chapter 6

Proposed Real Time Software and Hardware Development for Testing of the Protective Relay

6.1 Introduction

This chapter discusses the relay development platform used to design, test, and debug the LOE relay algorithm. The platform is generic in nature so any real time protection algorithm could be easily implemented and tested by future students in the Real Time Power Systems Simulation Laboratory at the University of Saskatchewan. The processing is time critical, as a decision needs to be made in a very short time frame, i.e., within one or two power system fundamental frequency cycles, whenever a fault happens.

One of the main difficulties in debugging protective relaying algorithms with real signals is that the power system cannot be just paused at a desired time instant to analyze the performance of a given algorithm. This difficulty is addressed in the proposed platform by recording the signals for offline analysis and implementing a playback capability in the overall design.

Offline development is typically performed using specific processor development environment tools, which provide cycle and instruction accurate behavior. However, the use of a processor specific development environment is sometimes cumbersome, as either the em-

ulator board needs to be present or the processor instructions need to be emulated on a host computer. In the proposed platform, a processor independent code is used, so that development can be performed using native host computer development tools. By using the proposed platform independent code, offline testing can be performed either interactively or in batch mode for multiple case evaluation.

The exchange of power system signal information is made using the IEEE COMTRADE standard [189]. This is the typical format for exchange of relay recordings used by the protective relaying industry at the present time. By using the proposed architecture, cases can be generated using offline electromagnetic or real time simulation tools or using recordings of real power system scenarios of interest. In the proposed platform, a given COMTRADE file is played back to the protective algorithm under development.

The proposed platform is used to demonstrate a hardware implementation of the proposed SVM method for the detection of LOE conditions described in Chapter 4. The cases and tests previously performed used offline simulation of the proposed method with a software implementation embedded in the ATP electromagnetic simulation environment.

6.2 Hardware Implementation Considerations

The proposed platform is implemented using DSP development board 6713DSK (C6713 DSP Starter Kit) from Texas Instruments [190]. However, the discussions below are in most cases generally applicable to different embedded architecture development platforms for protective relaying.

6.2.1 Analog Inputs

6.2.1.1 Channels

The number and type of channels depends on the protective function being considered. Basically, there are two type of channels: voltage input and current input. For instance, a

numerical overcurrent relay typically uses three analog inputs, i.e., one for each current phase. A numerical distance relay uses six analog inputs, i.e., three voltage and three current input channels. Typically, a loss of excitation protection uses two analog inputs, i.e., one voltage channel and one current channel; however, this function is integrated within a multifunction numerical relay platform in current state of the art in relaying. To implement the proposed SVM method, one voltage input and one current input are used.

6.2.1.2 Sampling Rate

The state of the art in numerical relays uses a sampling rate, typically in the range of 64 to 128 samples/cycle. This sampling rate is equivalent to 3,840 to 7,680 Hz in power systems with a fundamental frequency of 60 Hz. The proposed platform on the 6713DSK board uses a sampling frequency of 8,000 Hz, which is equivalent to around 134 samples/cycle.

6.2.1.3 Range

Protective relay applications use normalized ranges for voltage and current inputs. The nominal voltage input on a relay is typically on the order of 100 to 120 V rms phase to phase considering a three phase system. This nominal range results in a range as given by (6.1).

$$V_{Nom-Peak} = \frac{120}{\sqrt{3}} \cdot \sqrt{2} = 97.98V \tag{6.1}$$

The voltage input for protective relay applications needs to provide a linear response during fault conditions beyond the normal range. The dynamic range for the voltage input signal in the proposed platform should cover most overvoltage conditions. Here, a maximum range of 220 V peak is used, which is equivalent to about 2.25 times the nominal.

The nominal current input on a relay is typically 1 A or 5 A. The smaller nominal value is more typically used outside North America, or when for a given application the relay location is very distant from the current transformers. Considering a typical 5 A relay, the

nominal range of the analog input is given by (6.2).

$$I_{Nom-Peak} = 5\sqrt{2} = 7.07A \tag{6.2}$$

The dynamic range for the current input signal should consider most fault conditions. The current signal during fault conditions in many cases presents DC offset due to the largely inductive nature of the power system network. This DC offset is superimposed on the fundamental frequency and theoretically may shift the AC waveform by 100%, in which case the range would need to be multiplied by 2.0. In practice, the most severe DC offset typically reaches 80% above the nominal, i.e., the range needs to be multiplied by 1.8. The main current transformers that scale down the currents from the power line down to 5 A are typically specified to saturate at about 20 times the nominal current, i.e., at around 100 A rms. Considering both factors with the nominal peak current, the maximum dynamic range for the current channel is obtained in (6.3).

$$I_{Dyn-Peak} = 5\sqrt{2} \cdot 1.8 \cdot 20.0 = 254.56A \tag{6.3}$$

Thus, a dynamic range of 250 A peak, which is equivalent to about 36 times the nominal, is used in the proposed platform.

6.2.1.4 Resolution

Resolution requirements depend on the type of channel and the sensitivity of the desired application. Voltage protection functions in typical applications use a minimum increment step of 0.1% of the nominal. Because the maximum range is about 225% of the nominal, the number of bits (resolution) needs to be at least that given by (6.4).

$$N_{Bits-V-Channel} = \frac{\log\left(\frac{225}{0.1}\right)}{\log\left(2\right)} = 11.1 \tag{6.4}$$

Overcurrent protection functions in typical applications also use a minimum increment step of 0.1% of the nominal. Because the maximum range is about 3600% of the nominal, the number of bits (resolution) needs to be larger than that for voltage channels, and is given by (6.5).

$$N_{Bits-I-Channel} = \frac{\log\left(\frac{3600}{0.1}\right)}{\log\left(2\right)} = 15.1 \tag{6.5}$$

It should be noted that the resolution specification applies to the total range of the A/D converter, i.e., plus and minus, although the calculation was done using only one side of the analog signal.

The proposed platform in the 6713DSK uses two analog channels with 16 bits of resolution, which satisfies typical input sensitivity requirements for both voltage and current.

6.2.1.5 Scaling

Scaling is platform dependent and requires knowledge of important parameters, such as the A/D binary output format, maximum/minimum signal levels, and the design specific values that these represent.

In the proposed platform implementation on the 6713DSK, the samples are obtained in 16 bit signed integer format, which has a range between -2^{15} and $+2^{15}-1$. The analog channels have a range from -3 V to +3 V. Based on these and the earlier discussion about input signal ranges, the equivalence is given in Table 6.1.

Table 6.1: Analog input channel ranges

A/D	Analog Input	Channel Type	Channel Value
-32768	-3 V	V	-220 Vpk
+32767	+3 V	V	+220 Vpk
-32768	-3 V	I	-250 Apk
+32767	+3 V	I	+250 Apk

6.2.2 Processor

The processor in protective relaying embedded architecture is selected based on the real time performance, type and number of peripherals to be associated with the particular processor, and the level of arithmetic processing required, among other criteria. There is no rule of thumb, but a typical numerical relay may use two types of processors: General Purpose Processors (GPP) and Digital Signal Processors (DSPs).

6.2.2.1 GPP or DSP

A GPP, i.e., general purpose CPU , is used to interface several types of temporary and permanent memory storage, timers, communication, human machine interface such as keyboard and display, binary I/O, analog to digital conversion, and other CPUs, and so on. This type of processor in many cases uses a multi-tasking operating system, with the highest priority task being the protection interrupt.

DSPs are used mainly in protective relaying for arithmetic computations, such as Discrete Fourier Transform (DFT), Finite Impulse Response (FIR) or Infinite Impulse Response (IIR) prefiltering, phasor magnitude and angle, and algorithm specific computations, among others. The operating system is typically linear, using a single task and few logic branches in the execution path.

The proposed platform was implemented using DSP type TMS320C6713 from Texas

Instruments on a hardware module DSP Starter Kit (DSK) from Digital Spectrum.

6.2.2.2 Protection Interrupt and Speed

The basic processing speed requirement is to perform all computations with the signal samples received from the A/D converter before the next set of samples arrive; this is typically the protection interrupt period. Application specific requirements may define the protection interrupt frequency based on the required decision time of the specific protection function. The CPU load usage is an important parameter in the development of a given embedded protective relaying platform, and needs to be measured at every stage of development.

For instance, time overcurrent protection using the IEEE moderately inverse time characteristic has a minimum operating time of $603ms$ for a current 10 times the pickup level if using a time multiplier of 0.5. In this case, a protection interrupt of $\frac{1}{2}$ power system cycle, i.e., 8.33 ms at 60 Hz, would be enough for the application requirement. With this protection interrupt frequency, 32 samples are processed per channel if using a 64 sample/cycle sampling rate.

Another important example is line protection using the impedance or distance function. Here, the fastest operating time possible is desired, typically ranging from 0.25 cycles up to 1.5 cycles. Thus, for the distance function case, a protection interrupt of around 1 ms is typically used, with the number of samples to be processed at about 8 samples per channel when using a 128 sample/cycle sampling rate.

The proposed platform was implemented using a protection interrupt time of 5 ms, with 40 samples to be processed per channel at a sampling rate is 8 kHz. The DSP clock used in this platform operates at 225 MHz.

6.2.2.3 Fixed/Floating Point

Fixed point arithmetic processing is less expensive in terms of computing effort compared with floating point arithmetic. However, the use of fixed point requires careful knowledge

of the range values of the computations to be performed at every stage to prevent overflow when handling large input signals. At the same time, fixed point requires careful knowledge to prevent losing significant bits when input signals are low. In spite of these difficulties, typical protective relaying embedded architectures use fixed point arithmetic, due to the number of channels and the amount of calculations required.

Typical fixed point processors currently use a 32 bit register size, which allows processing of 16 bit arithmetic without losing significant bits. One important factor to consider is the required dynamic range for the type of input signal. The voltage channel only requires a resolution of 12 bits based on the previous discussion. However, the dynamic range of current channels is larger and requires a resolution of 16 bits.

The proposed platform implementation uses fixed point arithmetic, but implements a pseudo floating point library in software to be used for some real and complex number computations. The advantage of this approach is that the portability of the resulting code eases development of the desired protection algorithms.

6.2.3 Storage

Protective relaying embedded architectures make use of several types of storage memory, such as Read Only Memory (ROM), Flash, and Random Access Memory (RAM). ROM is typically used for storing the boot loader program. The boot loader is active during system startup, to load the application code into program memory space, and also is used when upgrading the firmware into Flash memory. Flash memory is commonly used to store the firmware, protective relay settings, and parameters, but also is useful for storage of waveform recording as this requires a significant amount of space. RAM is used for the program space and working data space.

6.2.3.1 Platform Specific

In the proposed platform implementation, there are basically two memory areas: 256 KB of Internal RAM (IRAM on the 6713DSK) and 16 MB of External RAM (SDRAM on the 6713DSK) . The internal RAM memory is smaller but typically faster than the external RAM, so allocation between these two should be made carefully to obtain the best possible performance.

6.2.3.2 Application Code

Depending on the size of the program space, it is possible that all can be allocated in internal RAM; this will ensure good performance. In case the program space is larger than the available internal RAM, it is convenient at a minimum to allocate libraries or functions that are frequently used in internal RAM, keeping larger portions of code in external RAM.

In the proposed platform implementation, all of the program code was allocated to IRAM.

6.2.3.3 Data and Variables

A similar criteria for memory allocation is applicable for data and variables; at a minimum, the most frequently used variables or data should be allocated to internal RAM.

In the proposed platform implementation, most of the data, with the exception of waveform recordings, were allocated to IRAM.

6.2.3.4 Signal Recording

Protective relaying embedded architecture needs to consider space for waveform recording. This is typically an external Flash memory, because the waveform recording needs to remain available when the protective relay is powered down. When using Flash memory, the actual storage process is sometimes performed using a combination of external RAM for temporary storage plus a relatively low priority task outside the main protection interrupt

to perform the actual storage in Flash. This extra effort is required because writing to Flash is a relatively slow process.

In the proposed platform implementation, the waveform recording is performed in external RAM, i.e., SDRAM. The approximate use of SDRAM in this implementation is 50.00% for recording storage of IEEE COMTRADE waveforms with 30 s of information including input signals and output calculations.

6.2.4 Outputs

Most embedded relay architectures provide several types of outputs, such as contact output(s) for tripping breakers, LEDs for indication of a trip operation or other alarms, display for visualization of measurements or configuration parameters, and recording of calculation results and status of protection functions for fault analysis, among others.

In the proposed platform, three types of outputs were implemented: LED indication, calculation results recording, and protection bits recording.

6.2.4.1 LEDs

In the proposed platform implementation, only one LED was used to indicate that the protection algorithm was triggered and waveform recording was in process, as it stores 30 s of information.

6.2.4.2 Calculation Results

In the proposed platform implementation, several calculation results were recorded in COMTRADE format, including: a) current and voltage phasor values, b) complex apparent power and impedance values, c) SVM feature calculations, and d) traditional LOE detection pickup and trip decisions.

6.2.4.3 Protection Bits

In the proposed platform implementation, certain important bit status were also recorded, such as the waveform triggering signal.

6.3 Power Systems Simulation

The proposed platform was tested using the sample system described in Section 4.5 for comparison with results already published [1]. This platform was tested during the development cycle using two types of power system simulation: offline electromagnetic simulation with ATP/EMTP and real time digital simulation with RTDS.

6.3.1 Offline: ATP

The implementation of the SVM method of Chapter 4 was performed using the Foreign Models compiled object in ATP in four parts: a) phasor estimation, b) positive sequence phasor calculation, c) 10 Hz low pass filtering, and d) SVM and traditional LOE methods. The phasor estimation was implemented per phase and per channel using a recursive DFT method with a window size of 256 samples in C language. The positive sequence phasor calculation was implemented using TACS in ATP to calculate the positive sequence voltage and current phasors. The low pass filtering was also implemented using TACS in ATP to calculate the filtered real and imaginary components of the positive sequence that was the input for the SVM and LOE protection algorithms. The SVM and traditional LOE methods were implemented in C language in Chapter 4.

In this new platform, the original ATP simulation was used to produce IEEE COMTRADE waveforms that were used as inputs signals for testing in the development of the algorithms. The advantage of the proposed platform is that it is designed so that testing and debugging can be done offline as well as to capture cases during online testing for offline analysis and resolution.

6.3.2 Real Time: RTDS

An overview of the setup used for testing of the platform with RTDS is shown in Fig. 6.1 [38]. The implementation of the test system in RTDS was slightly different from the original ATP simulation. In RTDS, the analog signals for each voltage and current were transformed into positive sequence voltage and current analog signals using a filter similar to that used by analog solid state protective relays. Two analog output channels of 16 bit resolution were used to send the analog positive sequence voltage and current to the DSP implementation of the SVM and LOE algorithms. The phasor estimation using recursive DFT was performed inside the DSP platform, then the 10 Hz low pass filter was applied to the resulting real and imaginary values of these phasors. These filtered phasors were then used as input for the SVM and traditional LOE methods implemented in the proposed DSP platform.

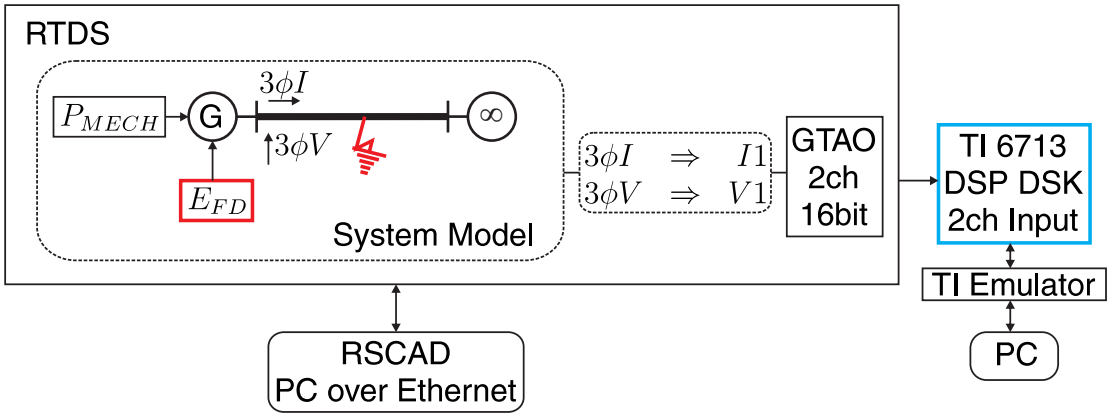

Figure 6.1: Hardware setup for RTDS testing of the SVM LOE algorithm on the DSP platform

One important consideration when interfacing the RTDS analog signals with a given DSP platform is the scaling and range. Two channels from the GT Analog Output (GTAO) card from RTDS were used, which have a +/- 10 V range and 16 bit resolution. There was almost a 2 bit loss in resolution due to the fact that the analog signal output needs to be scaled to match the +/- 3 V range of the DSP board.

The primary voltage and current signals in the power system model are scaled down by

a PT ratio of 13,800/120 V and CT ratio of 5,000/5 A. The scaling factor in the GTAO object inside RTDS represents the number of units, kV or kA, that correspond to a 5 V output. Using the information in Table 6.1, the CT and PT ratios, and the definition of the RTDS scaling factor, the specific scaling factors for this implementation are given by (6.6) and (6.7).

$$N_{RTDS-V} = 220Vpk \cdot \frac{5V}{3V} \cdot \frac{13800V}{120V} = 416.667\frac{kV}{5V} \tag{6.6}$$

$$N_{RTDS-I} = 250Apk \cdot \frac{5V}{3V} \cdot \frac{5000A}{5A} = 42.167\frac{kA}{5V} \tag{6.7}$$

6.4 Software Implementation: Platform Specific Considerations

6.4.1 Portability

An overview of the software architecture for the proposed relay development platform is shown in Fig. 6.2. One of the main criteria for the proposed platform was to make the application code portable so that the same exact code is used in both platforms, i.e., the PC simulator and the DSP platform.

6.4.1.1 Language: C

The language used in the proposed platform is C, a very flexible, well-known language. The performance may not be as fast as directly developing assembly language, but portability between DSP and PC platforms is almost completely ensured.

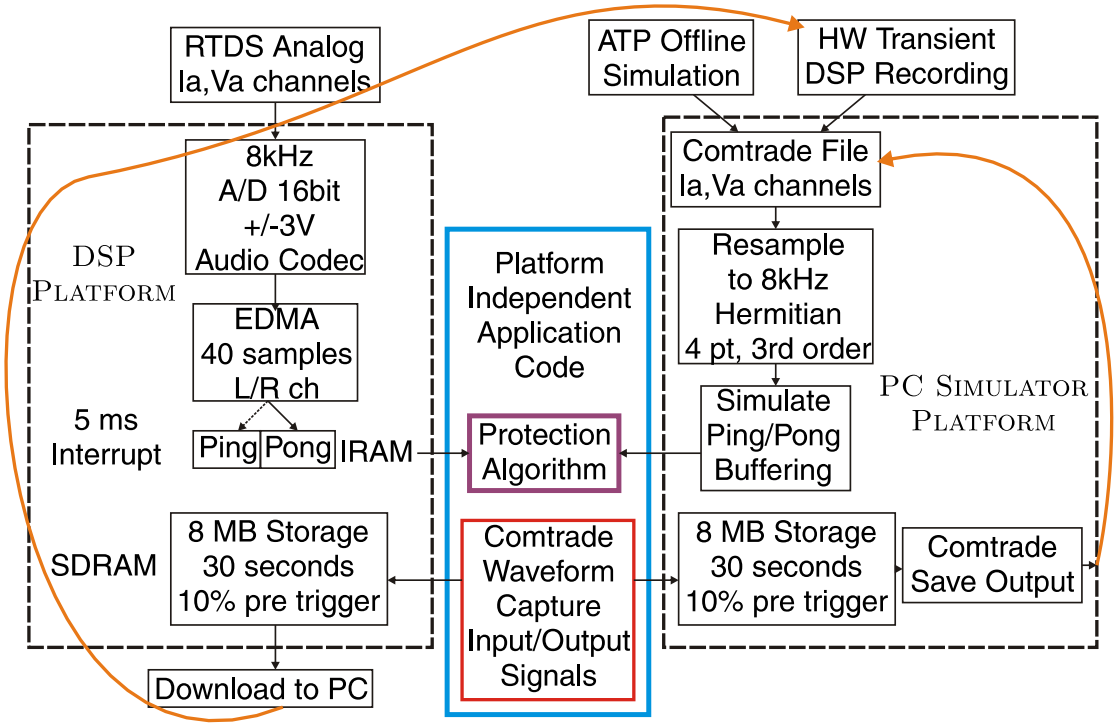

Figure 6.2: Software architecture of the proposed relay development platform

6.4.1.2 TI Code Composer

Some considerations observed during development apply to specific implementation of the development environment of the TI Code Composer. One of the considerations concerned memory alignment, as aligning 32 bit integer variables to a 2 byte address was required in order to assemble the COMTRADE sample record. The 6713DSK did not allow a 4 byte integer variable to be written directly into a region using 2 byte resolution address and it automatically realigned the data written to the next 4 byte address. This problem was solved by copying information byte by byte. Another consideration was initialization of static variables, which was assumed to be automatically zeroed. All initializations had to be programmed specifically. One last consideration was the assignment of specific variables to a specific address space. This was required to allocate memory storage for COMTRADE waveforms in external RAM in the DSP platform.

6.4.1.3 Open Watcom PC Development

The previous considerations discussed in the TI Code Composer were not necessary and in fact were not observed during development in the Open Watcom SDK [191] until the code was ported (copied and compiled) into the DSP platform. One consideration specific to this PC simulator platform was observed when trying to read a COMTRADE input file about 45 MB in size by using the fread() standard C function. The idea was to read the whole file in one operation and let the operating system handle the read optimally, but this was not possible. The solution was to split the total read into smaller pieces and find the optimum size to achieve the best possible reading performance. One important consideration is the type of variables used, as both the DSP and PC platforms are sharing the same exact code. This problem was solved by using specially defined variable types based on the platform specific types on a separate header file.

6.4.2 Platform Specific Code

The basic task of the platform specific code in the proposed design is to obtain the signal samples with the scale required by the application.

6.4.2.1 DSP: Base Architecture Initialization

An overview of the proposed software architecture for the DSP implementation is given in Fig. 6.3. In the DSP platform, several subsystems need to be initialized: a) the interrupt vector, b) the multitask operating system, c) the serial ports that interface with the A/D converter, d) the A/D converter, and e) the EDMA interface that receives the samples from the A/D. To ease the implementation process, a template example available from the TI Code Composer Studio was used, i.e., \examples\dsk6713\bsl\dsk_app.

The sampling rate was adjusted to 8 kHz, and the size of the input buffer for the EDMA transfer was adjusted to 80 samples, i.e., 40 samples times 2 channels, to match the 5 ms interrupt period. Only three function calls were inserted in the existing template example:

a) initdspmain(), b) ani(), and c) dspmain(). The initdspmain() is the initialization routine for the platform independent code, and is called before starting the protection interrupt and A/D converter. The ani() routine is the analog interface that uses knowledge of the specific format of data received from the A/D converter and performs the mapping and scaling to the internal protective relay input signal buffers. The pingPong control flag was made global so that the ani() interface can keep track of the current receiving buffer in the ping pong scheme of the DSP platform. The dspmain() is the actual main function of the platform independent protective relay program. LED number 1 was activated based on the status of the trig_active variable from the protective algorithm. A minor but important change was to eliminate the 25% of load() included by default in the original template to free CPU time for the desired protective algorithms to be implemented.

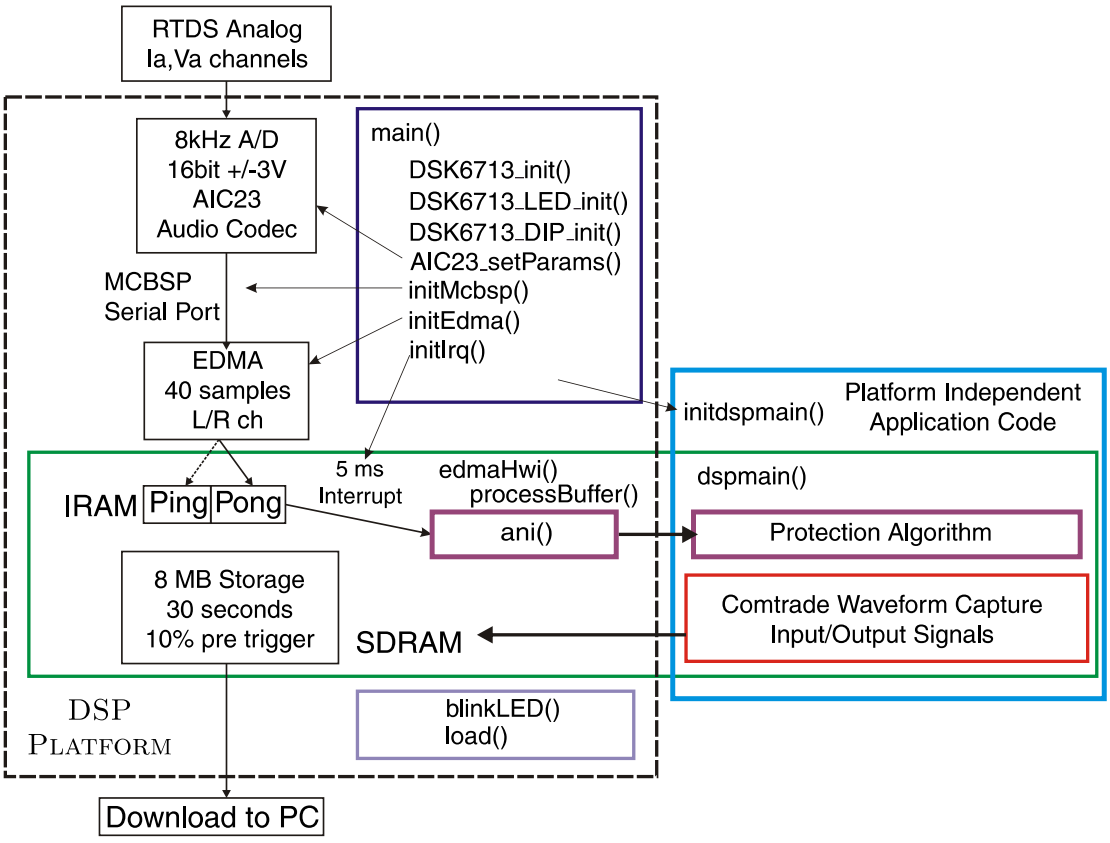

Figure 6.3: Software architecture DSP specific platform

6.4.2.2 PC: Basic DSP A/D input simulator, Playback of IEEE Comtrade Input file, and Resampling

An overview of the proposed software architecture for the PC simulator of the DSP implementation is given in Fig. 6.4. The PC simulator platform has to essentially replicate the behavior of the DSP, i.e., simulate the protection interrupt call, follow the ping pong scheme of the DSP platform, and provide the input samples to the protection algorithm.

The input samples are obtained and played back from an IEEE COMTRADE file containing the voltage and current channel samples. For this purpose, a routine ldoieee() was implemented that parses the channel parameters from the COMTRADE configuration file and is capable of loading either ASCII or BINARY data file formats into PC memory. The sampling rate of the signals in a COMTRADE file is not fixed and is specified in the configuration file, but may not necessarily match the sampling rate of the protective relay algorithm being tested.

In order for the COMTRADE input signals to match the required 8 kHz, a resampling function rsoieee() is implemented using the 4 point third-order Hermitian method of interpolation. Typically, a COMTRADE file generated by an electromagnetic simulation such as ATP would have a sampling frequency higher than 8 kHz. Thus, resampling is done to an oversampling frequency higher than the original COMTRADE but a multiple of the desired 8 kHz. Once resampling is performed, a 5th order low pass Butterworth filter is used as an anti-alias filter followed by an integer downsampling to the desired 8 kHz.

If the COMTRADE file was recorded by the DSP platform during RTDS testing, the sampling rate is 8 kHz and there is no need for resampling.

6.5 Platform Independent Software Implementation

An overview of the platform independent software architecture implementation is shown in Fig. 6.5, including the interaction between different software components such as phasor estimation, COMTRADE recording, the string and math libraries developed, and the SVM

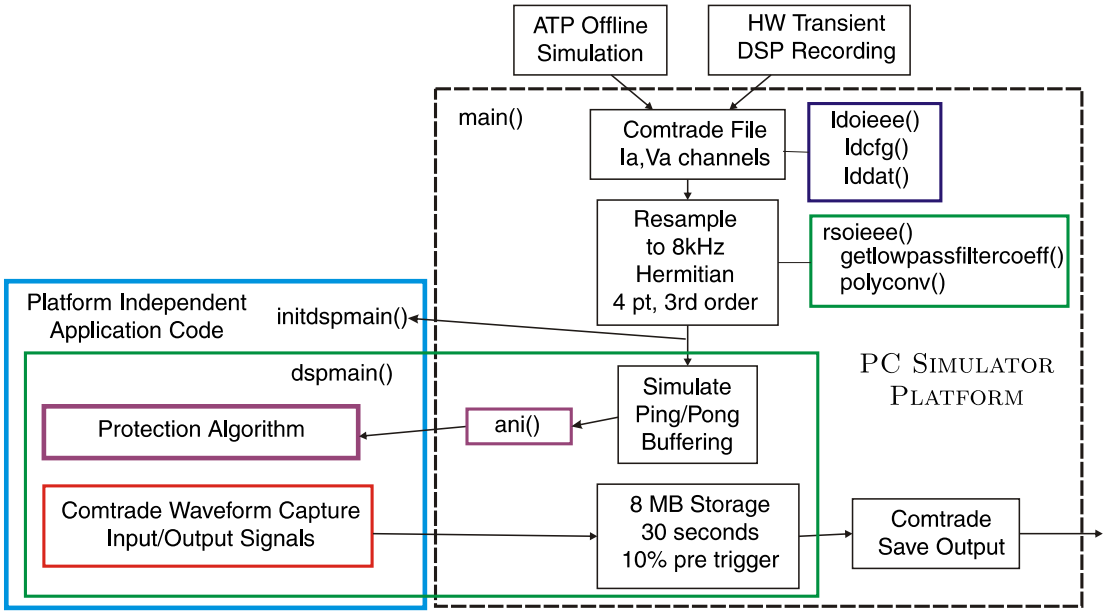

Figure 6.4: Software architecture PC specific platform

methodology implemented. The different components are described next.

6.5.1 Phasor Estimation

Phasor estimation is performed by using a recursive Discrete Fourier Transform (DFT) with full cycle window. The sine and cosine coefficients for the DFT are calculated and defined by an external macro in Octave (also compatible with Matlab) that creates a header that is included in the code. Because the arithmetic is fixed point, the coefficients are scaled to 15 bit value.

A rolling window of input signal samples is maintained for each channel, and is used to calculate the DFT. The design was implemented so that the DFT window size is defined at one location on header file dsp.h by the macro variable ONECYCLE. In the same header dsp.h, the number of samples received from the A/D converter at every protection interrupt by the macro NOFBUFSAMP as well as the total number of channels by the macro NOFDFTCHAN are also defined. In this way, the design is flexible enough to adapt to different hardware architectures with different sampling rates, protection interrupt time periods,

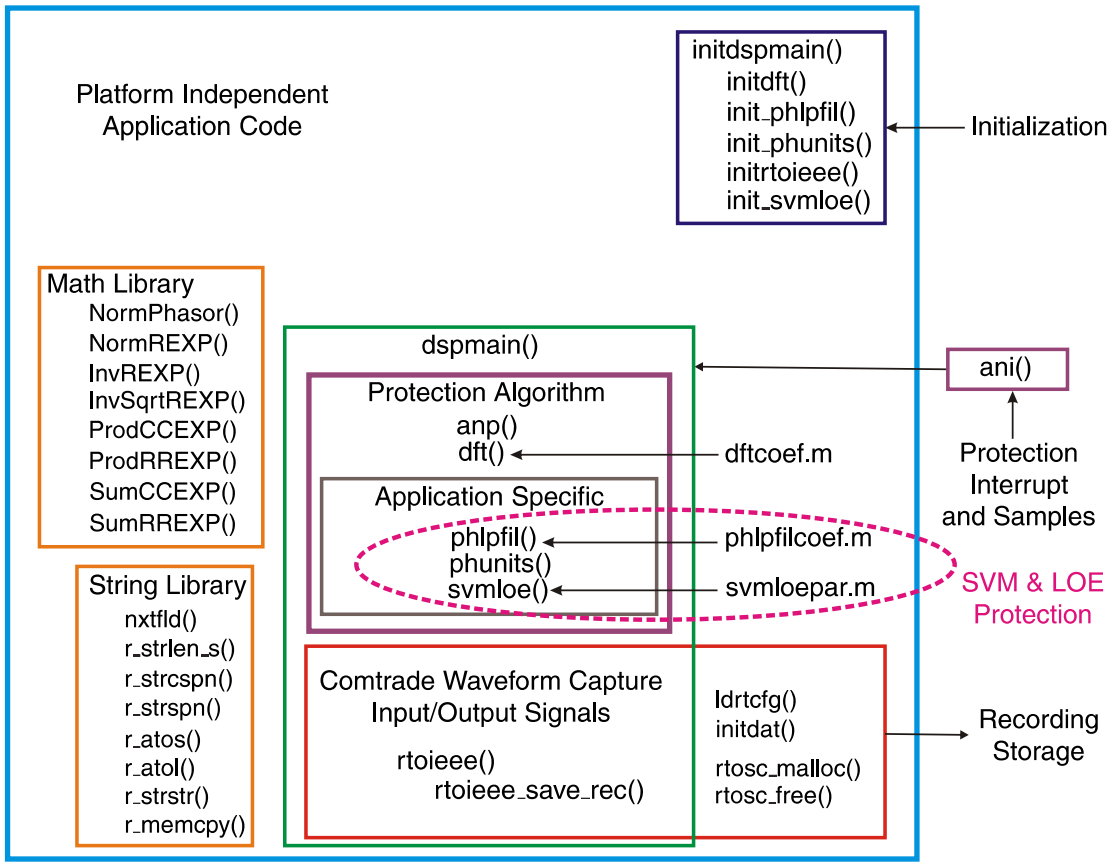

Figure 6.5: Software architecture platform independent implementation

and numbers of analog channels.

In the proposed implementation, the ONECYCLE window size is 134 samples, the NOFBUFSAMP is 40 samples, and the NOFDFTCHAN is 2 channels for DFT. It should be noted that a ONECYCLE window size of 134 samples does not exactly synchronize the window size with a fundamental frequency period on 60 Hz systems, and this produces a small error in angle and magnitude estimation. To achieve synchronization of sampling rate, window size, and the power system signal, a frequency of 8040 Hz, i.e., $= 134 \cdot 60$, would be required instead of the 8 kHz used.

6.5.1.1 Recursive DFT

The recursive DFT method is implemented by rotating the set of sine and cosine coefficients in time. For instance, if a new phasor is calculated at every sample instant, the sequence of coefficients will be as given by (6.8).

$$\underbrace{\begin{bmatrix} t_0 \\ t_0 + \Delta t \\ t_0 + 2\Delta t \\ \vdots \end{bmatrix}}_{\text{Time}} \Longleftrightarrow \underbrace{\begin{bmatrix} 1, & 2, & \cdots & , & N \\ 2, & 3, & \cdots & N, & 1 \\ 3, & 4, & \cdots & 1, & 2 \\ \vdots, & \vdots, & \cdots & \vdots & \vdots \end{bmatrix}}_{\text{Coefficient Index}} \tag{6.8}$$

where:

t_0: time in which original sequence occurs

Δt: sampling period, i.e., time between samples

N: DFT window size

Every N samples, the sequence repeats again. The effect, i.e., advantage, of recursivity is that each sample is multiplied once by a given sine or cosine coefficient. Because the DFT is calculated every time a new set of samples is received from the A/D, there are NOFBUFSAMP multiplications and additions to perform for each real and imaginary component, resulting in a partial sum for each of these components. The real and imaginary partial sums are referred to as phaselets. Using each phaselet just obtained, a full window sum is performed with prior phaselets to obtain the real and imaginary components of the desired phasor.

One difficulty, i.e., flexibility, resulting from the proposed platform is that no restriction was imposed on the sampling rate relationship with the protection interrupt interval. In typical protective relaying platforms, the protection interrupt time period is selected so that

the fundamental frequency of the power system has a period that is a multiple integer of the protection interrupt time period. In this way, the ONECYCLE number of samples is required to be a multiple of the NOFBUSAMP number of samples received from the A/D for each protection interrupt.

The proposed platform is flexible in that ONECYCLE does not need to be a multiple of NOFBUFSAMP. This flexibility was implemented by using an incomplete phaselet concept. The number of phaselets to assemble a full cycle window is given in a macro variable NOFPHASELETS. In the special case that ONECYCLE is an integer multiple of NOFBUFSAMP, the following relationship (6.9) applies.

$$\text{ONECYCLE} = \text{NOFPHASELETS} \cdot \text{NOFBUFSAMP} \tag{6.9}$$

In a general case, where ONECYCLE is not a multiple of NOFBUFSAMP, the (NOFPHASELETS - 1) phaselets are equal and the oldest one will be incomplete, i.e., will have less than NOFBUSAMP samples. The end result is that adding all NOFPHASELETS phaselets provides the desired phasor.

6.5.1.2 Optimized Fixed Point

The use of fixed point arithmetic in the proposed platform requires careful consideration in terms of the scaling and ranges of the values used. Consider the basic equation to calculate the real component V_{RE} of the fundamental frequency voltage phasor using DFT, given by equation (6.10):

$$V_{RE} = \frac{2}{N} \sum_{k=1}^{N} v_k \cdot c_k \tag{6.10}$$

where

N: window size, i.e., ONECYCLE

v_k: instantaneous voltage sample k

$c_k = \cos(\frac{2\pi k}{N})$: cosine coefficient k

The equation (6.10) is implemented in the proposed platform using 15 bit plus sign fixed point arithmetic and, assuming the input signal v_k is already in 15 bit format, it can be rewritten as (6.11).

$$V_{RE} = \frac{2}{N} \sum_{k=1}^{N} v_k \cdot \left(\frac{c_k \cdot 2^{15}}{2^{15}} \right) \tag{6.11}$$

In equation (6.11), it is reasonable to assume that if the signal v_k is a full scale signal, i.e., +/- 15 bit, in the time window considered, the value of V_{RE} may also give as a result a 15 bit number. Also, from equation (6.11) it is derived that the result of performing the sum is a value $N/2$ times larger than V_{RE}. Considering our proposed implementation with $N = 134$ so $N/2 = 67$, which is slightly larger than a 7 bit number, rearranging (6.11) results in (6.12):

$$V_{RE} = \left(\frac{1}{2^{15}} \right) \frac{2}{N} \sum_{k=1}^{N} \underbrace{(v_k)}_{15 \text{ bit}} \cdot \underbrace{\left(c_k \cdot 2^{15}\right)}_{15 \text{ bit}} \tag{6.12}$$

From equation, (6.12) it is noted that each product of signal (v_k) times cosine coefficient $(c_k \cdot 2^{15})$ results in a 30 bit number. If we keep performing the sum of equation (6.12), the result is a 30 bit number plus 7 bit number from the $N/2$ factor, i.e., a 37 bit number, and thus overflow occurs in a 32 bit processor.

To overcome this problem in the proposed platform, two ranges of scaling are used inside the DFT method. The maximum and minimum levels of the input signal are measured as soon as the signal is received from the A/D converter. Each product $(v_k) \cdot (c_k \cdot 2^{15})$ is

scaled down by a number $2^{\text{LOWHIGHEXP}}$ if the maximum absolute range of the signal v_k is larger than a threshold $2^{\text{LOWHIGHLIMIT}}$. The macro variable LOWHIGHEXP is the number of bits corresponding to the $N/2$ factor. The relationship between LOWHIGHEXP and LOWHIGHLIMIT proposed is given by (6.13).

$$\text{LOWHIGHEXP} + \text{LOWHIGHLIMIT} = 15 \tag{6.13}$$

The reason for the proposed approach, instead of just scaling down each product $(v_k)\cdot(c_k \cdot 2^{15})$ by 15 bits, becomes clear when low input signal levels are measured. Considering that the input signal v_k is low and only has 4 bits of information, immediately scaling down by 15 bits after each product would result in a number with only 4 bits. Because each product inside the sum results in 19 bits of information, i.e., 15 bit plus 4 bit, there are 11 bits of space available in the 32 bit register not considering the sign. In the proposed implementation that considers $N/2 = 67$ is an 8 bit number, performing the complete DFT sum would result in 27 bits, i.e., 19 bit plus 8 bit, and thus no overflow of the 32 bit processor.

Summarizing, if the input signal is low, the resulting DFT product is used without scaling down in order not to lose bit resolution; however, if the input signal is large, the resulting DFT product is scaled down by a factor of $2^{LOWHIGHEXP}$. In order to keep track of the actual scaling being used, a pseudo exponent is associated with each number.

6.5.2 IEEE Comtrade Recording

The proposed platform implements recording of input signals and calculation result outputs in IEEE COMTRADE format. The design allows flexibility in the configuration of several parameters, including the number of channels, type of channels, sampling rate, and length of recording. To achieve this flexibility, a simple memory allocation library is implemented and is composed of three functions: rtosc_malloc_init(), rtosc_malloc(), and rtosc_free(). These routines manage the space in the external RAM allocated to waveform recording.

The channels are configured by editing the COMTRADE configuration file embedded in the rtoieee.c source file. The mapping between channels and the protection functions that may generate them is also done in the rtoieee.c source file. This configuration is read by the ldrtcfg() routine, which parses the COMTRADE configuration parameters and initializes structures and pointers that are used to assemble the sample records to produce the COMTRADE data file.

6.5.2.1 Prefault Time

The main waveform recording routine is rtoieee() and consists of a state machine that switches between three states: prefault, fault, and copy prefault. The default and initial state is the prefault state. The next state in the sequence is the fault state, which is activated when a trigger condition is satisfied. The prior state in the sequence is the copy prefault state, which is the last procedure performed to record a COMTRADE waveform.

For a prefault condition, the rtoieee() routine is continuously saving the current set of samples to a rotating prefault buffer. The prefault buffer is a space independent from the actual COMTRADE file location with a size that is large enough to store the number of samples indicated by the parameter value pretrigger, which is a percentage of the total length.

6.5.2.2 Trigger Algorithm

The trigger for waveform recording is enabled or disabled by a dip switch on the hardware board to help during RTDS testing of the proposed platform. The trigger is activated by monitoring the rising edge of the trigflag variable, which causes the state machine to switch from the prefault to fault state. The trigflag variable is associated with a desired protection function for which recording is desired.

As soon as the trigflag triggers recording, the variable trig_active, which controls the LED indication that recording is active, is activated. The trig_active flag is active during the fault

and the copy prefault states.

During the fault state, the current set of samples is saved to the actual corresponding COMTRADE files, until they are full. Also during the fault state, the prefault buffer remains frozen with the last information stored just before the trigger picked up.

When all of the fault data are recorded in the COMTRADE file, the state machine switches to the copy prefault state. In this state, the rtoieee() routine copies all information from the prefault buffer to its final destination in the COMTRADE file. Once the prefault copy is completed, the state machine switches back to the default prefault state and clears the LED via the trig_active flag to indicate that the protective relay is ready for recording a new case.

In the proposed platform, only one waveform recording for the input signals and for the calculation results was implemented, which would overwrite any preexisting COMTRADE files in the memory. The COMTRADE file had to be downloaded from the hardware board before testing a new case. It should be noted that a length of 30 s of recording in a single COMTRADE file is very seldom found in typical relays currently available. The more common record lengths vary from 500 ms to 2 s. The trigger signal of interest in the implementation of the proposed SVM method is activated when the magnitude of a change in the complex value of the apparent power ΔS within 1.0 s time window exceeds 0.1 pu.

6.5.2.3 Input Signal Recording

The input channels recorded in the proposed implementation of the SVM method are shown in Table 6.2. The sampling rate for the recording is 8 kHz, which means that 40 samples are stored for each protection interrupt. The configuration file is stored in ASCII format, while the data samples file is stored in BINARY format to save space.

Table 6.2: COMTRADE input channels

No.	Chan.ID	Type	Description
1	IA	An.	Positive sequence analog current input
2	VA	An.	Positive sequence analog voltage input

Type: An.:Analog

6.5.2.4 Output Results Recording

The channels where calculation results are recorded in the proposed implementation of the SVM method are shown in Table 6.3. The sampling rate for the recording is 200 Hz, which means that one sample is stored for each protection interrupt. The configuration file is stored in ASCII format, while the data samples file is stored in BINARY format to save space.

Table 6.3: COMTRADE output channels

No.	Chan.ID	Type	Description
1	VA1PU_R	An.	Real component of positive sequence phasor VA1
2	VA1PU_I	An.	Imaginary component of positive sequence phasor VA1
3	VA1PU_E	An.	Exponent of positive sequence phasor VA1
4	IA1PU_R	An.	Real component of positive sequence phasor IA1
5	IA1PU_I	An.	Imaginary component of positive sequence phasor IA1
6	IA1PU_E	An.	Exponent of positive sequence phasor IA1
7	SPU_R	An.	Real component of apparent power SPU, i.e. P in *pu*
8	SPU_I	An.	Imaginary component of apparent power SPU, Q in *pu*
9	SPU_E	An.	Exponent of apparent power SPU
10	ZPU_R	An.	Real component of impedance ZPU, i.e. R in *pu*
11	ZPU_I	An.	Imaginary component of impedance ZPU, i.e. X in *pu*
12	ZPU_E	An.	Exponent of impedance ZPU

13	X1_R	An.	Magnitude of first SVM feature X1
14	X1_E	An.	Exponent of first SVM feature X1
15	X2_R	An.	Magnitude of second SVM feature X2
16	X2_E	An.	Exponent of second SVM feature X2
17	X3_R	An.	Magnitude of third SVM feature X3
18	X3_E	An.	Exponent of third SVM feature X3
19	X4_R	An.	Magnitude of fourth SVM feature X4
20	X4_E	An.	Exponent of fourth SVM feature X4
21	O1_R	An.	Magnitude of SVM classifier output
22	O1_E	An.	Exponent of SVM classifier output
23	O2P_R	An.	Magnitude of Zone 1 Mho LOE pick up output
24	O2P_E	An.	Exponent of Zone 1 Mho LOE pick up output
25	O2T_R	An.	Magnitude of Zone 1 Mho LOE trip output
26	O2T_E	An.	Exponent of Zone 1 Mho LOE trip output
27	O3P_R	An.	Magnitude of Zone 2 Mho LOE pick up output
28	O3P_E	An.	Exponent of Zone 2 Mho LOE pick up output
29	O3T_R	An.	Magnitude of Zone 2 Mho LOE trip output
30	O3T_E	An.	Exponent of Zone 2 Mho LOE trip output
31	DSDT	Di.	Status of delta of SPU detector

Type: An.:Analog, Di.:Digital

6.5.3 String Libraries: to avoid using C standard libraries (stdio)

In the proposed platform, some functions from the standard C library were implemented so that the code was not dependent on these standard libraries and headers. A list and brief description of the functions implemented is given next.

nxtfld() : this function behaves as strtok() with only one character as a delimiter, except that it returns an empty string if there is no space between delimiters; that is, it does not skip repeated delimiter characters in searching for the next field.

r_strlen_s() : this function is similar to the standard strlen() function, and obtains the length of a given string.

r_strcspn() : this function is similar to the standard strcspn() function, and obtains the length of string before reaching a set of specified delimiters.

r_strspn() : this function is similar to the standard strspn() function, and obtains the length of a string that contains only a set of specified characters.

r_atos() : this function is similar to the standard atoi() function, except that it returns a short integer, i.e., 16 bit signed integer, given a string of input characters.

r_atol() : this function is similar to the standard atol() function, and converts a given string to its long integer, i.e., 32 bit signed integer, representation.

r_strstr() : this function is similar to the standard strstr() function, and locates one string within another.

r_memcpy() : this function is similar to the standard memcpy() function, and copies contents of one memory location to another.

6.5.4 Math Libraries

Implementing protective relaying algorithms requires that some basic calculations be performed, such as complex and real arithmetic including sum and product, real division, and real square root as a minimum. All of these calculations need to handle a large dynamic range not possible with just regular fixed point arithmetic. To achieve this, the proposed platform implements a pseudo floating approach that is described below.

6.5.4.1 Pseudo Floating Point

In the pseudo floating point approach, two types of variables are defined: complex type CEXP and real type REXP. The complex type CEXP is a structure with three fields, as shown in Table 6.4.

Table 6.4: Pseudo floating complex number structure CEXP

Field Name	Type	Description
Real	Int32	Real component mantissa
Imag	Int32	Imaginary component mantissa
Exp	Int16	Exponent in base 2

CEXP value = $(Real + j \cdot Imag) \cdot 2^{Exp}$

The real type REXP is a structure with two fields, as shown in Table 6.5.

Table 6.5: Pseudo floating real number structure REXP

Field Name	Type	Description
Real	Int32	Real component mantissa
Exp	Int16	Exponent in base 2

REXP value = $Real \cdot 2^{Exp}$

6.5.4.2 Portability

Portability of the math libraries is ensured by using portable type definitions that are based on the specific platform definitions. These definitions are made on header file types.h specific to each platform. The equivalences between the proposed portable definitions for DSP and PC platforms is given in Table 6.6.

Table 6.6: Type equivalences for the proposed platform

Portable Type	DSP	PC	Description
Int16	short	signed short	16 bit signed integer
Int32	int	signed long	32 bit signed integer
Uint32	unsigned int	unsigned long	32 bit unsigned integer

6.5.4.3 Normalization

In the proposed platform, the pseudo floating variable is normalized to 15 bits. Two functions were implemented: NormPhasor() to normalize a complex CEXP value and NormREXP() to normalize a real value REXP. The normalization of the real variable REXP is performed based on the absolute value of the mantissa. The normalization is performed by rounding the last bit based on the value of the closest integer approach, i.e., using 1/2 of the last bit as the boundary for rounding. As a result of normalization, the mantissa has a value between 0.5 and 1.0 times the maximum integer, i.e., between 2^{14} and $(2^{15} - 1)$.

The normalization for complex variable CEXP is slightly different, because only one exponent is used for both the real and the imaginary components. Here, the normalization is performed based on the largest absolute value of real or imaginary components taken individually. As a result of normalization, the mantissa of the largest component has a value between 0.5 and 1.0 times the maximum integer, and the smaller component may have a value that depends on the absolute ratio between these two components while keeping the original signs for each.

6.5.4.4 Optimized Complex/Real Math

Four arithmetic functions were implemented in the proposed platform, as described below.

ProdRREXP() : this function performs the product of two real REXP numbers, and returns the result in a new REXP structure. For the product operation, care was taken to not lose significant bits during the operation, as the magnitude of the result may vary between $0.25 = 0.5 \cdot 0.5$ up to $1.0 = 1.0 \cdot 1.0$. Two additional bits were considered inside this function for the intermediate operations until the final rounding and normalization was performed.

ProdCCEXP() : this function performs the product of two complex CEXP numbers, and returns the result in a new CEXP structure. A similar approach for not losing significant bits was taken in this operation.

Sum RREXP() : this function performs the sum of two complex REXP numbers, and returns the result in a new REXP structure. For the sum operation, two real numbers need to equalize the exponents before adding the mantissas. One simple approach is to calculate the difference $d = Exp_1 - Exp_2$ between exponents and multiply the number with the larger exponent by 2^d. This approach is expensive later during normalization, as the larger the difference d the greater the number of iterations to normalize. In our proposed arithmetic, the proposed mantissas use 15 bit resolution so a maximum of 4 extra bits are used in the intermediate operations if $d > 4$. That is, instead of multiplying by 2^d, the number with the larger exponent is multiplied by 2^4 and the other number is divided by 2^{d-4}.

Sum CCEXP() : this function performs the sum of two complex CEXP numbers, and returns the result in a new CEXP structure. A similar approach for equalizing the exponents is used in this operation.

6.5.4.5 Inverse 1/x

The inverse of a real number is mainly needed to perform division. That is, a division n/d becomes a multiplication $(n) \cdot (1/d)$. The inverse $1/x$ is implemented in two steps: binary search and the Newton-Raphson method. The function InvREXP() was implemented for this task.

For the binary search, a 16 point lookup table is used, knowing that the mantissa $x \in [0.5, 1)$ so the inverse $1/x \in (1, 2]$. The binary search provides 4 significant bits of the desired result. Once the 1/16 interval corresponding to the desired value is obtained, then the Newton-Raphson method is performed using the relationship (6.14). Only two iterations of the Newton-Raphson method are required to obtain the remaining 11 bits and thus complete the desired 15 significant bits:

$$y_k = 2 \cdot y_{k-1} - x \cdot y_{k-1}^2 \tag{6.14}$$

where:

y the estimated value of $1/x$

k current iteration number

6.5.4.6 Square Root Inverse $1/\sqrt{x}$

The inverse square root is needed to obtain the square root of a real number, as it is less expensive in terms of processing effort to obtain the inverse square root than to obtain the square root directly. The square root of x is obtained by multiplying $(x)\cdot(1/\sqrt{x})$. The inverse square root $1/\sqrt{x}$ is implemented in two steps: a binary search and the Newton-Raphson method. The function InvSqrtREXP() was implemented for this task.

For the binary search, a 16 point lookup table is used knowing that if the mantissa $x \in [0.5, 1)$ then the inverse square root $1/\sqrt{x} \in \left(1, \sqrt{2}\right]$. The binary search provides approximately 4 significant bits of the desired result. Once the 1/16 interval corresponding to the desired value is obtained, then the Newton-Raphson method is performed using the relationship (6.15). Only two iterations of the Newton-Raphson method are required to obtain 10 of the remaining bits, for a total of 14 significant bits:

$$y_k = \frac{3 \cdot y_{k-1} - x \cdot y_{k-1}^3}{2} \tag{6.15}$$

where:

y is the estimated value of $1/\sqrt{x}$

k is the current iteration number

6.6 Application Specific Code

Using the proposed relay development platform, the SVM method for detection of LOE conditions was implemented, and is described next.

6.6.1 Low Pass Filter 10 Hz Antialias Code

The output from the DFT method for phasor estimation is filtered by a second order low pass Butterworth filter with a cutoff of 10 Hz. The coefficients for this filter are calculated for the protection interrupt frequency, i.e., 200 Hz, and with fixed point resolution of 15 bit by using an external Octave (or Matlab) macro that generates a header file phlpfilcoef.h. The function implemented for this task is phlpfil(). This function performs low pass filtering of the real and imaginary components of the positive sequence voltage and current phasors, with a total of four signals being filtered.

6.6.2 Impedance (Z) and Power (S) in per unit

The scale of the phasors up to this point uses the 15 bit word size with no design specific scale applied. Two scalings are applied: hardware platform specific scaling and application specific scaling.

One function was implemented to perform the hardware specific scaling to obtain voltage and current phasors in physical units according to the 220 Vpk and 250 Apk specifications indicated in Subsection 6.2.1.5.

The scaling specific to the SVM method being implemented is performed inside the svmloe() function because it has knowledge of the specific power system parameters. The parameters needed to scale the voltage and current phasors are generated by an external Octave (or Matlab) macro and written on a header file svmloepar.h, as part of all parameter inputs to the proposed SVM method. This scaling simply converts the voltage and current phasors to per unit by dividing by the corresponding voltage and current base.

The apparent power is calculated simply as the product of voltage times the conjugate of the current, i.e., $S_{PU} = V_{PU} \cdot I^*_{PU}$. The apparent impedance is typically calculated by dividing the voltage by the current, i.e. $Z_{PU} = V_{PU}/I_{PU}$. However, because complex division arithmetic function is not considered in this implementation, an equivalent relationship is used, i.e., $Z_{PU} = (V_{PU} \cdot I^*_{PU})/(I_{PU} \cdot I^*_{PU})$. With this approach, the denominator is a real number, and the division is converted to multiplication by the inverse $1/|I_{PU}|^2$. One consideration made is to avoid division by zero; therefore, the magnitude of the quantity $|I_{PU}|^2$ is monitored and a minimum real value is used if it becomes zero.

6.6.3 Disturbance Detector: Comtrade Triggering

To trigger the COMTRADE waveform recording, a disturbance detector was implemented in the proposed platform based on the absolute value of the change in apparent power $|\Delta S|$ in a one second window. A threshold value of 0.1 pu was used for this disturbance detector, designated as _OUT_DSDT. The time resolution of this detector is the same as the protection interrupt, i.e., 5 ms.

6.6.4 SVM Classifier Implementation

Specific details of the SVM implementation are described below.

20 Point Time Window : The proposed implementation of the SVM method for LOE detection maintains a rolling window of 200 points and from these it takes one point every 10 to complete the 20 points used by the method.

Feature Vector Computation : Once the 20 points have been selected, the features are calculated as described in Subsection 4.3.3.

Considerations for Division by Zero : The implementation of the third feature of the proposed SVM method needed careful consideration when the denominator of (4.18) becomes zero. To avoid division by zero, the magnitude of this denominator $|S_{19} - S_0|$ was monitored and a minimum value was used if it became zero.

Minimize Division Instances : One criterion used was to avoid division at all costs in the real time processing, unless absolutely necessary for the algorithm implemented. If a division was performed by a constant or a configuration parameter, this was converted to a multiplication by using the inverse of the number. Only two divisions are carried out in the protection interrupt for the proposed implementation of the SVM method. One is to calculate the apparent impedance, and the other is to calculate the third feature X_3 of the proposed method.

6.6.5 Traditional LOE Detection

The two mho zone detection method of Berdy and Mason [141] was implemented for comparison with the proposed SVM method.

6.6.5.1 Zone 1, Zone 2

The implementation of the mho characteristics for the traditional LOE zones is based on two fixed points that define the diameter of this circle. Consider that the first point in the voltage plane is defined by $V_{P1} = I_X \cdot Z_{P1}$ and the second point is defined by $V_{P2} = I_X \cdot Z_{P2}$. A point V_X satisfies the boundary condition (i.e., is inside the border of the mho circle) when the angle between the two complex values $(V_X - V_{P1})$ and $(V_X - V_{P2})$ is 90 degrees. If these

two complex values form an angle of less than 90 degrees, the point V_X is outside of the mho zone. Thus, for the mho zone to pickup, the two complex numbers need to form an angle larger than 90 degrees, as given by (6.16).

$$\Re\{(V_X - V_{P1}) \cdot (V_X - V_{P2})^*\} < 0 \tag{6.16}$$

The impedance values that define the diameter of the smaller mho zone, i.e., Zone 1, are $Z_{P1} = -j \cdot X'_d/2$ and $Z_{P2} = -j \cdot (X'_d/2 + 1.0)$. The impedance values that define the diameter of the larger mho zone, i.e., Zone 2, are $Z_{P1} = -j \cdot X'_d/2$ and $Z_{P2} = -j \cdot (X'_d/2 + X_d)$.

6.6.5.2 Pickup and Trip

The operating times of the mho zones are measured by the pickup and trip times. The pickup is the time when the operating point just enters the mho zone. The trip decision is made based on a time delay measured from the pickup time. In the proposed implementation of the mho LOE zones, the trip delay time is 400 ms for zone 1 and 1.0 s for zone 2.

6.7 Profiling

6.7.1 Measuring CPU Time: Per Function, Total

The CPU load was measured by using a timer clock available in the hardware architecture with a frequency of 56.25 MHz. The load for different functions is listed in Table 6.7 and for the math library is listed in Table 6.8. The load percentage is calculated treating 100% as a 5 ms interrupt.

Table 6.7: CPU load measurement for the proposed implementation

Function	Load %	Clocks cycles	Time μs
A/D to V,I	0.17	478	8.5
V,I preprocess	0.64	1800	32.0
DFT	1.05	2953	52.5
Low Pass 10 Hz	1.41	3966	70.5
Physical Units	0.06	177	3.2
SVM & LOE	8.60	24176	429.8
COMTRADE save	3.81	10708	190.4
Overall	15.60	43875	780.0

Table 6.8: CPU load measurement for math libraries

Function	Load %	Clocks cycles	Time μs
$1/x$	0.0706	199	3.53
$1/\sqrt{x}$	0.0810	228	4.05
$z \cdot z$	0.0454	128	2.27
$x \cdot x$	0.0330	93	1.65
$z + z$	0.0708	199	3.54
$x + x$	0.0566	159	2.83

x : real, z : complex

6.8 Test Results

The test case scenario from Subsection 4.5.3.1 was used as a reference for comparison. The proposed implementation of the SVM method was tested with RTDS and the results

are given in Tables 6.9 and 6.10.

Table 6.9: SVM method in DSP tested with RTDS - two MHO zone LOE

				Two MHO zone			
				Large MHO Time, s		Small MHO Time, s	
Case No.	Load/PF	Initial P+jQ,*pu*	Type of case	Pickup	Trip	Pickup	Trip
1	LL/lag.	0.10+j0.68	LOE	8.54	9.53	-	-
3	LL/lead.	0.03-j0.55	LOE	0.93	1.945	-	-
4	HL/lag.	0.78+j0.41	LOE	2.564	3.556	3.424	3.816
6	HL/lead.	0.79-j0.49	LOE	0.771	1.763	1.618	2.013
				Pickup	Reset	Pickup	Reset
7	LL/lag.	0.10+j0.68	PS-3P	-	-	-	-
9	LL/lead.	0.03-j0.55	PS-3P	0.251	1.239	0.251	0.647
10	HL/lag.	0.78+j0.41	PS-3P	0.251	0.297	0.261	0.267
12	HL/lead.	0.79-j0.49	PS-3P	0.226	0.767	0.226	0.571

LL: light load, HL: heavy load, PS: power swing, 3P: 3 phase fault used

Table 6.10: SVM method in DSP tested with RTDS - SVM Method

				SVM Time, s		
Case No.	Load/PF	Initial P+jQ, *pu*	Type of case	Pickup	Reset	Loss of Synch. time, s
1	LL/lag.	0.10+j0.68	LOE	0.558	-	
3	LL/lead.	0.03-j0.55	LOE	0.345	-	
4	HL/lag.	0.78+j0.41	LOE	0.188	4.578	
6	HL/lead.	0.79-j0.49	LOE	0.406	2.766	

LL: light load, HL: heavy load, PS: power swing, 3P: 3 phase fault used

The results for detection of LOE conditions of Tables 4.3, 4.4, 6.9, and 6.10 are illustrated in Figs. 6.6 and 6.7.

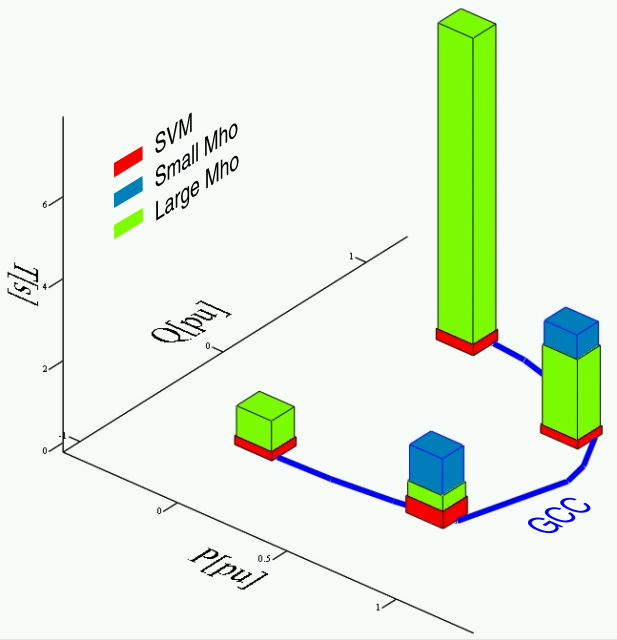

Figure 6.6: Proposed SVM Operating Pickup Times - IET paper [1]

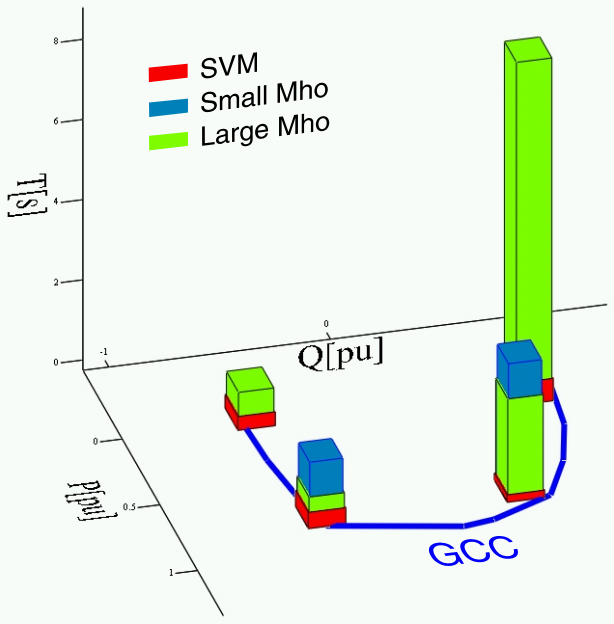

Figure 6.7: Proposed SVM Operating Pickup Times - DSP and RTDS test

The results of power swing duration in the large and small mho zones from Tables 4.3

and 6.9 are illustrated in Figs. 6.8 and 6.9.

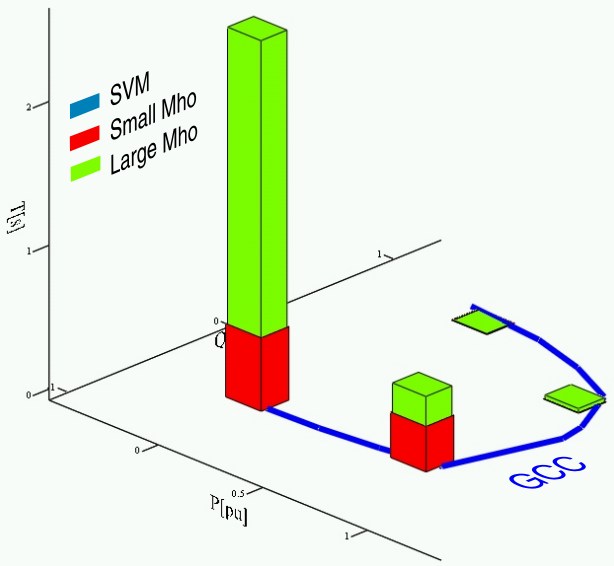

Figure 6.8: Power Swing Duration - IET paper [1]

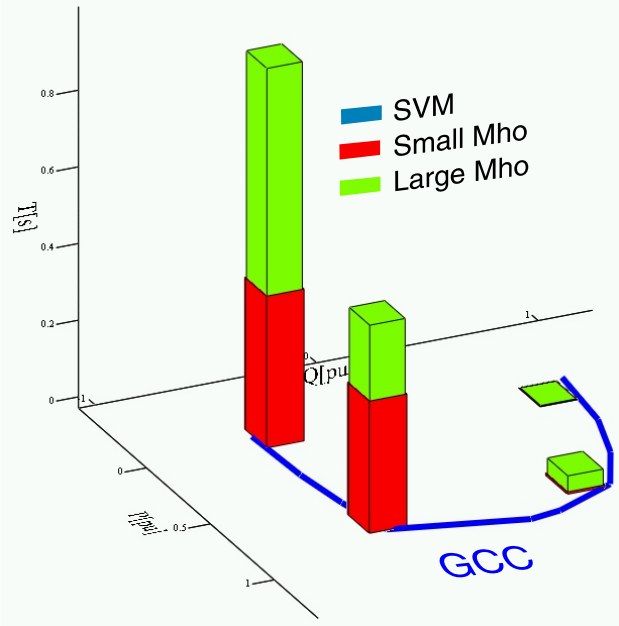

Figure 6.9: Power Swing Duration - DSP and RTDS test

The minimum improvements observed in Fig. 6.6 show that SVM is at least 0.36 s faster than the small mho zone and 1.24 s faster than the large mho zone. Similar improvements are observed in Fig. 6.7, with 0.37 s between SVM and the small mho zone and 1.21 s between

SVM and the large mho zone. The minimum improvements occur at the right bottom corner of the GCC curve, i.e., large active power and large negative reactive power. It should be noted that conditions with larger active power are of special importance because a loss of synchronism that typically follows an LOE presents a severe risk to the generator.

In Fig. 6.8, the maximum power swing durations observed were 2.57 s in the large mho zone and 0.51 s in the small mho zone (results are given in the IET publication [1]). Slightly different durations were observed for the power swing in Fig. 6.9, where results were 0.99 s ($0.988s = 1.239 - 0.251s$) in the large mho zone and 0.40 s ($0.396s = 0.647 - 0.251s$) in the small mho zone, corresponding to the RTDS simulation with the DSP hardware implementation. The differences observed between the IET paper results and the hardware implementation results (using the DSP and RTDS test) are mainly due to the different electromagnetic simulation tools used in each case. These maximum duration times are important in the context of the application of typical large and/or small mho zones, but they are rarely measured or estimated by simulations used in current industry practices. The SVM method did not pick-up up in any of the power swing conditions tested, as shown in these figures, i.e., the SVM was stable and ignored the non LOE conditions.

6.9 Summary

In this section, a generic type of protective relaying development platform was first described, followed by the proposed SVM method for LOE detection implemented in the proposed platform for hardware-in-the-loop testing. Various items that need to be taken into consideration in the design of this relay development platform were described in detail. Hardware considerations, such as analog inputs processing, CPU choice, memory storage, and physical outputs, were some of the most important considerations. The use of electromagnetic offline and real time simulations for validation and debugging was discussed, combined with the IEEE COMTRADE standard for signal recording and playback. Software considerations, such as portability to enable development in a native PC environment and use of the same exact application code in the specific embedded DSP platform, were also

discussed. The approach for a platform specific interface for the protection interrupt, sample processing, COMTRADE recording storage, and other considerations were described. The platform independent software blocks, such as phasor estimation, string and math libraries, COMTRADE triggering and recording, up to the interface with the application specific software block were introduced. The implementation of the proposed SVM method for LOE detection was described and the experimental test results were compared with previous work in this thesis performed with an offline electromagnetic simulation tool.

In the next chapter, the summary, conclusions, and contributions of this thesis as well as proposed future work are presented.

Chapter 7

Summary and Conclusions

7.1 Summary

The thesis consists of seven chapters. In Chapter 1, a brief introduction to power systems protection, numerical relays, and power systems controls was provided. The importance of coordination between protection and control was described, and the difficulties in coordination with the current techniques being used in the industry were explained. Also in this chapter, the need for including a detailed $d-q-0$ model of the synchronous machine in the studies was discussed as well as the importance of including the Canay reactance [29] in the estimation of the $d-q-0$ parameters. This is especially important for dynamic modeling of the overexcitation limiter (OEL). With the current models used in the industry, the actual field current behavior does not match the field current waveforms because the Canay reactance is not included. Dynamic simulations (transient stability simulations, electromagnetic simulations, hardware-in-the-loop simulations) and tools types were discussed. The chapter concluded with a thesis statement, objectives, and thesis outline.

In Chapter 2, a detailed discussion of generator protection was provided. The most common protection functions, and especially the protection functions where the excitation controls have an impact, were discussed. A similar discussion about the most important generator excitation controls, such as the automatic voltage regulator, the power system stabilizer, the overexcitation and underexcitation limiters, and their role in the coordination problem were also presented. Finally, the current state of the art in coordination for generator protection and control, the concept of static and dynamic coordination, as well as basic considerations for the coordination in overexcited, underexcited, and loss of synchronism

conditions were given.

In Chapter 3, the overexcitation capability of synchronous generators, the steady state, and transient overload limits were described. The interaction between different modes of control in the overexcited region and the requirement for coordination with the corresponding field overcurrent protection were discussed. Two approaches for modeling the overexcitation limiter were considered: custom modeling and the use of an existing IEEE proposal for a generic OEL. In the first approach, a proposed custom model to complement existing standard excitation control models from IEEE was described in detail. In the second approach, improvements to the existing IEEE generic OEL were proposed to match the performance obtained by the custom model. This modeling was used to study some severe reactive overload conditions that are practical to do through simulations. These cases are important to verify whether the coordination functionalities are able to successfully support the system.

In Chapter 4, a new method was proposed to detect a loss of excitation condition using the Support Vector Machine method. The chapter starts with an introduction to the loss of excitation problems, types of risks it poses for the machine and the power systems, as well as typical detection methods. A literature review of the techniques for the detection of loss of excitation conditions was provided. The concept of pattern recognition was introduced, including the concepts of feature vector, training, mapping functions, and, in particular, the Support Vector Machine classification method. The new loss of excitation detection method was discussed, in particular the selection of features based on careful study of the trajectories in the power plane and the impedance plane. Another key component of the new method was training to cover a wide range of operating conditions of the generator. Finally, test results and a sensitivity study provided a validation of the accuracy and robustness of the proposed method.

In Chapter 5, the proposed methodology for coordination in the underexcited region of synchronous generators was proposed, followed by a case study of coordination for a real power generator connected to Alberta power system network. The chapter starts with a discussion of limitations of existing coordination methods as well as a literature review of previous work on dynamic coordination. A discussion of different limits to be considered,

such as thermal and stability limits, and the reliability aspects of the excitation system being used was presented. The modeling and validation of excitation and limiter controls was discussed. The chapter also highlighted the fact that the limiters are not typically present in utility network databases. The static and the proposed dynamic coordination methodologies were described and then tested in different scenarios in which these protection and control functions need to be coordinated. The new SVM described earlier in this thesis was trained and tested with this real generator, and its performance demonstrated coordination with excitation control functions.

In Chapter 6, a generic type of protective relaying development platform was first described, followed by the proposed SVM method for LOE detection implemented in the proposed platform for hardware-in-the-loop testing. Various items that need to be taken into consideration in the design of this relay development platform were described in detail. Hardware specifications, such as analog inputs processing, CPU choice, memory storage, and physical outputs, were some of the most important considerations. The use of electromagnetic offline and real time simulations for validation and debugging was discussed, combined with the IEEE COMTRADE standard for signal recording and playback. Software considerations, such as portability to enable development in a native PC environment and use of the same exact application code in the specific embedded DSP platform, were also discussed. The approach for a platform specific interface for the protection interrupt, sample processing, COMTRADE recording storage, and other considerations were described. The platform independent software blocks, such as phasor estimation, string and math libraries, COMTRADE triggering and recording, up to the interface with the application specific software block were introduced. The implementation of the proposed SVM method for LOE detection was described and the experimental test results compared to previous work in this thesis performed with an offline electromagnetic simulation tool.

7.2 Thesis Contributions

Following are the main contributions of this thesis:

1. This thesis proposes an overexcitation limiter (OEL) custom model that interfaces with the IEEE ST1A standard excitation model. The current ST1A model does not completely represent the OEL dynamics. Dynamic coordination can be analyzed using the proposed OEL model, along with models for the automatic voltage regulator, power system stabilizer, and protective relays.

   This thesis also proposes improvements to the generic OEL proposed by the IEEE in 1995 in order to properly represent the dynamics of existing limiters. The modified IEEE OEL provides the same response as the custom OEL.

   The proposed OEL models can be used with EMTP (high bandwidth) simulations, either offline or in real time. The existing simplified OEL in the ST1A or the generic OEL in the IEEE 1995 paper are intended for low bandwidth simulations only, such as transient or small signal stability studies.

   The performance of the proposed OEL model was demonstrated through a coordination example. Test scenarios that are not physically performed due to risk to the machine were simulated to determine the validity of the coordination. These scenarios are often not verified due to lack of proper models. These considerations become more critical for round rotor machines.

2. This thesis proposed a new method using the Support Vector Machine (SVM) pattern technique to identify loss of excitation (LOE) conditions from other conditions such as power swing or faults. By combining the proposed classifier with a traditional mho zone, it is possible to improve the detection times of loss of excitation conditions by 300 ms or more while preserving the security of the technique against other disturbances that may encroach on the mho characteristic. The operating times (i.e., tripping times) are typically 1.0 s after the LOE detection is made, thus the overall operating time improvements achieved are on the order of 1.3 s ($= 0.3s + 1.0s$) or more in the most severe LOE scenario. The proposed LOE detection method eliminates the need for additional functions, such as a second mho zone or directional or undervoltage supervision for LOE operation. The training requirements for the proposed SVM LOE detection method are based on the limit points of the generator capability (GCC) area in the

power plane as well as the network condition with the strongest system interconnection with the generator. The proposed method is stable over several conditions, such as different generator loadings, different fault types followed by a power swing, different interconnection impedances, and generator parameter variations of up to 5%.

This thesis proposed four feature vectors as inputs to the SVM classification method based on a careful analysis of the inputs analyzed in the classical methods. A very common approach is to use generic functions (e.g., Gaussian or polynomial) to map a given set of nonlinearly separable feature vectors into a new space. This approach expects to achieve linear separation of the mapped feature vectors in this new space by tuning the coefficients of the generic mapping functions. This traditional approach was not used in this work. The proposed approach for obtaining the features to be used is based on two main ideas. The first idea is the study of the dynamic behaviour of the synchronous generator for the different conditions under study, such as loss of excitation, faults, power swing, and switching operations, among others. The second idea is to analyze the behavior of the synchronous generator at different levels of complexity, such as raw samples and sampling rate, phasors estimated, complex power and impedance planes, time window size, sampling rate of classification algorithm, and trajectory characteristics in power and impedance planes. Using this approach, the features obtained can clearly differentiate an LOE condition from others. The features obtained also have closer correlation with the physical behavior of the machine being studied.

This thesis developed an embedded relay model in the ATP/EMTP simulation program. In this relay model, the phasor estimation based on the DFT method is performed in a 'C' language routine compiled and linked with the ATP main library to produce a new ATP executable. Other calculations required, such as positive sequence and complex low pass filtering for the 50 ms SVM LOE sampling rate, are implemented using the TACS and MODELS capabilities of ATP. Another 'C' language routine is used to implement a traditional two mho zone LOE detection function and the proposed SVM classifier. These relay models allow study of the performance in offline

mode in a closed loop fashion.

3. This thesis proposes a methodology for coordination of generator protection and control in the underexcited region that consolidates the associated technical problems and challenges. One of the issues discussed throughout this thesis work is the use of dynamic simulation to verify the performance of the generator for various conditions instead of using existing coordination methods based only on static characteristics. Another important consideration is identifying the actual stability limit to see if it needs to take part in the coordination, instead of just using the manual voltage control steady state stability limit. Emphasis is given to correct modeling of the excitation control system, including the automatic voltage regulator, power system stabilizer, and, most importantly, the underexcitation limiter control. One last consideration is the selection of credible but severe disturbances that exercise these limits, such as stable power swings or temporary system overvoltages.

4. This thesis proposes a development platform for protective relaying algorithms that addresses the challenges imposed by the real time signal processing and critical operating time constraints for a protective decision whenever a fault happens in the power system. One of the challenges is the fact that the power system cannot just be paused to analyze and debug the algorithm; this is addressed by implementing recording and playback following the IEEE COMTRADE file format. Another challenge is portability, as protective algorithm analysis requires the playback and study of numerous cases for regression testing every time a modification to the algorithm is tried; processor specific tools make this process cumbersome and slow. This challenge is addressed by implementing a careful, portable, and modular design that allows development using the exact same code on a host computer.

7.3 Conclusions

The following conclusions are drawn from this thesis work:

1. In the overexcited region, coordination between excitation control, the overexcitation limiter, field overcurrent protection, and generator capability is important to meet present industry requirements for the use of the reactive overload capabilities of synchronous generators to the fullest extent.

2. For proper coordination in the overexcited region, several modeling considerations need to be addressed. One consideration is correct representation of the rotor field current behavior, which requires knowledge of an additional generator parameter, such as Canay's reactance X_C. Another consideration is correct representation of the overexcitation limiter dynamics, which requires modeling of field forcing time measurements, inverse time measurements, control loop representation, and limiter pickup and reset levels and logic.

3. Existing overexcitation limiter modeling proposed by the IEEE in 1995 requires modifications to properly represent the dynamics of existing limiters. The improvements required include restricting ramp up/down variables controlling the pickup level, including hysteresis for proper reset of the function, providing integral as well as proportional control loop, and including an integrating timer to measure field forcing duration.

4. Traditional loss of excitation protection functions that are based on fixed characteristics on the complex impedance or power planes are susceptible to maloperation for severe disturbances that may enter these characteristics; therefore, time delays are used to ride through these disturbances and prevent incorrect operations.

5. Traditional loss of excitation protection methods are based on the study of synchronous generator behavior in the complex impedance or power plane for these conditions. In this study, characteristics in the impedance or power planes were used to identify the loss of excitation condition. The use of these types of characteristics for fault identification falls within the definition of a pattern classification method.

6. In the method proposed for detection of loss of excitation conditions, the selection of features based on careful study of the synchronous machine behavior during these con-

ditions contributes significantly to improved detection of loss of excitation conditions while correctly detecting and ignoring other disturbances (e.g., faults, power swings, switching operations).

7. In addition to a careful selection of features, another factor that contributes to improved detection of loss of excitation conditions by the proposed method is careful training, which includes generator and system modeling, selecting extreme cases, as well as restricting the time window to the loss of excitation condition prior to the consequent loss of synchronism.

8. In the underexcited region, coordination between excitation control, the underexcitation limiter, stability limits, loss of excitation protection, and generator capability is important to meet power system requirements for full utilization of this capability either during normal conditions or during degraded conditions in which the generator contribution to system stability is important.

9. For proper coordination in the underexcited region, several considerations need to be addressed. One consideration is to assess whether the stability limit needs to be considered and estimate its characteristic limit in the power or impedance plane to be used for analysis. Another consideration is correct representation of the generator dynamics, considering the excitation control, underexcitation limiter, and power system stabilizer if applicable. One more consideration is representation of the specific loss of excitation protection function applied to protect the generator, including details such as frequency dependence in case this relay is susceptible to this effect. The last consideration is careful selection of credible and severe disturbances to be simulated, such as a temporary system overvoltage, stable power swing, or unstable power swing, while paying close attention to the generator loading condition.

7.4 Future Work

Based on this thesis work, the following studies are recommended for future investigations:

1. Further investigation of generator loss of excitation, phase backup protection, dynamic overexcitation limiters, and under excitation limiters. One aspect to look at would be validating the EMTP models against the standard IEEE models, which are simplified for low bandwidth simulations. Another aspect to look at are different failure modes in the excitation systems and their impact on generator protection (such as partial loss of excitation). Such studies are only possible with complete electromagnetic transient EMTP models for simulations.

2. Field verification in collaboration with the Saskatchewan Power Corporation to measure some of the real dynamic limits (e.g., measuring the end core limit characteristics). To make the research meaningful for the utility, it is important to develop these dynamic models in some of the commercial software platforms used by Canadian utilities for power system studies, such as DSA Tools, PSS/E, DiGSILENT, MiPower, ATP, PSCAD/EMDTC, EMTP-RV, etc.

3. Current research works mostly deal with automatic voltage regulators (AVRs), power systems stabilizers (PSS), and control limiters. Looking at the control loops for the excitation limiters and investigating their behavior during stressed conditions and methodologies for their proper tuning would be useful research contributions.

4. Experimental testing of the new technologies by interfacing or implementing them on commercial hardware platforms and testing them in closed-loop using real-time power systems simulations (power hardware-in-the-loop testing).

5. The sensitivity study in Chapter 4 was done making an ideal assumption that generator parameters are independent from each other. This is not always the case and percentage error in one parameter means errors in another parameter as well which needs to be taken into account.

References

[1] E. Pajuelo, R. Gokaraju, and M. Sachdev, "Identification of generator loss of excitation from power swing conditions using a fast pattern classification method," *IET Generation, Transmission and Distribution*, vol. 7, no. 1, pp. 24–36, 2013.

[2] J. F. Daume, "Summer of our disconnects - 1996 western systems coordinating council power system disturbances," in *Western Protective Relay Conference*, 1997, pp. 1–21.

[3] NERC, "Technical analysis of the august 14, 2003, blackout: What happened, why, and what did we learn?" 2004. [Online]. Available: http://www.nerc.com/pa/rrm/ea/August%2014%202003%20Blackout%20Investigation%20DL/NERC_Final_Blackout_Report_07_13_04.pdf

[4] MRO, "August 29, 2009 - south dakota disturbance," 2009. [Online]. Available: http://www.midwestreliability.org/00_events/MRO_August-29_Event_Public_Report_7-28-10.pdf

[5] NERC, "Arizona-southern california outages on september 8, 2011," 2012. [Online]. Available: http://www.nerc.com/pa/rrm/ea/September%202011%20Southwest%20Blackout%20Event%20Document%20L/AZOutage_Report_01MAY12.pdf

[6] S. Patel, K. Stephan, M. Bajpai, R. Das, T. J. Domin, E. Fennel, J. D. Gardell, I. Gibbs, C. Henville, P. M. Kerrigan, H. J. King, P. Kumar, C. J. Mozina, M. Reichard, J. Uchiyama, S. Usman, D. L. Viers, D. Wardlow, and M. Yalla, "Performance of generator protection during major system disturbances," *IEEE Transactions on Power Delivery*, vol. 19, no. 4, pp. 1650–1662, October 2004.

[7] D. Tziouvaras, "Relay performance during major system disturbances," in *60th Annual Conference of Protective Relay Engineers - Texas A & M*, 2007, pp. 251–270.

[8] D. Novosel, G. J. Bartok, G. Henneberg, P. Mysore, D. Tziouvaras, and S. Ward, "Ieee psrc report on performance of relaying during wide-area stressed conditions," *IEEE Transactions on Power Delivery*, vol. 25, no. 25, pp. 3–16, January 2010.

[9] L. Pereira, "Introduction and backgroiund to synchronous unit testing and model validation in the WSCC," in *IEEE PES Winter Meeting*, vol. 1, 1999, pp. 151–156.

[10] "Power plant and transmission system protection coordination," NERC, Tech. Rep. Rev.1, July 2010, NERC System Protection and Control Subcommittee. [Online]. Available: http://www.nerc.com/comm/PC/System%20Protection%20and%20Control%20Subcommittee%20SPCS%20DL/Gen%20Prot%20Coord%20Rev1%20Final%2007-30-2010.pdf

[11] G. R. Berube and L. M. Hajagos, "Coordination of underexcitation limiters and loss of excitation relays with generator capability," in *IEEE PES GM*, Calgary, Alberta, Canada, 2009.

[12] D. Reimert, *Protective Relaying for Power Generation Systems*. CRC Press, 2006.

[13] R. Thornton-Jones, I. Golightly, N. Gutteridge, C. Huizer, and D. Navratil, "Review of generator and excitation system specification and test requirements to satisfy multiple international grid code standards," in *IEEE PES GM*, 2012, pp. 1–6.

[14] C. J. Mozina, M. Reichard, Z. Bukhala, S. Conrad, T. Crawley, J. Gardell, R. Hamilton, I. Hasenwinkle, D. Herbst, L. Henrikssen, G. Johnson, P. Kerrigan, S. Khan, G. Kobet, P. Kumar, S. Patel, B. Nelson, D. Sevcik, M. Thompson, J. Uchiyama, S. Usman, P. Waudby, and M. Yalla, "Coordination of generator protection with generator excitation control and generator capability," in *Power Engineering Society General Meeting*. Tampa, Florida, USA: IEEE, June 2007, pp. 1–17, working Group J-5 of the Rotating Machinery Subcommittee of the Power System Relay Committee.

[15] R. H. Park, "Two-reaction theory of synchronous machines - generalized method of analysis - part i," *AIEE Transactions*, vol. 48, pp. 716–730, 1929.

[16] P. L. Dandeno, P. Kundur, A. T. Poray, and M. E. Coultes, "Validation of turbogenerator stability models by comparisons with power system tests," *IEEE Transactions on Power Apparatus and Systems*, vol. PAS-100, no. 4, pp. 1637–1645, April 1981.

[17] P. L. Dandeno, P. Kundur, A. T. Poray, and H. M. Zein El-Din, "Adaptation and validation of turbogenerator model parameters through on-line frequency response measurements," *IEEE Transactions on Power Apparatus and Systems*, vol. PAS-100, no. 4, pp. 1656–1664, April 1981.

[18] A. G. Jack and T. J. Bedford, "A study of the frequency of turbogenerators with special reference to nanticoke g. s." *IEEE Transactions on Energy Conversion*, vol. EC-2, no. 3, pp. 496–505, September 1987.

[19] P. L. Dandeno and A. T. Poray, "Development of detailed turbogenerator equivalent circuits from stanstill frequency response measurements," *IEEE Transactions on Power Apparatus and Systems*, vol. PAS-100, no. 4, pp. 1646–1655, April 1981.

[20] I. M. Canay, "Advance calculation of the characteristic quantities of synchronous machines and comparison with measured values," *IEE Proceedings - Electric Power Applications*, vol. 141, no. 1, pp. 13–18, January 1994.

[21] J. W. Dougherty, S. M. Minnich, and S. H. Minnich, "Finite element modeling of large turbine generators; calculations versus load test data," *IEEE Transactions on Power Apparatus and Systems*, vol. PAS-100, no. 8, pp. 3921–3929, August 1981.

[22] A. M. El-Serafi and J. Wu, "A new method for determining the armature leakage reactance of synchronous machines," *IEEE Transactions on Energy Conversion*, vol. 6, no. 1, pp. 120–125, March 1991.

[23] IEEE/PES Electric Machinery Committee, "IEEE Guide for Synchronous Generator Modeling Practices and Applications in Power System Stability Analyses," *IEEE Std 1110-2002*, November 2003.

[24] MRO, "Mro generator testing guidelines," 2007. [Online]. Available: http://www.midwestreliability.org/03_reliability/06_gtrtf/Documents/MRO_Generator_Testing_Requirements_Rev.pdf

[25] L. M. Hajagos, J. Barton, G. R. Berube, M. E. Coultes, J. Feltes, G. Lanier, S. Patterson, L. Pereira, P. Porbeik, A. Schneider, and R. Thornton-Jones, "Guidelines for generator stability model validation testing," in *IEEE PES GM*, 2007, pp. 1–16.

[26] M. Ghomi and Y. N. Sarem, "Review of synchronous generator parameters estimation and model identification," in *42nd International Universities Power Engineering Conference*, 2007, pp. 228–235.

[27] P. Kundur and P. L. Dandeno, "Implementation of advanced generator models into power system stability programs," *IEEE Transactions on Power Apparatus and Systems*, vol. PAS-102, no. 7, pp. 2047–2054, July 1983.

[28] V. Brandwajn, "Synchronous generator models for the simulation of electromagnetic transients," Ph.D. dissertation, University of British Columbia, 1977. [Online]. Available: http://hdl.handle.net/2429/20635

[29] I. M. Canay, "Causes of discrepancies on calculation of rotor quantities and exact equivalent diagrams of the synchronous machine," *IEEE Transactions on Power Apparatus and Systems*, vol. PAS-88, no. 7, pp. 1114–1120, July 1969.

[30] ——, "Equivalent circuits of synchronous machines for calculating quantities of the rotor during transient processes and asynchronous starting - part i: Turbogenerators," *Brown Boveri Review*, vol. 56, pp. 60–71, 1969.

[31] ——, "Equivalent circuits of synchronous machines for calculating quantities of the rotor during transient processes and asynchronous starting - part ii: Salient-pole machines," *Brown Boveri Review*, vol. 57, pp. 134–143, 1970.

[32] ——, "Extended synchronous-machine model for the calculation of transient processes and stability," *Electric Machines and Electromechanics*, vol. 1, pp. 137–150, 1977.

[33] ——, "Determination of model parameters of synchronous machines," *Proceedings of the IEE*, vol. 130, no. 2, pp. 86–94, March 1983.

[34] NERC, "Project 2007-09 generator verification," 2013. [Online]. Available: http://www.nerc.com/pa/Stand/Pages/Project2007-09-Generator-Verification.aspx

[35] P. Kundur, *Power System Stability and Control*. Mc Graw Hill, 1994.

[36] H. W. Dommel, "Digital computer solution of electromagnetic transients in single- and multi-phase networks," *IEEE Transactions on Power Apparatus and Systems*, vol. PAS-88, no. 2, pp. 734–741, 1969.

[37] D. Nemec, M. Stojsavljevic, H. Bulat, and C. Klapcic, "Loss of excitation protection testing by transient playback of emtp simulation results," in *Proceedings of the 14th International Conference on Power System Protection*, 2001. [Online]. Available: http://bib.irb.hr/prikazi-rad?&rad=287269

[38] *Real Time Digital Simulator for the Power Industry*, RTDS, 2012, manual Set.

[39] *Hypersim*, OPAL-RT, 2014, brochure.

[40] *PSS/E 32.0.5 Online Documentation*, Siemens PTI, October 2010.

[41] *Alternative Transients Program Rule Book*, Canadian / American EMTP User Group, 2002.

[42] C. J. Mozina, "Lessons learned from generator tripping events," *IEEE Industry Applications Magazine*, vol. 16, no. 5, pp. 29–36, Sept/Oct 2010.

[43] IEEE/PES Power System Relaying Committee, *Tutorial on the Protection of Synchronous Generators*, 2nd ed. IEEE, 2011, special Publication of the IEEE Power System Relaying Committee.

[44] *Rotating Eletrical Machines - Part 3: Specific Requirements for Synchronous Generators Driven by Steam Turbines or Combustion Gas Turbines, IEC Standard 600034-3*, IEC Std., November 2007.

[45] W. C. New, "Load shedding and underfrequency relays," General Electric Company, Tech. Rep., gET-6449.

[46] D. W. Smaha, C. R. Rowland, and J. W. Pope, "Coordination of load conservation with turbine-generator underfrequency protection," *IEEE Transactions on Power Apparatus and Systems*, vol. PAS-99, no. 3, pp. 1137–1150, May/June 1980.

[47] C. K. Seetharaman, S. P. Verma, and A. M. El-Serafi, "Operation of synchronous generators in the asynchronous mode," *IEEE Transactions on Power Apparatus and Systems*, vol. PAS-93, no. 3, pp. 928–939, May 1974.

[48] K. Z. Guo, W. D. Zhu, F. W. Tan, R. L. Jin, and G. Wang, "Analysis of large turbo-generator's asynchronous operation during loss of field," in *International Conference on Power System Technology*, 1998, pp. 935–940.

[49] M. Amini, M. Sanaye-Pasand, M. Navabi, M. Davarpanah, and H. Asadi, "Generator loss of field and its effects on voltage stability in power systems," in *Proceedings of The International Conference on Electrical Engineering*, 2008, pp. 1–6.

[50] H. G. Darron, J. L. Koepfinger, J. R. Mather, and P. A. Rusche, "The influence of generator loss of excitation on bulk power system reliability," *IEEE Transactions on Power Apparatus and Systems*, vol. PAS-95, no. 5, pp. 1473–1483, September/October 1975.

[51] O. Rodriguez and A. Medina, "Stability analysis of the synchronous machine under unbalance and loss of excitation conditions," in *IEEE PES GM*, 2003, pp. 1508–1511.

[52] L. Tao, Z. Qian, W. Xiangheng, S. Pengsheng, and W. Weijian, "Dynamic performance for turbo generator under low excitation and loss of field," in *Proceedings of the 5th International Conference on Electrical Machines and Systems*, 2001.

[53] K. Zhang, X. Yin, D. Chen, Z. Zhang, and W. Chen, "Simulation analysis of dynamic performance for hydro-generator under loss of excitation condition," in *Proceedings of the 41st International Universities Power Engineering Conference*, 2006.

[54] L. Yang-ling, G. Bao-jun, L. Cui-cui, T. Da-jun, and Z. Zhi-qiang, "Analysis of high-voltage generator stator windings sudden three-phase short-circuit and loss of excitation fault," in *International Conference on Sustainable Power Generation and Supply*, 2009.

[55] P. J. Tavner and A. F. Anderson, "Core faults in large generators," *IEE Proceedings on Electric Power Applications*, vol. 152, no. 6, pp. 1427–1439, November 2005.

[56] E. F. Alves and M. A. D. Souza, "Analysis of overexcitation relaying set up in synchronous generators for hydro power plants," in *Proceedings of the IEEE Transmission and Distribution Conference and Exposition: Latin America*, 2010, pp. 298–303.

[57] G. W. Alexander, S. L. Corbin, and W. J. McNutt, "Influence of design and operating practices on excitation of generator step-up transformers," *IEEE Transactions on Power Apparatus and Systems*, vol. PAS-85, no. 8, pp. 901–909, August 1966.

[58] IEEE/PES Electric Machinery Committee, "IEEE Standard for Cylindrical-Rotor 50 Hz and 60 Hz Synchronous Generators Rated 10 MVA and Above," *IEEE Std. C50.13 - 2005*, February 2006.

[59] B. Badrzadeh and V. Davidov, "Generator out of step protection for a combined heat and power (chp) plant," in *IEEE PES GM*, 2010, pp. 1–8.

[60] K. Malmedal, P. K. Sen, and J. P. Nelson, "Application of out-of-step relaying for small generators in distributed generation," *IEEE Transactions on Industry Applications*, vol. 41, no. 6, pp. 1506–1514, November/December 2005.

[61] J. S. Joyce, T. Kulig, and D. Lambrecht, "Torsional fatigue of turbine-generator shafts caused by different electrical system faults and switching operations," *IEEE Transactions on Power Apparatus and Systems*, vol. PAS-97, no. 5, pp. 1965–1977, Sept/Oct 1978.

[62] J. M. Undrill and L. N. Hannet, "Turbine-generator impact torques in routine and fault operations," *IEEE Transactions on Power Apparatus and Systems*, vol. PAS-98, no. 2, pp. 618–628, March/April 1979.

[63] C. G. Kaloudas, P. N. Papadopoulos, T. A. Papadopoulos, A. G. Marinopoulos, and G. K. Papagiannis, "Short-circuit analysis of an isolated generator and comparative study of iec, ansi and dynamic simulation," in *7th Mediterranean Conference and Exhibition on Power Generation, Transmission, Distribution and Energy Conversion*, 2010, pp. 1–7.

[64] K. Dartawan and C. R. S. Pierre, "Evaluating generator breakers short-circuit duty using ieee std. c37.010 and c37.013," in *48th Industrial and Commercial Power Systems Technical Conference*, 2012, pp. 1–7.

[65] R. E. Owen and W. A. Lewis, "Asymmetry characteristics of progressive short-circuits on large synchronous generators," *IEEE Transactions on Power Apparatus and Systems*, vol. PAS-90, no. 2, pp. 587–596, March/April 1971.

[66] J. C. Das, "Calculations of generator source short- circuit current according to ansi/ieee and iec standards, with emtp verifications," in *Annual Pulp and Paper Industry Technical Conference*, 2009, pp. 205–215.

[67] IEEE/PES Electric Machinery Committee, "IEEE Standard for Salient-Pole 50 Hz and 60 Hz Synchronous Generators and Generator/Motors Rated 5 MVA and Above," *IEEE Std. C50.12 - 2005*, February 2006.

[68] IEEE/PES Energy Development and Power Generation Committee, "IEEE Recommended Practice for Excitation System Models for Power System Stability Studies," *IEEE Std. 421.5 - 2005*, April 2006.

[69] V. Slenduhhov and J. Kilter, "Modeling and analysis of the synchronous generators excitation systems," in *13th International Symposium PARNU 2013 TOPICAL PROBLEMS IN THE FIELD OF ELECTRICAL AND POWER ENGINEERING*, 2013, pp. 252–258.

[70] J. Hurley, L. N. Bize, and C. R. Mummert, "The adverse effects of excitation system var and power factor controllers," *IEEE Transactions on Energy Conversion*, vol. 14, no. 4, pp. 1636–1645, December 1999.

[71] A. Glaninger-Katschnig, F. Nowak, M. Bachle, and J. Taborda, "New digital excitation system models in addition to ieee.421.5 2005," in *IEEE PES GM*, 2010.

[72] D. E. A. T. F. of the Excitation Systems Subcommittee, "Digital excitation technology - a review of features, functions and benefits," *IEEE Transactions on Energy Conversion*, vol. 12, no. 3, pp. 255–258, September 1997.

[73] C. A. Morse, C. R. Mummert, R. F. Martinez, and I. Gibbs, "New multi-processor digital excitation system," in *IEEE PES SM*, 2000.

[74] A. Godhwani and M. J. Basler, "A digital excitation control system for use on brushless excited synchronous generators," *IEEE Transactions on Energy Conversion*, vol. 11, no. 3, pp. 616–620, September 1996.

[75] IEEE/PES Energy Development and Power Generation Committee, *Power System Stabilization via Excitation Control*. IEEE, 2011.

[76] IEEE/PES Power Generation Committee, "IEEE Guide for Identification, Testing, and Evaluation of the Dynamic Performance of Excitation Control Systems," *IEEE Std. 421.2 - 1990*, May 1990.

[77] A. Murdoch and M. J. D'Antonio, "Generator excitation systems - performance specification to meet interconnection requirements," in *Proceedings of Electric Machines and Drives Conference*, 2001, pp. 317–322.

[78] E. L. Busby, J. D. Hurley, F. W. Keay, and C. Raczkowski, "Dynamic stability improvement at monticello station - analytical study and field tests," *IEEE Transactions on Power Apparatus and Systems*, vol. PAS-98, no. 3, pp. 889–901, May/June 1979.

[79] D. C. Lee, R. E. Beaulieu, and J. R. R. Service, "A power system stabilizer using speed and electrical power inputs - design and field experience," *IEEE Transactions on Power Apparatus and Systems*, vol. PAS-100, no. 9, pp. 4151–4157, September 1981.

[80] N. E. Nilsson and J. Mercurio, "Synchronous generator capability curve testing and evaluation," *IEEE Transactions on Power Delivery*, vol. 9, no. 9, pp. 414–424, January 1994.

[81] A. Panvini and T. J. Yohn, "Field assessment of generators reactive capability," *IEEE Transactions on Power Systems*, vol. 10, no. 1, pp. 288–296, February 1995.

[82] D. Zlatanovici, P. Budulan, and R. Zlatanovici, "Assessment of hydrogenerators capacity to provide the system service of voltage control in the secondary band," in *IEEE Power Tech Conference Proceedings*, vol. 4, June 2003.

[83] M. M. Adibi and D. P. Milanicz, "Reactive capability limitation of synchronous machines," *IEEE Transactions on Power Systems*, vol. 9, no. 1, pp. 29–40, February 1994.

[84] T. W. Eberly and R. C. Schaefer, "Minimum / maximum excitation limiter performance goals for small generation," *IEEE Transactions on Energy Conversion*, vol. 10, no. 4, pp. 714–721, December 1995.

[85] M. Baechle, V. Knazkis, P. A. Smulders, and D. Stutz, "Improving the performance of the stator current limiter of excitation control systems," in *IEEE PES GM*, 2012.

[86] A. Godhwani, K. Kim, and M. J. Basler, "An under and over excitation limiter implementation in a digital excitation system for synchronous generators," in *IEEE PES Winter Meeting*, 1999, pp. 193–195.

[87] M. S. Baldwin and D. P. McFadden, "Power systems performance as affected by turbine-generator controls response during frequency disturbances," *IEEE Transactions on Power Apparatus and Systems*, vol. PAS-100, no. 5, pp. 2486–2494, May 1981.

[88] J. D. Hurley, J. C. Agee, R. E. Beaulieu, G. R. Berube, C. R. Mummert, A. Murdoch, J. R. Ribeiro, and R. C. Schaefer, "Underexcitation limiter models for power system stability studies," *IEEE Transactions on Energy Conversion*, vol. 10, no. 3, pp. 524–531, September 1995, performance and Modeling Working Group of the Excitation Systems Subcommittee, Energy Development and Power Generation Committee.

[89] E. G. Potamianakis and C. D. Vournas, "Short-term voltage instability: Effects on

synchronous and induction machines," *IEEE Transactions on Power Systems*, vol. 21, no. 2, pp. 791–798, May 2006.

[90] C. Aumuller and T. K. Saha, "Investigating voltage collapse and subsequent transient instability in a large power system," in *IEEE PES GM*, 2003.

[91] J. C. Agee, R. Beaulieu, G. R. Berube, J. Hurley, C. Taylor, P. Kundur, G. K. Morison, B. Gao, and J. Ribeiro, "Recommended models for overexcitation limiting devices," *IEEE Transactions on Energy Conversion*, vol. 10, no. 4, pp. 706–713, December 1995.

[92] G. Quinonez-Varela and A. Cruden, "Experimental testing and model validation of a small-scale generator set for stability analysis," in *IEEE Powertech*, June 2003.

[93] A. B. Piardi, J. R. Presente, R. B. Otto, and R. A. Ramos, "Evaluation of volts/hertz and over-excitation limiters acting under unbalanced load conditions," in *IEEE PES GM*, 2013, pp. 1–5.

[94] A. S. Rubenstein and M. Temoshok, "Underexcited reactive ampere limit for modern amplidyne voltage regulator," *AIEE Transactions Part III : Power Apparatus and Systems*, vol. 73, no. 1, pp. 1433–1438, 1954.

[95] J. T. Carleton, P. O. Bobo, and D. A. Burt, "Minimum excitation limit for magnetic amplifier regulating system," *AIEE Transactions Part III : Power Apparatus and Systems*, vol. 73, no. 1, pp. 869–874, 1954.

[96] Y. Takeda and B. Adkins, "Determination of synchronous - machine parameters allowing for unequal mutual inductances," *Proceedings of the IEE*, vol. 121, no. 12, pp. 1501–1504, December 1974.

[97] F. DeMello and L. N. Hannet, "Validation of synchronous machine models and derivation of model parameters from tests," *IEEE Transactions on Power Apparatus and Systems*, vol. PAS-100, no. 2, pp. 662–672, February 1981.

[98] G. Shackshaft and A. T. Poray, "Implementation of new approach to determination of synchronous-machine parameters from tests," *Proceedings of the IEE*, vol. 124, no. 12, pp. 1170–1178, December 1977.

[99] G. Shackshaft, "New approach to the determination of synchronous - machine parameters from tests," *Proceedings of the IEE*, vol. 121, no. 11, pp. 1385–1392, November 1974.

[100] F. P. DeMello and J. R. Ribeiro, "Derivation of synchronous machine parameters from tests," *IEEE Transactions on Power Apparatus and Systems*, vol. PAS-96, no. 4, pp. 1211–1218, July/August 1977.

[101] M. E. Coultes and W. Watson, "Synchronous machine models by standstill frequency response tests," *IEEE Transactions on Power Apparatus and Systems*, vol. PAS-100, no. 4, pp. 1480–1489, April 1981.

[102] G. Quinonez-Varela and A. Cruden, "Development of a small-scale generator set model for local network voltage and frequency stability analysis," *IEEE Transactions on Energy Conversion*, vol. 22, no. 2, pp. 368–375, June 2007.

[103] J. L. Aguero, P. L. Arnera, R. E. L. Bianchi, M. C. Beroqui, and M. B. Barbieri, "Synchronous compensators. models verified by tests of: Automatic voltage regulator, reactive power control and voltage joint control," in *Transmission and Distribution Conference and Exposition: Latin America*, 2006.

[104] J. L. Aguero, P. L. Arnera, R. E. Bianchi Lastra, and M. C. Beroqui, "Synchronous compensators: Models verified by tests of automatic voltage regulator, reactive power control, and voltage joint control," *IEEE Transactions on Power Systems*, vol. 21, no. 4, pp. 1798–1807, November 2006.

[105] R. M. Rifaat, "Independent power producers (ipp) perspectives and experiences with wscc requirements for generator model validation tests," *IEEE Transactions on Industry Applications*, vol. 37, no. 4, pp. 1210–1216, Jul/Aug 2001.

[106] *PSS/E Model Library*, Siemens PTI, October 2010.

[107] *TSAT Transient Security Assessment Tool, Model Manual*, Powertech, August 2010.

[108] AESO, "Base cases 2012," 2012. [Online]. Available: http://www.aeso.ca/transmission/261.html

[109] R. D. Pettigrew, "Generator protection: The value of periodic settings review," in *59th Annual Conference for Protective Relay Engineers - Texas A & M*, April 2006.

[110] R. C. Schaefer, D. Janse, S. McMullen, and P. Rao, "Coordination of digital excitation system settings for reliable operation," in *IEEE PES GM*, 2009.

[111] C. J. Mozina, "Implementing nerc guidelines for coordinating generator and transmission protection," in *65th Annual Conference for Protective Relay Engineers*, 2012, pp. 491–504.

[112] ——, "Coordinating generator protection with transmission protection and generator controlnerc standards and pending requirements," in *63rd Annual Conference for Protective Relay Engineers*, 2010, pp. 1–12.

[113] R. Sandoval, A. Guzman, and H. J. Altuve, "Dynamic simulations help improve generator protection," in *Power Systems Conference: Advanced Metering, Protection, Control, Communication, and Distributed Resources*, 2007, pp. 16–38.

[114] M. S. Baldwin, W. A. Elmore, and J. J. Bonk, "Improve turbine-generator protection for increased plant reliability," *IEEE Transactions on Power Apparatus and Systems*, vol. PAS-99, no. 3, pp. 982–989, May/June 1980.

[115] T. V. Cutsem, "Voltage instability: Phenomena, countermeasures, and analysis methods," *Proceedings of the IEEE*, vol. 88, no. 2, pp. 208–227, February 2000.

[116] M. M. Elkateb and M. F. Dias, "Performance analysis and design of loss-of-excitation relays part i," in *Proceedings of the 3rd AFRICON Conference*, 1992, pp. 426–429.

[117] C. R. S. Pierre, "Loss-of-excitation protection for synchronous generators on isolated systems," *IEEE Transactions on Industry Applications*, vol. IA-21, no. 1, pp. 81–98, January/February 1985.

[118] M. F. Dias and M. M. Elkateb, "Case study into loss-of-excitation relays during simultaneous faults part ii," in *Proceedings of the 3rd AFRICON Conference*, 1992, pp. 430–433.

[119] C. R. Arndt and M. C. Rogers, "A study of loss-of-excitation relaying and stability of a 595-MVA generator on the Detroit Edison system," *IEEE Transactions on Power Apparatus and Systems*, vol. PAS-94, no. 5, pp. 1449–1456, September/October 1975.

[120] Agee, "Maximizing benefits of temporary generator overexcited capability: A special technical session on new operating concepts," in *Proceedings of IEEE PES WM*, 2001, pp. 203–204.

[121] A. Murdoch, R. W. Delmerico, R. A. Venkataraman, J. E. Curran, and W. R. Pearson, "Excitation system protective limiters and their effect on volt/var control-design, computer modeling, and field testing," *IEEE Transactions on Energy Conversion*, vol. 15, no. 4, pp. 440–450, December 2000.

[122] C. R. Mummert, "Excitation system limiter models for use in system stability studies," in *Proceedings of the Power Engineering Society Winter Meeting*, vol. 1, Jan./Feb. 1999, pp. 197–192.

[123] A. Murdoch, G. E. Boukarim, M. J. D'Antonio, and R. A. Lawson, "Generator over excitation capability and excitation system limiters," in *Proceedings of the Power Engineering Society Winter Meeting*, vol. 1, Jan./Feb. 2001, pp. 215–220.

[124] IEEE/PES Power System Relaying Committee, "IEEE Guide for AC Generator Protection," *IEEE Std. C37.102 - 2006*, February 2007.

[125] J. C. Agee and H. D. Vu, "Overexcitation limiter testing and modeling," in *IEEE PES WM*, 1999.

[126] G. K. Girgis and H. D. Vu, "Verification of limiter performance in modern excitation control systems," *IEEE Transactions on Energy Conversion*, vol. 10, no. 3, pp. 538–542, September 1995.

[127] IEEE/PES Digital Excitation Task Force of the Excitation System Subcommittee, "Computer models for representation of digital-based excitation systems," *IEEE Transactions on Energy Conversion*, vol. 11, pp. 607–615, September 1996.

[128] K. Kim, M. J. Basler, and A. Godhwani, "Supplemental control in a modern digital excitation system," in *IEEE PES WM*, 2000, pp. 603–608.

[129] M. Orozco and H. Vasquez, "Dynamic performance of an excitation system built in a digital way," in *IEEE ICIECA*, 2005.

[130] M. Shimomura, Y. Xia, M. Wakabayashi, and J. Paserba, "A new advanced over excitation limiter for enhancing the voltage stability of power systems," in *IEEE PES WM*, 2001.

[131] A. W. Goldman, "Selection of generator stepup transformer ratings," *IEEE Transactions on Power Apparatus and Systems*, vol. PAS-100, no. 7, pp. 3425–3431, July 1981.

[132] C. D. Vournas, G. A. Manos, P. W. Sauer, and M. A. Pai, "Effect of overexcitation limiters on power system long-term modeling," *IEEE Transactions on Energy Conversion*, vol. 14, no. 4, pp. 1529–1536, December 1999.

[133] S. Patterson, "Overexcitation limiter modeling for power system studies," in *IEEE PES GM*, 2005.

[134] Kestrel, "Analysis/Modeling/Testing of Poplar River Unit G2 - SaskPower - MAPP Verification Program," Nov 2006.

[135] R. D. Rana, R. P. Shulz, M. Heyeck, and T. R. Boyer, "Generator loss of field study for aep's rockport plant," *IEEE Computer Applications in Power*, vol. 3, no. 2, pp. 44–49, April 1990.

[136] C. R. Mason, "A new loss-of-excitation relay for synchronous generators," *AIEE Transactions Part III : Power Apparatus and Systems*, vol. 68, pp. 1240–1245, 1949.

[137] R. L. Tremaine and J. L. Blackburn, "Loss-of-field protection for synchronous machines," *AIEE Transactions Part III : Power Apparatus and Systems*, vol. 73, no. 1, pp. 765–772, 1954.

[138] J. M. Bisbee, M. F. Rosol, C. L. Wagner, and E. W. Woody, "A partial survey of relay protection of steam-driven a-c generators," *AIEE Transactions Part III : Power Apparatus and Systems*, vol. 80, pp. 954–957, 1962.

[139] P. J. Moore and A. Stangenberg, "An investigation into the impedance characteristics of a synchronous generator under loss of excitation condition," in *Proceedings of Energy Management and Power Delivery*, 1998.

[140] W. F. Mackenzie, J. A. Imhof, C. Dewey, E. J. Emmerling, F. H. Freer, S. H. Horowitz, and C. L. Wagner, "Loss-of-field relay operation during system disturbances working group report - june 1971," *IEEE Transactions on Power Apparatus and Systems*, vol. PAS-94, no. 5, pp. 1464–1472, Sep./Oct. 1975.

[141] J. Berdy, "Loss of excitation protection for modern synchronous generators," *IEEE Transactions on Power Apparatus and Systems*, vol. PAS-94, no. 5, pp. 1457–1463, 1975.

[142] D. C. Lee, P. Kundur, and R. D. Brown, "A high speed, discriminating generator loss of excitation protection," *IEEE Transactions on Power Apparatus and Systems*, vol. PAS-98, no. 6, pp. 1895–1899, 1979.

[143] H. J. Herrman and A. Smit, "Increased sensitivity of loss of field protection based on admittance measurement," in *Western Protective Relay Conference*. Washington State University, 2009, pp. 1–15.

[144] S. R. Tambay and Y. G. Paithankar, "A new adaptive loss of excitation relay augmented by rate of change of reactance," in *Proceedings of IEEE Power Engineering Society General Meeting*, vol. 2, June 2005, pp. 1831–1835.

[145] L. Li., S. Caixin, and M. Daohuai, "Study on the excitation protection and control of synchronous generator based on the delta and s," in *Proceedings IEEE PES Trans-*

mission and Distribution Conference Exhibition: Asia and Pacific, August 2005, pp. 1–4.

[146] O. Usta, M. H. Musa, M. Bayrak, and M. A. Redfern, "A new relaying algorithm to detect loss of excitation of synchronous generators," *Turkey Journal of Electrical Engineering*, vol. 15, no. 3, pp. 339–349, 2007.

[147] H. Yaghobi, H. Mortazavi, K. Ansari, H. R. Mashhadi, H. K. Zadeh, and H. Borzoe, "A novel flux-based method for synchronous generator loss of excitation protection," in *Proceeding of 25th International Power System Conference*, 2010, pp. 1–14.

[148] Z. P. Shi, J. P. Wang, Z. Gajic, C. Sao, and M. Ghandhari, "The comparison and analysis for loss of excitation protection schemes in generator protection," in *International Conference on Developments in Power System Protection*, 2012, pp. 1–6.

[149] Z. Shi, "Investigation on generator loss of excitation protection in generator protection coordination," Master's thesis, School of Electrical Engineering - Royal Institute of Technology, 2010. [Online]. Available: http://kth.diva-portal.org/smash/record.jsf?pid=diva2:610188

[150] C. H. Lee, L. S. Ma, C. H. Weng, and B. K. Chen, "Lessons learned from the generator loss of field at a cogeneration thermal plant in taiwan," *IEEE Transactions on Power Systems*, vol. 26, no. 4, pp. 2093–2100, 2011.

[151] Y. Siwang, W. Weijian, L. Ling, G. Lin, and Q. Arui, "Discussion on setting calculation of loss-of-excitation protection for large turbogenerator," in *International Conference on Electrical Machines and Systems*, 2010, pp. 1413–1416.

[152] A. P. Morais, G. Cardoso, L. Mariotto, and L. N. Canha, "Performance evaluation of the adaptive loss of field protection in synchronous generators by means of the positive offset method," *IEEE Latin America Transactions*, vol. 7, no. 6, pp. 643–649, December 2009.

[153] A. M. Sharaf and T. T. Lie, "Ann based pattern classification of synchronous generator

stability and loss of excitation," *IEEE Transactions on Energy Conversion*, vol. 9, no. 4, pp. 753–759, December 1994.

[154] K. H. So, J. Y. Heo, R. K. Aggarwal, and K. B. Song, "Out-of-step detection algorithm using frequency deviation of voltage," *IET Generation, Transmission and Distribution*, vol. 1, no. 1, pp. 119–126, January 2007.

[155] F. Bo, L. Xiaoquan, X. Peng, and L. Junjie, "The research ul-p of loss of excitation protection for generator based on the artificial neural networks," in *Asia Pacific Power and Energy Engineering Conference*, 2009, pp. 1–4.

[156] A. P. Morais, G. Cardoso, and L. Mariotto, "An innovative loss-of-excitation protection based on the fuzzy inference mechanism," *IEEE Transactions on Power Delivery*, vol. 25, no. 4, pp. 2197–2204, October 2010.

[157] T. Bi, J. Sui, H. Yu, and Q. Yang, "Adaptive loss of field protection based on phasor measurements," in *Power and Energy Society General Meeting*, 2011, pp. 1–4.

[158] R. O. Duda, P. E. Hart, and D. G. Stork, *Pattern Classification*, 2nd ed. John Wiley and Sons, 2001.

[159] S. S. Choi, R. Larkin, M. T. Bastick, and A. W. Ferres, "Effects of underexcitation limiters on operation of remote generating station," *IEE Proceedings - C*, vol. 138, no. 6, pp. 560–566, November 1991.

[160] J. R. Ribeiro, "Minimum excitation limiter effects on generator response to system disturbances," *IEEE Transactions on Energy Conversion*, vol. 6, no. 1, pp. 29–38, March 1991.

[161] G. R. Berube, L. M. Hajagos, and R. E. Beaulieu, "A utility perspective on underexcitation limiters," *IEEE Transactions on Energy Conversion*, vol. 10, no. 3, pp. 532–537, September 1995.

[162] A. J. P. Ramos, L. R. Lins, E. H. D. Fittipaldi, and L. Monteath, "Performance of underexcitation limiters of synchronous machines for system critical disturbances," *IEEE Transactions on Power Systems*, vol. 12, no. 4, pp. 1702–1707, November 1997.

[163] J. P. Hunt, "Capability curves and excitation requirements of saturated cylindrical rotor synchronous machines," *IEEE Transactions on Power Apparatus and Systems*, vol. PAS-86, no. 7, pp. 855–859, July 1967.

[164] J. Kekela and L. Firestone, "Underexcited operation of generators," *IEEE Electrical Engineering*, vol. 82, no. 12, pp. 811–817, August 1963.

[165] G. L. Langdreen, "Extended use of generator reactive capability by a dual underexcitation limiter," *IEEE Transactions on Power Apparatus and Systems*, vol. PAS-99, no. 4, pp. 1381–1385, Jul/Aug 1980.

[166] S. S. Choi and X. M. Jia, "Under excitation limiter and its role in preventing excessive synchronous generator stator end-core heating," *IEEE Transactions on Power Systems*, vol. 15, no. 1, pp. 95–101, February 2000.

[167] A. G. Jack and B. C. Mecrow, "A method to calculate turbogenerator end region fields and losses and validation using measured results," *IEEE Transactions on Energy Conversion*, vol. EC-2, no. 1, pp. 100–107, March 1987.

[168] B. C. Mecrow, A. G. Jack, and K. W. Cowan, "Stator core end heating in air and hydrogen indirectly cooled turbogenerators," in *Fifth Internation Conference on Electrical Machine and Drives*, 1991, pp. 290–294.

[169] G. K. M. Khan, G. W. Buckley, R. B. Bennett, and N. Brooks, "An integrated approach for the calculation of losses and temperatures in the end-region of large turbine generators," *IEEE Transactions on Energy Conversion*, vol. 5, no. 1, pp. 183–194, March 1990.

[170] Y. Liu and S. Hjarne, "Computations of losses and temperatures in the core ends of high voltage turbo-generator," in *Eight International Conference on Electrical Machines and Systems*, 2005, pp. 2091–2096.

[171] S. Doi, K. Ito, and S. Nonaka, "Three-dimensional thermal analysis of stator end-core for large turbine-generators using flow visualization results," *IEEE Transactions on Power Apparatus and Systems*, vol. PAS-104, no. 7, pp. 1856–1862, July 1985.

[172] G. Hui, Y. Yingying, F. Youtong, and Y. Shiyou, "The dynamic performance and temperature distribution of turbine generator under loss of excitation by using coupled fe analysis," in *14th Biennial IEEE Conference on Electromagnetic Field Computation*, 2010.

[173] L. Junqing, L. Heming, and L. Zhiping, "Research on temperature-rise of stator iron-core end region of turbine generator," in *Fifth International Conference on Power Electronics and Drive Systems*, 2003, pp. 766–770.

[174] Y. Yao, H. Xia, G. Ni, X. Liang, and Z. Xian, "Analysis of magnetic-thermal coupled fields in the end region of large turbine-generators," in *World Automation Congress*, 2008.

[175] Z. Maljkovic and I. Gasparac, "Operating limits of underexcited synchronous generator," in *4th International Conference on Power Engineering, Energy and Electrical Drives*, May 2013.

[176] S. Mohajeryami, Z. Salami, and I. N. Moghaddam, "Study of effectiveness of under-excitation limiter in dynamic modeling of diesel generators," in *Power and Energy Conference at Illinois*, 2014, pp. 1–5.

[177] C. C. DeMello, F.P., "Concepts of synchronous machine stability as affected by excitation control," *IEEE Transactions on Power Apparatus and Systems*, vol. PAS-88, no. 5, pp. 316–329, 1969.

[178] S. S. Choi and X. M. Jia, "Tuning under excitation limiters in the multi-machine power system environment," in *IEEE PES WM*, 2000.

[179] A. J. Saavedra-Montes and J. M. Ramirez, "Parameter estimation of under-excitation limiter from the registers of startup of a generation unit," in *IEEE PES Transmission and Distribution Conference and Exposition Latin America*, 2008.

[180] S. S. Choi and X. M. Jia, "Application of a coordinated design method for under-excitation limiters in a multi-machine power system," in *IEEE PES WM*, 2001.

[181] ——, "Coordinated design of under-excitation limiters and power system stabilizers," *IEEE Transactions on Power Systems*, vol. 15, pp. 937–944, 2000.

[182] X. M. Jia and S. S. Choi, "Design of volts per hertz limiter with consideration of the under-excitation limiter control actions," *IEEE Transactions on Energy Conversion*, vol. 16, no. 2, pp. 140–147, June 2001.

[183] S. E. M. d. Oliveira and M. G. d. Santos, "Impact of under-excitation limit control on power system dynamic performance," *IEEE Transactions on Power Systems*, vol. 10, no. 4, pp. 1863–1869, November 1995.

[184] S. S. Choi and X. M. Jia, "A technique for tuning under excitation limiters," *IEEE Transactions on Power Systems*, vol. 14, no. 4, pp. 1279–1284, November 1999.

[185] S. S. Choi and R. Larkin, "Steady state stability of a remote gas-turbine generating station: Field tests and validation of computer simulation results," *IEEE Transactions on Power Systems*, vol. 8, no. 4, pp. 1518–1524, November 1993.

[186] M. L. Crenshaw, K. E. Bollinger, R. R. Byerly, R. L. Cresap, L. E. Eilt, D. E. Eyre, F. W. Keay, P. Kundur, E. V. Larsen, D. C. Lee, J. F. Luini, R. G. Pillote, P. L. Dandeno, K. C. Bess, H. H. Chen, and D. G. Ramey, "Excitation system models for power system stability studies," *IEEE Transactions on Power Apparatus and Systems*, vol. 2, pp. 494–509, 1981, prepared by the Working Group on Computer Modelling of Excitation Systems.

[187] J. C. Agee, S. Patterson, and J. Seitz, "Excitation system testing and model validation," in *IEEE PES WM*, 1999.

[188] C. A. Morse, C. R. Mummert, R. F. Martinez, I. A. Gibbs, and T. Reynolds, "Functional testing of a new digital excitation system," in *IEEE PES Summer Meeting*, 2000, pp. 637–642.

[189] IEEE/PES Power System Relaying Committee, "IEEE Standard Common Format for Transient Data Exchange (COMTRADE) for Power Systems," *IEEE C37.111*, 1999.

[190] *TMS320C6713 DSK Technical Reference*, Digital Spectrum Incorporated, 2003.

[191] "Openwatcom," version 1.9. [Online]. Available: http://www.openwatcom.org

[192] G. Benmouyal, "The impact of synchronous generators excitation supply on protection and relays," in *Western Protective Relay Conference*, 2007, pp. 1–16.

Appendix
Stability Limit Calculation using DeMello 'K' Factors

The calculation of the stability limit using DeMello 'K' factors was described by Reimert [12]. Reimert provided detailed derivation for the limits when no AVR action was considered, However, Reimert's derivation for the case with AVR action included and no PSS was not detailed and had an error in the synchronizing torque component. Another approach was proposed by Benmouyal [192] based on Reimert's work but using state space instead of algebraic derivation of the torque components. Benmouyal's approach was demonstrated including AVR and PSS control action. In this thesis, the error in Reimert approach is corrected and the resulting equations are used for the calculation of the stability limits with and without AVR action but without including PSS action.

To obtain the stability limits a single machine supplying an infinite bus through an external impedance including the effects of AVR is considered. A linearized block diagram for this simplified system is shown in Fig. A.1, this figure is almost identical to that used by DeMello [177] with only minor modifications for clarity.

From Fig. A.1 equations (A.1) and (A.2) can be derived directly from inspection.

$$\Delta E_{fd} = \frac{-K_e}{1+sT_e}[K_5\Delta\delta + \Delta e_{t_{ref}} + K_6\Delta E_q{}'] \tag{A.1}$$

$$\Delta E_q{}' = \frac{K_3}{1+sK_3T'_{do}}[-K_4\Delta\delta + \Delta E_{fd}] \tag{A.2}$$

Substituting (A.2) into (A.1) we obtain (A.3):

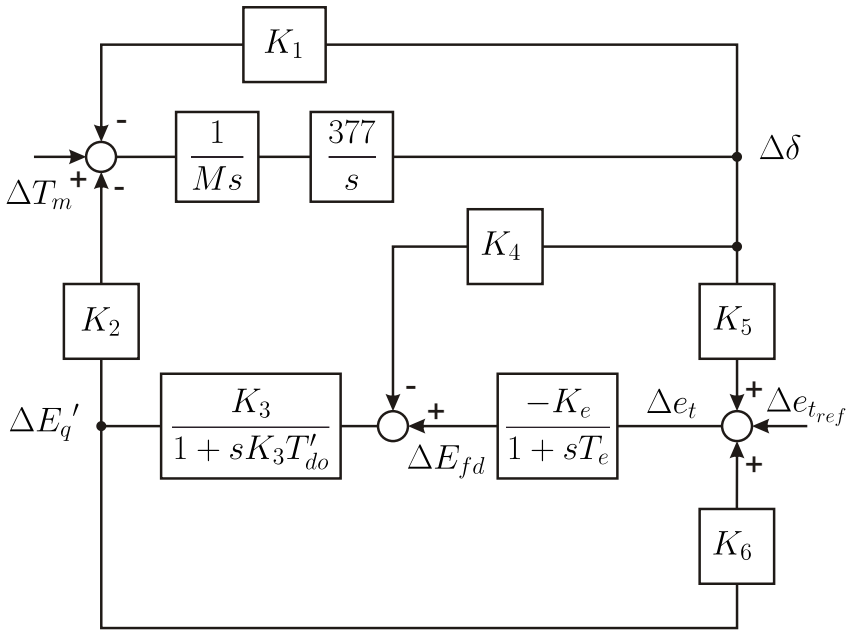

Figure A.1: Single machine supplying an infinite bus through external impedance including effects of voltage regulator

$$\Delta E_{fd} = \frac{-K_e}{1+sT_e}\left[K_5\Delta\delta + \Delta e_{t_{ref}} + K_6\frac{K_3}{1+sK_3T'_{do}}[-K_4\Delta\delta + \Delta E_{fd}]\right] \tag{A.3}$$

Rearranging (A.3) to have E_{fd} in one side results in (A.4).

$$\left[1 + \frac{K_eK_6K_3}{(1+sT_e)(1+sK_3T'_{do})}\right]\Delta E_{fd} = \frac{-K_e}{1+sT_e}\left[\left(K_5 - \frac{K_3K_4K_6}{1+sK_3T'_{do}}\right)\Delta\delta + \Delta e_{t_{ref}}\right] \tag{A.4}$$

In Fig. A.1 the electrical torque ΔT_e corresponds to the sum of the two subtracting inputs opposing the mechanical torque ΔT_m, thus resulting (A.5).

$$\Delta T_e = K_1\Delta\delta + \frac{K_2K_3}{1+sK_3T'_{do}}(-K_4\Delta\delta + \Delta E_{fd}) \tag{A.5}$$

From (A.4) considering no PSS action means that the input $\Delta e_{t_{ref}}$ is zero. Solving for E_{fd} in (A.4) and substituting in (A.5) results in (A.6).

$$\begin{aligned}\Delta T_e = & \\ & K_1\Delta\delta \\ & + \frac{K_2K_3}{(1+sK_3T'_{do})}\left[-K_4\Delta\delta\right. \\ & \left. - \frac{Ke\left(K_5[1+sK_3T'_{do}] - K_3K_4K_6\right)\Delta\delta}{[(1+sK_3T'_{do})(1+sT_e)+K_eK_6K_3]}\right]\end{aligned} \tag{A.6}$$

Simplifying (A.6) gives (A.7).

$$\begin{aligned}\Delta T_e = & \\ & K_1\Delta\delta \\ & + K_2K_3\frac{-K_eK_5 - K_4 - sK_4T_e}{[(1+sK_3T'_{do})(1+sT_e)+K_eK_6K_3]}\Delta\delta\end{aligned} \tag{A.7}$$

The synchronizing torque for steady state stability limit results from substituting $s = 0$ in (A.7), which gives (A.8).

$$\begin{aligned}\Delta T_e|_{s=0} = & \\ & K_1\Delta\delta \\ & + K_2K_3\frac{-K_eK_5 - K_4}{[1+K_eK_6K_3]}\Delta\delta\end{aligned} \tag{A.8}$$

The damping torque at the dynamic stability limit results from substituting $s = j\omega$ ($\omega = \omega_n$, natural frequency) in (A.7) and taking the imaginary component, which gives (A.9).

$$\begin{aligned}\Im\{\Delta T_e|_{s=j\omega}\} = & \\ & - K_2K_3\omega\frac{(K_3T'_{do}+T_e)(-K_eK_5-K_4)+K_4T_e(1-\omega^2K_3T'_{do}T_e+K_eK_6K_3)}{([1-\omega^2K_3T'_{do}T_e+K_eK_6K_3]^2+\omega^2[K_3T'_{do}+T_e]^2)}\Delta\delta\end{aligned} \tag{A.9}$$

The case for no AVR action, i.e., manual control, is obtained substituting $K_e = 0$ and $T_e = 0$ in (A.8) and (A.9).

The method used to obtain the limits uses a search in the PQ plane following radial paths from the origin and looking for a change in sign in the synchronizing and damping torques. The information values needed are listed in table A.1.

Table A.1: Parameters Needed for 'K' Factors Method

Description	Parameter
Terminal voltage	e_t
Synchronous reactance	X_d
	X_q
Transient reactance	X'_d
Transient OC Time Constant	T_{do}
Inertia Constant	H
System impedance	X_e
	r_e
AVR gain and time constant	K_e
	T_e

For a given operating point S_0 in the PQ plane the initial values are calculated.

$$e_{t_0} = e_t \tag{A.10}$$

$$i_{t_0} = \left| \frac{S_0}{e_{t_0}} \right|^* \tag{A.11}$$

$$E_Q = e_{t_0} + i_{t_0} j X_q \tag{A.12}$$

$$E_{sy} = e_{t_0} - i_{t_0}(r_e + jX_e) \tag{A.13}$$

$$e_{d_0} = |e_{t_0}| \sin \angle(E_Q e^*_{t_0}) \tag{A.14}$$

$$e_{q_0} = |e_{t_0}| \cos \angle(E_Q e^*_{t_0}) \tag{A.15}$$

$$i_{d_0} = |i_{t_0}| \sin \angle(E_Q i^*_{t_0}) \tag{A.16}$$

$$i_{q_0} = |i_{t_0}| \cos \angle(E_Q i^*_{t_0}) \tag{A.17}$$

Some additional variables to calculate the 'K' factors.

$$E_{q_0} = |E_Q| \tag{A.18}$$

$$E_0 = |E_{sy}| \tag{A.19}$$

$$\delta_0 = \angle E_Q E^*_{sy} \tag{A.20}$$

The 'K' factors need to be recalculated for each operating point S_0 being considered, using the following expressions [177]

$$A = r_e^2 + (X_e + X'_d)(X_q + X_e) \tag{A.21}$$

$$\begin{aligned} K_1 = {} & \frac{E_{q_0} E_0}{A}(r_e \sin(\delta_0) + (X_e + X'_d)\cos(\delta_0)) \\ & + \frac{i_{q_0} E_0}{A}((X_q - X'_d)(X_e + X_q)\sin(\delta_0)) \\ & - r_e(X_q - X'_d)\cos(\delta_0)) \end{aligned} \tag{A.22}$$

$$K_2 = \left[\frac{r_e E_{q_0}}{A} + i_{q_0}\left(1 + \frac{(X_e + X_q)(X_q - X'_d)}{A}\right)\right] \tag{A.23}$$

$$K_3 = \left[1 + \frac{(X_e + X_q)(X_d - X'_d)}{A}\right]^{-1} \tag{A.24}$$

$$K_4 = \frac{E_0(X_d - X'_d)}{A}[(X_e + X_q)\sin(\delta_0) - r_e\cos(\delta_0)] \tag{A.25}$$

$$\begin{aligned} K_5 = \frac{e_{d_0}}{e_{t_0}} X_q \left[\frac{r_e E_0 \sin(\delta_0) + (X_e + X'_d)E_0\cos(\delta_0))}{A}\right] \\ + \frac{e_{q_0}}{e_{t_0}} X'_d \left[\frac{r_e E_0 \cos(\delta_0) - (X_e + X_q)E_0\sin(\delta_0)}{A}\right] \end{aligned} \tag{A.26}$$

$$K_6 = \frac{e_{q_0}}{e_{t_0}}\left[1 - \frac{X'_d(X_e + X_q)}{A}\right] + \frac{e_{d_0}}{e_{t_0}} X_q \frac{r_e}{A} \tag{A.27}$$

The natural frequency of the system is calculated by (A.28).

$$\omega_n = \frac{sign(K_1) + 1}{2}\sqrt{\frac{2\pi 60 K_1}{2H}} \tag{A.28}$$